frontiers | Research Topics

Aquatic photosynthetic organisms under global change

Edited by
Benoit Schoefs and Justine Marchand

Published in
Frontiers in Plant Science

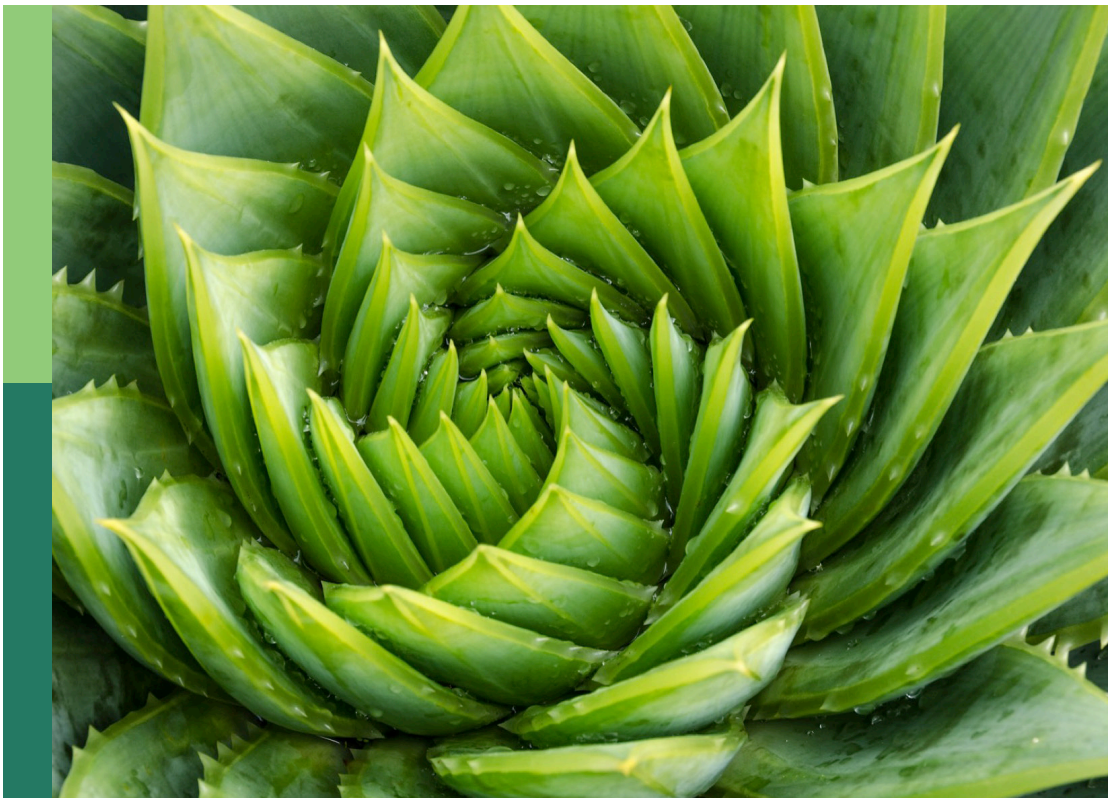

ISSN 1664-8714
ISBN 978-2-8325-5967-3
DOI 10.3389/978-2-8325-5967-3

About Frontiers

Frontiers is more than just an open access publisher of scholarly articles: it is a pioneering approach to the world of academia, radically improving the way scholarly research is managed. The grand vision of Frontiers is a world where all people have an equal opportunity to seek, share and generate knowledge. Frontiers provides immediate and permanent online open access to all its publications, but this alone is not enough to realize our grand goals.

Frontiers journal series

The Frontiers journal series is a multi-tier and interdisciplinary set of open-access, online journals, promising a paradigm shift from the current review, selection and dissemination processes in academic publishing. All Frontiers journals are driven by researchers for researchers; therefore, they constitute a service to the scholarly community. At the same time, the *Frontiers journal series* operates on a revolutionary invention, the tiered publishing system, initially addressing specific communities of scholars, and gradually climbing up to broader public understanding, thus serving the interests of the lay society, too.

Dedication to quality

Each Frontiers article is a landmark of the highest quality, thanks to genuinely collaborative interactions between authors and review editors, who include some of the world's best academicians. Research must be certified by peers before entering a stream of knowledge that may eventually reach the public - and shape society; therefore, Frontiers only applies the most rigorous and unbiased reviews. Frontiers revolutionizes research publishing by freely delivering the most outstanding research, evaluated with no bias from both the academic and social point of view. By applying the most advanced information technologies, Frontiers is catapulting scholarly publishing into a new generation.

What are Frontiers Research Topics?

Frontiers Research Topics are very popular trademarks of the *Frontiers journals series*: they are collections of at least ten articles, all centered on a particular subject. With their unique mix of varied contributions from Original Research to Review Articles, Frontiers Research Topics unify the most influential researchers, the latest key findings and historical advances in a hot research area.

Find out more on how to host your own Frontiers Research Topic or contribute to one as an author by contacting the Frontiers editorial office: frontiersin.org/about/contact

Aquatic photosynthetic organisms under global change

Topic editors

Benoit Schoefs — Le Mans Université, France

Justine Marchand — Le Mans Université, France

Citation

Schoefs, B., Marchand, J., eds. (2025). *Aquatic photosynthetic organisms under global change*. Lausanne: Frontiers Media SA. doi: 10.3389/978-2-8325-5967-3

Table of contents

frontiers | Frontiers in Plant Science

TYPE Editorial
PUBLISHED 23 January 2025
DOI 10.3389/fpls.2024.1539716

OPEN ACCESS

EDITED AND REVIEWED BY
Miroslav Obornik,
Czech Academy of Sciences, Czechia

*CORRESPONDENCE
Benoît Schoefs
benoit.schoefs@univ-lemans.fr

RECEIVED 04 December 2024
ACCEPTED 30 December 2024
PUBLISHED 23 January 2025

CITATION
Marchand J and Schoefs B (2025) Editorial: Aquatic photosynthetic organisms under global change.
Front. Plant Sci. 15:1539716.
doi: 10.3389/fpls.2024.1539716

Editorial: Aquatic photosynthetic organisms under global change

Justine Marchand and Benoît Schoefs*

Metabolism, Molecular Engineering of Microalgae and Applications, Laboratory Biology of Organisms, Stress, Health and Environment, IUML – FR 3473 CNRS, Le Mans University, Le Mans, France

KEYWORDS

adaptation, algae, carbon metabolism, freshwater, global warming, photosynthesis, plant, ocean

Editorial on the Research Topic
Aquatic photosynthetic organisms under global change

From space, Earth looks like a masterful stone marquetry such as can be admired in Florence, Italy. In this stone painting, large areas and thinner lines of lapis lazuli would represent oceans (97%) and rivers (3%), respectively. Together, they occupy 71% of the Earth's surface. Despite their different chemical composition, oceans and rivers host a large number of living organisms, including phototrophs. Their diversity is also great with anoxygenic and oxygenic bacteria, and unicellular and multicellular eukaryotes, including some flowering plants. For example, the number of identified alga species lies in the range of 40–60,000 (Guiry, 2024), a number that increases annually (e.g., Schoefs et al., 2020; Morin et al., 2025). As primary producers, aquatic photosynthetic organisms fulfill crucial ecosystem services for the planet. This includes approximately half of the global oxygen production (Benoiston et al., 2017) and photosynthetic carbon fixation (Falkowski and Raven, 2013). Aquatic photosynthetic organisms are also involved in many spectacular symbioses with non-photosynthetic organisms such as the symbiosis between the ciliate *Paramecium bursaria* and the green freshwater microalga *Chlorella variabilis* (Kodama and Sumita, 2022), allowing the partners to develop during dedicated phase or accompanying them all along their life like the symbiotic dinoflagellates in corals. In addition to the obvious freshwater, brackish water, and saline water habitats, aquatic photosynthetic organisms are also present in more surprising and/or drastic niches such as solid water (e.g., Procházková et al., 2024), hot springs (Smith et al., 2013), radioactive natural springs (Millan et al., 2020), and loggerhead sea turtles (Majewska et al., 2020). Each of these aquatic organisms develops according to its ecological optimum. When one ecological factor deviates from its optimum, aquatic photosynthetic organisms start to acclimate.

Global warming has direct and indirect impacts on the climate and therefore on the ecological parameters of every ecological niche, including aquatic ones. This Research Topic "*Aquatic photosynthetic organisms under global change*" focuses on the direct and indirect effects of climate change on the life of microalga, macroalga, and aquatic angiosperms.

The increase in ocean temperature together with the increase of CO_2 dissolution in the oceans leads to a change in the physico-chemical properties of seawater, including a decrease in pH, known as ocean acidification (Feely et al., 2009). Ocean acidification has pleiotropic effects on aquatic photosynthetic organisms because it promotes or decreases microalgal division rate (Gao et al., 2019), reduces the calcification of algae (Jin et al., 2017),

increases the exposure of algae to UV radiation, and can negatively impact the symbiotic relationship between corals and microalgae (Fautin and Buddemeier, 2004), including the thermo-tolerant microalga *Symbiochlorum hainanensis* (Gong et al.). In this article Research Topic, Gong et al. reported on the impacts of elevated temperature and acidification alone or in combination on the biology of *S. hainanensis*. Overall, the data reveal that chloroplast adaptation constitutes one of the most important challenges of the adaptation of algae to climate change. Indeed, the contribution to this article Research Topic by Zhang et al. confirms and extends this conclusion to red macroalgae living in the intertidal zone, a very unique and challenging ecosystem because they are exposed, albeit temporarily, to extreme conditions such as fresh air, high light intensity, and UV radiation irradiation. High light exposure reduces photosynthesis and growth rate significantly. Moderate UV-A (315–400 nm) levels are beneficial for carbon fixation, nitrate uptake (Viñegla et al., 2006; Xu and Gao, 2010), and/or development of conchospores (Jiang et al., 2007) of some macroalgae but not all, including the red commercial macroalga genus *Pyropia* (Zhang et al., 2020) (formerly known as *Porphyra*; Sutherland et al., 2011). In this Research Topic, Zhang et al. also demonstrated that seawater acidification mitigates UV radiation on *Pyropia yezoensis* photosynthesis by modulating the synergy between photosystems. Mitochondrial metabolism is also important because it is involved in the control of the bloom of the dinoflagellate *Karenia mikimotoi* when nutrient availability and seawater acidity are altered (Liu et al.). Interestingly, it was found that nutrient limitations, especially phosphorous, can alleviate the negative impacts of acidification. Research in this field is particularly timely because these two factors are typical of global change (e.g., Gobler et al., 2017). Conversely, eutrophication can also increase the abundance of toxic microalgae (Anderson et al., 2002). The use of filter-feeding bivalve mollusks and submerged macrophytes can be an alternative to reduce indirectly the abundance of blooms. In this Research Topic, Du et al. presented a characterization of their impacts on phytoplankton bloom development by alleviating the eutrophication. In a nutrient-enriched freshwater mesocosm experiment, combining the filter-feeding bivalve *Cristaria plicata*, the cockscomb pearl mussel, and the macrophyte *Hydrilla verticillata* was highly efficient in decreasing the availability of nutrients, resulting in the suppression of bloom development, particularly by excluding cyanobacteria. While eutrophication can promote the occurrence of taxa, it can also jeopardize the survival of some of them such as the European aquatic plant *Luronium natans* (Alismataceae) (Makuch et al.).

In addition to aquatic photosynthetic organisms, submerged macrophytes occupy an important place in aquatic ecosystems, especially in shallow lakes and rivers (Hao et al., 2017), because they can maintain the physico-chemical properties and transparency of water (Wu et al., 2021). Like phytoplankton, submerged macrophytes also suffer from climate warming and eutrophication due to changes in abiotic variables alone or in combination with biotic variables (Hao et al., 2018; Matsuzaki et al., 2018). In their contribution, Wu et al. used mesocosms to determine the effects of climate warming and eutrophication on the growth of two aquatic plants, *Potamogeton crispus* and *Elodea canadensis*, at a seasonal scale (Zoppi et al. 2024). The latter taxon is recognized as an invasive species worldwide. The authors suggest that the variables explaining the variation in biomass are different for each season and that a synergetic effect of temperature and nutrients occurred rarely. At the annual scale, the overall results showed a direct positive effect of temperature rather than nutrient concentrations on *E. canadensis* biomass. Surprisingly, nutrient enrichment affected biomass by increasing competition among primary producers. Altogether, the study shows that ongoing climate warming and eutrophication will cause a transition in aquatic plant communities through selection effects.

Obviously, carbon metabolism is at the core of every reaction of photosynthetic organisms, in which the supply of inorganic carbon is of primary importance. This is particularly true for submerged organisms such as algae (e.g., Schoefs et al., 2017) but also for aquatic plants. In this Research Topic, two different cases are reported. The first one is the completely submerged marine land plant *Zoostera marina* (eelgrass) and the freshwater land plant *Ottela ovalifolia* with submerged and floating leaves. These plants differ not only in their autoecology but also in the source of inorganic carbon to which they have access. *Z. marina* only has access to HCO_3^-, whereas *O. ovalifolia* can fix either HCO_3^- or CO_2, depending on whether the leaves are submerged or emerged. *Z. marina* is a C_3 plant, meaning that its photosynthetic capacity is limited by the activity of photorespiration, the efficiency of which decreases as the inorganic carbon concentration in the environment increases, a condition that drives global change. As explained previously, the CO_2 accumulation in the ocean leads to its acidification, a process that, in turn, can impact photosynthesis. Using outdoor controlled *Z. marina* cultures, Celebi-Ergin et al. studied their responses to different inorganic carbon concentrations ranging from 55 to 2,121 µM. The data reveal a dynamic regulatory mechanism coupling i) energy capture capacity by pigments, ii) dissipation of the excess of absorbed energy through non-radiative energy dissipation mechanisms, typically non-photochemical quenching processes, and iii) photorespiration activity. Altogether, these three components of the photosynthetic machinery allow *Z. marina* to acclimate to the changing availability of inorganic carbon in the ocean. For their part, Liao et al. investigated how the freshwater aquatic plant *O. ovalifolia*, with two types of leaves uses CO_2-concentrating mechanisms to optimize the uptake of inorganic carbon. At least two levels of adaptation were established. The first one concerns the morphological level with submerged leaves. Actually, submerged leaves are characterized by a larger specific surface area than floating leaves, so submerged leaves can better absorb dissolved inorganic carbon. The second level of adaptation relies on the involved carbon fixation cycle. In floating leaves, inorganic carbon is fixed directly on ribulose bisphosphate by ribulose-1,5-bisphosphate carboxylase oxygenase in the Calvin–Benson–Bassham cycle (C_3 metabolism), whereas in submerged leaves, inorganic carbon is pre-fixed on phospho*enol*pyruvate in the Hatch and Slack cycle (C_4 metabolism). This difference, together with an activation of the external carbonic anhydrases, allows an optimized supply of dissolved inorganic carbon to the submerged leaves.

Global change is leading to an additional shortage of various natural resources, including water and fertilizers, which have already become scarce due to the growing populations and shrinking arable lands. To slow down this shortage, recycling processes need to be introduced, especially for wastewater, including that from aquaculture, which is enriched with organic nutrients. Recycling wastewater to produce biomass is interesting in the context of a circular economy. The paper presented by Villanova et al. fits into this framework. Three microalgae were tested for their ability to remove nitrogen and phosphate from the recirculating marine aquaculture wastewater to produce high-quality biomass. As expected, wastewater supported high biomass production, and its enrichment with valuable compounds only occurred when the biomass was stressed (e.g., Sayanova et al., 2017). Interestingly, using this two-step process, the biomass of all tested strains was rich in proteins, polyunsaturated fatty acids (PUFAs), and carotenoids.

The contributions to this thematic Research Topic clearly confirm that global change is already affecting all living organisms, even the smallest ones. Despite the continuous accumulation of data, it is still difficult to determine exactly what will happen to each of them and how communities and ecosystems will change. Many aspects of these transformations remain to be studied, described, and, above all, understood. Multidisciplinary approaches are needed to achieve these goals. This information may also be of interest for the development of new biotechnological approaches and/or the improvement of current processes to make them more environmentally sustainable.

Author contributions

JM: Writing – review & editing. BS: Writing – review & editing, Writing – original draft.

Conflict of interest

The authors declare that the research was conducted in the absence of any commercial or financial relationships that could be construed as a potential conflict of interest.

The author(s) declared that they were an editorial board member of Frontiers, at the time of submission. This had no impact on the peer review process and the final decision.

Publisher's note

References

Anderson, D. M., Glibert, P. M., and Burkholder, J. M. (2002). Harmful algal blooms and eutrophication: Nutrient sources, composition, and consequences. *Estuaries* 25, 704–726. doi: 10.1007/BF02804901

Benoiston, A.-S., Ibarbalz, F. M., Bittner, L., Guidi, L., Jahn, O., Dutkiewicz, S., et al. (2017). The evolution of diatoms and their biogeochemical functions. *Philos. Trans. R. Soc. B: Biol. Sci.* 372, 20160397. doi: 10.1098/rstb.2016.0397

Falkowski, P. G., and Raven, J. A. (2013). *Aquatic photosynthesis* (Princeton, NY, USA: Princeton University Press).

Fautin, D. G., and Buddemeier, R. W. (2004). Adaptive bleaching: a general phenomenon. *Hydrobiologia* 530, 459–467.

Feely, R. A., Doney, S. C., and Cooley, S. R. (2009). Ocean acidification: Present conditions and future changes in a high-CO_2 world. *Oceanography* 22, 36–47. doi: 10.5670/oceanog.2009.95

Gao, K., Beardall, J., Häder, D.-P., Hall-Spencer, J. M., Gao, G., and Hutchins, D. A. (2019). Effects of ocean acidification on marine photosynthetic organisms under the concurrent influences of warming, UV radiation, and deoxygenation. *Front. Mar. Sci.* 6, 322. doi: 10.3389/fmars.2019.00322

Gobler, C. J., Hattenrath-Lehmann, T. K., Doherty, O. M., Griffith, A. W., Kang, Y., Litaker, R. W., et al. (2017). Reply to Dees: Ocean warming promotes species-specific increases in the cellular growth rates of harmful algal blooms. *Proc. Natl. Acad. Sci.* 114, E9765–E9766. doi: 10.1073/pnas.1715749114

Guiry, M. D. (2024). How many species of algae are there? A reprise. Four kingdoms, 14 phyla, 63 classes and still growing. *J. Phycology* 60, 214–228. doi: 10.1111/jpy.13431

Hao, B., Roejkjaer, A. F., Wu, H., Cao, Y., Jeppesen, E., and Li, W. (2018). Responses of primary producers in shallow lakes to elevated temperature: a mesocosm experiment during the growing season of Potamogeton crispus. *Aquat. Sci.* 80, 34. doi: 10.1007/s00027-018-0585-0

Hao, B., Wu, H., Cao, Y., Xing, W., Jeppesen, E., and Li, W. (2017). Comparison of periphyton communities on natural and artificial macrophytes with contrasting morphological structures. *Freshw. Biol.* 62, 1783–1793. doi: 10.1111/fwb.2017.62.issue-10

Jiang, H., Gao, K., and Helbling, E. W. (2007). Effects of solar UV radiation on germination of conchospores and morphogenesis of sporelings in *Porphyra haitanensis* (Rhodophyta). *Mar. Biol.* 151, 1751–1759. doi: 10.1007/s00227-007-0632-1

Jin, P., Ding, J., Xing, T., Riebesell, U., and Gao, K. (2017). High levels of solar radiation offset impacts of ocean acidification on *Emiliania huxleyi*, with special reference to calcifying and non-calcifying strains. *Mar. Ecol. Prog. Ser.* 568, 47–58. doi: 10.3354/meps12042

Kodama, Y., and Sumita, H. (2022). The ciliate *Paramecium bursaria* allows budding of symbiotic *Chlorella variabilis* cells singly from the digestive vacuole membrane into the cytoplasm during algal reinfection. *Protoplasma* 259, 117–125. doi: 10.1007/s00709-021-01645-x

Majewska, R., Robert, K., Van De Vijver, B., and Nel, R. (2020). A new species of *Lucanicum* (Cyclophorales, Bacillariophyta) associated with loggerhead sea turtles from South Africa. *Bot. Lett.* 167, 7–14. doi: 10.1080/23818107.2019.1691648

Matsuzaki, S. S., Suzuki, K., Kadoya, T., Nakagawa, M., and Takamura, N. (2018). Bottom-up linkages between primary production, zooplankton, and fish in a shallow, hypereutrophic lake. *Ecology* 99, 2025–2036. doi: 10.1002/ecy.2018.99.issue-9

Millan, F., Izere, C., Breton, V., Voldoire, O., Biron, D. G., Wetzel, C. E., et al. (2020). The effect of natural radioactivity on diatom communities in mineral springs. *Bot. Lett.* 167, 95–113. doi: 10.1080/23818107.2019.1691051

Morin, S., Peeters, V., and Schoefs, B. (2025). From traditional taxonomy to the inclusion of web applications to improve diatom-based ecosystem's health assessment. *Bot. Letters.* 172. doi: 10.1080/23818107.2024.2446810

Procházková, L., Remias, D., Suzuki, H., Kociánová, M., and Nedbalová, L. (2024). *Chloromonas rubrosalmonea* sp. nov. (Chlorophyta) causes blooms of salmon-red snow due to high astaxanthin and low chlorophyll content. *Bot. Lett.* 172, 1–19. doi: 10.1080/23818107.2023.2301608

Sayanova, O., Mimouni, V., Ulmann, L., Morant-Manceau, A., Pasquet, V., Schoefs, B., et al. (2017). Modulation of lipid biosynthesis by stress in diatoms. *Philos. Trans. R. Soc. B: Biol. Sci.* 372, 20160407. doi: 10.1098/rstb.2016.0407

Schoefs, B., Hu, H., and Kroth, P. G. (2017). The peculiar carbon metabolism in diatoms. *Philos. Trans. R. Soc. B: Biol. Sci.* 372, 20160405. doi: 10.1098/rstb.2016.0405

Schoefs, B., Van De Vijver, B., Wetzel, C., and Ector, L. (2020). From diatom species identification to ecological and biotechnological applications. *Bot. Lett.* 167, 2–6. doi: 10.1080/23818107.2020.1719883

Smith, T., Manoylov, K., and Packard, A. (2013). Algal extremophile community persistence from Hot Springs National Park (Arkansas, U.S.A.). *Int. J. Algae* 13, 65–76. doi: 10.1615/InterJAlgae.v15.i1.50

Sutherland, J. E., Lindstrom, S. C., Nelson, W. A., Brodie, J., Lynch, M. D. J., Hwang, M. S., et al. (2011). A new look at an ancient order: Generic revision of the Bangiales (Rhodophyta). *J. Phycology* 47, 1131–1151. doi: 10.1111/j.1529-8817.2011.01052.x

Viñegla, B., Segovia, M., and Figueroa, F. L. (2006). Effect of artificial UV radiation on carbon and nitrogen metabolism in the macroalgae *Fucus spiralis* L. and *Ulva olivascens* Dangeard. *Hydrobiologia* 560, 31–42. doi: 10.1007/s10750-005-1097-1

Wu, H., Hao, B., Cai, Y., Liu, G., and Xing, W. (2021). Effects of submerged vegetation on sediment nitrogen-cycling bacterial communities in Honghu Lake (China). *Sci. Total Environ.* 755, 142541. doi: 10.1016/j.scitotenv.2020.142541

Xu, J., and Gao, K. (2010). UV-A enhanced growth and UV-B induced positive effects in the recovery of photochemical yield in *Gracilaria lemaneiformis* (Rhodophyta). *J. Photochem. Photobiol. B-Biology* 100, 117–122. doi: 10.1016/j.jphotobiol.2010.05.010

Zhang, D., Xu, J., Bao, M., Yan, D., Beer, S., Beardall, J., et al. (2020). Elevated CO_2 concentration alleviates UVR-induced inhibition of photosynthetic light reactions and growth in an intertidal red macroalga. *J. Photochem. Photobiol. B: Biol.* 213, 112074. doi: 10.1016/j.jphotobiol.2020.112074

Zoppi, M., Falasco, E., Schoefs, B., and Bona, F. (2024). "Turning waste into resources: A comprehensive review on the valorisation of Elodea nuttallii biomass." *J. Environ. Manag.* 369, 122258.

frontiers in Plant Science

ORIGINAL RESEARCH
published: 17 November 2020
doi: 10.3389/fpls.2020.585202

Ocean Acidification and Warming Lead to Increased Growth and Altered Chloroplast Morphology in the Thermo-Tolerant Alga *Symbiochlorum hainanensis*

*Sanqiang Gong[1,2,3], Xuejie Jin[2,3], Yilin Xiao[1] and Zhiyong Li[1]**

[1] Marine Biotechnology Laboratory, State Key Laboratory of Microbial Metabolism and School of Life Sciences and Biotechnology, Shanghai Jiao Tong University, Shanghai, China, [2] Key Laboratory of Tropical Marine Bio-Resources and Ecology, Guangdong Provincial Key Laboratory of Applied Marine Biology, South China Sea Institute of Oceanology, Chinese Academy of Sciences, Guangzhou, China, [3] Southern Marine Science and Engineering Guangdong Laboratory, Guangzhou, China

Ocean acidification and warming affect the growth and predominance of algae. However, the effects of ocean acidification and warming on the growth and gene transcription of thermo-tolerant algae are poorly understood. Here we determined the effects of elevated temperature (H) and acidification (A) on a recently discovered coral-associated thermo-tolerant alga *Symbiochlorum hainanensis* by culturing it under two temperature settings (26.0 and 32.0°C) crossed with two pH levels (8.16 and 7.81). The results showed that the growth of *S. hainanensis* was positively affected by H, A, and the combined treatment (AH). However, no superimposition effect of H and A on the growth of *S. hainanensis* was observed under AH. The analysis of chlorophyll fluorescence, pigment content, and subcellular morphology indicated that the chloroplast morphogenesis (enlargement) along with the increase of chlorophyll fluorescence and pigment content of *S. hainanensis* might be a universal mechanism for promoting the growth of *S. hainanensis*. Transcriptomic profiles revealed the effect of elevated temperature on the response of *S. hainanensis* to acidification involved in the down-regulation of photosynthesis- and carbohydrate metabolism-related genes but not the up-regulation of genes related to antioxidant and ubiquitination processes. Overall, this study firstly reports the growth, morphology, and molecular response of the thermo-tolerant alga *S. hainanensis* to future climate changes, suggesting the predominance of S. *hainanensis* in its associated corals and/or coral reefs in the future.

Keywords: acidification, warming, thermophilic, *Symbiochlorum hainanensis*, coral reef algae

OPEN ACCESS

Edited by:
Peter J. Lammers, Arizona State University, United States

Reviewed by:
Justin Findinier, Carnegie Institution for Science, United States
Ansgar Gruber, Academy of Sciences of the Czech Republic (ASCR), Czechia

***Correspondence:**
Zhiyong Li
zyli@sjtu.edu.cn

Specialty section:
This article was submitted to Marine and Freshwater Plants, a section of the journal Frontiers in Plant Science

Received: *27 July 2020*
Accepted: *21 October 2020*
Published: *17 November 2020*

Citation:
Gong S, Jin X, Xiao Y and Li Z (2020) Ocean Acidification and Warming Lead to Increased Growth and Altered Chloroplast Morphology in the Thermo-Tolerant Alga Symbiochlorum hainanensis. Front. Plant Sci. 11:585202. doi: 10.3389/fpls.2020.585202

INTRODUCTION

Ocean acidification and warming have led to shifts in seawater chemistry and carbonate saturation, which will potentially affect the physiology, behavior, and predominance of a range of organisms in marine ecosystems (Hoegh–Guldberg and Bruno, 2010). In recent decades, the mean pH value of surface seawater has declined by an average of 0.1 units, owing to the uptake of CO_2

(Feely et al., 2009). Further decreases of 0.3–0.5 pH units and warming of 1–7°C are projected to occur by the end of this century (Feely et al., 2009; IPCC, 2014).

As primary producers, marine photosynthetic algae account for approximately half of global photosynthetic carbon fixation (Falkowski and Raven, 2013). Increasing evidence shows that ocean acidification influences the growth and/or gene transcription of algae, and the responses of algae to acidification are modulated by temperature, light, UV, and nutrient availability (Gao and Campbell, 2014; Gao et al., 2017; Boyd et al., 2018). For example, acidification may enhance the N_2 fixation activity of cyanobacteria, but trace metal availability may neutralize or even reverse this effect (Zhang et al., 2019). Elevated CO_2 enhances the growth of diatoms at low levels of sunlight but inhibits their growth at high levels (Gao et al., 2019). For most calcifying macroalgae, acidification under elevated solar UV and/or elevated temperature reduces their calcification (Jin et al., 2017; Martin and Hall-Spencer, 2017). Non-calcifying macroalgae, on the other hand, appear to benefit from elevated CO_2 and show an enhanced growth rate (Gao et al., 1993; Cornwall et al., 2015, 2017). Furthermore, the geographic distribution and/or predominance of algae are also affected by future ocean acidification and warming conditions (Wernberg et al., 2011). A study of over 20,000 herbarium records of algae collected over 70 years from the Pacific and the Indian oceans around the Australian coast showed that a pole-ward shift of several temperate algal species is already occurring (Wernberg et al., 2011). Acquiring resistant Symbiodiniaceae from the environment or changing the relative abundance of Symbiodiniaceae associated with corals under elevated temperature have been reported (Baker et al., 2004; Fautin and Buddemeier, 2004). One field study provides evidence that acidification can lead to a predominance of macroalgae on reefs (Johnson et al., 2014). Those studies reveal that the response of algae to ocean acidification and warming are species specific, and certain thermophilic and/or stress-tolerant algae might have the ability to acclimate to future global climate changes and become predominant in the future. However, the individual and specifically combined effects of ocean acidification and warming on the growth and gene transcription of the thermophilic and/or stress-tolerant algae in the ocean remain poorly understood.

Symbiochlorum hainanensis, a recently discovered unicellular alga affiliated with Ulvophyceae, is widely associated with corals in the tropical coral reef areas of the South China Sea (SCS), where the annual average temperature is approximately 26°C (Gong et al., 2018, 2019). The optimal growth temperature of this alga is approximately 32°C (**Supplementary Figure 1**), which is higher than that of coral-symbiotic *Cladocopium* spp. (dominant Symbiodiniaceae associated with corals in the SCS; **Supplementary Figure 2**). Besides that, *S. hainanensis* can maintain rapid growth when it is cultured at 35°C (**Supplementary Figure 1**). Hence, *S. hainanensis* is a thermo-tolerant alga, and we propose that it may outcompete *Cladocopium* spp. and be the predominant species in coral–algae symbiont areas and/or coral reef areas in the future. However, how it will respond to future ocean acidification and warming conditions is unclear. Therefore, the present study performed a 28-day lab-scale experiment in which *S. hainanensis* was cultured under two temperature settings (∼26.0°C, $n = 3$ and ∼32.0°C, $n = 3$) crossed with two pH levels (∼8.16, $n = 3$ and ∼7.81, $n = 3$) to mainly explore the growth and the molecular-level response of *S. hainanensis* to the individual and combined effects of future ocean acidification and warming conditions.

MATERIALS AND METHODS

Cultures and Experimental Setup

Cultures of *S. hainanensis* (CCTCC M2018096), isolated from coral species *Porites lutea* in the tropical reef regions of the SCS (Gong et al., 2018, 2019), were incubated in 250-ml Erlenmeyer flasks with 100 ml autoclaved artificial seawater medium (Formula grade A Reef Sea Salt, Formula, Japan) under an *in situ* temperature of 26°C, light intensity of 90 μmol photon m^{-2} s^{-1} with a 12-h/12-h light/dark cycle. The cultures were shaken at least three times a day. Cells in the mid-exponential phase were collected by centrifugation (5,000 rpm for 10 min) and washed three times with sterile phosphate-buffered saline. Then, cell pellets were re-suspended in autoclaved artificial seawater medium and used for further experiments.

Cultures of *S. hainanensis* were acclimated to four conditions: (1) pCO_2 level 1,000 μatm (pH = 7.81), 26°C (A, $n = 3$), (2) pCO_2 level 395 μatm (pH = 8.16), 32°C (H, $n = 3$), (3) pCO_2 level 1,000 μatm (pH = 7.81), 32°C (AH, $n = 3$), and (4) pCO_2 level 395 μatm (pH = 8.16), 26°C (C, $n = 3$). To achieve the different pCO_2/pH conditions, 1,000-ml Erlenmeyer flasks with 500 ml autoclaved artificial seawater medium were bubbled with sterilized air containing either ambient (395 μatm, pH = 8.16) or elevated (1,000 μatm, pH = 7.81, **Supplementary Figure 3**) CO_2 concentrations using outdoor air and CO_2 chambers (HP1000G-D, China). To achieve the different temperature conditions, the Erlenmeyer flasks were incubated in water baths (26 or 32°C, **Supplementary Figure 4**). For each treatment, triplicate cultures were incubated under cool white fluorescent light intensity of 90 μmol photons m^{-2} s^{-1}.

Cell Growth and Morphology Observation

The cell concentration of *S. hainanensis* under the A ($n = 3$), H ($n = 3$), AH ($n = 3$), and C ($n = 3$) conditions was monitored every 2 days by optical density (OD) value at 750 nm with a UV spectrophotometer (UV-7504, China) at 750 nm. The growth rate was calculated based on the cell concentration variations of *S. hainanensis* at exponential phase (day 2 to day 24). The dry cell weight in the mid-exponential phase under the A ($n = 3$), H ($n = 3$), AH ($n = 3$), and C ($n = 3$) conditions was measured by filtering the algal suspension through a pre-dried and pre-weighted 0.45-μm cellulose nitrate membrane filter (Whatman, United States) and drying in an oven at 80°C for 24 h.

Chlorophyll fluorescence of *S. hainanensis* under the A ($n = 3$), H ($n = 3$), AH ($n = 3$), and C ($n = 3$) conditions was measured using a Turner fluorometer with the *in vivo* module (Trilogy, Turner Design, Sunnyvale, CA, United States). Algal cells in the mid-exponential phase under the A ($n = 3$), H ($n = 3$), AH

(n = 3), and C (n = 3) conditions were sampled for chlorophyll *a*, chlorophyll b, and total carotenoids measurements according to the acetone-based method (Dere et al., 1998).

Cells of *S. hainanensis* in the mid-exponential phase under different conditions (A, H, AH, and C) were determined based on scanning electron and transmission electron microscopy observations according to our previous study (Gong et al., 2018).

RNA Extraction, Purification, and Sequencing

Algal cells under the A (n = 3), H (n = 3), AH (n = 3), and C (n = 3) conditions were harvested in the mid-exponential phase by centrifugation at 5,000 rpm for 5 min at 4°C for total RNA extraction and RNA-seq. In detail, cell pellets under different conditions were snap-frozen in liquid nitrogen and stored at −80°C before RNA extraction. Total RNA was extracted from algal cells as previously described (Rosic and Hoegh–Guldberg, 2010). The RNA quantity and integrity were analyzed using a NanoDrop ND-1000 spectrometer (Wilmington, DE, United States) and an Agilent 2100 Bioanalyzer (Santa Clara, CA, United States). RNA samples with high purity (OD260/280 between 1.8 and 2.2) and high integrity (RNA integrity number > 8) were used for cDNA library construction. The size and the concentration of the cDNA libraries were determined by the Agilent 2100 Bioanalyzer (Santa Clara, CA, United States). All cDNA libraries were layered on a separate Illumina flow cell and sequenced using Illumina HiSeq 2000 (Illumina, Inc.). The raw sequence data produced in this study were deposited in the Sequence Read Archive (PRJNA662215) at the National Center for Biotechnology Information (NCBI).

Quality Control and Short Read Assembly

Raw RNA-Seq reads under the A (n = 3), H (n = 3), AH (n = 3), and C (n = 3) conditions were processed using Trimmomatic v0.33 for trimming adapters as well as low-quality bases from the ends of the reads (Bolger et al., 2014). Poor-quality reads with average Phred quality score <20 and reads with lengths <55 were filtered out. The resulting set of good quality reads was then assembled with Trinity v2.1.1 software using default parameters (Grabherr et al., 2011; Haas et al., 2013). The assembly validation was performed using Bowtie2 aligner, where the filtered reads were mapped back to the assembled unigenes. Furthermore, non-redundant unigenes were retrieved with the aid of CD-HIT-EST software[1] that clustered the unigenes with an identity parameter of 95%.

Functional Annotation and Identification of Differentially Transcribed Genes

The *de novo*-assembled unigenes were searched against NCBI's non-redundant protein and Swiss-Prot database using the BLASTX algorithm with an *e*-value cutoff of 10^{-5}. Unigenes with significant matches were annotated using the Blast2GO platform (Conesa et al., 2005). Additional annotations were obtained through the Kyoto Encyclopedia of Genes and Genomes (KEGG) database through the KEGG Automatic Annotation Server (v1.6a) (Moriya et al., 2007). The cluster in the eggNOG database was employed to classify and group the putative and definitively identified proteins. The expression quantity of each unigene (fragments per kilobase of exon model per million mapped fragments) was estimated using RSEM (Li and Dewey, 2011). Differentially transcribed genes were selected using edge R as the method of choice (Robinson et al., 2010). Fold change differences were considered significant when a P-value <0.01 was achieved based on Benjamin and Hochberg's false discovery rate procedure. A correlation analysis of differentially transcribed genes among different conditions was performed using the program package in the R software package (R 3.1.2). Bray–Curtis dissimilarity-based principal coordinate analysis (PCoA) pictures of differentially transcribed genes were drawn using Primer-e[2] for comparing differentially expressed genes under different conditions.

Quantitative Polymerase Chain Reaction

To validate the RNA-seq results, the expression level of 17 differentially transcribed genes under the A (n = 3), H (n = 3), AH (n = 3), and C (n = 3) conditions was measured using quantitative PCR (qPCR). The list of genes and primers is available in the electronic **Supplementary Material** (**Supplementary Table 1**). Complementary DNA was synthesized from 1 μg of total RNA, and qPCR was performed with an ABI ViiA 7 Real-Time PCR System (Applied Biosystems, United States) using FAST START SYBR green master mix according to the manufacturer's instructions. The following procedure was used: 95°C for 10 min and one cycle for cDNA denaturation, 95°C for 10 s, 60°C for 20 s, 36 cycles for amplification, and one cycle for melting curve analysis (from 60 to 95°C) to verify the presence of a single product. qPCR was performed in triplicate for each sample. The relative expression levels were measured using Relative Expression Software Tool (REST).

Statistical Analysis

All results are presented in the text as mean ± standard error. Significant differences (P < 0.01) in the OD value, dry cell weight, chlorophyll fluorescence, and pigment content under the A (n = 3), H (n = 3), AH (n = 3), and C (n = 3) conditions were tested by ANOVA using the stats package in R software (R Core Team, 2014). Significant (P < 0.01) differences in the Bray–Curtis distances of differentially transcribed genes under the A (n = 3), H (n = 3), AH (n = 3), and C (n = 3) conditions were determined by permutational multivariate analysis of variance (MANOVA) in Primer-e (see text footnote 2). Significant (P < 0.01) differences in qPCR-measured genes under the A (n = 3), H (n = 3), AH (n = 3), and C (n = 3) conditions were calculated using the pair-wise fixed reallocation randomization test in REST.

[1] http://weizhongli-lab.org/cd-hit/

[2] http://www.primer-e.com/

RESULTS

Growth and Morphological Responses of *S. hainanensis* to H, A, and AH

The cell concentration, as measured by OD_{750} (**Figure 1A**) and cell dry weight (**Figure 1B**) of *S. hainanensis*, was significantly promoted by elevated temperature (H, $n = 3$), acidification (A, $n = 3$), and the combined treatment (AH, $n = 3$) compared with the control (C, $n = 3$; $P < 0.01$). The growth rate of *S. hainanensis* increased 1.05-fold but decreased 1.04-fold in the combined treatment compared with individual elevated temperature (AH-VS-H, $P < 0.01$) and acidification (AH-VS-A, $P < 0.01$), respectively (**Supplementary Figure 5**). In addition, chlorophyll fluorescence (**Figure 1C**) and pigment content (**Figure 1D**) showed similar variation trends with the algal growth of *S. hainanensis* under different conditions.

The features of the cell morphology of *S. hainanensis* under different conditions were documented (**Figure 2**). The cell wall of *S. hainanensis* was furrowed (A2–A4), and the shape of the chloroplast changed (i.e., the volume of chloroplast became larger under acidification and warming conditions; B2–B4). More starch granules under acidification and warming conditions were observed (B2–B4). Moreover, the sporangium of *S. hainanensis* was observed under acidification condition (C1–C4).

Transcriptomic Profiles of *S. hainanensis* Response to H, A, and AH

A total of 12 transcriptomic sequencing libraries were generated for the four conditions (C, H, A, and AH) with three biological replicates. These libraries were sequenced with an Illumina platform with an output of 88.36 G clean reads (an average of 7.36 G reads per sample) (**Supplementary Table 2**). The clean reads were pooled together and assembled into 95,827 unique genes, with an average length of 1,277 bp and a N50 value of 3,768 bp (**Supplementary Table 3**).

The PCoA analysis revealed that the gene transcription of *S. hainanensis* was significantly different under the C, H, A, and AH conditions (**Figure 3**, MANOVA, $P < 0.001$). The PCoA analysis showed the following order of the effect of different conditions on gene transcription: A-VS-C > AH-VS-H > H-VS-C. Among the detected genes, 688 genes were significantly differentially transcribed, and more than half of these genes had unknown functions (**Supplementary File 1**).

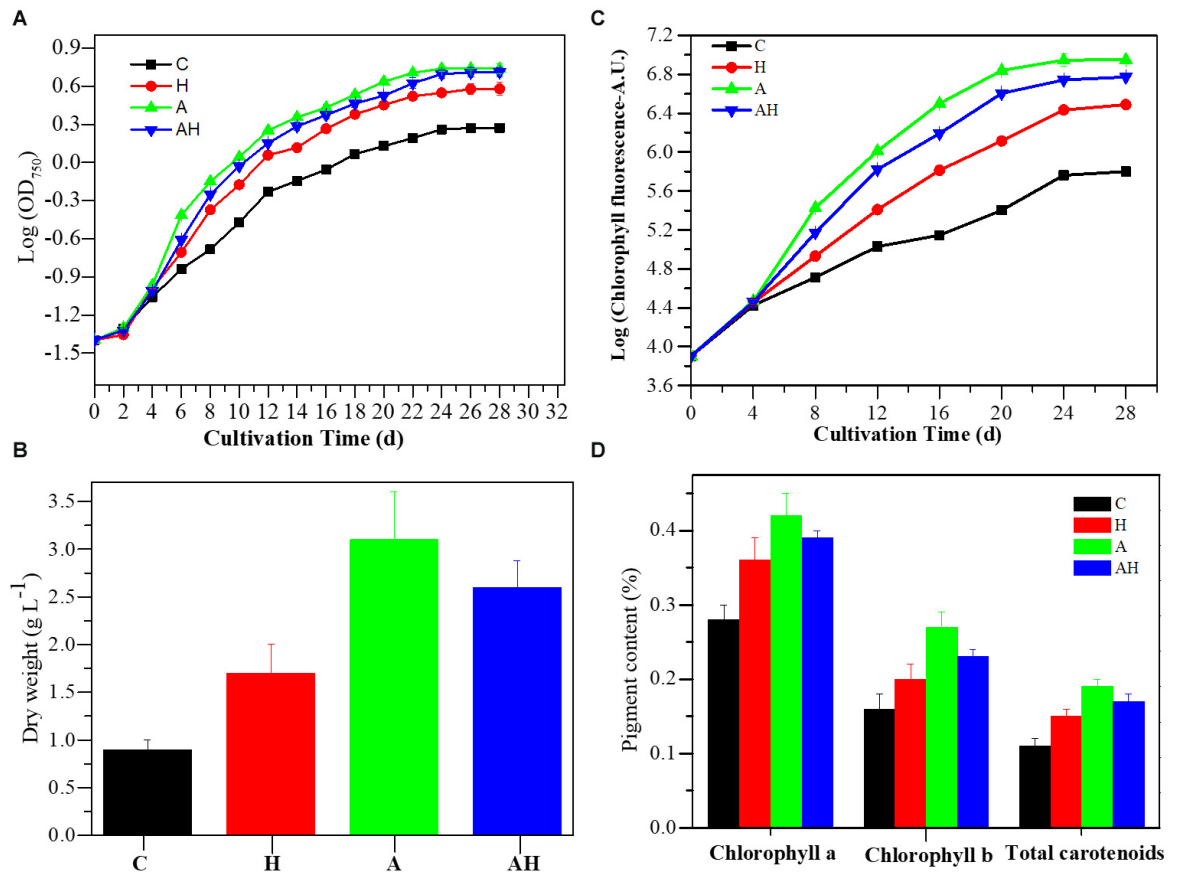

FIGURE 1 | Growth characteristics of *Symbiochlorum hainanensis* in response to acidification and warming conditions. Growth curves **(A)**, cellular dry weight [**(B)** day 20], chlorophyll fluorescence **(C)**, and pigment content [**(D)** day 20] of *S. hainanensis* under the control (*in situ* temperature)—C ($n = 3$), elevated temperature—H ($n = 3$), acidification—A ($n = 3$), and combined treatment—AH ($n = 3$). All results are presented in the text as mean ± standard error.

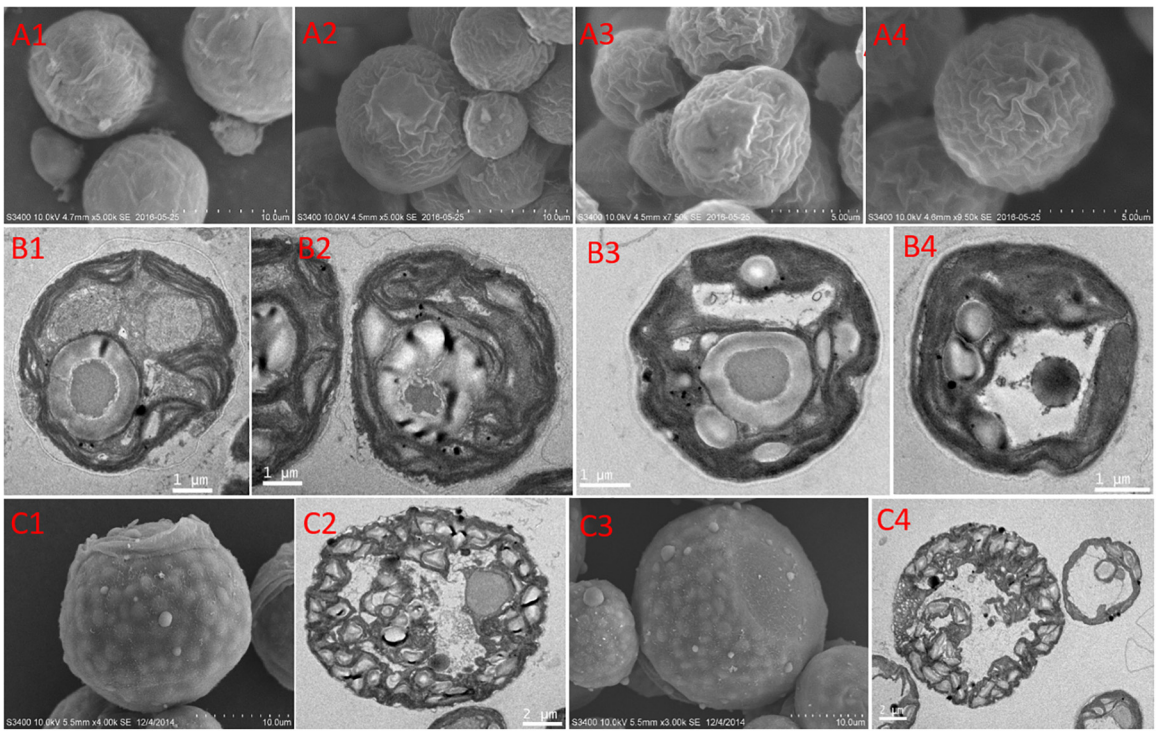

FIGURE 2 | Morphological characteristics of *Symbiochlorum hainanensis* in response to acidification and warming. Scanning electron microscopic presentations of the vegetative cells of *S. hainanensis* under the control **(A1)**, elevated temperature **(A2)**, acidification **(A3)**, and combined treatment **(A4)**. Transmission electron microscopic presentations of vegetative cells of *S. hainanensis* under the control **(B1)**, elevated temperature **(B2)**, acidification **(B3)**, and combined treatment **(B4)**. Scanning and transmission electron microscopic presentations of aplanosporangiums of *S. hainanensis* under acidification conditions **(C1–C4)**.

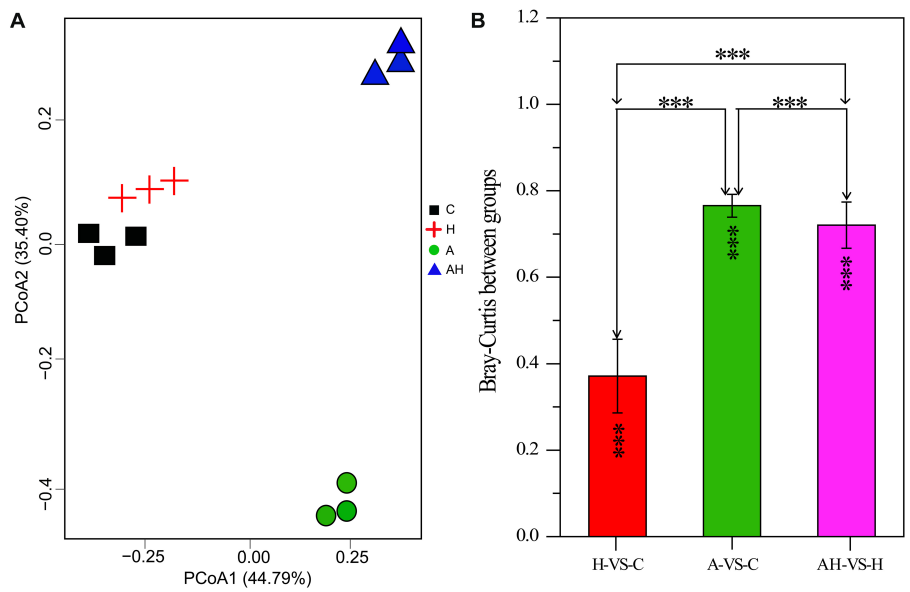

FIGURE 3 | Plots of principal coordinate analysis **(A)** and permutational multivariate analysis of variance analysis **(B)** of differentially transcribed genes under different conditions: control—C (n = 3), elevated temperature—H (n = 3), acidification—A (n = 3), and combined treatment—AH (n = 3). Significant differences ($P < 0.01$) in Bray–Curtis distances of differentially transcribed genes under different conditions were determined using Primer-e. All results are presented in the text as mean ± standard error.

The genes related to photosynthesis, CO_2 biofixation, carbohydrate metabolism, cell cycle and control, nutrient input, transport and metabolism, stress response, and intracellular homeostasis were differentially transcribed under acidification and warming conditions (**Figure 4**). Other genes involved in flagella-related components, extracellular matrix (fasciclin-like protein, glycoprotein of tenascin, and the expansin superfamily of proteins), and transcriptional regulation also changed under different conditions (**Supplementary File 1**).

To validate the RNA-seq results, several key genes were selected for qPCR analysis. The results exhibited the same trends as the results of RNA-seq, confirming the reliability of our present analysis (**Supplementary Table 1**).

Photosynthesis-Related Gene Responses to H, A, and AH

The transcription of genes related to photosynthesis was minimally affected by elevated temperature (H-VS-C) (**Figure 4**), while gene transcription was obviously affected by acidification (A-VS-C) and the combined treatment (AH) (**Figures 4–6**). Specifically, nearly all differentially transcribed genes related to photosynthesis were significantly down-regulated under the combined treatment. For example, the genes of *psaA*, *psaJ*, and *ycf3* involved in photosystem I, *psbB*, *psbC*, *psbE*, *psbH*, *psbP*, and *psbS* involved in photosystem II, *lhcB*, *chlB*, *chlP*, and *chl11* involved in light-harvesting complex (LHC) protein, and *atpA* and *atpB* involved in photosynthetic ATP synthesis were down-regulated more than 1–15-fold by the combined treatment (AH) (**Figures 4**, **6**). In addition, the *lci* and *cah1* genes encoding low CO_2-inducible protein and soluble carbonic anhydrase related to carbon acquisition by CO_2 concentrating mechanism (CCM) were significantly down-regulated more than fourfold by individual acidification and the combined treatment (**Figures 4–6**).

Carbohydrate Metabolism-Related Gene Responses to H, A, and AH

Acidification and elevated temperature had different effects on the genes related to the carbohydrate metabolism of *S. hainanensis* (**Figures 4–6**). Almost all the differentially transcribed genes involved in carbohydrate metabolism were up-regulated by acidification (A-VS-C), while most were minimally affected by elevated temperature and the combined treatment (both H-VS-C and AH-VS-H). Compared with the control (C), individual acidification (A) caused the genes *fba*, *clsa11*, *ugdh3*, *ugdh4*, *man1*, *man5*, *msp130*, *mindh*, and *aox4* related to the citric acid cycle (TCA), cell wall polysaccharide synthesis, and β oxidation of fatty acids to be significantly up-regulated more than threefold. However, the transcription of those genes was down-regulated approximately 1–17-fold by the combined treatment (AH).

Cell and Life Cycle-Related Gene Responses to H, A, and AH

Elevated temperature (H) also had a minimal effect on the transcription of genes involved in the cell and life cycles. However, almost all of these genes were up-regulated by individual acidification (A-VS-C), while most of them were down-regulated by the combined treatment (AH-VS-H) (**Figures 4–6**). Genes encoding DUF724 domain-containing protein and circumsporozoite protein related to sporulation were up-regulated by both individual acidification (A) and the combined treatment (AH). Specifically, the gene encoding DUF724 domain-containing protein was up-regulated approximately 66-fold by individual acidification (A). In addition, the key gene *ftsZ*, which is involved in chloroplast division, was significantly up-regulated by A, H, and AH compared with the control (C).

Nutrient Transport- and Metabolism-Related Gene Responses to H, A, and AH

The transcription of genes related to nutrient transport and metabolism is illustrated in **Figures 4–6**. Genes encoding alkaline phosphatase and ABC-type phosphate transporter involved in phosphate metabolism were up-regulated more than 10-fold, whereas genes encoding NO_3^- transporter and nitrate reductase involved in nitrogen metabolism were down-regulated over threefold under elevated temperature (H-VS-C). Under the combined treatment (AH), genes involved in nitrogen and phosphate metabolism were up-regulated over threefold relative to the acidification treatment (A). In addition, the gene encoding transferrin involved in Fe^{3+} transporter showed a higher transcription under the control (C) and elevated temperature (H) conditions than under the other conditions, and it was significantly down-regulated approximately fivefold by acidification (A) and the combined treatment (AH).

Stress- and Intracellular Homeostasis-Related Gene Responses to H, A, and AH

Genes encoding glutathione S-transferase, catalase isozyme, UvrB/uvrC motif, heat shock 22-kDa protein, and chaperones were differentially transcribed under single acidification (A) or elevated temperature condition (H) (**Figures 4–6**). Specifically, the transcription of these genes was up-regulated more than twofold by the combined treatment (AH) than by individual acidification (A), except for one gene encoding chaperone DnaJ. Moreover, genes related to ubiquitination processes were highly transcribed under different conditions.

DISCUSSION

In this study, we mainly explored the growth, morphology, and molecular level response of *S. hainanensis*, a recently discovered coral-associated thermo-tolerant alga, to future ocean acidification and warming conditions by culturing it under two temperature settings (∼26.0 and ∼32.0°C) crossed with two pH levels (∼8.16 and ∼7.81) in a 28-day lab-scale experiment. We found that this thermo-tolerant alga exhibited a positive growth response to individual acidification, elevated

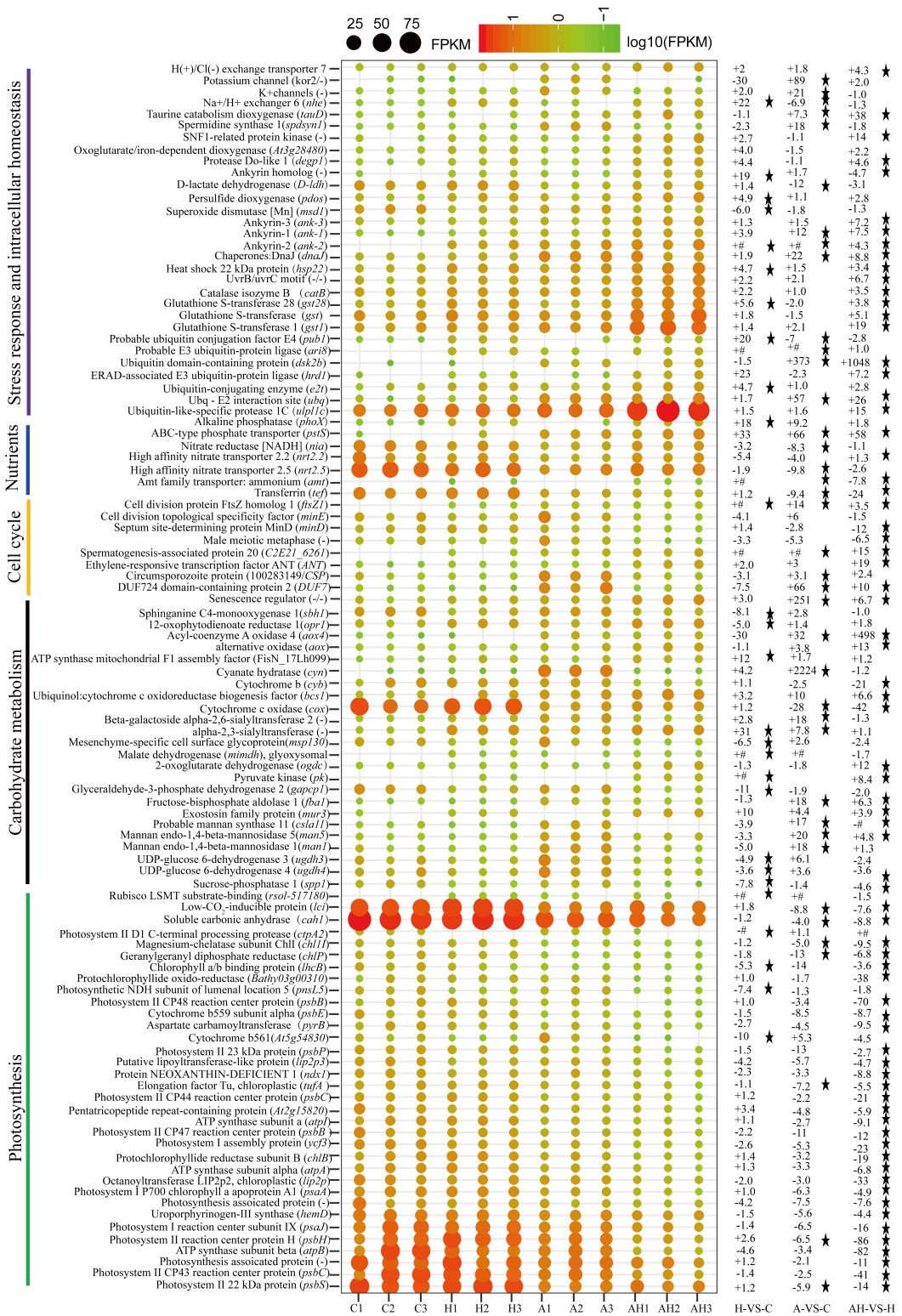

FIGURE 4 | Profiles of differentially transcribed genes involved in key pathways under acidification and warming conditions. The control—C (n = 3), elevated temperature—H (n = 3), acidification—A (n = 3), and combined treatment—AH (n = 3). + signs represents up-regulated genes, – signs represent down-regulated genes, and star represents significantly changed genes under different conditions. All results are presented in the text as mean ± standard error.

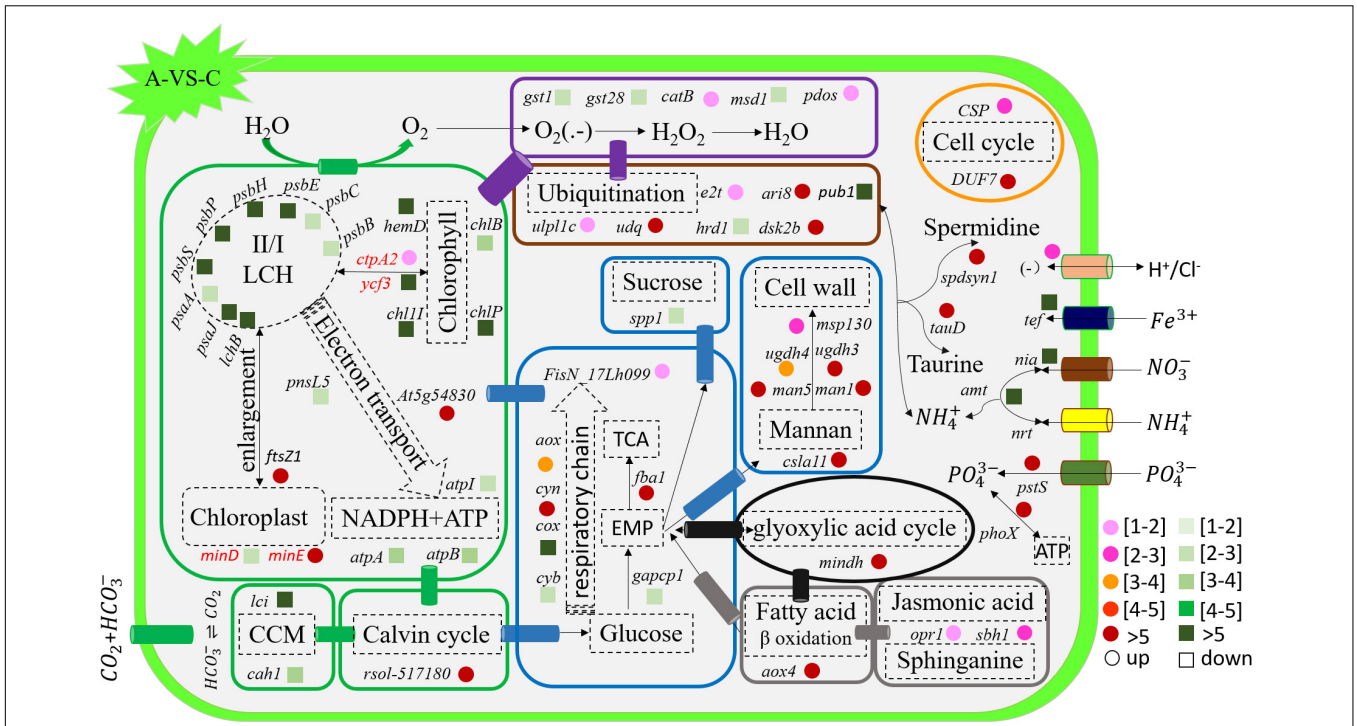

FIGURE 5 | Schematic summary of the gene functions affected by acidification compared with the control (n = 3) of *in situ* temperature (n = 3). All results are presented in the text as mean ± standard error.

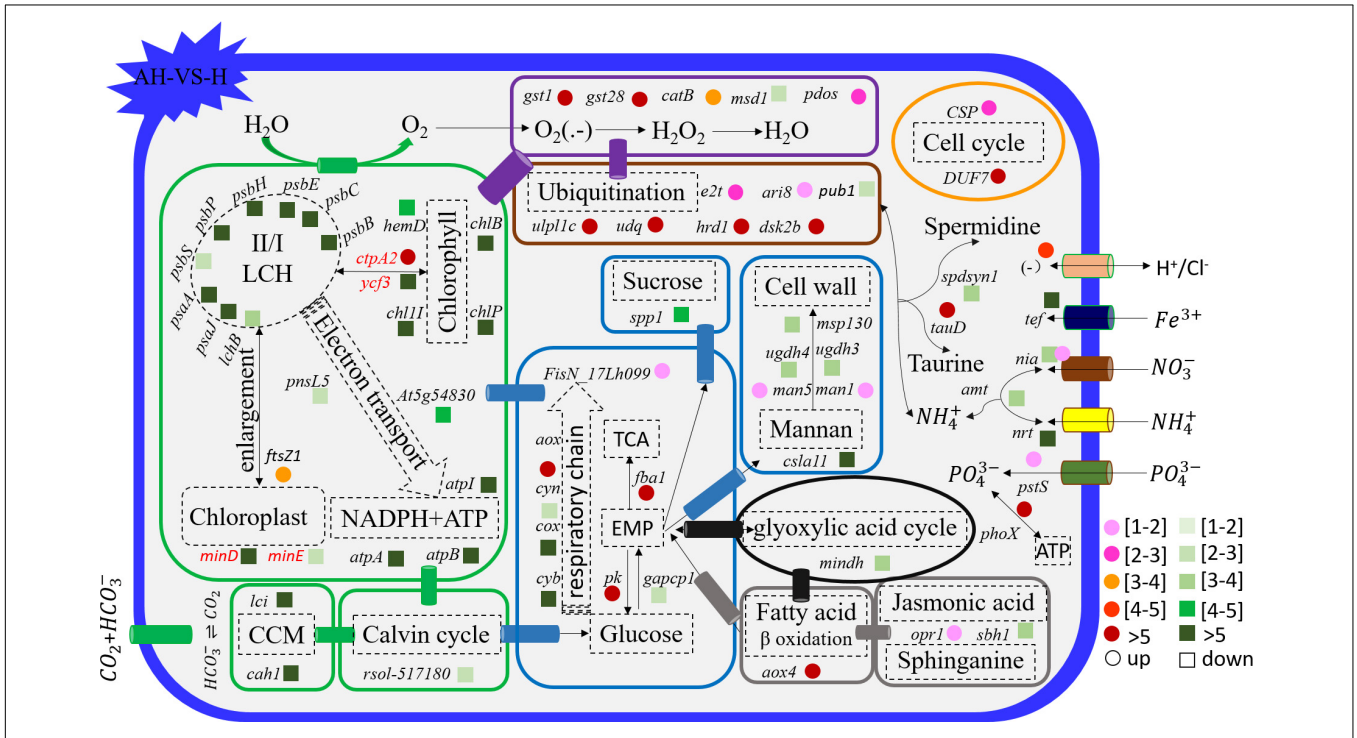

FIGURE 6 | Schematic summary of the gene functions affected by the combined treatment (n = 3) compared with elevated temperature (n = 3). All results are presented in the text as mean ± standard error.

temperature, and the combined treatment. We observed a no-superimposition effect of individual acidification and elevated temperature on the growth of *S. hainanensis* compared with the combined treatment of acidification and elevated temperature. Interestingly, our present data indicated that the chloroplast enlargement (possibly controlled by the *ftsZ* gene) along with the increase of chlorophyll fluorescence and pigment content might be a universal mechanism for the stimulative growth of *S. hainanensis* under ocean acidification and warming conditions, implying the predominance of *S. hainanensis* in its associated corals and/or coral reef areas in the future. This study provides novel insights into the growth, morphology, and molecular-level responses of thermo-tolerant algae to ocean warming and acidification conditions.

The stimulative growth response of *S. hainanensis* to ocean acidification reported in this study is consistent with the previous studies in several species of cyanobacteria, diatoms, and dinoflagellates (Brading et al., 2011; Wu et al., 2014; Walworth et al., 2016; Huang et al., 2018). The enhanced growth may be attributed to more carbon resources and down-regulated CCMs (an efficient process needs energy and resources for CO_2 fixation by algae) caused by the increasing partial pressure of CO_2 (pCO_2) in seawater under acidification (Riebesell et al., 1993; Tortell et al., 2008). Our transcriptomic results also showed that two genes encoding low CO_2-inducible protein (*lci*) and soluble carbonic anhydrase (*cah1*) associated with CCMs were significantly down-regulated by acidification. Although the genes encoding RubisCO for CO_2 fixation were not differentially transcribed in *S. hainanensis* under acidification, one gene encoding RubisCO LSMT was significantly up-regulated. RubisCO LSMT was reported to exhibit methyltransferase activity toward RubisCO (Ying et al., 1999); thus, we propose that the up-regulation of the gene encoding RubisCO LSMT might be involved in the regulation of CO_2 fixation in *S. hainanensis* under acidification. In addition, we observed that acidification enhanced the transcription of genes related to cell activity and growth (i.e., sucrose and cell wall polysaccharide synthesis, EMP, TCA, glyoxylic acid cycle, β-oxidation of fatty acid, and cyanide-resistant respiration), which might contribute to the enhanced growth of *S. hainanensis* as well. Similar results were also reported in higher plants under elevated CO_2 or stresses (Solomos, 1977; Li et al., 2008). Notably, our results showed that almost all genes involved in photosynthesis (i.e., *psbB-psbS* of photosynthetic II, *psaA* and *psaJ* of photosynthetic I, and *lchB* of LHC) were down-regulated by acidification. According to one previous study of diatom (Goldman et al., 2017), a likely reason for the variability in the response of *S. hainanensis* (excluding potential modulation by other environmental factors, i.e., temperature) to acidification is that the increasing pCO_2 (carbon resource) and the concomitantly decreasing pH (acidification) separately have different effects on the growth and photosynthesis. Interestingly, we observed that the chlorophyll fluorescence and pigment content of *S. hainanensis* significantly increased under acidification. Concomitantly, enlargement of chloroplast and significant up-regulation of one key gene *ftsZ* (encoding cell division protein homolog 1) for controlling chloroplast division and/or morphogenesis (Strepp et al., 1998; Wang et al., 2002) were observed under acidification in *S. hainanensis*. Therefore, we speculated that the significant up-regulation of *ftsZ* gene might contribute to the enlargement of chloroplast and the enhancement of chlorophyll fluorescence and pigment content of *S. hainanensis* under acidification.

The present results showed that the growth of *S. hainanensis* was greatly promoted by an elevated temperature of 32°C. To our knowledge, this was the first report of a positive response of marine algae to an elevated temperature up to 32°C. A previous study suggested that marine algae may exhibit much lower optimal growth temperature than tropical seagrasses and macroalgae which showed optimal growth temperature ranging from 27 to 33°C (Koch et al., 2013). Biber (2007) reported that the biomass of Florida algae significantly decreased when the temperatures were above 31°C. Fleshy, branching tropical macroalgae species maintain relatively consistent net productivity rates at 32°C (Mejia et al., 2012). The photosynthesis of the tropical *Codium edule* (macroalgae) was disrupted and inhibited at 32 and 35°C, respectively (Lee and Hsu, 2010). Even for the generally considered thermo-tolerant Symbiodiniaceae (*Durusdinium* spp.) associated with corals, both net growth and negative effect of photosynthesis at 32°C were reported (Karim et al., 2015). Notably, our results showed that *S. hainanensis* isolated from tropical reefs in the South China Sea exhibited a high optimal growth temperature of 32°C, which was higher than those of previously reported algal species. In reality, *S. hainanensis* could maintain a rapid growth even when it was cultured at 35°C. The transcriptomic results showed that, in addition to up-regulating genes involved in protein folding, oxidative stress, and ubiquitination processes, elevated temperature had a minimal effect on the transcription of genes involved in the basic metabolism of *S. hainanensis*, such as photosynthesis, carbohydrate metabolism, the cell cycle, and nutrient metabolism. As what previous studies have suggested for other organisms (Kumar et al., 2017; Ruocco et al., 2017), the up-regulation of genes related to protein folding (i.e., heat shock protein and chaperone) might contribute to the thermal acclimation of *S. hainanensis*. It is widely believed that the production of reactive oxygen species increases under elevated temperatures or other stresses, and plants/algae must activate their antioxidant defense mechanisms to protect themselves from oxidative damage (Ledford and Niyogi, 2005; Lazaro et al., 2016). Similarly, genes encoding glutathione S-transferase, catalase, and persulfide dioxygenase related to antioxidant defense mechanisms were up-regulated in *S. hainanensis*. The ubiquitination processes may also have aided in the ability of this alga to acclimate to high temperatures given the up-regulation in the transcription of the respective genes, such as up-regulating genes encoding ubiquitin ligase (over 23-fold) (Mayfield et al., 2014). In addition, the increase of chlorophyll fluorescence and pigment content, the enlargement of chloroplast, and the significant up-regulation of *ftsZ* gene encoding cell division protein homolog 1 were also observed under elevated temperature in *S. hainanensis*, which might also contribute to the enhanced growth of *S. hainanensis* under elevated temperature.

Laboratory studies have shown that the effects of the combined treatment of elevated temperature and acidification on the growth of marine algae are species specific (Hyun et al., 2014; Gao et al., 2019). For example, the growth of the picoplanktonic cyanobacterium *Synechococcus* was promoted by the combined treatment, whereas elevated temperature and acidification had no effects on *Prochlorococcus* (Fu et al., 2007). Similarly, the combined treatment promoted the growth of the diatom *Skeletonema* (Kremp et al., 2012), but it had no obvious effects on *Thalassiosira* and *Chaetoceros* (Hyun et al., 2014). The growth of coccolithophore *E. huxleyi* was inhibited by the combined treatment (Listmann et al., 2016). Our present results indicated that the combination of elevated temperature and acidification (AH) had a positive effect on the growth of *S. hainanensis* (AH-VS-C). Meanwhile, we observed no superimposition effect on the growth of *S. hainanensis* in response to acidification and elevated temperature alone, compared to the combined treatment.

For transcriptional profiles, the effects of individual acidification and warming conditions on the response of marine algae and terrestrial plant have been widely reported (Li et al., 2008; Kumar et al., 2017; Ruocco et al., 2017). To our knowledge, however, data on the effect of the combined treatment of elevated temperature and acidification (AH) on marine algae have not been reported, and we do not know the mechanisms involved. Differently from the no-superimposition effect in the growth of *S. hainanensis*, a superimposition effect of the individual elevated temperature (H) and acidification (A) on the gene transcription of *S. hainanensis* was observed under combined treatment (AH). Meanwhile, our present transcriptomic data revealed a balanced strategy used by *S. hainanensis* for maintaining moderate growth under the combined treatment of elevated temperature and acidification (AH). For example, the transcription of genes related to photosynthesis, CO_2 biofixation, and carbohydrate metabolism was inhibited, but genes related to antioxidant and ubiquitination processes were promoted under combined treatment (AH) compared with individual elevated temperature (H) and acidification (A).

CONCLUSION

This study mainly describes the growth, morphology, and molecular response of *S. hainanensis*, a recently discovered coral-associated thermo-tolerant alga, to future ocean acidification and warming conditions. The promoted growth of *S. hainanensis* under these conditions suggests the strong acclimation of this alga to future ocean environmental changes. An antagonistic effect on the growth of *S. hainanensis* was observed between elevated temperature and acidification, which are involved in the balance of gene transcription related to basic metabolism and stress responses. The present data revealed that chloroplast morphogenesis (possibly controlled by *ftsZ* gene) along with increasing chlorophyll fluorescence and pigment content might serve as a universal mechanism for promoting the growth of this alga under both acidification and warming conditions. This alga is also ecologically important because it is highly abundant in corals in the SCS, and the optimum growth temperature of 32°C for *S. hainanensis* isolated from bleached corals in the SCS is higher than those of the symbiotic *Cladocopium* spp. and *Durusdinium* spp. (thermal-sensitive and thermal-tolerant Symbiodiniaceae majorly associated with corals in the SCS). The present study provides novel and valuable data on the growth of *S. hainanensis* and improves the knowledge of the molecular functions underpinning the growth response of thermo-tolerant algae to future ocean acidification and warming. This study also lays a foundation for a further evaluation of the distribution and the ecological significance of *S. hainanensis* in coral–algae symbionts and/or coral reef areas.

DATA AVAILABILITY STATEMENT

The datasets presented in this study can be found in online repositories. The names of the repository/repositories and accession number(s) can be found in the article/**Supplementary Material**.

AUTHOR CONTRIBUTIONS

SG and ZL conceived and designed the experiments. SG and YX performed the cultivation experiment and sampling. SG performed the molecular and bioinformatic analyses. SG, XJ, and ZL wrote the manuscript. All the authors read and approved the final manuscript.

FUNDING

This work was funded by the Major National Scientific Research Project, China (2013CB956103) and the National Natural Science Foundation of China (41906135). This work was supported by the Key Special Project for Introduced Talents Team of Southern Marine Science and Engineering Guangdong Laboratory (Guangzhou; GML2019ZD0405).

SUPPLEMENTARY MATERIAL

The Supplementary Material for this article can be found online at: https://www.frontiersin.org/articles/10.3389/fpls.2020.585202/full#supplementary-material

REFERENCES

Baker, A., Starger, C., and Mcclanahan, T. (2004). Corals' adaptive response to climate. *Nature* 430:74.

Biber, P. D. (2007). Hydrodynamic transport of drifting macroalgae through a tidal cut. *Estuar. Coastal Shelf Sci.* 74, 565–569. doi: 10.1016/j.ecss.2007.04.019

Bolger, A. M., Lohse, M., and Usadel, B. (2014). Trimmomatic: a flexible trimmer for illumina sequence data. *Bioinformatics* 30, 2114–2120. doi: 10.1093/bioinformatics/btu170

Boyd, P., Collins, S., Dupont, S., Fabricius, K., Gattuso, J. P., and Havenhand, J. (2018). Experimental strategies to assess the biological ramifications of multiple drivers of ocean global ocean—a

review. *Global Change Biol.* 24, 2239–2261. doi: 10.1111/gcb.14102

Brading, P., Warner, M. E., Davey, P., Smith, D. J., Achterberg, E. P., and Suggett, D. J. (2011). Differential effects of ocean acidification on growth and photosynthesis among phylotypes of *Symbiodinium* (dinophyceae). *Limnol. Oceanogr.* 56, 927–938. doi: 10.4319/lo.2011.56.3.0927

Conesa, A., Götz, S., Garcíagómez, J. M., Terol, J., Talón, M., and Robles, M. (2005). Blast2go: a universal tool for annotation, visualization and analysis in functional genomics research. *Bioinformatics* 21, 3674–3676. doi: 10.1093/bioinformatics/bti610

Cornwall, C. E., Revill, A. T., Hall–Spencer, J. M., Milazzo, M., Raven, J. A., and Hurd, C. L. (2017). Inorganic carbon physiology underpins macroalgal responses to elevated CO_2. *Sci. Rep.* 7:46297.

Cornwall, C. E., Revill, A. T., and Hurd, C. L. (2015). High prevalence of diffusive uptake of CO_2 by macroalgae in a temperate subtidal ecosystem. *Photosynth. Res.* 124, 181–190. doi: 10.1007/s11120-015-0114-0

Dere, S., Gunes, T., and Sivaci, R. (1998). Spectrophotometric determination of chlorophyll-a, b and total carotenoid contents of some algae species using different solvents. *Botany* 22, 13–17.

Falkowski, P. G., and Raven, J. A. (2013). *Aquatic Photosynthesis*. Princeton, NY: Princeton University Press.

Fautin, D. G., and Buddemeier, R. W. (2004). Adaptive bleaching: a general phenomenon. *Hydrobiologia* 530–531, 459–467. doi: 10.1007/978-1-4020-2762-8_52

Feely, R. A., Doney, S. C., and Cooley, S. R. (2009). Ocean acidification: Present conditions and future changes in a high-CO_2 world. *Oceanography* 22, 36–47. doi: 10.5670/oceanog.2009.95

Fu, F. X., Warner, M. E., Zhang, Y., Feng, Y., and Hutchins, D. A. (2007). Effects of increased temperature and CO_2 on photosynthesis, growth, and elemental ratios in marine *Synechococcus* and *Prochlorococcus* (Cyanobacteria). *J. Phycol.* 43, 485–496. doi: 10.1111/j.1529-8817.2007.00355.x

Gao, G., Clare, A. S., Rose, C., and Caldwell, G. S. (2017). Eutrophication and warming-driven green tides (*Ulva rigida*) are predicted to increase under future climate change scenarios. *Mar. Pollut. Bull.* 114, 439–447. doi: 10.1016/j.marpolbul.2016.10.003

Gao, K. S., Aruga, Y., Asada, K., Ishihara, T., Akano, T., and Kiyohara, M. (1993). Calcification in the articulated coralline alga *Corallina pilulifera*, with special reference to the effect of elevated CO_2 concentration. *Mar. Biol.* 117, 129–132. doi: 10.1007/bf00346434

Gao, K. S., Beardall, J., Häder, D. P., Hall-Spencer, J. M., Gao, G., and Hutchins, D. A. (2019). Effects of ocean acidification on marine photosynthetic organisms under the concurrent influences of warming, UV radiation, and deoxygenation. *Front. Mar. Sci.* 6:322.

Gao, K. S., and Campbell, D. (2014). Photophysiological responses of marine diatoms to elevated CO_2 and decreased pH: a review. *Funct. Plant Biol.* 41, 449–459. doi: 10.1071/fp13247

Goldman, J. A. L., Bender, M. L., and Morel, F. M. M. (2017). The effects of pH and pCO_2 on photosynthesis and respiration in the diatom *Thalassiosira weissflogii*. *Photosynth. Res.* 132, 1–11. doi: 10.1007/978-3-319-23534-9_1

Gong, S. Q., Li, Z. Y., Zhang, F. L., Xiao, Y. L., and Chen, H. (2018). *Symbiochlorum hainanensis*, gen. et sp. nov. (ulvophyceae, chlorophyta) isolated from bleached corals living in the south china sea. *J. Phycol.* 54, 811–817. doi: 10.1111/jpy.12779

Gong, S. Q., Xu, L. J., Yu, K. F., Zhang, F. L., and Li, Z. Y. (2019). Differences in Symbiodiniaceae communities and photosynthesis following thermal bleaching of massive corals in the northern part of the South China Sea. *Mar. Pollut. Bull.* 144, 196–204. doi: 10.1016/j.marpolbul.2019.04.069

Grabherr, M. G., Haas, B. J., Yassour, M., Levin, J. Z., Thompson, D. A., and Amit, I. (2011). Full-length transcriptome assembly from RNA-seq data without a reference genome. *Nat. Biotechnol.* 29:644. doi: 10.1038/nbt.1883

Haas, B. J., Papanicolaou, A., Yassour, M., Grabherr, M., Blood, P. D., and Couger, M. B. (2013). De novo transcript sequence reconstruction from RNA-seq using the trinity platform for reference generation and analysis. *Nat. Protoc.* 8, 1494–1512. doi: 10.1038/nprot.2013.084

Hoegh–Guldberg, O., and Bruno, J. F. (2010). The impact of climate change on the world's marine ecosystems. *Science* 328, 1523–1528. doi: 10.1126/science.1189930

Huang, Y. B., Liu, X., Laws, E. A., Chen, B. Z., Li, Y., and Xie, Y. (2018). Effects of increasing atmospheric CO_2 on the marine phytoplankton and bacterial metabolism during a bloom: a coastal mesocosm study. *Sci. Total Environ.* 633, 618–629. doi: 10.1016/j.scitotenv.2018.03.222

Hyun, B., Choi, K. H., Jang, P. G., Jang, M. C., Lee, W. J., Moon, C. H., et al. (2014). Effects of increased CO_2 and temperature on the growth of four diatom species (*Chaetoceros debilis*, *Chaetoceros didymus*, *Skeletonema costatum* and *Thalassiosira nordenskioeldii*) in laboratory experiments. *J. Environ. Sci. Int.* 23, 1003–1012. doi: 10.5322/jesi.2014.23.6.1003

IPCC (2014). *Climate change 2014: Impacts, Adaptation, and Vulnerability. Part B: Regional Aspects Contribution of Working Group II to the Fifth Assessment Report of the Intergovernmental Panel on Climate Change*. Geneva: IPCC.

Jin, P., Ding, J. C., Xing, T., Riebesell, U., and Gao, K. S. (2017). High levels of solar radiation offset impacts of ocean acidification on calcifying and non-calcifying strains of *Emiliania huxleyi*. *Mar. Ecol. Prog. Ser.* 568, 47–58. doi: 10.3354/meps12042

Johnson, M. D., Price, N. N., and Smith, J. E. (2014). Contrasting effects of ocean acidification on tropical fleshy and calcareous algae. *PeerJ* 2:411.

Karim, W., Nakaema, S., and Hidaka, M. (2015). Temperature effects on the growth rates and photosynthetic activities of *Symbiodinium* cells. *J. Mar. Sci. Eng.* 3, 368–381. doi: 10.3390/jmse3020368

Koch, M., Bowes, G., Ross, C., and Zhang, X. H. (2013). Climate change and ocean acidification effects on seagrass and marine macroalgae. *Global Change Biol.* 19, 103–132. doi: 10.1111/j.1365-2486.2012.02791.x

Kremp, A., Godhe, A., Egardt, J., Dupont, S., Suikkanen, S., Casabianca, S., et al. (2012). Intraspecific variability in the response of bloom-forming marine microalgae to changed climate conditions. *Ecol. Evolut.* 2, 1195–1207. doi: 10.1002/ece3.245

Kumar, A., Castellano, I., Patti, F. P., Delledonne, M., and Buia, M. C. (2017). Molecular response of *Sargassum vulgare* to acidification at volcanic CO_2 vents-insights from de novo transcriptomic analysis. *Mol. Ecol.* 26, 2276–2290. doi: 10.1111/mec.14034

Lazaro, M. G., Juan, M. R., Dattolo, E., Rocio, G. M., and Gabriele, P. (2016). Physiological and molecular evidence of differential short-term heat tolerance in mediterranean seagrasses. *Sci. Rep.* 6:28615.

Ledford, H. K., and Niyogi, K. K. (2005). Singlet oxygen and photo-oxidative stress management in plants and algae. *Plant Cell Environ.* 28, 1037–1045. doi: 10.1111/j.1365-3040.2005.01374.x

Lee, T. C., and Hsu, B. D. (2010). Disintegration of the cells of siphonous green alga *Codium edule* (bryopsidales, chlorophyta) under mild heat stress. *J. Phycol.* 45, 348–356. doi: 10.1111/j.1529-8817.2009.00656.x

Li, B., and Dewey, C. N. (2011). RSEM: accurate transcript quantification from RNA seq data with or without a reference genome. *BMC Bioinform.* 12:323.

Li, P., Ainsworth, E. A., Leakey, A. D., Ulanov, A., Lozovaya, V., Ort, D. R., et al. (2008). *Arabidopsis* transcript and metabolite profiles: ecotype-specific responses to open-air elevated [CO_2]. *Plant Cell Environ.* 31, 1673–1687. doi: 10.1111/j.1365-3040.2008.01874.x

Listmann, L., Leroch, M., Schlüter, L., Thomas, M. K., and Reusch, T. B. H. (2016). Swift thermal reaction norm evolution in a key marine phytoplankton species. *Evolut. Appl.* 9, 1156–1164. doi: 10.1111/eva.12362

Martin, S., and Hall-Spencer, J. M. (2017). "Effects of ocean warming and acidification on rhodolith/maërl beds," in *Rhodolith/Maërl Beds: A Global Perspective*, eds R. Riosmena-Rodríguez, W. Nelson, and J. Aguirre (Cham: Springer), 55–85. doi: 10.1007/978-3-319-29315-8_3

Mayfield, A. B., Wang, Y. B., Chen, C. S., Lin, C. Y., and Chen, S. H. (2014). Compartment-specific transcriptomics in a reef-building coral exposed to elevated temperatures. *Mol. Ecol.* 23, 5816–5830. doi: 10.1111/mec.12982

Mejia, A. Y., Puncher, G. N., and Engelen, A. H. (2012). "Macroalgae in tropical marine coastal systems," in *Seaweed Biology. Ecological Studies (Analysis and Synthesis)*, Vol. 219, eds C. Wiencke and K. Bischof (Berlin: Springer).

Moriya, Y., Itoh, M., Okuda, S., Yoshizawa, A. C., and Kanehisa, M. (2007). KAAS: an automatic genome annotation and pathway reconstruction server. *Nucleic Acids Res.* 35, 182–185.

R Core Team (2014). *R: A Language and Environment for Statistical Computing*. Vienna: R Core Team.

Riebesell, U., Wolf-Gladrow, D. A., and Smetacek, V. (1993). Carbon dioxide limitation of marine phytoplankton growth rates. *Nature* 361, 249–251. doi: 10.1038/361249a0

Robinson, M. D., McCarthy, D. J., and Smyth, G. K. (2010). edgeR: a Bioconductor package for differential expression analysis of digital gene expression data. *Bioinformatics* 26, 139–140. doi: 10.1093/bioinformatics/btp616

Rosic, N. N., and Hoegh–Guldberg, O. (2010). A method for extracting a high-quality RNA from *Symbiodinium* sp. *J. Appl. Phycol.* 22, 139–146. doi: 10.1007/s10811-009-9433-x

Ruocco, M., Musacchia, F., Olivé, I., Costa, M. M., Barrote, I., and Santos, R. (2017). Genomewide transcriptional reprogramming in the seagrass *Cymodocea nodosa* under experimental ocean acidification. *Mol. Ecol.* 26, 4241–4259.

Solomos, T. (1977). Cyanide-resistant respiration in higher plants. *Ann. Rev. Physiol.* 28, 279–297. doi: 10.1146/annurev.pp.28.060177.001431

Strepp, R., Scholz, S., Kruse, S., Speth, V., and Reski, R. (1998). Plant nuclear gene knockout reveals a role in plastid division for the homolog of the bacterial cell division protein ftsz, an ancestral tubulin. *Proc. Natl. Acad. Sci. U.S.A.* 95, 4368–4373. doi: 10.1073/pnas.95.8.4368

Tortell, P. D., Payne, C. D., Li, Y., Trimborn, S., Rost, B., Smith, W. O., et al. (2008). CO_2 sensitivity of southern ocean phytoplankton. *Geophys. Res. Lett.* 35:L04605.

Walworth, N. G., Lee, M. D., Fu, F. X., Hutchins, D. A., and Webb, E. A. (2016). Molecular and physiological evidence of genetic assimilation to high CO_2 in the marine nitrogen fixer *Trichodesmium*. *Proc. Natl. Acad. Sci. U.S.A.* 11, 7367–7374.

Wang, D., Kong, D. D., Ju, C. L., Hu, Y., He, Y. K., and Sun, J. S. (2002). Effects of tabacco plastid division genes NtFtsZ1 and NtFtsZ2 on the division and morphology of chloroplasts. *Acta Bot. Sin.* 44, 838–844.

Wernberg, T., Russell, B. D., Moore, P. J., Ling, S. D., Smale, D. A., and Campbell, A. (2011). Impacts of climate change in a global hotspot for temperate marine biodiversity and ocean warming. *J. Exp. Mar. Biol. Ecol.* 400, 7–16. doi: 10.1016/j.jembe.2011.02.021

Wu, Y., Campbell, D. A., Irwin, A. J., Suggett, D. J., and Finkel, Z. V. (2014). Ocean acidification enhances the growth rate of larger diatoms. *Limnol. Oceanogr.* 59, 1027–1034. doi: 10.4319/lo.2014.59.3.1027

Ying, Z. T., Mulligan, R. M., Janney, N., and Houtz, R. L. (1999). Rubisco small and large subunit N-methyltransferases. *J. Biol. Chem.* 274, 36750–36756. doi: 10.1074/jbc.274.51.36750

Zhang, F., Hong, H., Kranz, S. A., Shen, R., and Shi, D. (2019). Proteomic responses to ocean acidification of the marine diazotroph *trichodesmium* under iron-replete and iron limited conditions. *Photosynth. Res.* 142, 17–34. doi: 10.1007/s11120-019-00643-8

Conflict of Interest: The authors declare that the research was conducted in the absence of any commercial or financial relationships that could be construed as a potential conflict of interest.

frontiers in Plant Science

ORIGINAL RESEARCH
published: 16 September 2021
doi: 10.3389/fpls.2021.726538

Increased CO_2 Relevant to Future Ocean Acidification Alleviates the Sensitivity of a Red Macroalgae to Solar Ultraviolet Irradiance by Modulating the Synergy Between Photosystems II and I

*Di Zhang[1], Juntian Xu[2], Sven Beer[3], John Beardall[1,4], Cong Zhou[1] and Kunshan Gao[1]**

[1]State Key Laboratory of Marine Environmental Science & College of Ocean and Earth Sciences, Xiamen University, Xiamen, China, [2]Jiangsu Key Laboratory of Marine Bioresources and Environment, Jiangsu Ocean University, Lianyungang, China, [3]Department of Plant Sciences and Food Security, Faculty of Life Sciences, Tel Aviv University, Tel Aviv, Israel, [4]School of Biological Sciences, Monash University, Clayton, VIC, Australia

OPEN ACCESS

Edited by:
Jan de Vries, University of Göttingen, Germany

Reviewed by:
Gregor Christa, University of Wuppertal, Germany
Mattia Pierangelini, University of Liège, Belgium

***Correspondence:**
Kunshan Gao
ksgao@xmu.edu.cn

Specialty section:
This article was submitted to Marine and Freshwater Plants, a section of the journal Frontiers in Plant Science

Received: *17 June 2021*
Accepted: *16 August 2021*
Published: *16 September 2021*

Citation:
Zhang D, Xu J, Beer S, Beardall J, Zhou C and Gao K (2021) Increased CO_2 Relevant to Future Ocean Acidification Alleviates the Sensitivity of a Red Macroalgae to Solar Ultraviolet Irradiance by Modulating the Synergy Between Photosystems II and I. Front. Plant Sci. 12:726538. doi: 10.3389/fpls.2021.726538

While intertidal macroalgae are exposed to drastic changes in solar photosynthetically active radiation (PAR) and ultraviolet radiation (UVR) during a diel cycle, and to ocean acidification (OA) associated with increasing CO_2 levels, little is known about their photosynthetic performance under the combined influences of these drivers. In this work, we examined the photoprotective strategies controlling electron flow through photosystems II (PSII) and photosystem I (PSI) in response to solar radiation with or without UVR and an elevated CO_2 concentration in the intertidal, commercially important, red macroalgae *Pyropia* (previously *Porphyra*) *yezoensis*. By using chlorophyll fluorescence techniques, we found that high levels of PAR alone induced photoinhibition of the inter-photosystem electron transport carriers, as evidenced by the increase of chlorophyll fluorescence in both the J- and I-steps of Kautsky curves. In the presence of UVR, photoinduced inhibition was mainly identified in the O_2-evolving complex (OEC) and PSII, as evidenced by a significant increase in the variable fluorescence at the K-step (F_k) of Kautsky curves relative to the amplitude of F_J–F_o (W_k) and a decrease of the maximum quantum yield of PSII (F_v/F_m). Such inhibition appeared to ameliorate the function of downstream electron acceptors, protecting PSI from over-reduction. In turn, the stable PSI activity increased the efficiency of cyclic electron transport (CET) around PSI, dissipating excess energy and supplying ATP for CO_2 assimilation. When the algal thalli were grown under increased CO_2 and OA conditions, the CET activity became further enhanced, which maintained the OEC stability and thus markedly alleviating the UVR-induced photoinhibition. In conclusion, the well-established coordination between PSII and PSI endows *P. yezoensis* with a highly efficient photochemical performance in response to UVR, especially under the scenario of future increased CO_2 levels and OA.

Keywords: chlorophyll fluorescence, CO_2 enrichment, ocean acidification, photosystems II and I, photoinhibition, *Pyropia yezoensis*, ultraviolet-radiation

INTRODUCTION

Living in the intertidal zone, macroalgae are often exposed to periodic harsh light fluctuations and air exposure associated with changes in tide levels. High levels of solar irradiance can significantly decrease photosynthesis and growth rates in macroalgae (Aline et al., 2006; Martin and Gattuso, 2009; Ji and Gao, 2020), while limited light would entail an insufficient energy supply and thus decrease photosynthesis and growth. Under limited light conditions, longer wavelengths within the range of ultraviolet radiation (UVR, 280–400 nm), generally considered to be detrimental to aquatic ecosystems, can be used as light energy for photosynthesis (Gao et al., 2007). Moderate levels of UVA (315–400 nm) are beneficial for carbon fixation in several macroalgae (Gao and Xu, 2008; Xu and Gao, 2010), and can also act as a signal to stimulate the activity of carbonic anhydrase and nitrate reductase (Viñegla et al., 2006), or prompt morphological development during germination of conchospores (Jiang et al., 2007). Furthermore, the effects of UVR also depend strongly on interactions with other environmental factors. For example, increased ocean temperatures result in stratification and shoaling of the upper mixed layer and thus expose organisms to increased levels of solar photosynthetically active radiation (PAR) and UVR (Häder and Barnes, 2019 and reference therein), and the global warming-induced melting of ice and snow would also aggravate the transmission of UVR and increase UVR exposure in polar regions (Williamson et al., 2019; Neale et al., 2021 and references therein). These interactive effects control the levels of exposure of macroalgae to UVR, and may modulate their photosynthetic performance, production of photoprotective compounds and/or repair mechanisms in response to UVR (see the review by Ji and Gao, 2020 and references therein).

As a consequence of anthropogenic CO_2 emissions, the atmospheric CO_2 concentration has been predicted to increase to above 1,000 μatm by the end of this century (e.g., IPCC, 2014). In addition to possible direct effects of higher aqueous CO_2, this will also result in an increase in proton concentration in the seawater (a drop in pH from 8.1 to 7.8), known as ocean acidification (OA). A number of previous studies have shown that OA hindered calcification processes (Gao et al., 1993; Semesi et al., 2009; Gao and Zheng, 2010; Büdenbender et al., 2011) and thus exposed calcified algae to more UVR exposure. In contrast, the elevated availability of dissolved inorganic carbon (DIC) in seawater has been reported to stimulate both photosynthesis and growth in a number of non-calcified macroalgae such as in *Pyropia* sp. (Gao et al., 1991; Zhang et al., 2020), *Palmaria* sp. (Beer and Koch, 1996), *Gloiopeltis* sp., *Gigartina* sp. (Zou and Gao, 2005), *Gracilaria* sp. (Andría et al., 1999, 2001), *Hypnea* sp. (Suárez-Álvarez et al., 2012), and *Ellisolandia* sp. (Korbee et al., 2014). In addition, the increased DIC would also down-regulate the CO_2-concentrating mechanisms (CCMs), which utilize HCO_3^- to compensate for the limitation of CO_2 in seawater and maintain high intracellular CO_2 levels for photosynthesis and growth of the macroalgae (e.g., a green algae *Ulva prolifera* in Xu and Gao, 2012, and a red algae *Pyropia yezoensis* in Li et al., 2016). Since down-regulation of CCMs is known to save operational energy cost (Raven et al., 2014 and references therein), the energy savings can either stimulate algal growth under low light and increase the risk of photoinhibition under high light (especially with the presence of UVR; see the review by Gao et al., 2019 and references therein).

Pyropia (previously known as *Porphyra*; Rhodophyta), an economically important marine crop worth ~US$1.3 billion per year (Blouin et al., 2011), has been widely cultivated in both China and other Asian countries. Previously, we showed that UVR inhibited both carbon assimilation and growth of *P. yezoensis*, while elevated CO_2 exhibited a positive effect and participated in the alleviation of the UVR-induced inhibition (Zhang et al., 2020). In that work, increases of non-photochemical quenching (NPQ) and UV-absorbing compounds (UVACs) were suggested to dissipate and/or absorb the excess energy originating from UVR, while little attention was paid to the transfer of such absorbed energy. In red algae, phycobilisomes (PBS) form the light-harvesting antennae on the outer surface of thylakoid membranes, in the proximity of photosystem II (PSII), the specific mechanisms for this are unclear but may involve state transitions or mobility of PBS, redistributing the energy between the two photosystems and thus altering photosynthetic electron transport and supply of energy for CO_2 fixation and reduction (Su et al., 2010 and references therein). Moreover, regulation of photosynthetic electron transport, e.g., *via* alternative electron transport chains, including cyclic electron transport (CET) around photosystem I PSI, photorespiration and the water-water cycle along with reactive oxygen species (ROS)-scavenging systems, has also been supposed to protect photosynthetic systems from photoinhibition/photodamage (Eberhard et al., 2008 and references therein, Miyake, 2010). In *P. yezoensis*, CET has been verified to play a vital role in photoprotection when thalli suffered from dehydration (Gao and Wang, 2012), severe salt stress (Lu et al., 2016; Yu et al., 2018), and irradiance stress (Niu et al., 2016). The active CET not only participates in NPQ, but also alleviates the over-reduction of plastoquinone and, thus, balance the redox state of the photosynthetic electron transport chain (Miyake, 2010).

In the present study, effects of OA and UVR on the photosynthetic performance of *P. yezoensis* were investigated by growing these algae under incident solar radiation with or without UVR at ambient and elevated CO_2 concentrations projected for future OA by the end of 2100. While high CO_2 and the concomitant OA may have separate effects on algal physiology in nature (Hurd et al., 2020), technically, it is hard to distinguish the specific effects of pH or CO_2. Moreover, pH and CO_2 covary oppositely even in algal blooms or with progressive OA, thus we did not attempt to disentangle the interactions between these two variables. Our aims are 1) characterized the electron transport flux from PSII to PSIl, 2) examined an alternative electron sink, i.e., CET; and 3) evaluated the coordination between PSII and PSI, under the influences of UVR and OA.

MATERIALS AND METHODS

Experimental Treatments and Measurements of UV Irradiance and pH

Thalli of *P. yezoensis* (Ueda) M.S.Hwang & H.G.Choi were collected from rafts offshore of Gaogong Island (34°43′31′ N, 119°31′57′ E), Lianyungang, Jiangsu Province, China, on December 12, 2017, and transported to the laboratory in a cooled Styrofoam box within 2 h. Following rinsing, thalli of ~0.05 *g* fresh weight were grown outdoors for 9 days in 1 L open-ended quartz tubes filled with natural seawater, which were partly immersed in a flow-through water bath to maintain the seawater temperature at 8 ± 1°C. The seawater in each tube was continuously aerated (300 ml per min) with air containing 400 ± 20 or 1,000 ± 50 μatm CO_2, and was renewed every day. The low-CO_2 air was directly obtained with an air pump while the high-CO_2 level was obtained from a CO_2 enricher (HP 1000 G-D, Ruihua Instruments, Wuhan, China), which controls the CO_2 concentration with less than 5% variation. Different radiation treatments were achieved by covering the quartz tubes with Ultraphan film 395 (UV Opak, Digefra, Munich, Germany), Folex 320 film (Montagefolie, Folex, Dreieich, Germany), or Ultraphan film 295 (Digefra), respectively, so that the thalli were exposed to irradiances above 395 nm (PAR alone), above 320 nm (PA, PAR + UVA) and above 295 nm (PAB, PAR + UV-A + B), respectively. Considering the low density of algal blades in the tubes, the self-shading in our present study can be considered minimal. Measurements of photochemical activities (see below) were carried out around 14:00 on the 10th day of treatments. A total of 18 tubes containing different individual thalli were used for measurements, and three independent thalli were used as replicates for each parameter. According to published papers (Mercado et al., 1999; Zou, 2005; Chen et al., 2016, 2017), and also based on our previous experience (Zou et al., 2003; Xu and Gao, 2008, 2010), 10 days culture is enough for full acclimation of the photosynthetic and other biochemical traits in *Pyropia* spp. and other tested marine macroalgae.

The pH_{NBS} was measured at the end of each day by a pH meter (pH 700, Eutech Instruments, Singapore) equipped with an Orion® 8102BN Ross combination electrode (Thermo Electron Co., United States), which was calibrated with NBS standard buffers every day during the experiment (Thermo Fisher Scientific Inc., United States). Total alkalinity (TA) was measured with a TA analyzer (AS-ALK1, Apollo SciTech, United States) by Gran acidimetric titrations. The values of other carbonate chemistry parameters (total inorganic carbon concentration, TIC, bicarbonate and carbonate ions) were calculated by the Excel program CO2SYS (Pierrot et al., 2006) according to the measured values of TA and pH_{NBS}.

The incident solar irradiances were continuously monitored and recorded every minute by a broadband solar radiometer (EKO Instruments Co., LTD, Japan), which has three separate channels, for (PAR, 400–700 nm), UVA (315–400 nm), and UVB (280–315 nm), respectively.

Before the final measurements, the *in situ* diurnal variations (daytime) of pH and CO_2 were measured. These results showed that the total alkalinity (TA) was around ~2,400 μm throughout the day, pH ranged from ~8.2 to 8.4 and the dissolved CO_2 ranged from about 10 to 13 μm. The maximal and daily average PAR values during the experimental period were 812.6 ± 57.4 and 186.1 ± 35.1 μmol photons m^{-2} s^{-1}, respectively, while the corresponding values for UVA were 8.1 ± 0.7 and 1.9 ± 0.3 W m^{-2}, and that for UVB 0.3 ± 0.03 and 0.1 ± 0.01 W m^{-2}. PAR, UVA and UVB levels were 635 μmol photons m^{-2} s^{-1} and 6.5 and 0.2 W m^{-2}, respectively, when the following parameters were measured at 14:00 on the 10th day. During the experiment, the enhanced CO_2 level (from 400 to 1000 μatm in the air phase) resulted a pH drop from 8.24 ± 0.03 to 7.92 ± 0.03 ($n = 27$). While TA remained unaltered, the TIC increased from 2,131 ± 20 to 2,310 ± 20 μm and that of CO_2 from 12 ± 1 to 28 ± 3 μm ($n = 27$) under the high-CO_2 treatment.

Chlorophyll Fluorescence Measurements and Analyses

A dual-wavelength pulse-amplitude-modulated (PAM) fluorescence monitoring system (Dual-PAM-100, Walz, Effeltrich, Germany) was employed to simultaneously measure the performance of PSII and PSI. To avoid the effect of phycobiliproteins on chlorophyll fluorescence, blue light (440 nm) was used as excitation light in the following measurements. Rapid fluorescence induction kinetics (Kautsky curves) showed a typical polyphasic rise pattern between O (the minimum fluorescence) and P (the maximum fluorescence) during the first second of illumination (Neubauer and Schreiber, 1987). The typical Kaustsky curve plotted against a logarithmic time scale represented different processes of photosynthetic electron transport (**Supplementary Figure S1**). According to Strasser and Strasser (1995) and Guisse et al. (1995), the fluorescence characterized of several different phases, where the time-specific steps were labeled as O, K (at ~300 μs), J (at ~2 ms), I (at ~30 ms) and P. Fluorescence intensities at different phases were noted as F_o, F_k, F_J, F_I and F_m. The standardized fluorescence intensity from the O- to P-phase was calculated as $V_t = (F_t - F_o)/(F_m - F_o)$. To assess the donor side activity of PSII, the normalized variable fluorescence at the K-step relative to the amplitude of $F_J - F_o$ (W_k) was calculated as $W_k = (F_k - F_o)/(F_J - F_o)$. To evaluate the activity of PSII, the maximum quantum yield of PSII (F_v/F_m) was calculated as $F_v/F_m = (F_m - F_o)/F_m$. The acceptor side activity of PSII, i.e., the probability that a trapped exciton moves an electron into the electron transport chain beyond Q_A^- (ψ_{ET2O}) and the quantum yield of electron transport (φ_{Eo}) was calculated as $\psi_{ET2O} = 1 - V_J$ and $\varphi_{Eo} = (1 - F_o/F_m) \times (1 - V_J)$, respectively. The redox state of inter-photosystem electron carriers and the acceptor side activity of PSI, i.e., the probability that an electron moves from reduced Q_A beyond PSI (ψ_{RE1O}), and the quantum yield for reduction of the end electron acceptors on the PSI acceptor side (φ_{Ro}), were calculated as $\psi_{RE1O} = 1 - V_I$ and $\varphi_{Ro} = (1\text{-}F_o/F_m) \times (1 - V_I)$, respectively. All these parameters were derived from JIP-tests (Strasser and Strasser, 1995; Strasser et al., 2004). According to the theory of energy fluxes in biomembranes (Strasser, 1981), the density of the PSII reaction

center per excited cross section (RC/CSo), the absorbed flux (ABS), the trapping flux (TRo), the electron transport flux (ETo), and the dissipated energy flux (DIo) by active reaction centers were calculated as.

$$RC/CSo = F_v/F_m \times V_J/V_K/4 \times F_O,$$
$$ABS/RC = 4 \times (F_K - F_O) \times F_m/(F_J - F_O) \times F_v,$$
$$TRo/RC = 4 \times (F_K - F_O)/(F_I - F_O),$$
$$ETo/RC = 4 \times (F_K - F_O) \times (F_m - F_J)/(F_J - F_O) \times F_v$$

and

$$DIo/RC = ABS/RC - TRo/RC.$$

P700 Measurements and Analyses

As suggested by Klughammer and Schreiber (1994), the $P700^+$ signal measured with the dual-wavelength (830/875 nm) unit of the instrument was taken as a measure of the redox state of P700. After 10 s exposure to far-red light, a saturation flash was applied to determine the maximum $P700^+$ signal (P_m). The steady-state $P700^+$ signal (P) was monitored under actinic light generated by the instrument at similar PAR levels as the natural sunlight (~800 μmol photons m^{-2} s^{-1}). The 0.8 s saturating flash of ~10, 000 μmol photons m^{-2} s^{-1} was applied to induce the maximum $P700^+$ value (P_m'). The effective quantum yield of PSI (YI) was calculated as $(P_m' - P)/P_m$.

In *Pyropia* spp., several published papers have demonstrated that the CET around PSI could account for up to 97.7% of total electron flow when algal blades suffered from severe desiccation (Gao and Wang, 2012). This was thus supposed to be one of the most important alternative electron transport pathway during exposure to stresses (Gao et al., 2013; Yu et al., 2018). Accordingly, our present study paid more attention on the physiological role of CET during the exposure to UVR and high-CO_2 induced OA. CET around PSI was evaluated by the measurement of the re-reduction kinetics of $P700^+$. After ~10 s exposure to far-red light, the applied saturation flash drives $P700^+$ to combine with electrons, and the initial linear slope of the re-reduction of $P700^+$ indicated the activity of CET.

All measured and calculated parameters are summarised in **Table 1**.

Statistical Analyses

In the present study, UVR-induced inhibition for a particular parameter was calculated as $(P_{PAR} - P_{PAR+UVR})/P_{PAR} \times 100\%$, where P_{PAR} and $P_{PAR+UVR}$ represent the values of the physiological parameter for the thalli grown under PAR alone or PAR + UVR, respectively. UVB-induced inhibition was derived from the difference in the values between the PAB (PAR + UVA + B) and PA (PAR + UVA) treatments.

Statistical analyses were performed using SPSS 19.0 (SPSS Inc., Chicago, IL, United States). The homogeneity of variance was examined using Levene's test before all statistical analyses. One-way ANOVA and *t*-test were used to establish differences among treatments. A two-way ANOVA was used to identify the effects of CO_2 concentration, light, UV, and their interactions. Differences were considered to be statistically significant at $p < 0.05$.

TABLE 1 | Measured and calculated parameters used in this paper.

Parameters	Physiological interpretation
Kautsky curves	
F_o, F_k, F_J, F_I, F_P	fluorescence intensity at O, K, J, I, P phases
V_t	relative variable fluorescence at time *t*
$W_k = (F_k - F_o)/(F_J - F_o)$	normalized variable fluorescence at the K-step relative to the amplitude of $F_J - F_o$
$F_v/F_m = (F_m - F_o)/F_m$	maximum photochemical efficiency of PSII
$RC/CS_o = F_v/F_m \times V_J/V_K/4 \times F_o$	density of PSII RC per excited cross sections
$\psi_{ET2O} = 1 - V_J$	probability that a trapped excition moves an electron into the electron transport chain beyond Q_A^-
$\varphi_{Eo} = (1 - F_o/F_m) \times (1 - V_J)$	quantum yield of electron transport
$\psi_{RE1O} = 1 - V_I$	probability that an electron moves from reduced Q_A beyond PSI
$\varphi_{Ro} = (1 - F_o/F_m) \times (1 - V_I)$	quantum yield for reduction of the end electron acceptors on the PSI acceptor side
$ABS/RC = 4 \times (F_k - F_o) \times F_m/(F_J - F_o) \times F_v$	absorbed flux by active RCs
$TR_o/RC = 4 \times (F_k - F_o)/(F_I - F_o)$	trapping flux by active RCs
$ET_o/RC = 4 \times (F_k - F_o) \times (F_m - F_J)/(F_J - F_o) \times F_v$	electron transport flux by active RCs
$DI_o/RC = ABS/RC - TR_o/RC$	dissipated energy flux by active RCs
P700 measurements	
P, P_m, P_m'	real-time, maximum, and maximum steady state, absorption signal of $P700^+$
$YI = (P_m' - P)/P_m$	effective photochemical quantum yield of PSI
$P700^+$ re-reduction	the activity of cyclic electron transport (CET) around PSI

PSII, photosystem II; PSI, photosystem I; RC, reaction center; CS, cross section.

RESULTS

Under the ambient CO_2 conditions (low-CO_2), the presence of UVR significantly inhibited the O_2-evolving complex (OEC) of PSII activities as evidenced by an increase of the variable fluorescence at the K-step of the Kautsky curve relative to the amplitude of $F_J - F_O$ (W_K; *t*-test, $p < 0.05$; **Figure 1**) and a decrease of the maximum quantum yield of PSII (F_v/F_m; *t*-test, $p < 0.05$; **Figure 2**). Furthermore, UVB-induced inhibition of the OEC, with an amplitude of up to ~24%, was significantly higher than that induced by UVA (~16%; *t*-test, $p < 0.05$). In contrast, the PSII acceptor side activity (ψ_{ET2O}; **Figure 3A**), quantum yield of electron transport (φ_{Eo}; **Figure 3B**), PSI donor side activity (ψ_{RE1O}; **Figure 3C**), and quantum yield for reduction of PSI acceptor side (φ_{Ro}; **Figure 3D**) were significantly increased by UVR, as shown here by the negative inhibition values (*t*-test, $p < 0.05$ for these four parameters). However, under the low-CO_2 conditions, the effective quantum yield of PSI showed no significant change (*t*-test, $p = 0.487$; **Figure 4**) between PAR and PAR + UVR treatments, indicating that PSI activity was less affected by UVR. However, an increase in the re-reduction rate of $P700^+$ showed that UVR significantly stimulated the activity of CET around PSI, especially in the presence of UVB,

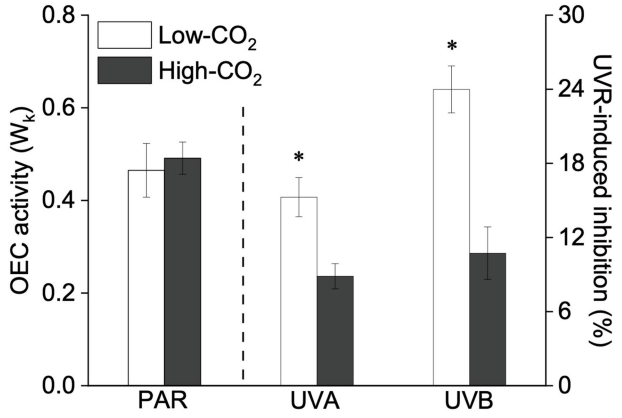

FIGURE 1 | Values (a.u., left pair of bars) and UVR-induced inhibition (%, right two pairs of bars) on the O_2-evolving complex (OEC) activity (the normalized variable fluorescence at the K-step relative to the amplitude of F_J–F_o, W_k) of *Pyropia yezoensis* growing for 9 days at low (~400 μatm, open bars) and high (~1000 μatm, closed bars) CO_2 conditions. Data are means ± *SD* ($n = 3$). The symbol "*" indicates a significant ($p < 0.05$, *t*-tests) difference between the treatments in each pair.

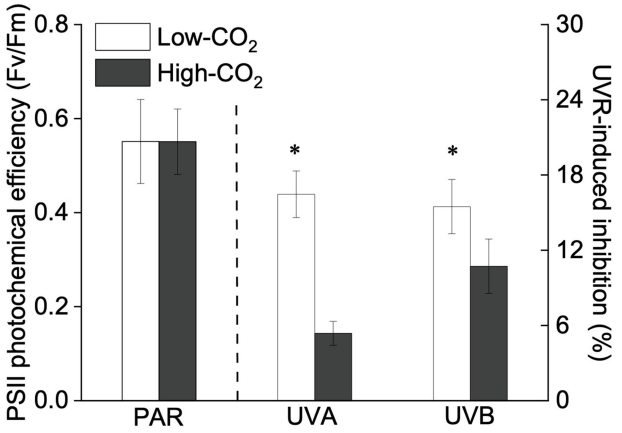

FIGURE 2 | Values (a.u., left pair of bars) and UVR-induced inhibition (%, right two pairs of bars) of PSII photochemical efficiency (F_v/F_m) of *P. yezoensis* growing for 9 days at low (~400 μatm, open bars) and high (~1000 μatm, closed bars) CO_2 conditions. Data are means ± *SD* ($n = 3$). The symbols "*" indicates a significant ($p < 0.05$, *t*-tests) difference between the treatments in each pair.

with increasing amplitude by up to ~17% (~7% for UVA and ~10% for UVB, respectively; *t*-test, $p < 0.05$ for both UVA and UVB treatments; **Figure 5**). Due to the fact that CET relates to electron transport rate in both PSII and PSI [as it could be calcultated by the difference between ETRI and ETRII (Yamori et al., 2011; Gao and Wang, 2012)], the asynchronous variation between PSI activity and CET was mainly attributed to the decrease of PSII photochemical efficiency. The active CET thus compensates for the loss of linear electron transport rate, maintaining a high efficiency of generating ATP. Analyses of the specific energy fluxes of PSII showed that UVR significantly inhibited the density of PSII reaction centers (RC/CSo), the absorbed photon flux (ABS), the trapping photon flux (TRo) and the electron transport flux (ETo; *t*-test, $p < 0.05$ for these four parameters), while there was an up-regulation of the dissipated energy flux (DIo; *t*-test, $p < 0.05$; **Figure 6**).

In the future-simulated high-CO_2 conditions, leading also to ocean acidification (OA), PAR alone did not induce any significant changes in W_k and F_v/F_m (*t*-test, $p = 0.378$ and 0.523, respectively; **Figures 1, 2**), indicating that both OEC and PSII were unaffected. The enhancements of ψ_{ET2O} (**Figure 3A**), φ_{Eo} (**Figure 3B**), ψ_{RE1O} (**Figure 3C**), and φ_{Ro} (**Figure 3D**) suggested that more electrons were transferred through the intersystem electron carriers under OA (*t*-test, $p < 0.05$ for these four parameters). Regarding the downstream electron transport chain, YI (**Figure 4**) and re-reduction rate of $P700^+$ (**Figure 5**) increased by up to ~11% and ~23%, respectively, implying an up-regulation in PSI and CET (*t*-test, $p < 0.05$ for these two parameters). Changes of the specific energy fluxes of PSII indicated the efficiency of active PSII reaction centers were enhanced by OA (*t*-test, $p < 0.05$; **Figure 6**).

A two-way ANOVA analysis showed that both CO_2 concentration, UVR, and their interaction, significantly affected OEC, PSII, the intersystem electron transport and CET activities, but not always PSI (**Table 2**). Under the high CO_2 condition, UVR-induced inhibition of both OEC and PSII photochemical efficiency significantly decreased, with UVA- and UVB-induced inhibition of OEC decreased from ~15% to ~9%, and from ~24% to ~11%, respectively (*t*-test, $p < 0.05$ for both UVA and UVB treatment); that of PSII by UVA and UVB ranged from ~16% to ~5%, and from ~15% to ~10%, respectively (*t*-test, $p < 0.05$ for both UVA and UVB treatment; **Figures 1, 2**). Although the extent of UVR-induced inhibition on ψ_{ET2O}, φ_{Eo}, ψ_{RE1O}, and φ_{Ro} exhibited significant differences between low- and high-CO_2 conditions (**Figure 3**), the absolute values of these parameters were less affected (*t*-test, $p = 0.647$, 0.548, 0.398 and 0.712 respectively). The significant difference in $P700^+$ re-reduction between low- and high-CO_2 indicated that there was a synergistic effect between increased CO_2/OA and UVR, the high-CO_2 further enhanced CET activity by up to ~4% and ~5% under the influences of UVA and UVB, respectively (*t*-test, $p < 0.05$ for both UVA and UVB treatment; **Table 2, Figure 5**). In PSII, UVR-induced inhibition on the density of PSII reaction centers (RC/CSo), the absorbed photon flux (ABS), the trapping photon flux (TRo), and the electron transport flux (ETo) was alleviated by the high-CO_2 treatment (*t*-test, $p < 0.05$ for both UVA and UVB treatment; **Figure 6**). Meanwhile, UVR-induced up-regulation of dissipated energy flux (DIo) was further enhanced under the high-CO_2/OA condition (*t*-test, $p < 0.05$ for both UVA and UVB treatment; **Figure 6**).

DISCUSSION

Our results suggest that in the red algae *P. yezoensis* (Ueda) M. S. Hwang and H. G. Choi, future elevated CO_2 and ocean acidification (OA) can alleviate both UVB- and UVA-induced inhibition on PSII by modulating the synergy between PSII

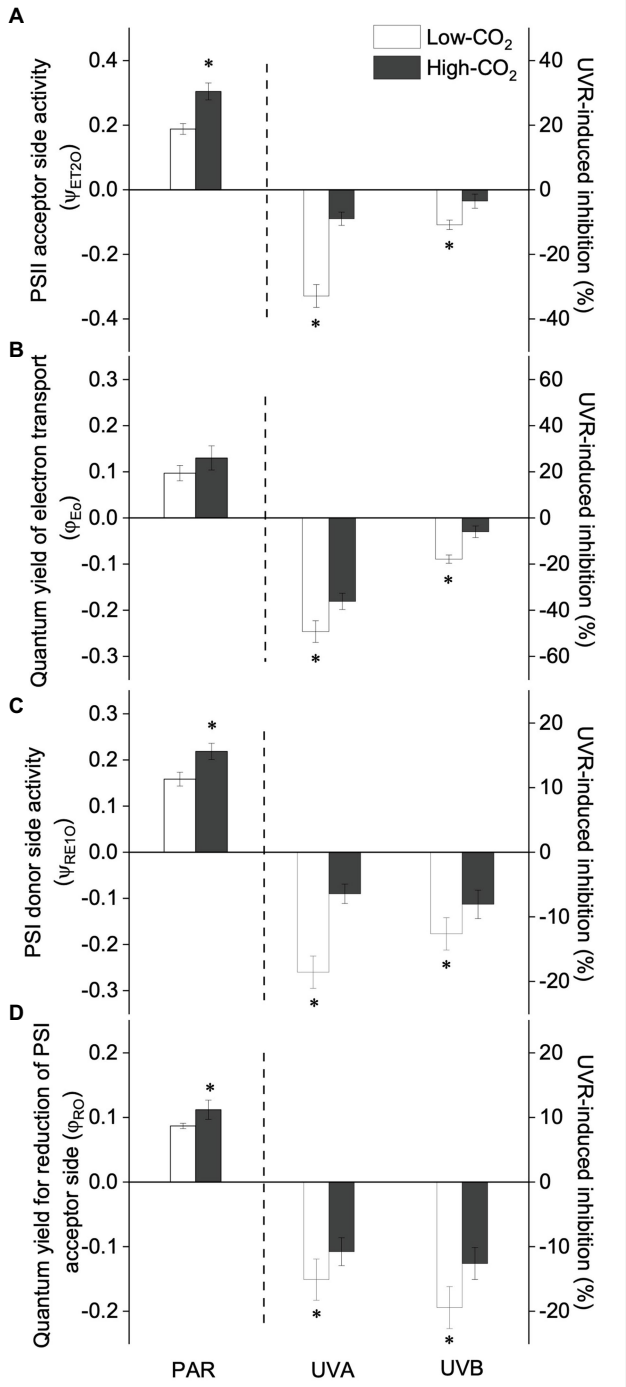

FIGURE 3 | Values (a.u., left pair of bars) and UVR-induced inhibition (%, right two pairs of bars) of PSII acceptor side activity [the probability that trapped excitons move electrons into the electron transport chain beyond Q_A^-, Ψ_{ET2O}, panel **(A)**], quantum yield of electron transport [φ_{Eo}, panel **(B)**], PSI donor side activity [the probability that an electron moves from reduced Q_A beyond PSI, Ψ_{RE1O}, panel **(C)**] and the quantum yield for reduction of PSI acceptor side [φ_{Ro}, panel **(D)**] of *P. yezoensis* growing for 9 days at low (~400 μatm, open bars) and high (~1000 μatm, closed bars) CO_2 conditions. Data are means ± *SD* ($n = 3$). The symbols "*" indicates a significant ($p < 0.05$, *t*-tests) difference between the treatments in each pair.

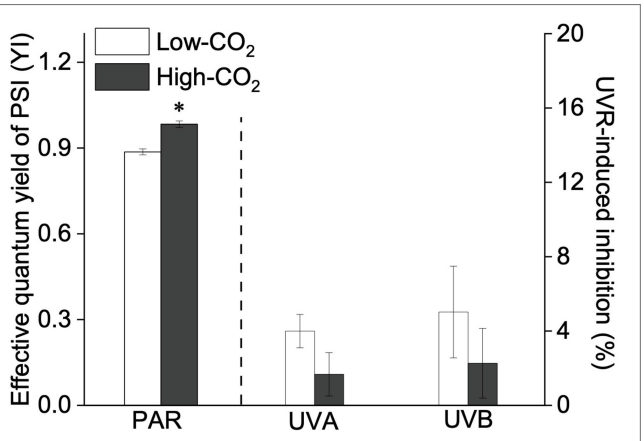

FIGURE 4 | Values (a.u., left pair of bars) and UVR-induced inhibition (%, right two pairs of bars) of the effective quantum yield of PSII (YI) of *P. yezoensis* growing for 9 days at low (~400 μatm, open bars) and high (~1000 μatm, closed bars) CO_2 conditions. Data are means ± *SD* ($n = 3$). The symbols "*" indicates a significant ($p < 0.05$, *t*-tests) difference between the treatments in each pair.

and PSI. Such synergy was found to relate mainly to the up-regulation of the intersystem electron transport efficiencies and CET around PSI (see **Figure 7**). In contrast with high-light-induced over-reduction of inter-photosystem electron transfer carriers (**Figure 7A**), UVR (especially UVB)-induced photoinhibition, characterized by the inhibition of OEC and PSII (**Figure 7B**), significantly decreased its quantum yield (**Figure 2**), which should be responsible for the reduced rates of carbon assimilation and growth (**Figure 7B**; Zhang et al., 2020). When grown and acclimated in the high-CO_2 condition (**Figure 7C**), the well- established coordination between PSII and PSI, as well as the enhanced CET around PSI sustain the efficient electron transport, consequently increasing the resilience of *P. yezoensis* to PAR and/or UVR.

Previous studies have shown that the presence of UVR would reduce primary productivity in cyanobacteria and of phytoplankton assemblages by about 20% due to the concomitant photoinhibition (Helbling et al., 2003; Neale and Thomas, 2017; Williamson et al., 2019). In our previous study (Zhang et al., 2020), UVR-induced growth inhibition of *P. yezoensis* was ~31%, with only about 5% being attributable to UVB, implying that UVR-induced loss of carbon fixation was mainly driven by the negative effects of UVA. However, here, we show that both UVA and UVB significantly inhibited the OEC and PSII, and the presence of UVB markedly exacerbated photoinhibition by 24% for OEC and 15% for PSII (**Figures 1, 2**). Macroalgae have evolved several adaptive mechanisms to cope with photoinhibition, by increasing NPQ and UVACs(Gao and Xu, 2008; Zheng and Gao, 2009; Zhang et al., 2020), enhancing the xanthophyll cycle (Häder et al., 2002; Aigner et al., 2017; Xie et al., 2020) as well as antioxidant systems (Sureda et al., 2008; Li et al., 2010). In the present work, the responses of photosynthetic electron transport to UVR (UVA and UVB) and the related modulations between the photosystems are

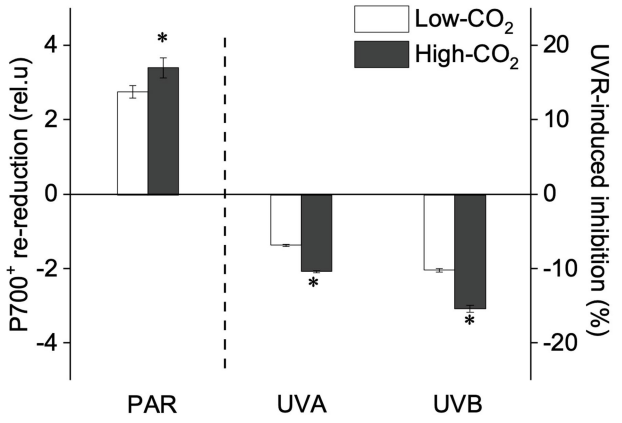

FIGURE 5 | Values (a.u., left pair of bars) and UVR-induced inhibition (%, right two pairs of bars) of CET activity (the $P700^+$ re-reduction rate) of *P. yezoensis* growing for 9 days at low (~400 μatm, open bars) and high (~1000 μatm, closed bars) CO_2 conditions. Data are means ± *SD* ($n = 3$). The symbols "*" indicates a significant ($p < 0.05$, *t*-tests) difference between the treatments in each pair.

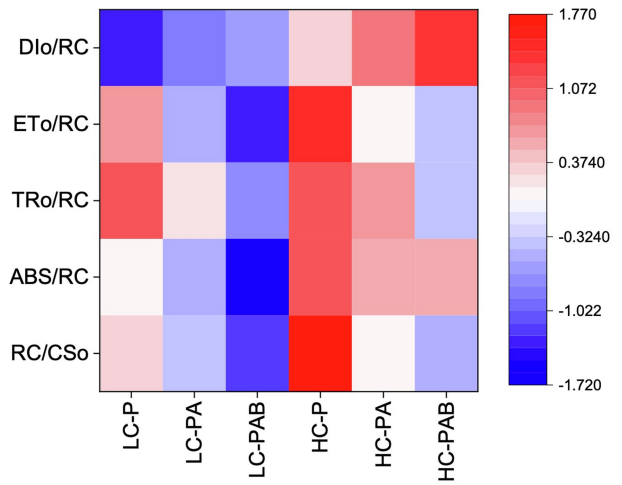

FIGURE 6 | Variations in the density of the PSII reaction centers per excited cross section (RC/CSo) and the specific energy fluxes [the absorbed flux (ABS/RC), the trapping flux (TRo/RC), the electron transport flux (ETo/RC), and the dissipated energy flux (DIo/RC)] of *P. yezoensis* growing for 9 days. LC and HC stand for low (~400 μatm) and high (~1000 μatm) CO_2 conditions, respectively. P, PA, and PAB stand for PAR only, PAR + UVA, and PAR + UVA + UVB, respectively.

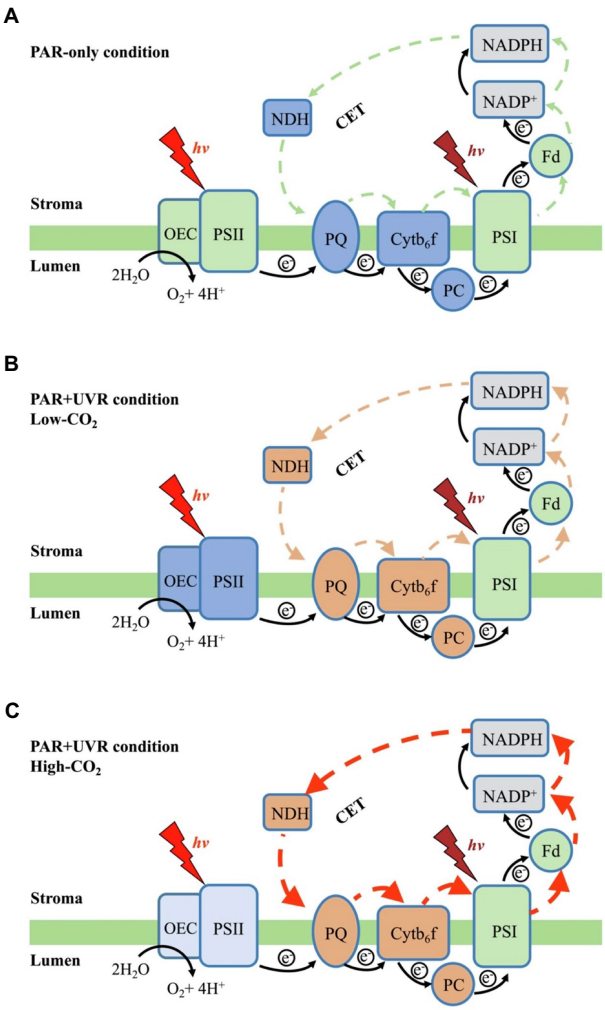

FIGURE 7 | Schematic representation of the coordination in *P. yezoensis* photosynthetic electron transport when exposed to PAR-only **(A)**, or to PAR + UVR under low-CO_2 **(B)** or high-CO_2 **(C)** concentrations. The green area indicates a normal state, the dark blue areas indicated a more severe inhibition, the light blue indicates a moderate inhibition, the orange area indicates an up-regulation, and the gray areas represent the unmeasured sites. Black arrows indicate linear electron transport flow, the colored arrows CET around PSI and the orange/red arrows indicate the up-regulation of CET.

speculated to be responsible for the observed asymmetric responses between photoinhibition and growth.

Under the influence of UVR, the deactivation of OEC would lower the efficiency of water splitting, and thus the excess excitation energy would also result in an accumulation of ROS, as well as $P680^+$ (Turcsányi and Vass, 2000; Tyystjärvi, 2008). These oxidized components can damage the D1 protein and lead to PSII photoinhibition (Zsiros et al., 2006). Our present study suggested that UVR inhibited the catalytic manganese cluster of the water-oxidizing complex, which has also been shown in other photosynthetic organisms (Vass et al., 1996; Turcsányi and Vass, 2000). Such damages are correlated with decreased O_2 evolution in the tested species of *Pyropia* (**Supplementary Table S1**, Figueroa et al., 1997; Aguilera et al., 1999, 2008). Nevertheless, such photoinhibition could lower electron transport from PSII to PSI and thus protect the intersystem electron carriers and PSI from over-reduction and alleviating PSI from photoinhibition (**Figures 4, 5, 7C**; as suggested also by Larosa et al., 2018).

In view of the impacts of increased CO_2 and OA, a number of previous studies have shown that high CO_2/OA treatments did benefit O_2 evolution and carbon assimilation in *Pyropia* spp. (**Supplementary Table S2**, Gao et al., 1991; Mercado et al.,

TABLE 2 | Two-way ANOVA for the effects of CO_2 (~400 and ~ 1,000 μatm) and irradiance quality photosynthetically active radiation (PAR, PAR + UVA and PAR + UVA + UVB) on the OEC activity (W_k), photosystem II (PSII) photochemical efficiency (F_v/F_m), intersystem electron transport efficiencies (ψ_{ET2O}, φ_{Eo}, ψ_{RE1O}, φ_{Ro}), photosystem I (PSI) activity (YI) and CET activity ($P700^+$ re-reduction).

	Irradiance quality		CO_2		Irradiance quality × CO_2	
	F	***p***	**F**	***p***	**F**	***p***
OEC activity (W_k)	45.06	<0.001	12.89	0.004	5.72	0.018
PSII photochemical efficiency (F_v/F_m)	354.51	<0.001	21.52	0.001	5.38	0.021
PSII acceptor side activity (ψ_{ET2O})	32.17	<0.001	34.66	<0.001	8.73	0.005
Quantum yield of electron transport (φ_{Eo})	7.33	0.008	49.49	<0.001	4.90	0.028
PSI donor side activity (ψ_{RE1O})	79.26	<0.001	13.24	0.003	5.28	0.023
Quantum yield for reduction of PSI acceptor side (φ_{Ro})	5.58	0.019	26.87	<0.001	4.39	0.037
Effective quantum yield of PSI (YI)	1.94	0.186	22.12	0.001	0.70	0.515
CET activity ($P700^+$ re-reduction)	23.46	<0.001	146.14	<0.001	4.63	0.032

1999; Chen et al., 2016, 2017; Zhang et al., 2020). Our results showed here that both OEC and PSII of *P. yezoensis* were less affected under PAR-only conditions, with PSI and CET being significantly up-regulated (**Figures 4, 5**). In contrast to the donor side photoinhibition induced by UVR, high-light induced photoinhibition is usually related to the over-reduction of intersystem electron carriers (Vass et al., 2005; Tyystjärvi, 2008). In the present work, the enhancement of CET would work as an alternative electron flow sink, together with the oxidized PSI, promoting the intersystem electron carriers to become oxidized, as reflected in negative inhibition (i.e., enhancement; **Figure 3**). Moreover, the up-regulated CET could also regulate the energy balance by consuming NADPH and generating ATP; $NADP^+$ can also accept more electrons transferred from PSII and then oxidize the intersystem electron carriers (as suggested by Bukhov and Carpentier, 2004; Rumeau et al., 2007; Gao and Wang, 2012; Yu et al., 2018), thus contributing to the supply of energy for carboxylation.

The interactive effects of UVR and CO_2 enrichment have been previously reported to be species-specific and UV-intensity-dependent (Gordillo et al., 2015; Ji and Gao, 2020 and references therein). A moderate UVR exposure amplified the positive effects of CO_2 and OA on the red coralline algae *Corallina officinalis* under low PAR (Yildiz et al., 2013), while the synergistic effect of incident solar UVR and OA resulted in a decrease in both photosynthesis and calcification of the coralline algae *Corallina sessilis* (Gao and Zheng, 2010). In *P. yezoensis*, our results suggested that the increased CO_2 and associated OA alleviated UVR-induced inhibition of the photosynthetic processes. Under the high-CO_2 conditions, the up-regulation of CET would generate a higher trans-thylakoid proton gradient (ΔpH), which increase NPQ and could produce ATP for carbon assimilation. Moreover, the higher ΔpH-induced acidification of the lumen could also drive a Ca^{2+}/H^+ antiport to sequester Ca^{2+} into the lumen (Krieger and Weis, 1993; Ettinger et al., 1999), and thus aid in maintaining OEC stability, as reflected by our data showing alleviation of UVR-induced OEC inhibition by high CO_2 treatments (**Figure 1**). Accordingly, OEC inhibition-induced photo-oxidative damage was significantly decreased, as evidenced by the increase of PSII photochemical efficiency (**Figure 2**), as well as the enhancement of the efficiency of the active PSII reaction center (**Figure 6**). Similar response was also observed in a tropical tree species (Huang et al., 2016) and marine angiosperm (Tan et al., 2020).

As mentioned above, the elevated DIC/CO_2 in seawater can down-regulate the CCMs, which is also true for *P. yezoensis* (Li et al., 2016). However, little attention has been paid to the effects of high PAR/UVR as well as its combined effects with high CO_2-induced OA. According to several published papers, high PAR/UVR affects the CCMs in different ways, and the effect is species-specific and light intensity dependent. For example, UVR enhanced the activity of extracellular carbonic anhydrase in *Skeletonema costatum* and thus enhanced its CCM (Wu and Gao, 2009), while a short-term exposure to UVR did not affect the inorganic carbon acquisition in *Dunaliella tertiolecta* (Beardall et al., 2002). Considering the fact that inorganic carbon acquisition is the prerequisite for carbon assimilation, which is the main photosynthetic electron sink, investigations of CCMs under high PAR/UVR and high CO_2 are expected in future studies.

Under natural conditions in sea-farming areas, macroalgae experience low pH and high CO_2 during the early morning period due to respiratory CO_2 release at night. Our results imply that the red algae *P. yezoensis* can take advantage of the concomitant changes in the pCO_2 and pH to cope with increasing UV exposure following sunrise. In addition, progressive OA associated with CO_2 rise could positively enhance the alga's photosynthesis and growth even under the influences of UVR, owing to the modulated synergy between PSII and PSI.

DATA AVAILABILITY STATEMENT

The raw data supporting the conclusions of this article will be made available by the authors, without undue reservation.

AUTHOR CONTRIBUTIONS

DZ: conceptualization, data collection and curation, data analysis, visualization, writing – original draft, and review and editing. JX: data collection and curation and review and editing. SB and JB: data analysis, formal analysis, and writing – review and editing. CZ: formal analysis and writing – review and editing. KG: conceptualization, funding acquisition, project administration, writing – original draft, and review and editing. All authors contributed to the article and approved the submitted version.

FUNDING

This study was supported by the National Natural Science Foundation (41720104005, 41721005, and 41890803).

ACKNOWLEDGMENTS

We are grateful to Xianglan Zeng and Wenyan Zhao for their technical assistance.

SUPPLEMENTARY MATERIAL

The Supplementary Material for this article can be found online at: https://www.frontiersin.org/articles/10.3389/fpls.2021.726538/full#supplementary-material

REFERENCES

Aguilera, J., Figueroa, F. L., Häder, D. P., and Jiménez, C. (2008). Photoinhibition and photosynthetic pigment reorganisation dynamics in light/darkness cycles as photoprotective mechanisms of *Porphyra umbilicalis* against damaging effects of UV radiation. *Sci. Mar.* 72, 87–97. doi: 10.3989/scimar.2008.72n187

Aguilera, J., Jiménez, C., Figueroa, F. L., Lebert, M., and Häder, D. P. (1999). Effect of ultraviolet radiation on thallus absorption and photosynthetic pigments in the red alga *Porphyra umbilicalis*. *J. Photochem. Photobiol. B* 48, 75–82. doi: 10.1016/S1011-1344(99)00015-9

Aigner, S., Holzinger, A., Karsten, U., and Kranner, I. (2017). The freshwater red alga *Batrachospermum turfosum* (Florideophyceae) can acclimate to a wide range of light and temperature conditions. *Eur. J. Phycol.* 52, 238–249. doi: 10.1080/09670262.2016.1274430

Aline, T., Atkinson, M. J., and Christopher, L. (2006). Effects of elevated pCO_2 on epilithic and endolithic metabolism of reef carbonates. *Glob. Chang. Biol.* 12, 2200–2208. doi: 10.1111/j.1365-2486.2006.01249.x

Andría, J. R., Brun, F. G., Pérez-Lloréns, J. L., and Vergara, J. J. (2001). Acclimation responses of *Gracilaria* sp. (Rhodophyta) and *Enteromorpha intestinalis* (Chlorophyta) to changes in the external inorganic carbon concentration. *Bot. Mar.* 44, 361–370. doi: 10.1515/BOT.2001.046

Andría, J., Vergara, J., and Pérez-Lloréns, J. L. (1999). Biochemical responses and photosynthetic performance of *Gracilaria* sp. (Rhodophyta) from Cádiz, Spain, cultured under different inorganic carbon and nitrogen levels. *Eur. J. Phycol.* 34, 497–504.

Beardall, J., Heraud, P., Roberts, S., Shelly, K., and Stojkovic, S. (2002). Effects of UV-B radiation on inorganic carbon acquisition by the marine microalga *Dunaliella tertiolecta* (Chlorophyceae). *Phycologia* 41, 268–272. doi: 10.2216/i0031-8884-41-3-268.1

Beer, S., and Koch, E. (1996). Photosynthesis of marine macroalgae and seagrasses in globally changing CO_2 environments. *Mar. Ecol. Prog. Ser.* 141, 199–204. doi: 10.3354/meps141199

Blouin, N. A., Brodie, J. A., Grossman, A. C., Xu, P., and Brawley, S. H. (2011). *Porphyra*: a marine crop shaped by stress. *Trends Plant Sci.* 16, 29–37. doi: 10.1016/j.tplants.2010.10.004

Büdenbender, J., Riebesell, U., and Form, A. (2011). Calcification of the Arctic coralline red algae *Lithothamnion glaciale* in response to elevated CO_2. *Mar. Ecol. Prog. Ser.* 441, 79–87. doi: 10.3354/meps09405

Bukhov, N., and Carpentier, R. (2004). Alternative photosystem I-driven electron transport routes: mechanisms and functions. *Photosynth. Res.* 82, 17–33. doi: 10.1023/B:PRES.0000040442.59311.72

Chen, B., Zou, D., and Ma, J. (2016). Interactive effects of elevated CO_2 and nitrogen–phosphorus supply on the physiological properties of *Pyropia haitanensis* (Bangiales, Rhodophyta). *J. Appl. Phycol.* 28, 1235–1243. doi: 10.1007/s10811-015-0628-z

Chen, B., Zou, D., and Yang, Y. (2017). Increased iron availability resulting from increased CO_2 enhances carbon and nitrogen metabolism in the economical marine red macroalga *Pyropia haitanensis* (Rhodophyta). *Chemosphere* 173, 444–451. doi: 10.1016/j.chemosphere.2017.01.073

Eberhard, S., Finazzi, G., and Wollman, F. A. (2008). The dynamics of photosynthesis. *Annu. Rev. Genet.* 42, 463–515. doi: 10.1146/annurev.genet.42.110807.091452

Ettinger, W. F., Clear, A. M., Fanning, K. J., and Peck, M. L. (1999). Identification of a Ca^{2+}/H^+ antiport in the plant chloroplast thylakoid membrane. *Plant Physiol.* 119, 1379–1386. doi: 10.1104/pp.119.4.1379

Figueroa, F. L., Salles, S., Aguilera, J., Jiménez, C., Mercado, J., Viñegla, B., et al. (1997). Effects of solar radiation on photoinhibition and pigmentation in the red alga *Porphyra leucosticta*. *Mar. Ecol. Prog. Ser.* 151, 81–90. doi: 10.3354/meps151081

Gao, K., Aruga, Y., Asada, K., Ishihara, T., Akano, T., and Kiyohara, M. (1991). Enhanced growth of the red alga *Porphyra yezoensis* Ueda in high CO_2 concentrations. *J. Appl. Phycol.* 3, 355–362. doi: 10.1007/BF02392889

Gao, K., Aruga, Y., Asada, K., Ishihara, T., Akano, T., and Kiyohara, M. (1993). Calcification in the articulated coralline alga *Corallina pilulifera*, with special reference to the effect of elevated CO_2 concentration. *Mar. Biol.* 117, 129–132. doi: 10.1007/BF00346434

Gao, K., Beardall, J., Häder, D. P., Hall-Spencer, J. M., Gao, G., and Hutchins, D. A. (2019). Effects of ocean acidification on marine photosynthetic organisms under the concurrent influences of warming, UV radiation, and deoxygenation. *Front. Mar. Sci.* 6:322. doi: 10.3389/fmars.2019.00322

Gao, K., Guan, W., and Helbling, E. W. (2007). Effects of solar ultraviolet radiation on photosynthesis of the marine red tide alga *Heterosigma akashiwo* (Raphidophyceae). *J. Photochem. Photobiol. B* 86, 140–148. doi: 10.1016/j.jphotobiol.2006.05.007

Gao, S., Niu, J., Chen, W., Wang, G., Xie, X., Pan, G., et al. (2013). The physiological links of the increased photosystem II activity in moderately desiccated *Porphyra haitanensis* (Bangiales, Rhodophyta) to the cyclic electron flow during desiccation and re-hydration. *Photosynth. Res.* 116, 45–54. doi: 10.1007/s11120-013-9892-4

Gao, S., and Wang, G. (2012). The enhancement of cyclic electron flow around photosystem I improves the recovery of severely desiccated *Porphyra yezoensis* (Bangiales, Rhodophyta). *J. Exp. Bot.* 63, 4349–4358. doi: 10.1093/jxb/ers082

Gao, K., and Xu, J. (2008). Effects of solar UV radiation on diurnal photosynthetic performance and growth of *Gracilaria lemaneiformis* (Rhodophyta). *Eur. J. Phycol.* 43, 297–307. doi: 10.1080/09670260801986837

Gao, K., and Zheng, Y. (2010). Combined effects of ocean acidification and solar UV radiation on photosynthesis, growth, pigmentation and calcification of the coralline alga *Corallina sessilis* (Rhodophyta). *Glob. Chang. Biol.* 16, 2388–2398. doi: 10.1111/j.1365-2486.2009.02113.x

Gordillo, F. J., Aguilera, J., Wiencke, C., and Jiménez, C. (2015). Ocean acidification modulates the response of two Arctic kelps to ultraviolet radiation. *J. Plant Physiol.* 173, 41–50. doi: 10.1016/j.jplph.2014.09.008

Guisse, B., Srivastava, A., and Strasser, R. (1995). The polyphasic rise of the chlorophyll *a* fluorescence (OKJIP) in heat-stressed leaves. *Arch. Sci.* 48, 147–160. doi: 10.5169/SEALS-740252

Häder, D. P., and Barnes, P. W. (2019). Comparing the impacts of climate change on the responses and linkages between terrestrial and aquatic ecosystems. *Sci. Total Environ.* 682, 239–246. doi: 10.1016/j.scitotenv.2019.05.024

Häder, D. P., Lebert, M., Sinha, R. P., Barbieri, E. S., and Helbling, E. W. (2002). Role of protective and repair mechanisms in the inhibition of photosynthesis in marine macroalgae. *Photochem. Photobiol. Sci.* 1, 809–814. doi: 10.1039/B206152J

Helbling, E. W., Gao, K., Gonçalves, R. J., Wu, H., and Villafañe, V. E. (2003). Utilization of solar UV radiation by coastal phytoplankton assemblages off SE China when exposed to fast mixing. *Mar. Ecol. Prog. Ser.* 259, 59–66. doi: 10.3354/meps259059

Huang, W., Yang, Y. J., Hu, H., Zhang, S. B., and Cao, K. F. (2016). Evidence for the role of cyclic electron flow in photoprotection for oxygen-evolving complex. *J. Plant Physiol.* 194, 54–60. doi: 10.1016/j.jplph.2016.02.016

Hurd, C. L., Beardall, J., Comeau, S., Cornwall, C. E., Havenhand, J. N., Munday, P. L., et al. (2020). Ocean acidification as a multiple driver: how interactions between changing seawater carbonate parameters affect marine life. *Mar. Freshw. Res.* 71, 263–274. doi: 10.1071/MF19267

IPCC (2014) in *Climate Change 2014: Synthesis Report. Contribution of Working Groups I, II and III to the Fifth Assessment Report of the Intergovernmental Panel on Climate Change*. eds. Core Writing Team, R. K. Pachauri and L. A. Meyer (Geneva, Switzerland: IPCC), 151.

Ji, Y., and Gao, K. (2020). Effects of climate change factors on marine macroalgae: a review. *Adv. Mar. Biol.* 88, 91–136. doi: 10.1016/bs.amb.2020.11.001

Jiang, H., Gao, K., and Helbling, E. W. (2007). Effects of solar UV radiation on germination of conchospores and morphogenesis of sporelings in *Porphyra haitanensis* (Rhodophyta). *Mar. Biol.* 151, 1751–1759. doi: 10.1007/s00227-007-0632-1

Klughammer, C., and Schreiber, U. (1994). An improved method, using saturating light pulses, for the determination of photosystem I quantum yield via $P700^+$-absorbance changes at 830 nm. *Planta* 192, 261–268. doi: 10.1007/BF01089043

Korbee, N., Navarro, N. P., García-Sánchez, M., Celis-Plá, P. S. M., Quintano, E., Copertino, M. D. S., et al. (2014). A novel in situ system to evaluate the effect of high CO_2 on photosynthesis and biochemistry of seaweeds. *Aquat. Biol.* 22, 245–259. doi: 10.3354/ab00594

Krieger, A., and Weis, E. (1993). The role of calcium in the pH-dependent control of photosystem II. *Photosynth. Res.* 37, 117–130. doi: 10.1007/BF02187470

Larosa, V., Meneghesso, A., La Rocca, N., Steinbeck, J., Hippler, M., Szabò, I., et al. (2018). Mitochondria affect photosynthetic electron transport and photosensitivity in a green alga. *Plant Physiol.* 176, 2305–2314. doi: 10.1104/pp.17.01249

Li, X., Xu, J., and He, P. (2016). Comparative research on inorganic carbon acquisition by the macroalgae *Ulva prolifera* (Chlorophyta) and *Pyropia yezoensis* (Rhodophyta). *J. Appl. Phycol.* 28, 491–497. doi: 10.1007/s10811-015-0603-8

Li, L., Zhao, J., and Tang, X. (2010). Ultraviolet irradiation induced oxidative stress and response of antioxidant system in an intertidal macroalgae *Corallina officinalis* L. *J. Environ. Sci.* 22, 716–722. doi: 10.1016/S1001-0742(09)60168-6

Lu, X., Huan, L., Gao, S., Gao, S. (2016). NADPH from the oxidative pentose phosphate pathway drives the operation of cyclic electron flow around photosystem I in high-intertidal macroalgae under severe salt stress *Physiol. Plantarum.* 156, 397–406. doi: 10.1111/ppl.12383

Martin, S., and Gattuso, J. P. (2009). Response of Mediterranean coralline algae to ocean acidification and elevated temperature. *Glob. Chang. Biol.* 15, 2089–2100. doi: 10.1111/j.1365-2486.2009.01874.x

Mercado, J. M., Javier, F., Gordillo, L., Niell, F. X., and Figueroa, F. L. (1999). Effects of different levels of CO_2 on photosynthesis and cell components of the red alga *Porphyra leucosticta*. *J. Appl. Phycol.* 11, 455–461. doi: 10.1023/A:1008194223558

Miyake, C. (2010). Alternative electron flows (water–water cycle and cyclic electron flow around PSI) in photosynthesis: molecular mechanisms and physiological functions. *Plant Cell Physiol.* 51, 1951–1963. doi: 10.1093/pcp/pcq173

Neale, R. E., Barnes, P. W., Robson, T. M., Neale, P. J., Williamson, C. E., Zepp, R. G., et al. (2021). Environmental effects of stratospheric ozone depletion, UV radiation, and interactions with climate change: UNEP environmental effects assessment panel, update 2020. *Photochem. Photobiol. Sci.* 20, 1–67. doi: 10.1007/s43630-020-00001-x

Neale, P. J., and Thomas, B. C. (2017). Inhibition by ultraviolet and photosynthetically available radiation lowers model estimates of depth-integrated picophytoplankton photosynthesis: global predictions for *Prochlorococcus* and *Synechococcus*. *Glob. Chang. Biol.* 23, 293–306. doi: 10.1111/gcb.13356

Neubauer, C., and Schreiber, U. (1987). The polyphasic rise of chlorophyll fluorescence upon onset of strong continuous illumination: I. saturation characteristics and partial control by the photosystem II acceptor side. *Zeitschrift für Naturforschung C* 42, 1246–1254. doi: 10.1515/znc-1987-11-1217

Niu, J., Feng, J., Xie, X., Gao, S., and Wang, G. (2016). Involvement of cyclic electron flow in irradiance stress responding and its potential regulation of the mechanisms in *Pyropia yezoensis*. *Chin. J. Oceanol. Limnol.* 34, 730–739. doi: 10.1007/s00343-016-4236-9

Pierrot, D., Lewis, E., and Wallace, D. W. R. (2006). MS Excel program developed for CO_2 system calculations. ORNL/CDIAC-105a. *Environ. Sci.* doi: 10.3334/CDIAC/otg.CO2SYS_XLS_CDIAC105a

Raven, J. A., Beardall, J., and Giordano, M. (2014). Energy costs of carbon dioxide concentrating mechanisms in aquatic organisms. *Photosynth. Res.* 121, 111–124. doi: 10.1007/s11120-013-9962-7

Rumeau, D., Peltier, G., and Cournac, L. (2007). Chlororespiration and cyclic electron flow around PSI during photosynthesis and plant stress response. *Plant Cell Environ.* 30, 1041–1051. doi: 10.1111/j.1365-3040.2007.01675.x

Semesi, I. S., Kangwe, J., and Björk, M. (2009). Alterations in seawater pH and CO_2 affect calcification and photosynthesis in the tropical coralline alga, *Hydrolithon* sp. (Rhodophyta). *Estuar. Coast. Shelf Sci.* 84, 337–341. doi: 10.1016/j.ecss.2009.03.038

Strasser, R. J. (1981). "The grouping model of plant photosynthesis: heterogeneity of photosynthetic units in thylakoids," in *Photosynthesis III. Structure and Molecular Organisation of the Photosynthetic Apparatus*. ed. G. Akoyonoglou (Philadelphia: Balaban International Science Services), 727–737.

Strasser, B. J., and Strasser, R. J. (1995). "Measuring fast fluorescence transients to address environmental questions: The JIP-test," in *Photosynthesis: From Light to Biosphere*. ed. Mathis. Vol. 5 ed (Netherlands: Kluwer Academic Publishers), 977–980.

Strasser, R. J., Tsimilli-Michael, M., and Srivastava, A. (2004). "Analysis of the chlorophyll *a* fluorescence transient," in *Chlorophyll a Fluorescence*. eds. G. C. Papageorgiou and Govindjee (Dordrecht: Springer), 321–362.

Su, H. N., Xie, B. B., Zhang, X. Y., Zhou, B. C., and Zhang, Y. Z. (2010). The supramolecular architecture, function, and regulation of thylakoid membranes in red algae: an overview. *Photosynth. Res.* 106, 73–87. doi: 10.1007/s11120-010-9560-x

Suárez-Álvarez, S., Gómez-Pinchetti, J. L., and García-Reina, G. (2012). Effects of increased CO_2 levels on growth, photosynthesis, ammonium uptake and cell composition in the macroalga *Hypnea spinella* (Gigartinales, Rhodophyta). *J. Appl. Phycol.* 24, 815–823. doi: 10.1007/s10811-011-9700-5

Sureda, A., Box, A., Terrados, J., Deudero, S., and Pons, A. (2008). Antioxidant response of the seagrass Posidonia oceanica when epiphytized by the invasive macroalgae *Lophocladia lallemandii*. *Mar. Environ. Res.* 66, 359–363. doi: 10.1016/j.marenvres.2008.05.009

Tan, Y., Zhang, Q. S., Zhao, W., Liu, Z., Ma, M. Y., Zhong, M. Y., et al. (2020). The highly efficient NDH-dependent photosystem I cyclic electron flow pathway in the marine angiosperm *Zostera marina*. *Photosynth. Res.* 144, 49–62. doi: 10.1007/s11120-020-00732-z

Turcsányi, E., and Vass, I. (2000). Inhibition of photosynthetic electron transport by UV-A radiation targets the photosystem II complex. *Photochem. Photobiol.* 72, 513–520. doi: 10.1562/0031-8655(2000)072<0513:IOPETB>2.0.CO;2

Tyystjärvi, E. (2008). Photoinhibition of photosystem II and photodamage of the oxygen evolving manganese cluster. *Coord. Chem. Rev.* 252, 361–376. doi: 10.1016/j.ccr.2007.08.021

Vass, I., Sass, L., Spetea, C., Bakou, A., Ghanotakis, D. F., and Petrouleas, V. (1996). UV-B-induced inhibition of photosystem II electron transport studied by EPR and chlorophyll fluorescence. Impairment of donor and acceptor side components. *Biochemistry* 35, 8964–8973. doi: 10.1021/bi9530595

Vass, I., Szilárd, A., and Sicora, C. (2005). "Adverse effects of UV-B light on the structure and function of the photosynthetic apparatus," in *Handbook of Photosynthesis*. ed. Mohammad Pessarakli (Boca Raton, FL, USA: Francis and Taylor publisher), 43–63.

Viñegla, B., Segovia, M., and Figueroa, F. L. (2006). Effect of artificial UV radiation on carbon and nitrogen metabolism in the macroalgae *Fucus spiralis* L. and *Ulva olivascens* Dangeard. *Hydrobiologia* 560, 31–42. doi: 10.1007/s10750-005-1097-1

Williamson, C. E., Neale, P. J., Hylander, S., Rose, K. C., Figueroa, F. L., Robinson, S. A., et al. (2019). The interactive effects of stratospheric ozone depletion, UV radiation, and climate change on aquatic ecosystems. *Photochem. Photobiol. Sci.* 18, 717–746. doi: 10.1039/c8pp90062k

Wu, H., and Gao, K. (2009). Ultraviolet radiation stimulated activity of extracellular carbonic anhydrase in the marine diatom *Skeletonema costatum*. *Funct. Plant Biol.* 36, 137–143. doi: 10.1071/FP08172

Xie, X., Lu, X., Wang, L., He, L., and Wang, G. (2020). High light intensity increases the concentrations of β-carotene and zeaxanthin in marine red macroalgae. *Algal Res.* 47:101852. doi: 10.1016/j.algal.2020.101852

Xu, J., and Gao, K. (2008). Growth, pigments, UV-absorbing compounds and agar yield of the economic red seaweed *Gracilaria lemaneiformis* (Rhodophyta) grown at different depths in the coastal waters of the South China Sea. *J. Appl. Phycol.* 20, 681–686. doi: 10.1007/s10811-007-9247-7

Xu, J., and Gao, K. (2010). UV-A enhanced growth and UV-B induced positive effects in the recovery of photochemical yield in *Gracilaria lemaneiformis* (Rhodophyta). *J. Photochem. Photobiol. B* 100, 117–122. doi: 10.1016/j.jphotobiol.2010.05.010

Xu, J., and Gao, K. (2012). Future CO_2-induced ocean acidification mediates the physiological performance of a green tide alga. *Plant Physiol.* 160, 1762–1769. doi: 10.1104/pp.112.206961

Yamori, W., Sakata, N., Suzuki, Y., Shikanai, T., and Makino, A. (2011). Cyclic electron flow around photosystem I via chloroplast NAD (P) H dehydrogenase (NDH) complex performs a significant physiological role during photosynthesis and plant growth at low temperature in rice. *Plant J.* 68, 966–976. doi: 10.1111/j.1365-313X.2011.04747.x

Yildiz, G., Hofmann, L. C., Bischof, K., and Dere, Ş. (2013). Ultraviolet radiation modulates the physiological responses of the calcified rhodophyte *Corallina officinalis* to elevated CO_2. *Bot. Mar.* 56, 161–168. doi: 10.1515/bot-2012-0216

Yu, B., Niu, J., Feng, J., Xu, M., Xie, X., Gu, W., et al. (2018). Regulation of ferredoxin-$NADP^+$ oxidoreductase to cyclic electron transport in high salinity stressed *Pyropia yezoensis*. *Front. Plant Sci.* 9:1092. doi: 10.3389/fpls.2018.01092

Zhang, D., Xu, J., Bao, M., Yan, D., Beer, S., Beardall, J., et al. (2020). Elevated CO_2 concentration alleviates UVR-induced inhibition of photosynthetic light reactions and growth in an intertidal red macroalga. *J. Photochem. Photobiol. B* 213:112074. doi: 10.1016/j.jphotobiol.2020.112074

Zheng, Y., and Gao, K. (2009). Impacts of solar UV radiation on the photosynthesis, growth, and UV-absorbing compounds in *Gracilaria lemaneiformis* (Rhodophyta) grown at different nitrate concentrations. *J. Phycol.* 45, 314–323. doi: 10.1111/j.1529-8817.2009.00654.x

Zou, D. (2005). Effects of elevated atmospheric CO_2 on growth, photosynthesis and nitrogen metabolism in the economic brown seaweed, *Hizikia fusiforme* (Sargassaceae, Phaeophyta). *Aquaculture* 250, 726–735. doi: 10.1016/j.aquaculture.2005.05.014

Zou, D., and Gao, K. (2005). Ecophysiological characteristics of four intertidal marine macroalgae during emersion along Shantou coast of China, with a special reference to the relationship of photosynthesis and CO_2. *Acta Oceanol. Sin.* 24, 105–113.

Zou, D., Gao, K., and Xia, J. (2003). Photosynthetic utilization of inorganic carbon in the economic brown alga, *Hizikia Fusiforme* (Sargassaceae) from the South China Sea. *J. Phycol.* 39, 1095–1100. doi: 10.1111/j.0022-3646.2003.03-038.x

Zsiros, O., Allakhverdiev, S. I., Higashi, S., Watanabe, M., Nishiyama, Y., and Murata, N. (2006). Very strong UV-A light temporally separates the photoinhibition of photosystem II into light-induced inactivation and repair. *Biochim. Biophys. Acta* 1757, 123–129. doi: 10.1016/j.bbabio.2006.01.004

Conflict of Interest: The authors declare that the research was conducted in the absence of any commercial or financial relationships that could be construed as a potential conflict of interest.

Publisher's Note: All claims expressed in this article are solely those of the authors and do not necessarily represent those of their affiliated organizations, or those of the publisher, the editors and the reviewers. Any product that may be evaluated in this article, or claim that may be made by its manufacturer, is not guaranteed or endorsed by the publisher.

frontiers in Plant Science

ORIGINAL RESEARCH
published: 01 October 2021
doi: 10.3389/fpls.2021.678259

Seasonality and Species Specificity of Submerged Macrophyte Biomass in Shallow Lakes Under the Influence of Climate Warming and Eutrophication

Haoping Wu [1,2,3], *Beibei Hao* [1,2,3], *Hyunbin Jo* [3,4] *and Yanpeng Cai* [1,2*]

[1] *Guangdong Provincial Key Laboratory of Water Quality Improvement and Ecological Restoration for Watersheds, Institute of Environmental and Ecological Engineering, Guangdong University of Technology, Guangzhou, China,* [2] *Southern Marine Science and Engineering Guangdong Laboratory (Guangzhou), Guangzhou, China,* [3] *Department of Bioscience, Aarhus University, Silkeborg, Denmark,* [4] *Institute for Environment and Energy, Pusan National University, Busan, South Korea*

OPEN ACCESS

Edited by:
Eric Marechal,
UMR5168 Laboratoire de Physiologie Cellulaire Vegetale (LPCV), France

Reviewed by:
Xiaoke Zhang,
Anqing Normal University, China
Alberto Amato,
CEA Grenoble, France

****Correspondence:***
Yanpeng Cai
yanpeng.cai@gdut.edu.cn

Specialty section:
This article was submitted to Marine and Freshwater Plants, a section of the journal Frontiers in Plant Science

Received: *09 March 2021*
Accepted: *31 August 2021*
Published: *01 October 2021*

Citation:
Wu H, Hao B, Jo H and Cai Y (2021) Seasonality and Species Specificity of Submerged Macrophyte Biomass in Shallow Lakes Under the Influence of Climate Warming and Eutrophication. Front. Plant Sci. 12:678259. doi: 10.3389/fpls.2021.678259

Climate warming and eutrophication caused by anthropogenic activities strongly affect aquatic ecosystems. Submerged macrophytes usually play a key role in shallow lakes and can maintain a stable clear state. It is extremely important to study the effects of climate warming and eutrophication on the growth of submerged macrophytes in shallow lakes. However, the responses of submerged macrophytes to climate warming and eutrophication are still controversial. Additionally, the understanding of the main pathways impacting submerged macrophytes remains to be clarified. In addition, the influence of seasonality on the growth responses of submerged macrophytes to climate warming and eutrophication requires further elucidation. In this study, we conducted a series of mesocosm experiments with four replicates across four seasons to study the effects of rising temperature and nutrient enrichment on the biomass of two submerged macrophytes, *Potamogeton crispus* and *Elodea canadensis*. Our results demonstrated the seasonality and species specificity of plant biomass under the influence of climate warming and eutrophication, as well as the main explanatory factors in each season. Consistent with the seasonal results, the overall results showed that *E. canadensis* biomass was directly increased by rising temperature rather than by nutrient enrichment. Conversely, the overall results showed that *P. crispus* biomass was indirectly reduced by phosphorus enrichment *via* the strengthening of competition among primary producers. Distinct physiological and morphological traits may induce species-specific responses of submerged macrophytes to climate warming and eutrophication, indicating that further research should take interspecies differences into account.

Keywords: climate warming, eutrophication, submerged macrophyte, *Potamogeton crispus*, *Elodea canadensis*

INTRODUCTION

Because of anthropogenic activities, rapid changes, such as climate change and pollution have exerted strong stress on aquatic ecosystems globally (IPCC, 2014; Steffen et al., 2015). Climate warming resulting from accelerated urbanization has increased the water temperature of the hydrosphere over recent decades, and it is expected to continue to increase over this century (IPCC, 2014). On the other hand, the rapid development of agriculture and industrialization has led to massive inputs of nutrients, especially nitrogen (N) and phosphorus (P), in aquatic environments (Tilman et al., 2001). It has been suggested that the alteration of temperature and nutrient availability will change the ecosystem structure and thereafter threaten the ecological functioning of shallow lakes (Liboriussen et al., 2005; Özkan et al., 2010; Kosten et al., 2012; Hao et al., 2020). Submerged macrophytes are an important component in aquatic ecosystems and usually play a vital role in the ecological functioning of shallow lakes (Jeppesen et al., 2012; Hao et al., 2017). It is well-known that submerged macrophytes can maintain clear water by regulating nutrient retention and cycling in aquatic ecosystems (Jeppesen et al., 2012; Wu et al., 2021).

However, the growth of submerged macrophytes is sensitive to climate warming and eutrophication. Increasing temperatures within an optimal range can usually enhance the activity of enzymes and, therefore, promote photosynthesis in submerged macrophytes (Olesen and Madsen, 2000; Riis et al., 2012). Simultaneously, rising temperatures can accelerate dissimilation processes, such as respiration and senescence, and when dissimilation overtakes assimilation, a decline in the biomass of submerged macrophytes occurs (Lee et al., 2007; Hao et al., 2018). Although submerged macrophytes can take up N and P from the water column, satisfy metabolic demand, and stimulate plant growth (Elser et al., 2007; Kaldy, 2014), excessive nutrient loading in water may lead to algal blooms and then shift clear water to a stable turbid state; ultimately, competition with phytoplankton may induce the degradation of macrophytes (Jeppesen et al., 2012; Zhang et al., 2020). Indeed, both climate change and eutrophication usually arise simultaneously in natural systems (Cross et al., 2015). Previous studies have suggested that climate warming and eutrophication can interact to affect the biomass of aquatic plants (Cross et al., 2015; Zhang et al., 2020), while several studies have argued that the effects of temperature and nutrients on the growth of submerged macrophytes are not synergistic (Kaldy, 2014; Trochine et al., 2014). Thus, the effects of climate warming and eutrophication on the biomass of submerged macrophytes remain to be clarified.

Climate warming and eutrophication can directly affect the growth of submerged macrophytes. For example, Zhang et al. (2016, 2019) found that temperature and nutrient availability could significantly affect the growth of submerged macrophytes by altering individual ecological stoichiometry. However, Hao et al. (2018) and Jones et al. (2002) suggested that temperature and nutrients might regulate the growth of submerged macrophytes through the indirect pathway by which rising temperature and nutrient enrichment could induce environmental stress and then cause a decline in the biomass of submerged macrophytes. Furthermore, rising temperature and nutrient enrichment could change abiotic variables, such as dissolved oxygen (DO) and pH, and, thus, influence submerged macrophytes, because DO is necessary for respiration, and pH can determine the availability of inorganic carbon (C) for submerged macrophytes (Jones et al., 2002; Zhang et al., 2015; Dülger et al., 2017; Hao et al., 2020). On the other hand, temperature and nutrients could affect submerged macrophytes through effects on biotic variables, such as the biomass of phytoplankton, periphyton, and zooplankton, since stress from the same trophic level and higher trophic levels may threaten the growth of submerged macrophytes (Jones et al., 2002; Ventura et al., 2008; Hao et al., 2018; Matsuzaki et al., 2018; Yuan and Pollard, 2018). Previous studies have been commonly limited to either direct pathways or indirect pathways but have failed to determine the main pathway impacting the growth of submerged macrophytes, as well as the relative contributions of biotic and abiotic variables to the variation in the biomass of submerged macrophytes.

Taking the life history of an organism into account, seasonality may play a key role in the growth of submerged macrophytes under the influence of rising temperature and nutrient enrichment (Staehr and Sand-Jensen, 2006; Trochine et al., 2014; Zhang et al., 2019; Fu et al., 2020; Hao et al., 2020). For example, Riis et al. (2012) suggested that some submerged macrophyte species were controlled by high summer temperatures rather than low winter temperatures. Hao et al. (2020) found that low temperatures and lower light availability in winter created a harsh environment for primary producers and stressed changes in explanatory variables. However, the experimental cycle in similar studies has usually lasted only dozens of days or one season (Olesen and Madsen, 2000; Riis et al., 2012; Velthuis et al., 2017; Hao et al., 2018; Zhang et al., 2020), which has precluded observation of the response of submerged macrophytes to rising temperature and nutrient enrichment based on the seasonal scale, as well as determination of the main explanatory variables in each season.

Here, we established four mesocosm experiments in four seasons to study the effects of climate warming and eutrophication on the growth of submerged macrophytes at the seasonal scale. Two nutrient levels (enriched and unenriched) varied with three temperature scenarios (ambient, IPCC A2, and A2 + 50%) were applied to our mesocosm system. To better simulate the natural system and seasonality, the temperature gradient was set up on the basis of ambient temperature, and the increment in modeled temperature above ambient temperature in each season was different following IPCC climate scenario A2; therefore, the dynamics of modeled temperature varied with the ambient temperature in each season. Two dominant species of submerged macrophytes colonized naturally in most of the unenriched tanks, namely, *Potamogeton crispus* and *Elodea canadensis*, were selected as target species for our experiment. *P. crispus* is a Euro-Asiatic species, while *E. canadensis* originated from North America and has developed into the most common invasive species in Europe (Nichols and Shaw, 1986; Bolduan et al., 1994; Pilon et al., 2003; de Winton et al., 2009; Hussner, 2012; Riis et al., 2012; Wang et al., 2013; Zhang et al., 2015). Life

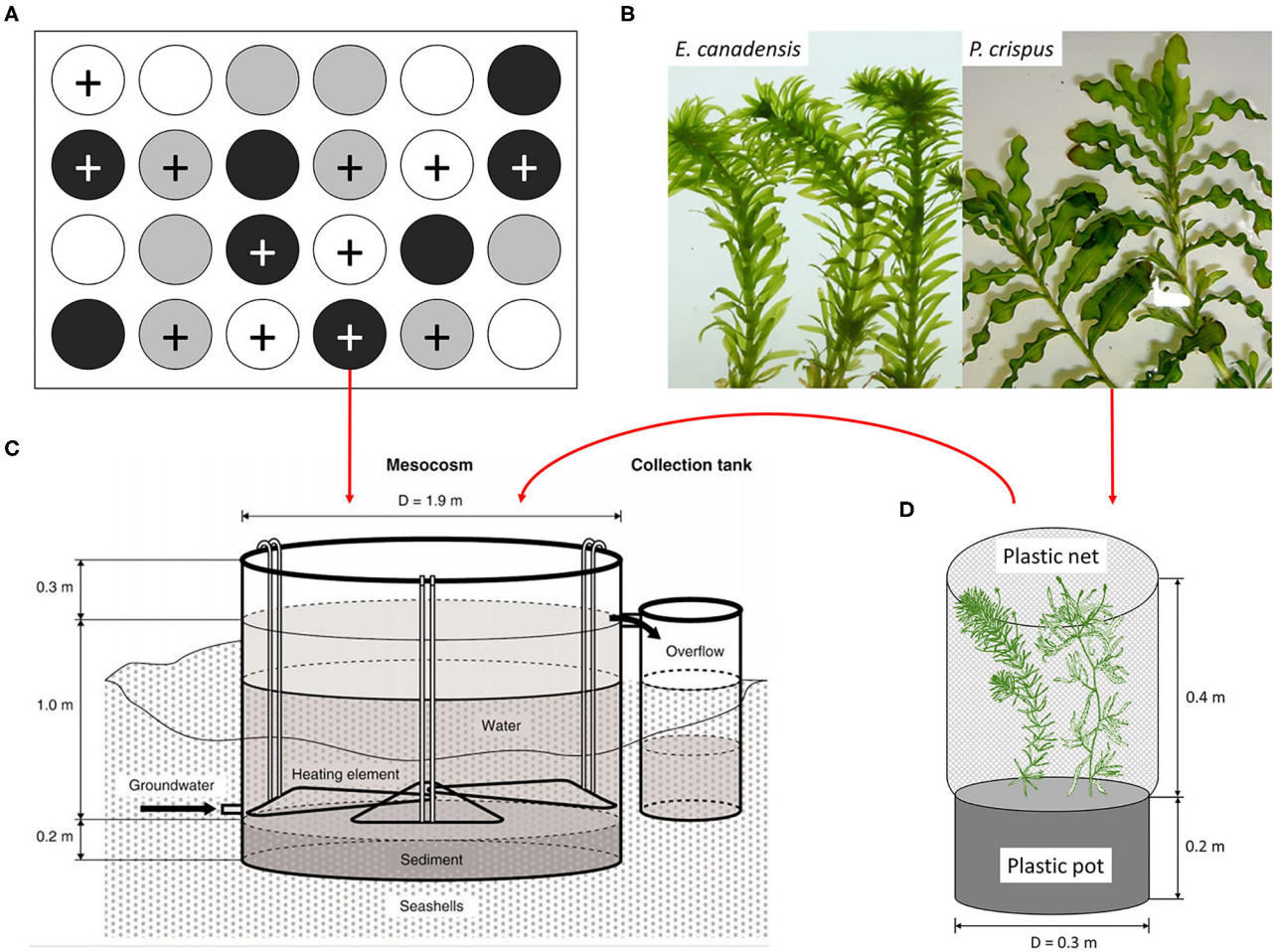

FIGURE 1 | (A) Diagram of the experimental design, **(B)** the experimental plant materials, **(C)** the mesocosm tank equipped with a flow-through system, and **(D)** the plastic pot planted with two individual plants, based on Liboriussen et al. (2005) and Trochine et al. (2014). The experimental design includes 24 tanks with two nutrient levels, unenriched (no symbol) and enriched (+ symbol), and three temperature scenarios, ambient (white), warming (gray), and enhanced warming (black).

history and morphological structure are conspicuously distinct between *P. crispus* and *E. canadensis* (Nichols and Shaw, 1986; Hao et al., 2020). Specifically, *P. crispus* has a thick branching stem accompanied with sparse strip leaves, while *E. canadensis* has a thin branching stem accompanied by dense whorled leaves (**Figure 1**). Additionally, *P. crispus* germinates in winter and blooms in summer, whereas *E. canadensis* grows faster in summer and spreads in autumn. Both two species have the same growth form (elodeid) and are equivalent competitors possess multiple adaptations, such as rapid propagation ability, opportunistic nature for nutrient acquisition, high tolerance for low temperature, high photosynthetic efficiency, which allow them to maintain stable coexistence in various regions (Nichols and Shaw, 1986; Vestergaard and Sand-Jensen, 2000; Burson et al., 2019). We hypothesized that the biomass of submerged macrophytes would be directly and indirectly affected by elevated temperature and nutrient enrichment, and that seasonality would contribute to the variance in plant biomass to a certain extent.

MATERIALS AND METHODS

Mesocosm Establishment

A mesocosm system, including 24 experimental tanks (**Figure 1**; diameter: 1.9 m, water depth: 1 m), was set up in a lowland valley in Central Jutland, Denmark (56° 14′N, 9°31′E) and has been running continuously since August 2003 (Liboriussen et al., 2005). These mesocosms simulate natural shallow lake ecosystems and have been used to study the long-term impacts of climate warming and eutrophication. Each tank was equipped with a flow-through system that automatically adds tap water and removes excess surface water. An experimental design consisting of three temperature scenarios and two nutrient levels (four replicates for each treatment) was applied to the mesocosm system. Briefly, eight tanks were heated according to IPCC climate scenario A2 (warming), eight tanks were heated according to A2 + 50% (enhanced warming), and eight tanks were unheated (ambient) and used as a reference. The IPCC climate scenarios A2 and A2 + 50% were formulated based on

regional downscaling (over five 25 km × 25 km grid cells) to the region and applied as the low- and high-warming scenarios, respectively. According to the IPCC, warming was calculated as the average air temperature increase in one particular month with respect to a reference period (1961–1990) and the modeled temperatures in the same month from 2071 to 2100 (Liboriussen et al., 2005). Additionally, climate scenario A2 takes seasonal variation into account, and the modeled temperatures are 2.74, 3.84, 3.76, and 2.76°C higher than the ambient temperatures in May, August, November, and February, respectively. Although IPCC scenarios are based on air temperature, water temperature is used as a surrogate for air temperature in our study, because air and water temperature have tended to be linearly correlated in many previous studies (Liboriussen et al., 2005; Caissie, 2006; Li et al., 2016). In fact, projected changes in aquatic environments under climate change conditions have been based on the strong correlation between water and air temperature, especially for small non-groundwater-dominated water bodies (Caissie, 2006). To mimic eutrophication, $Ca(NO_3)_2$ and Na_2HPO_4 solutions were added to 12 tanks weekly, maintaining a constant loading of 538 mg N and 54 mg P per tank each week. The other 12 tanks were treated as references, receiving nutrient input only from the tap water and remaining in an unenriched state (51–71 μg N L^{-1} and 2–20 μg P L^{-1}).

Experimental Design

This study was performed with the mesocosm system described above (**Figure 1**). The mesocosm system has been running continuously for 15 years before the initiation of our experiment, ensuring the reliability of the experiment, because the aquatic organisms in the mesocosm system may have evolved and adapted to the current conditions. To examine the effects of climate warming and eutrophication on the growth of submerged macrophytes, shoots of *P. crispus* and *E. canadensis* (**Figure 1**) were collected from the mesocosm system to conduct the experiment. For the purpose of distinguishing the effect of seasonality, four independent sub-experiments were conducted in May (spring), August (summer), November (autumn), and February (winter), and each sub-experiment lasted for 3 weeks.

The process for each sub-experiment was as follows: each shoot for a particular species was collected from the same stock plant to ensure the same growth stage, thoroughly rinsed to remove the surficial attachment, and weighed to ensure the same initial biomass (±0.05 g). One *P. crispus* and one *E. canadensis* were planted together in the same plastic pot and filled with sediment collected from the same mud and thereafter covered with a layer of 2-cm pure sand to prevent nutrient exchange between the sediment and the surface water (**Figure 1**). A plastic net was fixed around the edge of the plastic pot to protect the plants and associated epiphytic algae from snail herbivory. Subsequently, each plastic pot was randomly transferred to one tank and hung in the center of the tank at a depth of 25 cm. In all, 24 plastic pots planted with two kinds of shoots were hung in 24 tanks, corresponding to three temperature scenarios and two nutrient levels (four replicates for each treatment) (**Figure 1**).

Sampling and Parameter Detection

The entire plant was harvested from the tank for each submerged macrophyte, and the sediment was carefully removed *in situ*. Approximately 1 L of surface water was sampled from each tank before plant collection. All the samples were taken back to the laboratory for further examination.

All the biotic parameters were measured in the laboratory. Initially, each individual was rinsed thoroughly with distilled water, and the rinsing water was collected to examine periphyton attached to the surface of the leaves. Next, each whole plant was dried with absorbent paper and weighed to determine fresh biomass. Subsequently, each plant sample was flattened and placed under a lens, and a digital photograph was taken. After that, the photographs were scanned using the ImageJ software, and the scanned areas were multiplied by 2 to estimate the surface areas of the plant leaves. In addition, each rinsing water sample was adjusted to a volume of 1,000 ml and filtered through a GF/C filter membrane (0.45 μm; Whatman, Maidstone, United Kingdom), and the residue in the filter was placed in a 10-ml 95% ethanol solution to extract photosynthetic pigments and measure chlorophyll *a* (Chl-*a*) content *via* a spectrophotometer (UV-1800; Shimadzu, Jena, Germany). Consequently, periphyton Chl-*a* was estimated as the mass of Chl-*a* per leaf area of each plant (μg/cm^2) (Hao et al., 2020). Similarly, each acquired 500-ml surface water sample was filtered and extracted, and then phytoplankton Chl-*a* was measured. The identification and enumeration of zooplankton were performed under an inverted microscope.

Several abiotic environmental factors, such as water temperature (Temp), DO, electrical conductivity, and pH, were determined *in situ* using a water quality meter (YSI 6920; YSI Inc., Yellow Springs, OH, United States) before sampling, while the concentrations of total nitrogen (TN) and total phosphorus (TP) in water were determined using a UV-visible spectrophotometer (UV-1800; Shimadzu, Jena, Germany) in the laboratory.

Statistical Analysis

After the normality and homoscedasticity of the data were confirmed by the Shapiro-Wilk test, two-way ANOVA and *post-hoc* tests were performed to examine the effects of temperature and nutrients, and their interactions on the biomass of submerged macrophyte during each season. In addition, the Scheirer–Ray-Hare test was performed to examine the responses of environmental variables to temperature and nutrients. Thereafter, the pairwise Wilcoxon rank-sum test with Bonferroni–Holm adjustment was performed for *post-hoc* pairwise comparisons. In addition, the main factors explaining the variance in plant biomass in each season were analyzed by redundancy analysis (RDA). After Spearman correlation analysis, a structural equation model (SEM) was used to explore the direct and indirect pathways by which temperature and nutrients affected the growth of submerged macrophytes. The Shapiro–Wilk test, two-way ANOVA, and Spearman correlation analysis were performed with SPSS (Version 20.0; SPSS Inc., Chicago, IL, United States), while the Scheirer-Ray-Hare test, pairwise Wilcoxon rank-sum test, and RDA were performed in R (version

3.6.1) with the rcompanion and vegan packages. SEM was performed with AMOS (Version 21.0, IBM SPSS Amos; SPSS Inc., Chicago, IL, United States).

RESULTS

Responses of Plant Biomass to Temperature and Nutrients in Each Season

According to the results of two-way ANOVA, significant effects of temperature could be observed on *E. canadensis* biomass in spring ($p = 0.012$), summer ($p = 0.001$), and autumn ($p = 0.043$), and on *P. crispus* biomass only in spring ($p = 0.034$). On the other hand, the only significant effect of nutrients occurred on *P. crispus* biomass in autumn ($p = 0.043$). Furthermore, the interaction of temperature and nutrients significantly affected *E. canadensis* biomass in spring ($p = 0.012$), whereas neither temperature nor nutrients significantly affected the biomass of either species in winter.

Our results showed that the biomass of *P. crispus* decreased in the warming scenario, most significantly in the enhanced-warming scenario in spring, but that the responses of *P. crispus* biomass to the temperature gradients were ambiguous in other seasons (**Figure 2**). In contrast, *E. canadensis* biomass significantly increased in the warming scenario, especially in the enhanced-warming scenario, in most seasons except winter (**Figure 2**). In summer and autumn, *E. canadensis* biomass increased significantly with temperature across the two nutrient levels (**Figure 2**). Based on the nutrient levels, *P. crispus* biomass showed a decreasing tendency under the effect of nutrient enrichment in most seasons except in winter, as was especially evident with the significant decline that occurred in the warming scenario in autumn (**Figure 2**). Despite the significantly higher biomass of *E. canadensis* in enriched relative to unenriched conditions in the enhanced-warming scenario in spring, nutrients generally had little effect on *E. canadensis* biomass in most cases (**Figure 2**).

Responses of Environmental Factors to Temperature and Nutrients in Each Season

The temperature gradients and levels of nutrients, including TN and TP, clearly fit the experimental design well (**Figure 3**). Of several abiotic environmental factors, DO showed a decreasing tendency with increasing temperature in summer and autumn; in particular, there was a significant difference between the ambient and enhanced-warming scenarios (**Figure 3**). In contrast, the variation in pH might have been affected by nutrient enrichment, as higher pH was observed in enriched treatments in each season, most significantly in winter (**Figure 3**).

Although some results with strong variability seemed statistically unsupported, it was clear that the biotic environmental factors, including the biomass of zooplankton, phytoplankton, and periphyton, were generally higher in the enriched group than in the unenriched group on the basis of nutrient level; in particular, a significant increase in each biotic variable in the enriched treatment was found in summer (**Figure 4**). Furthermore, an opposing tendency was apparent between phytoplankton and periphyton; for example, the increase in phytoplankton was accompanied by a decline in periphyton in spring and summer and vice versa in autumn and winter (**Figure 4**). Despite the significantly higher biomass of periphyton on *E. canadensis* in the ambient than in the enhanced-warming scenario in summer, and the tendency of zooplankton to decrease with increasing temperature in enriched tanks, the overall trends of biotic variables in response to temperature remained ambiguous (**Figure 4**). Specifically, intense declines in the biomass of zooplankton, phytoplankton, and periphyton were observed in winter relative to their levels in the other seasons (**Figure 4**).

Key Environmental Factors Affecting Plant Biomass in Each Season

The RDA revealed the main explanatory factors contributing to the variance in submerged macrophyte biomass in each season except winter (**Figure 5**). In particular, temperature and DO were significant factors explaining 11 and 8%, respectively, of the variance (adjusted R^2) in spring; the former was positively correlated with *E. canadensis,* while the latter was positively correlated with *P. crispus*. Despite the nonsignificant contribution (3%) to the variance in spring, phytoplankton showed a notable negative correlation with *P. crispus*. Additionally, temperature and DO were both significant explanatory variables accounting for 22 and 16%, respectively, of the variance in summer. Moreover, a significant contribution (7%) by zooplankton to the variance and a positive relationship with *P. crispus* biomass could be observed in summer. In autumn, TP was the only significant explanatory factor, accounting for 10% of the variance, while temperature exhibited a noticeable contribution (4%) to the variance, and both of them were positively correlated with *E. canadensis* but negatively correlated with *P. crispus*. Unfortunately, no significant explanatory factor could be found in winter.

Pathways by Which Temperature and Nutrients Affect Plant Biomass

Based on the results of the Spearman correlation analysis, the variables that were significantly correlated with each other were selected to run the SEM. Here, the experimental treatments, including temperature, TN, and TP, were selected as promising explanatory factors; environmental variables, including abiotic and biotic factors, were selected as intermediate factors; and biomass values of submerged macrophytes were selected as the target variables. Consequently, the comparative fit index (CFI) value = 0.9 indicated that the final model was acceptable. The R^2 values were 0.21 and 0.39 for *P. crispus* biomass and *E. canadensis* biomass, respectively, implying a considerable contribution of other factors to variation in the target variables (**Figure 6**).

The results of the SEM analysis illustrated the direct and indirect pathways by which temperature and nutrients affected the biomass of submerged macrophytes (**Figure 6**). It was clear that temperature exerted a significant direct impact on *E. canadensis* biomass (0.63) and abiotic variables such as DO (−0.63) and pH (0.8) but not on *P. crispus* biomass or most

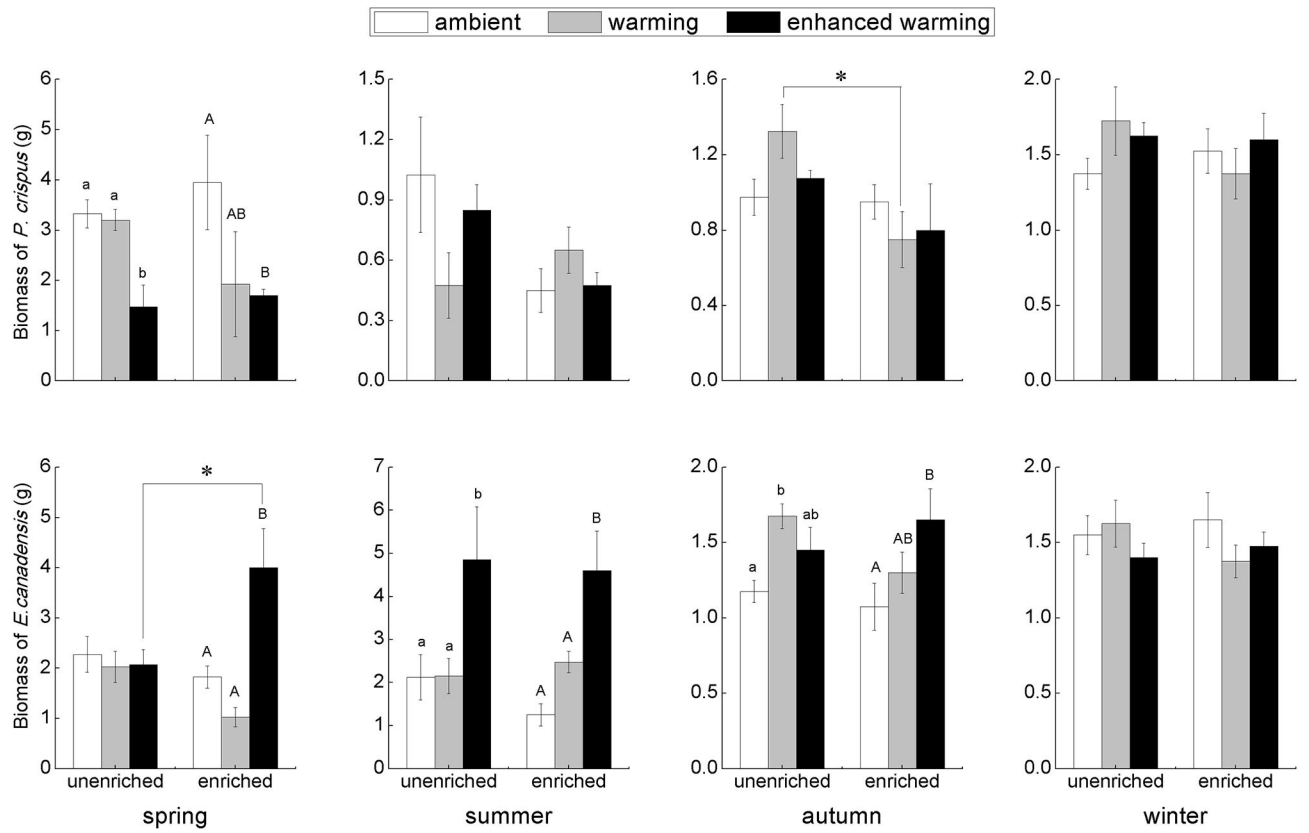

FIGURE 2 | The biomass (mean ± SE) of submerged macrophytes at different levels of temperature and nutrients in each season. Different letters indicate significant differences ($p < 0.05$) among the three temperature scenarios. The asterisks above the bars indicate significant differences ($p < 0.05$) between the two nutrient levels.

of the biotic variables such as phytoplankton, periphyton, and zooplankton (**Figure 6**). Although there was a little direct effect of nutrients on plant biomass, we found that TN could significantly and directly increase abiotic variables, including DO (0.17) and pH (0.33), while TP could significantly and directly increase biotic variables, including the biomass of phytoplankton (0.85), the biomass of periphyton on *P. crispus* (0.86), and biomass of periphyton on *E. canadensis* (0.52) (**Figure 6**). When the direct and indirect effects were combined into total effects, we found that *E. canadensis* biomass was strongly increased by rising temperature directly (**Figure 6**, **Table 1**). In contrast, *P. crispus* biomass was reduced directly by phytoplankton and periphyton and indirectly by TP but was increased directly by zooplankton (**Figure 6**, **Table 1**). Moreover, a positive relationship between zooplankton and periphyton and a negative relationship between phytoplankton and periphyton were demonstrated by the SEM (**Figure 6**).

DISCUSSION

Even though there were only four replications, our study compiled a large number of samples and demonstrated noticeable seasonality and species specificity in the growth of submerged macrophytes and in the variation of environmental factors under the influence of climate warming and nutrient enrichment, consistent with previous studies (Staehr and Sand-Jensen, 2006; Trochine et al., 2014; Zhang et al., 2019; Fu et al., 2020; Hao et al., 2020). Here, a significant negative effect of temperature on plant growth was observed only in *P. crispus* in spring, while a significant positive effect of temperature on plant growth appeared in *E. canadensis* in each season except winter (**Figure 2**). Moreover, a significant increase in *E. canadensis* biomass occurred with nutrient enrichment coupled with the enhanced-warming scenario in spring, indicating that the interaction of climate warming and nutrient enrichment only increased *E. canadensis* growth during spring (**Figure 2**). Similar results could be observed for several abiotic and biotic variables. For example, DO declined with increasing temperature in all the seasons except winter (**Figure 3**). In addition, the responses of sestonic and epiphytic algal biomass to nutrient enrichment were significant only in summer (**Figure 4**). The seasonality of plant biomass and environmental variables imply that the effects of climate warming and eutrophication on the aquatic ecosystems were sensitive to season.

Although the main factors affecting the growth of submerged macrophytes varied among seasons, the effects of temperature were sustained across the four seasons, suggesting the vital role

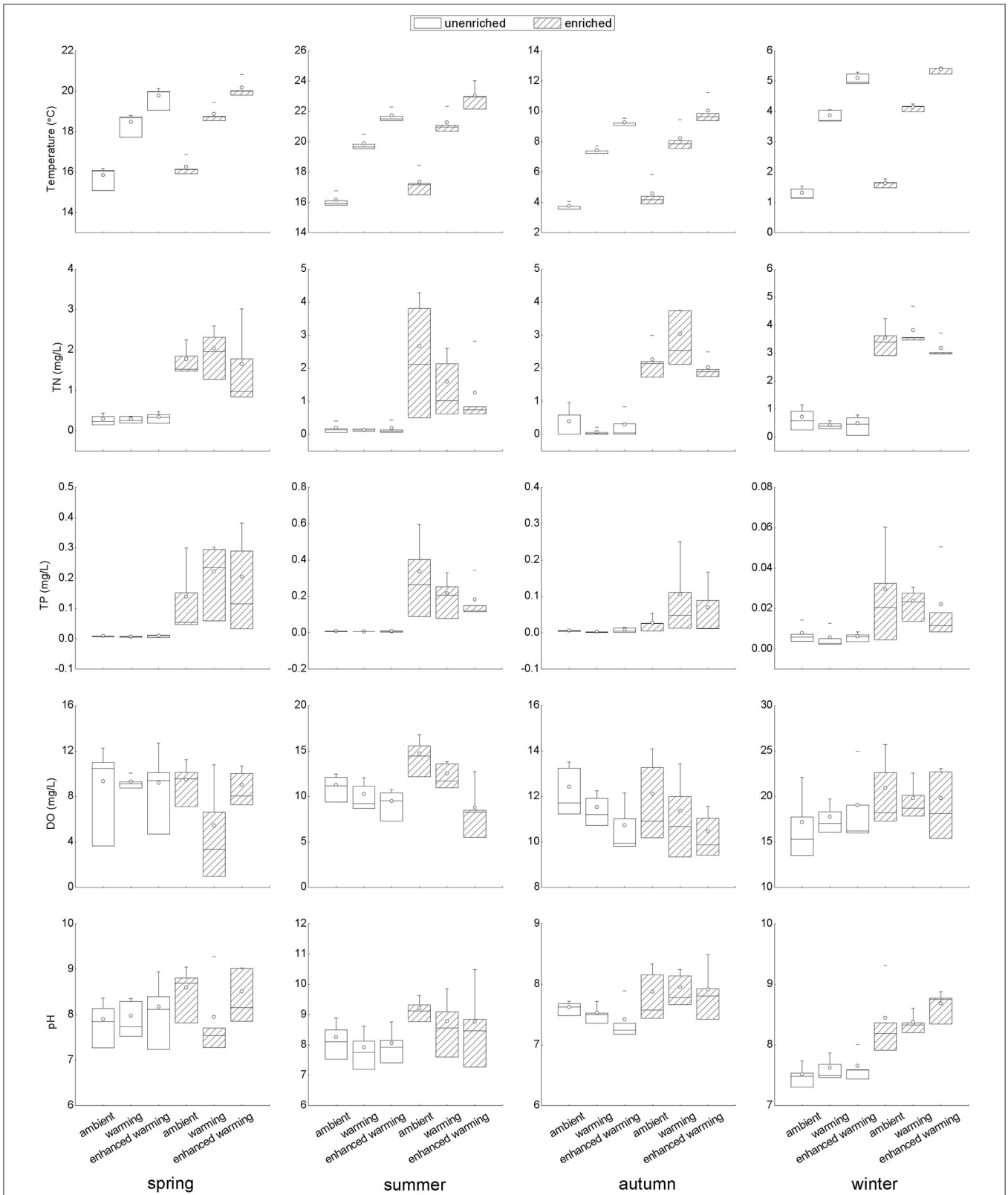

FIGURE 3 | Variation in temperature and nutrient concentrations and responses of abiotic variables to temperature and nutrients in each season. TN, total nitrogen in water; TP, total phosphorus in water; DO, dissolved oxygen.

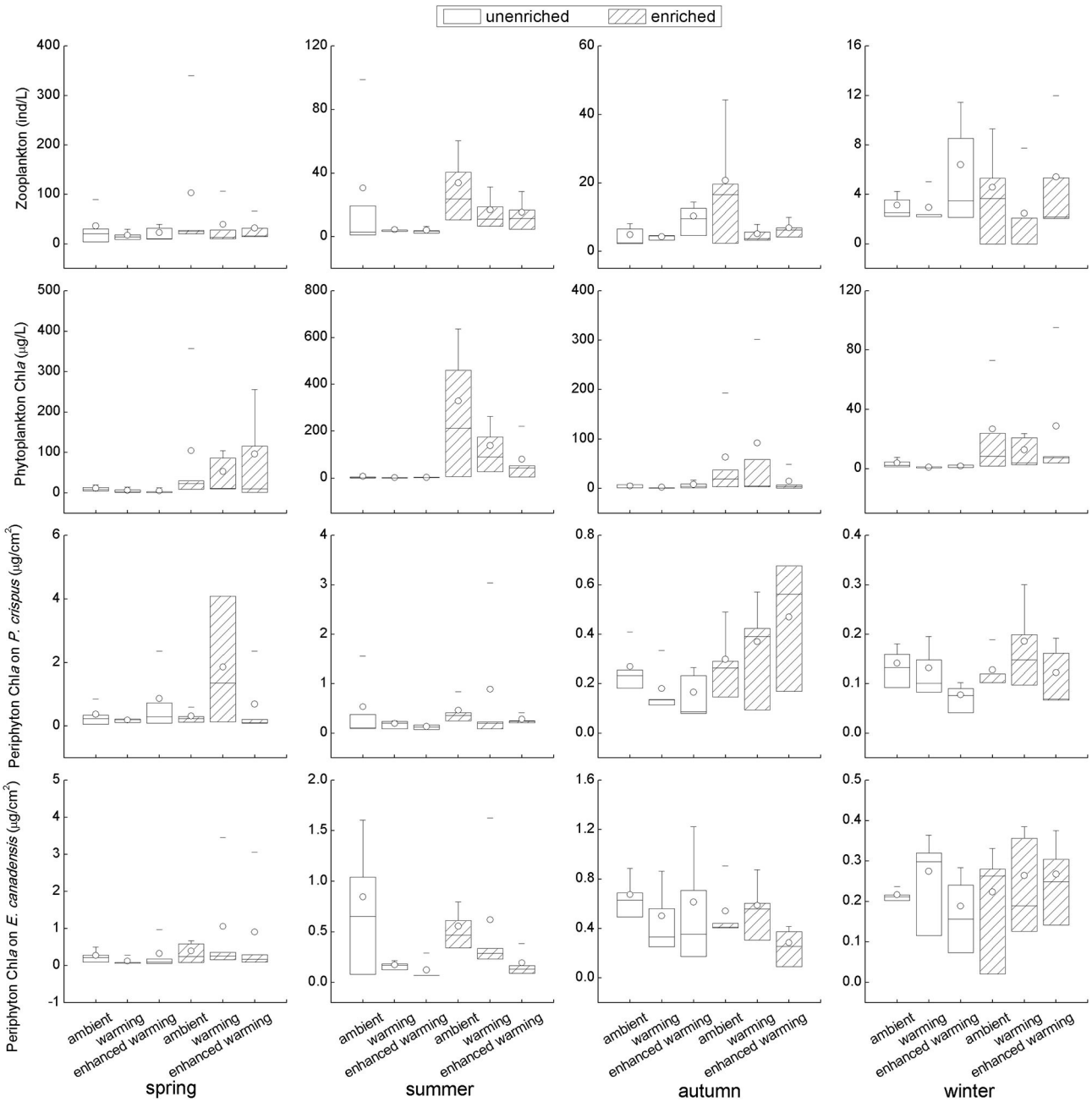

FIGURE 4 | Responses of biotic variables to temperature and nutrients in each season. It should be noted that the vertical scale in each figure was different among seasons.

climate warming played in the growth of submerged macrophytes (**Figure 5**). Such a strengthening effect of climate warming on the growth of *E. Canadensis* may be attributed to the stimulation of plant metabolism by high temperature, which is consistent with findings for the same species in previous studies (Olesen and Madsen, 2000; Riis et al., 2012; Zhang et al., 2015) and prevalent in many kinds of submerged macrophytes, such as *Callitriche cophocarpa*, *Zostera marina*, *Elodea nuttallii*, *Vallisneria spiralis*, and *Potamogeton lucens* (Olesen and Madsen, 2000; Kaldy, 2014; Zhang et al., 2019). In contrast, the restraining effect of high temperature on *P. crispus* during its growing season agrees with the results of a similar experiment conducted by Hao et al. (2018) in China and suggests that warming might accelerate the life cycle of *P. crispus* and increase respiration more than production, ultimately causing a decline in plant biomass during the growing period (Lee et al., 2007; Zhang et al., 2016; Hao et al., 2018). It is well-known that rising temperatures could significantly decrease DO concentrations in water because of

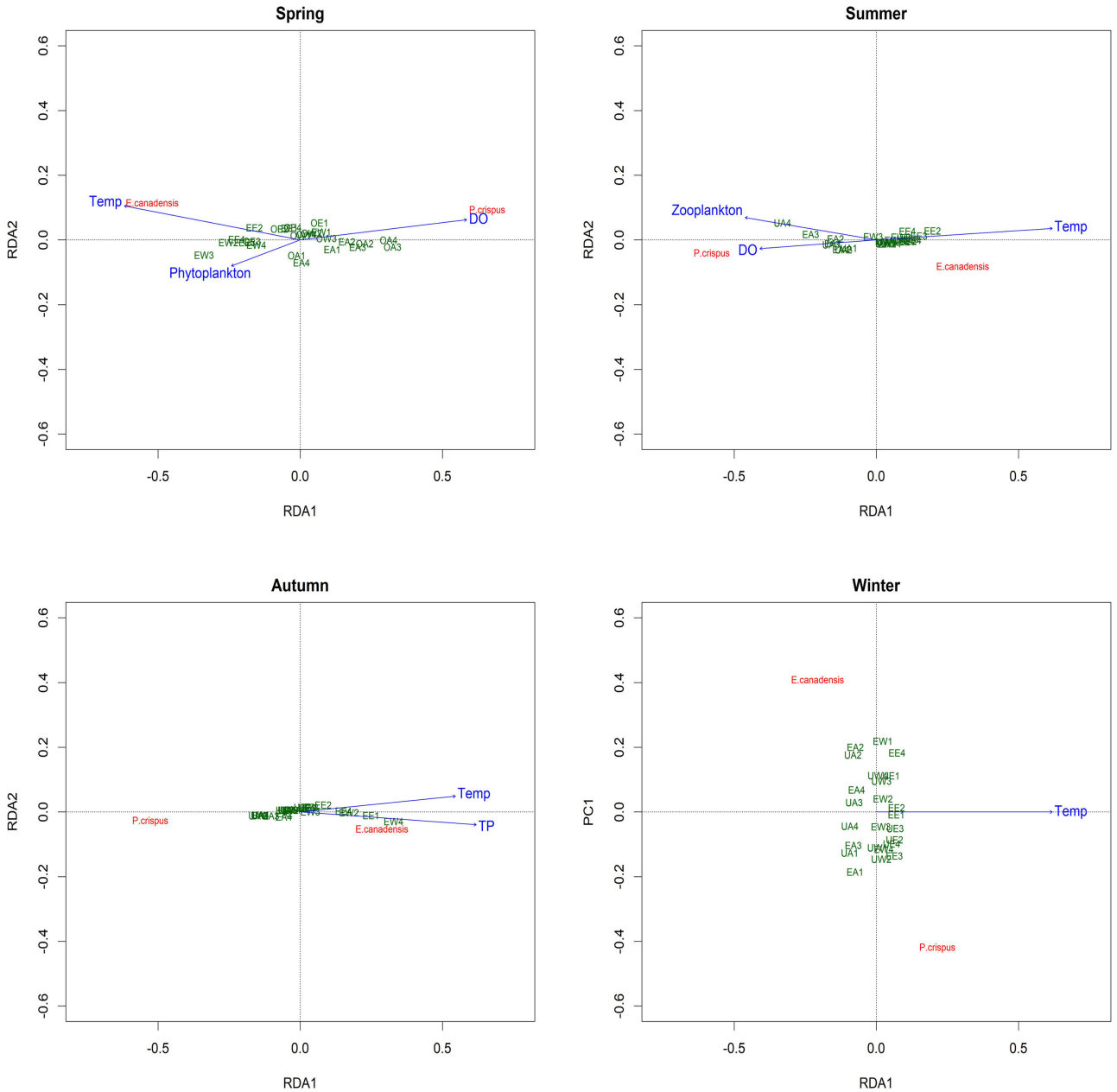

FIGURE 5 | Redundancy analysis (RDA) plot showing the analysis of the correlations between the biomass of submerged macrophytes and main explanatory factors in each season. Temp, temperature; DO, dissolved oxygen; TP, total phosphorus in water; UA, unenriched and ambient; UW, unenriched and warming; UE, unenriched and enhanced warming; EA, enriched and ambient; EW, enriched and warming; EE, enriched and enhanced warming.

enhanced oxygen consumption by intensive respiration from plant metabolism or from decomposition (Veraart et al., 2011; Zhang et al., 2015; Hao et al., 2020). A significant negative response of DO to rising temperature is confirmed in our study (**Figures 3**, **6**). The positive effect of DO on *P. crispus* in spring and summer (**Figure 5**) might be ascribed to the high demand for oxygen for enhanced respiration. Considering that the abundance of phytoplankton and zooplankton rose sharply in spring and summer (**Figure 3**), the negative effect of phytoplankton and the positive effect of zooplankton on *P. crispus* biomass were not surprising (**Figures 5**, **6**). Interestingly, in summer, the DO in enriched tanks in the enhanced-warming scenario was lowest (**Figure 3**), and concomitant lower *P. crispus* biomass and all biotic variables, but higher *E. canadensis* biomass could be found (**Figures 2**, **4**). This phenomenon probably provides speculation on how the two species and their ecosystems

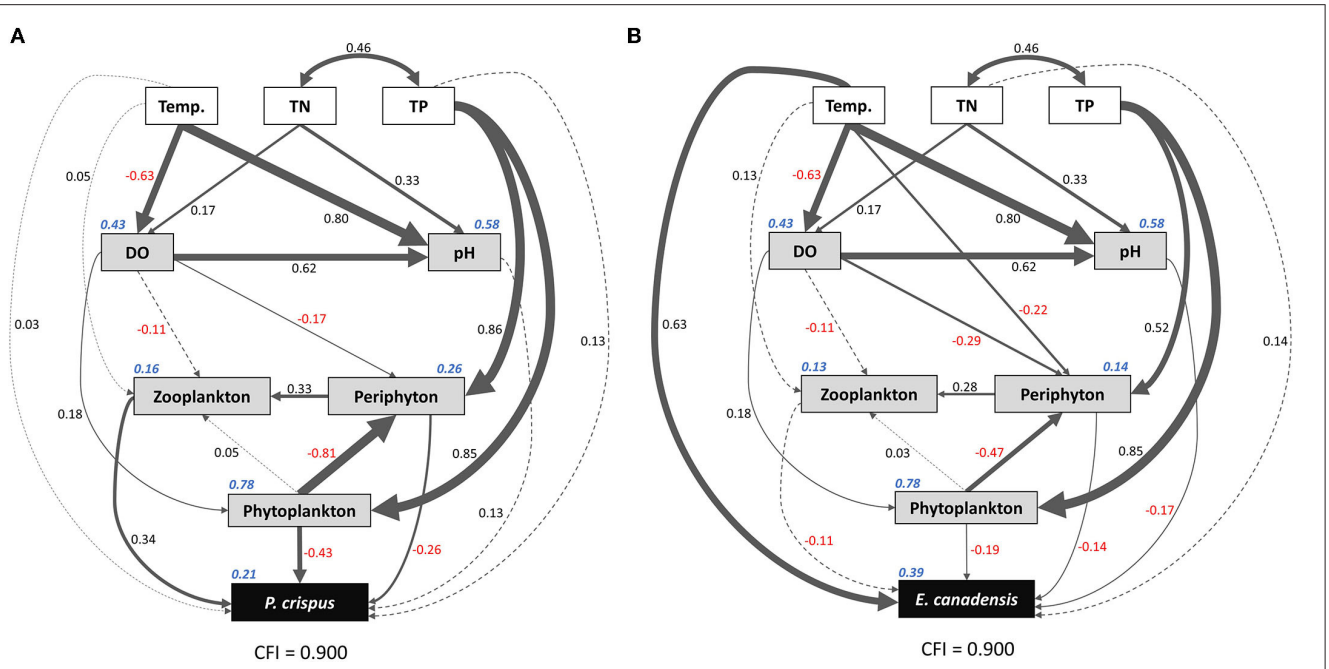

FIGURE 6 | Structural equation model (SEM) showing the direct and indirect pathways by which temperature and nutrients affected the biomass of *P. crispus* **(A)** and *E. canadensis* **(B)**. Single-headed arrows represent unidirectional causal relationships, and double-headed arrows represent non-causal covariances. Solid lines indicate significant ($p < 0.05$) or marginally significant ($p < 0.1$) effects, and dashed lines indicate non-significant effects. Numbers adjacent to the lines are standardized path coefficients, analogous to relative regression weights and indicative of the effect sizes of the corresponding relationships. The thickness of the arrows is proportional to the magnitudes of the standardized path coefficients or covariation coefficients. Numbers in italics adjacent to the boxes provide the R^2 values and denote the proportions of submerged macrophyte biomass explained by these parameters. Overall goodness-of-fit tests (CFIs) are shown at the bottom of each figure. Temp., temperature; TN, total nitrogen in water; TP, total phosphorus in water; DO, dissolved oxygen.

TABLE 1 | Standardized total, direct, and indirect effects of environmental factors on the biomass of submerged macrophytes in the SEM diagram.

	P. crispus			*E. canadensis*		
	Direct effect	**Indirect effect**	**Total effect**	**Direct effect**	**Indirect effect**	**Total effect**
Temp.	0.027	0.112	0.139	0.626	−0.072	0.554
TN	–	0.045	0.045	0.126	−0.067	0.059
TP	0.134	−0.377	−0.243	–	−0.186	−0.186
DO	–	0.014	0.014	–	−0.064	−0.064
pH	0.128	–	0.128	−0.170	–	−0.170
Zooplankton	0.341	–	0.341	−0.105	–	−0.105
Phytoplankton	−0.429	0.133	−0.295	−0.190	0.079	−0.112
Periphyton	−0.258	0.112	−0.146	−0.145	−0.029	−0.174

Direct effects are equal to the standardized path coefficients presented in ***Figure 6****. Indirect effects refer to the mathematical products of all possible paths. Total effects are the sums of direct and indirect effects. Temp., temperature; TN, total nitrogen in water; TP, total phosphorus in water; DO, dissolved oxygen.*

would vary in a scenario where temperature rises dramatically with consequent hypoxia and eutrophication.

However, the decline in microorganisms in cold seasons, namely, autumn and winter, may diminish the influence of biotic factors on submerged macrophytes, and the main contribution may be replaced by those of abiotic factors such as temperature or nutrients (Menge and Sutherland, 1987; Hao et al., 2020). In our study, the decline in *P. crispus* in the enriched treatment (**Figure 2**) in autumn was mainly induced by TP enrichment (**Figure 5**). The N:P ratio has been successfully used to predict the nature of community nutrient limitation in multiple aquatic ecosystems (Koerselman and Meuleman, 1996). In this study, an average N:P ratio below 6.1 indicated P overloading rather than P limitation for the plants (Wang et al., 2013). The supply of additional P at low P concentrations was conducive to the photosynthesis of *P. crispus*, while a high P concentration might negatively impact photosynthesis because of an imbalance in nutrient supply (Majerowicz and Kerbauy, 2002; Wang et al., 2013). Low P supply has been found to promote plant starch synthesis, leading to the release of inorganic P into the cytoplasm

from sugar-binding materials and maintenance of a constant cytoplasmic inorganic P concentration (Franco-Zorrilla et al., 2005). However, increasing water P levels might result in a lower capacity for starch synthesis in *P. crispus* and, thus, reduce inorganic P release into the cytoplasm (Wang et al., 2013). Owing to reduced solar radiation and persistent ice cover, winter is usually characterized by low temperature and limited light availability, which creates an unfavorable habitat for aquatic primary producers (Gustina and Hoffmann, 2000; Hao et al., 2020). Therefore, the lower ambient temperature (average 1.5°C in February vs. 16.8°C in August) and continuous ice cover on most of the experimental tanks in winter in our study would be expected to result in a great decline in plankton and periphyton (**Figures 3**, **4**). This may help explain why the environmental factors showed no significant effects accounting for the variance in plant biomass during winter, despite the apparent influence of temperature (**Figure 5**).

When variation from the four seasons was synthesized, the overall biomass of *E. canadensis* was positively affected primarily by temperature rather than nutrients, consistent with the results at the seasonal scale (**Figures 5**, **6**, **Table 1**). This result is unsurprising because the optimum temperature range for photosynthesis of submerged macrophytes is between 25 and 35°C when reviewing data across a series of submerged macrophyte species (Santamaría and van Vierssen, 1997). It has been widely confirmed that rising temperatures could enhance the growth of multiple aquatic plant species within their favorable temperature ranges (Madsen and Brix, 1997; Kaldy, 2014; Velthuis et al., 2017; Zhang et al., 2019). Aquatic plants can acclimate to thermal variation by phenotypic modifications of physiology and morphology (Barko et al., 1982; Madsen and Brix, 1997; Olesen and Madsen, 2000; Pilon and Santamaría, 2002; Zhang et al., 2015). For example, Olesen and Madsen (2000) and Riis et al. (2012) found that the relative growth rate and photosynthetic capacity of *E. canadensis* were enhanced by high temperatures. In addition, Pilon and Santamaría (2002) and Zhang et al. (2015) observed that the competitive traits of *Potamogeton pectinatus* and *E. canadensis*, such as leaf area, stem length, and root:shoot ratio, increased with increasing temperature, thereby promoting the growth and biomass of whole plants.

According to the hypothesis of temperature-plant physiology and enhanced nutrient-use efficiency (Reich and Oleksyn, 2004; An et al., 2005; De Senerpont Domis et al., 2014), elevated temperature would lead to an increased plant C:N ratio. As the temperature increases, on the one hand, aquatic plants invest fewer nutrients per mass of carbon to produce proteins to sustain biochemical reactions (Zhang et al., 2016, 2019). On the other hand, aquatic plants grow longer and accumulate additional biomass to develop their competitive capacity in response to rising temperatures, thereby diluting plant N and P contents (Velthuis et al., 2017; Zhang et al., 2020). In this study, the pH varied from 7 to 10 (**Figure 3**), which indicates that the major C source for the submerged macrophytes was bicarbonate (HCO_3^-) (Maberly and Gontero, 2017; Zhang et al., 2020). Previous experiments conducted in the same mesocosm system have reported that the alkalinity in each tank was always above 1 meq L^{-1} (Ventura et al., 2008; Zhang et al., 2015), signifying that the growth of *E. canadensis* is probably not limited by inorganic C availability (Vestergaard and Sand-Jensen, 2000; Zhang et al., 2019). Furthermore, nutrient enrichment compensated for the nutrient dilution effect, which was reflected by the interaction effect of rising temperature and nutrient enrichment on the growth of *E. canadensis* in spring (**Figure 2**).

For *P. crispus*, based on direct pathways, the overall variation in plant biomass was primarily affected by biotic factors rather than abiotic factors; meanwhile, based on the indirect pathways, it was primarily affected by P enrichment rather than temperature (**Figure 6**, **Table 1**). Numerous studies have revealed tight linkages among plankton, periphyton, and plants in aquatic ecosystems (Jones et al., 2002; Gyllström et al., 2005; Ventura et al., 2008; Özkan et al., 2010; Trochine et al., 2014; Hao et al., 2018, 2020; Matsuzaki et al., 2018; Yuan and Pollard, 2018; Zhang et al., 2020). The significant negative relationships between phytoplankton, periphyton, and plants in our study (**Figure 6**) indicate an intense direct competition among epiphytes, sestonic producers, and macrophytes, which is prevalent across the findings of a variety of studies (Jones et al., 2002; Ventura et al., 2008; Özkan et al., 2010; Trochine et al., 2014; Hao et al., 2020; Zhang et al., 2020). Phytoplankton, periphyton, and submerged macrophytes differ in their uptake of nutrients. Algae can take up nutrients from the water column even more efficiently than aquatic plants (Zhang et al., 2020). Similarly, free-floating algae can gain access to available nutrients in the water column more easily than adherent algae, which are constrained by the effects of the shape and boundary layer of biofilm (Trochine et al., 2014). In addition, the layer formed by epiphytes acts as a physical barrier to material exchange between plants and the aquatic environment (Jones et al., 2002; Ventura et al., 2008). Consequently, the flourishing of algae resulting from N and P enrichment would aggravate the competition for inorganic C acquisition among primary producers, thereby leading to C starvation of submerged macrophytes (Jones et al., 2002; Ventura et al., 2008; Dülger et al., 2017; Zhang et al., 2020). In addition, the increasing concentration of HCO_3^- due to the elevated water pH reduced the availability of inorganic C for submerged macrophytes, because the utilization of HCO_3^- incurred considerable physiological costs (Jones et al., 2002; Dülger et al., 2017). In addition to the C source, the requirement for light availability often shapes the intense competition among primary producers (Jones et al., 2002; Hao et al., 2018; Matsuzaki et al., 2018; Zhang et al., 2020). It has been explained that the increased abundance of epiphytes and sestonic and filamentous algae due to nutrient enrichment can restrict light availability through shading, thereby leading to the loss of submerged macrophytes (Phillips et al., 1978; Hao et al., 2018; Matsuzaki et al., 2018). Based on the annual scale, the probable fundamental cause for the decrease in the biomass of *P. crispus* in our study was external nutrient addition (through competition with increasing algae) rather than rising temperature (**Figure 6**, **Table 1**), which agrees with the results of multiple studies (Ventura et al., 2008).

Not only primary producers but also trophic cascades, including top-down and bottom-up control, could affect the

growth of submerged macrophytes (Jones et al., 2002; Ventura et al., 2008; Hao et al., 2018; Matsuzaki et al., 2018; Yuan and Pollard, 2018). In fact, nutrient enrichment significantly fueled the boom of algae initially, periphyton then significantly stimulated the development of zooplankton, and zooplankton significantly promoted the growth of *P. crispus* eventually. These sequential linkages in our experiment (**Figure 6**) indicate that cascading trophic effects had an impact on *P. crispus* through bottom-up control rather than top-down control. Of the zooplankton species in our mesocosm system, many copepods are carnivores or omnivores, while cladocerans and rotifers are grazers that feed on algae (Ventura et al., 2008; Matsuzaki et al., 2018). Carpenter et al. (2001) suggested that bottom-up control in primary production was stronger in lakes with three trophic levels than in lakes with the presence of a fourth trophic level. In addition, Costanza et al. (1993) and Frank et al. (2007) suggested that a shallow depth and temperate climate could promote the dominance of bottom-up control in lakes by accelerating efficient nutrient cycling. Specifically, the edibility of the phytoplankton, as measured by the proportions of edible and inedible algae (usually represented by cyanobacteria) within the phytoplankton assemblage, could determine the importance of bottom-up linkages (Gyllström et al., 2005; Matsuzaki et al., 2018; Yuan and Pollard, 2018). It has been demonstrated that the lack of highly unsaturated fatty acids in cyanobacteria, large size and accompanying gelatinous sheaths of cyanobacterial colonies, and toxins produced by cyanobacteria can threaten the growth of grazers (Wilson et al., 2006; Bednarska and Dawidowicz, 2007; Persson et al., 2007; Yuan and Pollard, 2018). Findings of previous studies have suggested that the dominance of cyanobacteria can be enhanced either by nutrient enrichment or rising temperature, which exerted stress on the bottom-up linkage and ultimately reduced the growth of aquatic plants (Gyllström et al., 2005; Kosten et al., 2012; Trochine et al., 2014; Matsuzaki et al., 2018; Schaum et al., 2018; Yuan and Pollard, 2018). In this study, phytoplankton growth was limited by P loading instead of N loading, and zooplankton was significantly increased by periphyton rather than by phytoplankton, implying that the assemblage of phytoplankton might be primarily composed of N-fixing cyanobacteria; therefore, the edibility of algae has shaped the herbivory strategy of grazers (**Figure 6**). On the other hand, the decline in zooplankton abundance with increasing temperature in the enriched mesocosms (**Figure 4**) might be ascribed to the increasing proportion of inedible algae. Thus, both nutrient enrichment and elevated temperature might result in the decline of *P. crispus* biomass by weakening bottom-up control, and this nonsignificant but visible interaction effect of nutrient enrichment and warming on the growth of *P. crispus* was present in autumn (**Figure 2**).

Although both *E. canadensis* and *P. crispus* are considered tolerant species that are, to some extent, capable of enduring alteration in nutrient loading and temperature (Riis et al., 2012; Zhang et al., 2015, 2016), their performance in response to nutrient enrichment and the rising temperature was conspicuously different in our study (**Figure 2**). There are three possible explanations for these discrepancies in their behaviors in response to climate warming and eutrophication. First, distinguishing aspects of specific lifecycles may result in differences in tolerance to elevated temperature. *E. canadensis* belongs to the Hydrocharitaceae family (de Winton et al., 2009; Hussner, 2012; Riis et al., 2012), grows faster in summer, and spreads in autumn, implying that elevated temperature would prolong the growing season and thereafter promote the productivity of *E. Canadensis* (Zhang et al., 2015; Hao et al., 2020). In contrast to *E. canadensis*, *P. crispus* usually germinates in winter, is more tolerant to colder temperatures, and thrives better at low temperatures (Bolduan et al., 1994; Pilon et al., 2003; Wang et al., 2013; Zhang et al., 2015). Second, the morphological complexity of submerged macrophytes can determine the underwater availability of light. Hao et al. (2017) compared the shading effects of several submerged macrophytes featuring morphological complexity gradients and found increasing underwater light attenuation with decreasing morphological complexity. Stronger light attenuation could induce lower light availability, thereby decreasing photosynthesis. *P. crispus* exhibits a simpler morphological complexity than *E. canadensis* (Hao et al., 2020). Thus, the middle and bottom leaves of *P. crispus* may experience low light availability and be sensitive to the turbidity induced by nutrient enrichment. Such a shading effect leading to the decreased survival of *P. crispus* has been demonstrated in a previous study (Hao et al., 2018). Third, the ability to utilize HCO_3^- efficiently may lead to superiority in competition for inorganic C sources. It has been verified that the mechanism by which *Elodea* and *Potamogeton* utilize HCO_3^- relies on leaf surface polarity. That is, HCO_3^- is converted into CO_2 in the cell walls and boundary layer by the activity of H^+ pumps located at the plasmalemmas of the lower cells *of Elodea* and *Potamogeton*, and released CO_2 subsequently diffuses into cells (Prins et al., 1982; Madsen et al., 1998). Therefore, *E. canadensis*, which possesses a higher leaf number and wider leaf surface area, may be able to take up HCO_3^- more efficiently than *P. crispus*. In addition, Sand-Jensen (1983) found that the photosynthetic rate of *P. crispus* was reduced by increasing pH, which could be attributed to the increasing capacity to buffer the efflux of H^+.

CONCLUSION

Taking into account the structuring role of submerged macrophytes in shallow lake ecosystems, it is of great importance to predict the response of submerged macrophytes to climate warming coupled with eutrophication (Jeppesen et al., 2012). In this study, we found that submerged macrophyte biomass showed noticeable seasonality and species specificity in response to climate warming and eutrophication. Additionally, the main explanatory variables accounting for the biomass of submerged macrophytes differed in each season. In addition, a significant interaction effect of temperature and nutrients on the growth of plants only occurred in rare cases. Based on the annual scale, the overall results showed a direct positive effect of temperature rather than nutrient concentrations on *E. canadensis* biomass, which was consistent with the seasonal results. However, the overall results showed that P enrichment negatively affected *P. crispus* biomass indirectly by altering the biotic environmental

factors, specifically by strengthening the competition among primary producers. Interestingly, we found that the growth of *P. crispus* was positively affected by a trophic cascade through bottom-up control rather than top-down control. In summary, it can be speculated that continuous climate warming and eutrophication would cause a transition in aquatic plant communities in shallow lakes through selection effects. Species-specific responses of submerged macrophytes to climate warming and eutrophication may be ascribed to their distinct physiological and morphological traits. These conclusions are drawn based on just four experimental replicates. We suggest that further research on the response of submerged vegetation in shallow lakes to climate warming and eutrophication should be conducted from the perspective of the population.

DATA AVAILABILITY STATEMENT

The raw data supporting the conclusions of this article will be made available by the authors, without undue reservation.

AUTHOR CONTRIBUTIONS

HW designed the study, performed the research, collected the samples, analyzed the data, and wrote the manuscript. BH collected the samples and analyzed the data. HJ collected the samples. YC contributed to data analysis and revisions. All authors have reviewed, discussed, agreed to the authorship, and submission of the manuscript for peer review.

FUNDING

This study was supported by the National Natural Science Foundation of China (51879007, 52000041, 51979043), the China Scholarship Council (CSC), the China Postdoctoral Science Foundation Grant (2019M662810), the Guangdong Provincial Key Laboratory Project (2019B121203011), the Guangdong Province Basic and Applied Basic Research Fund (2019A1515010378), and the KeySpecial Project for Introduced Talents Team of Southern Marine Science and Engineering Guangdong Laboratory (Guangzhou) (GML2019ZD0403).

ACKNOWLEDGMENTS

We thank Erik Jeppesen for the guidance and support during the mesocosm experiment.

REFERENCES

An, Y., Wan, S., Zhou, X., Subedar, A. A., Wallace, L. L., and Luo, Y. (2005). Plant nitrogen concentration, use efficiency, and contents in a tallgrass prairie ecosystem under experimental warming. *Glob. Change Biol.* 11, 1733–1744. doi: 10.1111/j.1365-2486.2005.01030.x

Barko, J. W., Hardin, D. G., and Matthews, M. S. (1982). Growth and morphology of submersed freshwater macrophytes in relation to light and temperature. *Can. J. Bot.* 60, 877–887. doi: 10.1139/b82-113

Bednarska, A., and Dawidowicz, P. (2007). Change in filter-screen morphology and depth selection: uncoupled responses of *Daphnia* to the presence of filamentous cyanobacteria. *Limnol. Oceanogr.* 52, 2358–2363. doi: 10.4319/lo.2007.52.6.2358

Bolduan, B. R., Van Eeckhout, G. C., Quade, H. W., and Gannon, J. E. (1994). *Potamogeton crispus*–the other invader. *Lake Reserv. Manag.* 10, 113–125. doi: 10.1080/07438149409354182

Burson, A., Stomp, M., Mekkes, L., and Huisman, J. (2019). Stable coexistence of equivalent nutrient competitors through niche differentiation in the light spectrum. *Ecology* 100:e02873. doi: 10.1002/ecy.2873

Caissie, D. (2006). The thermal regime of rivers: a review. *Freshw. Biol.* 51, 1389–1406. doi: 10.1111/j.1365-2427.2006.01597.x

Carpenter, S. R., Cole, J. J., Hodgson, J. R., Kitchell, J. F., Pace, M. L., Bade, D., et al. (2001). Trophic cascades, nutrients, and lake productivity: whole-lake experiments. *Ecol. Monogr.* 71, 163–186. doi: 10.1890/0012-9615(2001)0710163:TCNALP2.0.CO;2

Costanza, R., Kemp, W. M., and Boynton, W. R. (1993). Predictability, scale, and biodiversity in coastal and estuarine ecosystems: implications for management. *Ambio* 1993, 88–96.

Cross, W. F., Hood, J. M., Benstead, J. P., Huryn, A. D., and Nelson, D. (2015). Interactions between temperature and nutrients across levels of ecological organization. *Glob. Change Biol.* 21, 1025–1040. doi: 10.1111/gcb.12809

De Senerpont Domis, L. N., Van de Waal, D. B., Helmsing, N. R., Van Donk, E., and Mooij, W. M. (2014). Community stoichiometry in a changing world: combined effects of warming and eutrophication on phytoplankton dynamics. *Ecol.* 95, 1485–1495. doi: 10.1890/13-1251.1

de Winton, M. D., Champion, P. D., Clayton, J. S., and Wells, R. D. (2009). Spread and status of seven submerged pest plants in New Zealand lakes. *N. Z. J. Mar. Freshw. Res.* 43, 547–561. doi: 10.1080/00288330909510021

Dülger, E., Heidbüchel, P., Schumann, T., Mettler-Altmann, T., and Hussner, A. (2017). Interactive effects of nitrate concentrations and carbon dioxide on the stoichiometry, biomass allocation and growth rate of submerged aquatic plants. *Freshw. Biol.* 62, 1094–1104. doi: 10.1111/fwb.12928

Elser, J. J., Bracken, M. E., Cleland, E. E., Gruner, D. S., Harpole, W. S., Hillebrand, H., et al. (2007). Global analysis of nitrogen and phosphorus limitation of primary producers in freshwater, marine and terrestrial ecosystems. *Ecol. Lett.* 10, 1135–1142. doi: 10.1111/j.1461-0248.2007.01113.x

Franco-Zorrilla, J. M., Martín, A. C., Leyva, A., and Paz-Ares, J. (2005). Interaction between phosphate-starvation, sugar, and cytokinin signaling in Arabidopsis and the roles of cytokinin receptors CRE1/AHK4 and AHK3. *Plant Physiol.* 138, 847–857. doi: 10.1104/pp.105.060517

Frank, K. T., Petrie, B., and Shackell, N. L. (2007). The ups and downs of trophic control in continental shelf ecosystems. *Trends Ecol. Evol.* 22, 236–242. doi: 10.1016/j.tree.2007.03.002

Fu, H., Yuan, G., Özkan, K., Johansson, L. S., Søndergaard, M., Lauridsen, T. L., et al. (2020). Patterns of seasonal stability of lake phytoplankton mediated by resource and grazer control during two decades of re-oligotrophication. *Ecosystems* 20, 1–15. doi: 10.1007/s10021-020-00557-w

Gustina, G. W., and Hoffmann, J. P. (2000). Periphyton dynamics in a subalpine mountain stream during winter. *Arctic Antarctic Alpine Res.* 32, 127–134. doi: 10.1080/15230430.2000.12003348

Gyllström, M., Hansson, L. A., Jeppesen, E., Criado, F. G., Gross, E., Irvine, K., et al. (2005). The role of climate in shaping zooplankton communities of shallow lakes. *Limnol. Oceanogr.* 50, 2008–2021. doi: 10.4319/lo.2005.50.6.2008

Hao, B., Roejkjaer, A. F., Wu, H., Cao, Y., Jeppesen, E., and Li, W. (2018). Responses of primary producers in shallow lakes to elevated temperature: a mesocosm experiment during the growing season of *Potamogeton crispus*. *Aquatic Sci.* 80:34. doi: 10.1007/s00027-018-0585-0

Hao, B., Wu, H., Cao, Y., Xing, W., Jeppesen, E., and Li, W. (2017). Comparison of periphyton communities on natural and artificial macrophytes with contrasting

morphological structures. *Freshw. Biol.* 62, 1783–1793. doi: 10.1111/fwb.12991

Hao, B., Wu, H., Zhen, W., Jo, H., Cai, Y., Jeppesen, E., et al. (2020). Warming effects on periphyton community and abundance in different seasons are influenced by nutrient state and plant type: a shallow lake mesocosm study. *Front. Plant Sci.* 11:404. doi: 10.3389/fpls.2020.00404

Hussner, A. (2012). Alien aquatic plant species in European countries. *Weed Res.* 52, 297–306. doi: 10.1111/j.1365-3180.2012.00926.x

IPCC (2014). *Climate Change 2014: Synthesis Report. Contribution of WorkingGroups I, II and III to the Fifth Assessment Report of the Intergovernmental Panelon Climate Change*. Geneva: IPCC.

Jeppesen, E., Søndergaard, M., Søndergaard, M., and Christoffersen, K. (2012). *The Structuring Role of Submerged Macrophytes in Lakes, Vol. 131*. Berlin/Heidelberg: Springer Science & Business Media.

Jones, J. I., Young, J. O., Eaton, J. W., and Moss, B. (2002). The influence of nutrient loading, dissolved inorganic carbon and higher trophic levels on the interaction between submerged plants and periphyton. *J. Ecol.* 90, 12–24. doi: 10.1046/j.0022-0477.2001.00620.x

Kaldy, J. E. (2014). Effect of temperature and nutrient manipulations on eelgrass *Zostera marina* L. from the Pacific Northwest, USA. *J. Exp. Mar. Biol. Ecol.* 453, 108–115. doi: 10.1016/j.jembe.2013.12.020

Koerselman, W., and Meuleman, A. F. (1996). The vegetation N: P ratio: a new tool to detect the nature of nutrient limitation. *J. Appl. Ecol.* 10, 1441–1450. doi: 10.2307/2404783

Kosten, S., Huszar, V. L., Bécares, E., Costa, L. S., van Donk, E., Hansson, L. A., et al. (2012). Warmer climates boost cyanobacterial dominance in shallow lakes. *Glob. Change Biol.* 18, 118–126. doi: 10.1111/j.1365-2486.2011.02488.x

Lee, K. S., Park, S. R., and Kim, Y. K. (2007). Effects of irradiance, temperature, and nutrients on growth dynamics of seagrasses: a review. *J. Exp. Mar. Biol. Ecol.* 350, 144–175. doi: 10.1016/j.jembe.2007.06.016

Li, F., Shah, D. N., Pauls, S. U., Qu, X., Cai, Q., and Tachamo Shah, R. D. (2016). Elevational shifts of freshwater communities cannot catch up climate warming in the Himalaya. *Water* 8:327. doi: 10.3390/w8080327

Liboriussen, L., Landkildehus, F., Meerhoff, M., Bramm, M. E., Søndergaard, M., Christoffersen, K., et al. (2005). Global warming: design of a flow-through shallow lake mesocosm climate experiment. *Limnol. Oceanogr. Methods* 3, 1–9. doi: 10.4319/lom.2005.3.1

Maberly, S. C., and Gontero, B. (2017). Ecological imperatives for aquatic CO_2-concentrating mechanisms. *J. Exp. Bot.* 68, 3797–3814. doi: 10.1093/jxb/erx201

Madsen, T. V., and Brix, H. (1997). Growth, photosynthesis and acclimation by two submerged macrophytes in relation to temperature. *Oecologia* 110, 320–327. doi: 10.1007/s004420050165

Madsen, T. V., Hahn, P., and Johansen, J. (1998). Effects of inorganic carbon supply on the nitrogen requirement of two submerged macrophytes, *Elodea canadensis* and *Callitriche cophocarpa*. *Aquat. Bot.* 62, 95–106. doi: 10.1016/S0304-3770(98)00087-4

Majerowicz, N., and Kerbauy, G. B. (2002). Effects of nitrogen forms on dry matter partitioning and nitrogen metabolism in two contrasting genotypes of *Catasetum fimbriatum* (Orchidaceae). *Environ. Exp. Bot.* 47, 249–258. doi: 10.1016/S0098-8472(01)00131-9

Matsuzaki, S. I. S., Suzuki, K., Kadoya, T., Nakagawa, M., and Takamura, N. (2018). Bottom-up linkages between primary production, zooplankton, and fish in a shallow, hypereutrophic lake. *Ecology* 99, 2025–2036. doi: 10.1002/ecy.2414

Menge, B. A., and Sutherland, J. P. (1987). Community regulation: variation in disturbance, competition, and predation in relation to environmental stress and recruitment. *Am. Naturalist* 130, 730–757. doi: 10.1086/284741

Nichols, S. A., and Shaw, B. H. (1986). Ecological life histories of the three aquatic nuisance plants, *Myriophyllum spicatum*, *Potamogeton crispus*, and *Elodea canadensis*. *Hydrobiologia* 131, 3–21. doi: 10.1007/BF00008319

Olesen, B., and Madsen, T. V. (2000). Growth and physiological acclimation to temperature and inorganic carbon availability by two submerged aquatic macrophyte species, *Callitriche cophocarpa* and *Elodea canadensis*. *Funct. Ecol.* 14, 252–260. doi: 10.1046/j.1365-2435.2000.00412.x

Özkan, K., Jeppesen, E., Johansson, L. S., and Beklioglu, M. (2010). The response of periphyton and submerged macrophytes to nitrogen and phosphorus loading in shallow warm lakes: a mesocosm experiment. *Freshw. Biol.* 55, 463–475. doi: 10.1111/j.1365-2427.2009.02297.x

Persson, J., Brett, M. T., Vrede, T., and Ravet, J. L. (2007). Food quantity and quality regulation of trophic transfer between primary producers and a keystone grazer (*Daphnia*) in pelagic freshwater food webs. *Oikos* 116, 1152–1163. doi: 10.1111/j.0030-1299.2007.15639.x

Phillips, G. L., Eminson, D., and Moss, B. (1978). A mechanism to account for macrophyte decline in progressively eutrophicated freshwaters. *Aquat. Bot.* 4, 103–126. doi: 10.1016/0304-3770(78)90012-8

Pilon, J., and Santamaría, L. (2002). Clonal variation in the thermal response of the submerged aquatic macrophyte *Potamogeton pectinatus*. *J. Ecol.* 90, 141–152. doi: 10.1046/j.0022-0477.2001.00645.x

Pilon, J., Santamaría, L., Hootsmans, M., and van Vierssen, W. (2003). Latitudinal variation in life-cycle characteristics of *Potamogeton pectinatus* L.: vegetative growth and asexual reproduction. *Plant Ecol.* 165, 247–262. doi: 10.1023/A:1022252517488

Prins, H. B. A., Snel, J. F. H., Zanstra, P. E., and Helder, R. J. (1982). The mechanism of bicarbonate assimilation by the polar leaves of *Potamogeton* and *Elodea*. CO_2 concentrations at the leaf surface. *Plant Cell Environ.* 5, 207–214. doi: 10.1111/1365-3040.ep11571916

Reich, P. B., and Oleksyn, J. (2004). Global patterns of plant leaf N and P in relation to temperature and latitude. *Proc. Natl. Acad. Sci. U. S. A.* 101, 11001–11006. doi: 10.1073/pnas.0403588101

Riis, T., Olesen, B., Clayton, J. S., Lambertini, C., Brix, H., and Sorrell, B. K. (2012). Growth and morphology in relation to temperature and light availability during the establishment of three invasive aquatic plant species. *Aquat. Bot.* 102, 56–64. doi: 10.1016/j.aquabot.2012.05.002

Sand-Jensen, K. A. J. (1983). Photosynthetic carbon sources of stream macrophytes. *J. Exp. Bot.* 34, 198–210. doi: 10.1093/jxb/34.2.198

Santamaría, L., and van Vierssen, W. (1997). Photosynthetic temperature responses of fresh-and brackish-water macrophytes: a review. *Aquat. Bot.* 58, 135–150. doi: 10.1016/S0304-3770(97)00015-6

Schaum, C. E., Student Research Team, Ffrench-Constant, R., Lowe, C., Ólafsson, J. S., Padfield, D., et al. (2018). Temperature-driven selection on metabolic traits increases the strength of an algal–grazer interaction in naturally warmed streams. *Glob. Change Biol.* 24, 1793–1803. doi: 10.1111/gcb.14033

Staehr, P. A., and Sand-Jensen, K. A. J. (2006). Seasonal changes in temperature and nutrient control of photosynthesis, respiration and growth of natural phytoplankton communities. *Freshw. Biol.* 51, 249–262. doi: 10.1111/j.1365-2427.2005.01490.x

Steffen, W., Richardson, K., Rockström, J., Cornell, S. E., Fetzer, I., Bennett, E. M., et al. (2015). Planetary boundaries: guiding human development on a changing planet. *Science* 347:1259855. doi: 10.1126/science.1259855

Tilman, D., Fargione, J., Wolff, B., D'Antonio, C., Dobson, A., Howarth, R., et al. (2001). Forecasting agriculturally driven global environmental change. *Science* 292, 281–284. doi: 10.1126/science.1057544

Trochine, C., Guerrieri, M. E., Liboriussen, L., Lauridsen, T. L., and Jeppesen, E. (2014). Effects of nutrient loading, temperature regime and grazing pressure on nutrient limitation of periphyton in experimental ponds. *Freshw. Biol.* 59, 905–917. doi: 10.1111/fwb.12314

Velthuis, M., van Deelen, E., van Donk, E., Zhang, P., and Bakker, E. S. (2017). Impact of temperature and nutrients on carbon: nutrient tissue stoichiometry of submerged aquatic plants: an experiment and meta-analysis. *Front. Plant Sci.* 8:655. doi: 10.3389/fpls.2017.00655

Ventura, M., Liboriussen, L., Lauridsen, T., Søndergaard, M., Søndergaard, M., and Jeppesen, E. (2008). Effects of increased temperature and nutrient enrichment on the stoichiometry of primary producers and consumers in temperate shallow lakes. *Freshw. Biol.* 53, 1434–1452. doi: 10.1111/j.1365-2427.2008.01975.x

Veraart, A. J., De Klein, J. J., and Scheffer, M. (2011). Warming can boost denitrification disproportionately due to altered oxygen dynamics. *PLoS ONE* 6:e18508. doi: 10.1371/journal.pone.0018508

Vestergaard, O., and Sand-Jensen, K. (2000). Alkalinity and trophic state regulate aquatic plant distribution in Danish lakes. *Aquat. Bot.* 67, 85–107. doi: 10.1016/S0304-3770(00)00086-3

Wang, L., Yang, T., Zhu, D., Hamilton, D., Nie, Z., Liu, L., et al. (2013). Growth and turion formation of *Potamogeton crispus* in response to different phosphorus concentrations in water. *Aquat. Ecol.* 47, 87–97. doi: 10.1007/s10452-012-9427-7

Wilson, A. E., Sarnelle, O., and Tillmanns, A. R. (2006). Effects of cyanobacterial toxicity and morphology on the population growth of freshwater zooplankton:

meta-analyses of laboratory experiments. *Limnol. Oceanogr.* 51, 1915–1924. doi: 10.4319/lo.2006.51.4.1915

Wu, H., Hao, B., Cai, Y., Liu, G., and Xing, W. (2021). Effects of submerged vegetation on sediment nitrogen-cycling bacterial communities in Honghu Lake (China). *Sci. Total Environ.* 755:142541. doi: 10.1016/j.scitotenv.2020.142541

Yuan, L. L., and Pollard, A. I. (2018). Changes in the relationship between zooplankton and phytoplankton biomasses across a eutrophication gradient. *Limnol. Oceanogr.* 63, 2493–2507. doi: 10.1002/lno.10955

Zhang, P., Bakker, E. S., Zhang, M., and Xu, J. (2016). Effects of warming on *Potamogeton crispus* growth and tissue stoichiometry in the growing season. *Aquat. Bot.* 128, 13–17. doi: 10.1016/j.aquabot.2015.08.004

Zhang, P., Grutters, B., Van Leeuwen, C. H., Xu, J., Petruzzella, A., van den Berg, R. F., et al. (2019). Effects of rising temperature on the growth, stoichiometry, and palatability of aquatic plants. *Front. Plant Sci.* 9:1947. doi: 10.3389/fpls.2018.01947

Zhang, P., Kuramae, A., Van Leeuwen, C. H., Velthuis, M., van Donk, E., Xu, J., et al. (2020). Interactive effects of rising temperature and nutrient enrichment on aquatic plant growth, stoichiometry, and palatability. *Front. Plant Sci.* 11:58. doi: 10.3389/fpls.2020.00058

Zhang, X., Odgaard, R., Olesen, B. L., Lauridsen, T., Liboriussen, L., Søndergaard, M., et al. (2015). Warming shows differential effects on late-season growth and competitive capacity of *Elodea canadensis* and *Potamogeton crispus* in shallow lakes. *Inland Waters* 5, 421–432. doi: 10.5268/IW-5.4.830

Conflict of Interest: The authors declare that the research was conducted in the absence of any commercial or financial relationships that could be construed as a potential conflict of interest.

frontiers in Plant Science

ORIGINAL RESEARCH
published: 21 October 2021
doi: 10.3389/fpls.2021.739159

Nutrient Alteration Drives the Impacts of Seawater Acidification on the Bloom-Forming Dinoflagellate *Karenia mikimotoi*

Qian Liu[1,2†], Yanqun Wang[3†], Yuanyuan Li[1], Yijun Li[4], You Wang[1,2], Bin Zhou[1,2] and Zhongyuan Zhou[1,2]*

[1]College of Marine Life Science, Ocean University of China, Qingdao, China, [2]Laboratory for Marine Ecology and Environmental Science, Pilot National Laboratory for Marine Science and Technology, Qingdao, China, [3]College of Environmental Science and Engineering, Ocean University of China, Qingdao, China, [4]College of Life Sciences, Qingdao University, Qingdao, China

OPEN ACCESS

Edited by:
Benoit Schoefs,
Le Mans Université, France

Reviewed by:
Alina Corcoran,
New Mexico Consortium,
United States
David Dewez,
Université du Québec à Montréal,
Canada

***Correspondence:**
Zhongyuan Zhou
1071253114@qq.com

[†]These authors have contributed equally to this work

Specialty section:
This article was submitted to Marine and Freshwater Plants, a section of the journal Frontiers in Plant Science

Received: 10 July 2021
Accepted: 30 September 2021
Published: 21 October 2021

Citation:
Liu Q, Wang Y, Li Y, Li Y, Wang Y, Zhou B and Zhou Z (2021) Nutrient Alteration Drives the Impacts of Seawater Acidification on the Bloom-Forming Dinoflagellate Karenia mikimotoi. Front. Plant Sci. 12:739159. doi: 10.3389/fpls.2021.739159

Seawater acidification and nutrient alteration are two dominant environmental factors in coastal environments that influence the dynamics and succession of marine microalgae. However, the impacts of their combination have seldom been recorded. A simulated experimental system was set up to mimic the effects of elevated acidification on a bloom-forming dinoflagellate, *Karenia mikimotoi*, exposed to different nutrient conditions, and the possible mechanism was discussed. The results showed that acidification at different pH levels of 7.6 or 7.4 significantly influenced microalgal growth ($p < 0.05$) compared with the control at pH 8.0. Mitochondria, the key sites of aerobic respiration and energy production, were impaired in a pH-dependent manner, and a simultaneous alteration of reactive oxygen species (ROS) production occurred. Cytochrome c oxidase (COX) and citrate synthase (CS), two mitochondrial metabolism-related enzymes, were actively induced with acidification exposure, suggesting the involvement of the mitochondrial pathway in coping with acidification. Moreover, different nutrient statuses indicated by various N:P ratios of 7:1 (N limitation) and 52:1 (P limitation) dramatically altered the impacts of acidification compared with those exposed to an N:P ratio of 17:1 (control), microalgal growth at pH 7.4 was obviously accelerated with the elevation of the nutrient ratio compared to that at pH 8.1 ($p < 0.05$), and nutrient limitations seemed beneficial for growth in acidifying conditions. The production of alkaline phosphatase (AP) and acid phosphatase (AcP), an effective index indicating the microalgal growth status, significantly increased at the same time ($p < 0.05$), which further supported this speculation. However, nitrate reductase (NR) was slightly inhibited. Hemolytic toxin production showed an obvious increase as the N:P ratio increased when exposed to acidification. Taken together, mitochondrial metabolism was suspected to be involved in the process of coping with acidification, and nutrient alterations, especially P limitation, could effectively alleviate the negative impacts induced by acidification. The obtained results might be a possible explanation for the competitive fitness of *K. mikimotoi* during bloom development.

Keywords: seawater acidification, nutrient alteration, mitochondrial metabolism, hemolytic activity, *Karenia mikimotoi*

INTRODUCTION

Phytoplankton are the dominant primary producers and bases of marine ecosystems. However, the mass occurrence of microalgal species, especially those with toxic secondary metabolites (phycotoxins), harmful algal bloom (HAB) species, impair socioeconomic interests and human health in coastal regions worldwide and thus have aroused worldwide concern (Hallegraeff, 2003). Both suddenly massive occurrence and algal toxins production are mostly the result of complex interactions between environmental changes community processes (Wohlrab et al., 2020). It has been reported that the frequency and scale of HABs have steadily increased in scenarios of global changes (Nielsen et al., 2012; Wells et al., 2015; Gobler et al., 2017), including stimulated by seawater acidification (Riebesell et al., 2018; Wells et al., 2019) and related variations in nutrients (Wells et al., 2015; Zheng et al., 2016).

Generally, seawater acidification is said to affect the physiology of some HAB species by having consequences related to growth and toxin production (Wells et al., 2015; Brandenburg et al., 2019). Whether changes in physiological performance can lead to the expansion of HAB species under seawater acidification depends on how they affect the competitive fitness of HAB species over that of other coexisting species (Riebesell et al., 2018). Seawater acidification could directly affect the carbon acquisition of HAB species, for example, the CCM of dinoflagellate was downregulated under enhanced pCO_2 conditions, which could in turn result in energy reallocation from C-acquisition to other cellular processes (Bercel and Kranz, 2019; Van de Waal et al., 2019). Bercel and Kranz (2019) found that rising pCO_2 levels could result in increased toxicity of *Karenia brevis* blooms. Similarly, acidification may benefit the HAB-forming ichthyotoxic raphidophyte *Heterosigma akashiwo* (Nimer et al., 1997), which was easier to obtain competitive advantage than coexisting species. Therefore, increased in bloom occurrence in a future ocean may specifically benefit from seawater acidification (Van de Waal et al., 2013; Eberlein et al., 2014).

The concentrations of nitrogen (N) and phosphorus (P), as the most essential and frequent limiting nutrients, will influence the population dynamics and physiology of harmful algae at the species level (Glibert et al., 2006). Not only the contents but also their ratios (N:P) play essential roles in this process (Guan and Li, 2017), but how these changes influence the competitive success of HABs will depend in large part on their influence on nutrient uptake. In addition, it is commonly accepted that nutrient imbalance is one of the main driving forces involved in microalgal succession through toxin production (Glibert et al., 2018), and its effect is species-specific for different HAB groups (Fu et al., 2010; Radan and Cochlan, 2018; Wang et al., 2019b). For instance, N and P limitation of growth rate substantially increases brevetoxins in *K. brevis* blooms (Hardison et al., 2014). In fact, as a driver, nutrient availability was also proven to be helpful in modulating the impacts induced by seawater acidification (Sett et al., 2014; Taucher et al., 2015). Previous studies have shown that with the simultaneous intensification of acidification and nutrients, the cell growth of *Prorocentrum donghaiense* was significantly accelerated, that is, dinoflagellate was more adaptive than diatom (Zheng et al., 2016). In addition, some investigations in temperate regions reported that the responses of plankton communities to seawater acidification are most pronounced under conditions of nutrient limitations (Bach et al., 2016; Sala et al., 2016). Very few studies, however, have focused on the combined effects of seawater acidification and nutrient limitations on the physiological responses and toxin production of HAB species (Fu et al., 2010; Sun et al., 2011), despite its obvious relevance to phytoplankton growth in the present day and future coastal ocean. This inspires a question: what are the possible mechanisms of the underlying reason for seawater acidification altering the functional responses under different nutrient conditions?

Karenia mikimotoi is a common and representative harmful algal species in marine ecosystems, that often forms large algal blooms in the south Atlantic and east coast of United States and European coasts, especially in Asian areas (Brand et al., 2012; Li et al., 2019). Large-scale HABs occurred almost annually in the East China Sea from 2002 until now (Sun et al., 2007; Li et al., 2017), and the dinoflagellate *K. mikimotoi* was found to be one of the causative species (Chen et al., 2021). *K. mikimotoi* is evidenced to release toxins which threaten local fisheries and the health of the food web (Brand et al., 2012; Chen et al., 2021). At present, numerous studies into the population dynamics, nutritional characteristics, and toxicological mechanisms of *K. mikimotoi* blooms have been carried out (Sun et al., 2007; Zou et al., 2010; Guan and Li, 2017; Zhao et al., 2017). However, the ecological processes related to the formation of *K. mikimotoi* blooms remain largely unclear, and it cannot fully explain the mechanism behind this phenomenon. As global climate change adds new level of instability to complex marine ecosystems, expansion and intensification trends of HAB species need to be considered regionally and at the species level (Hallegraeff et al., 2021).

Increasingly higher atmospheric CO_2 is predicted in the near future in addition to the current imbalance of N:P ratios in coastal areas (Wang et al., 2019a; Tan et al., 2020). How does *K. mikimotoi* adapt to complex stress conditions and become dominant? Will its species dominance continue in the upcoming scenario? In addition to the series of physiological changes currently concerned that affect the competitive adaptability of HAB species, mitochondrial metabolism, as a multistep pathway that involves matrix- and membrane-associated enzymes and plays a key role in acclimation to variable environmental conditions (Leo et al., 2020). However, seawater acidification is seldom documented (Zheng et al., 2016). The above statements enabled us to perform the present study based on our previous studies that the ROS-initiated mitochondrial linked pathway was involved (Sun et al., 2016, 2017), and the effects of different pH levels when exposed to various nutrient statuses were analyzed regarding the physiological responses of *K. mikimotoi*. The present study sheds light on elucidating the adaptive strategy of *K. mikimotoi* when facing the combination of seawater acidification and nutrient limitations during the process of HAB development.

MATERIALS AND METHODS

Microalgal Cultivation

K. mikimotoi (MEL22) isolated from coastal Pingtan, Fujian Province and kindly provided to us by Institute of Oceanography, Chinese Academy of Sciences. Cells were cultured in 0.45-μm filtered natural seawater, which had been autoclaved (30 min, 121°C) and enriched with f/2 medium (Guillard, 1975). All cultures were incubated at 20 ± 1°C and illuminated under a 12-h light–dark cycle with radiance of 80 μmol photon m^{-2} s^{-1} provided by cool white fluorescent tubes in a constant temperature incubator. The pH and salinity were kept constant at 8.10 ± 0.02 and 30 ± 1.0, respectively. Flasks were manually shaken twice a day at a set time to avoid cell sedimentation. Cells in the exponential phase were used in the assays.

Acidifying System Set-Up

The establishment of the acidifying system was based on the methods of our previous study (Hu et al., 2017; Sun et al., 2017). Three pH levels were evaluated in the present study: pH 8.1 (present ambient seawater pH, $pCO_2 \approx 390$ ppm), pH 7.6 (predicted pH in 2100, $pCO_2 \approx 1{,}000$ ppm), and pH 7.4 (predicted pH in 2300, $pCO_2 \approx 2000$ ppm), obtained by gentle bubbling with 0.22-μm filtered ambient air and air/CO_2 mixtures. The air/CO_2 mixtures were generated by plant CO_2 chambers (HP400G-D, Ruihua Instrument & Equipment Ltd., Wuhan, China) with a variation of less than 5%. The pH values and salinity of the seawater in the flasks were measured by a pH meter (Seven Compact™ S210k, Mettler Toledo, Switzerland) and a handheld salinometer (WY028Y, HUARUI, CHN).

Experimental Design

Effects of Seawater Acidification

A control (pH 8.1) and two treatment groups (pH 7.6 and pH 7.4) were used in this experiment. The experiments were conducted in triplicate in 500-mL sterilized flasks containing 350 mL of medium. The initial density of *K. mikimotoi* was 1×10^4 cells mL^{-1}. The whole experiment lasted for 20 days and was performed in triplicate for each treatment. Samples were collected 8, 12, and 15 days after exposure for further physiological and biochemical analyses.

Effects of Seawater Acidification With Different Nutrient Conditions

Microalgae were exposed to a two-factor experimental design (2 × 3) with 2 pH levels of 8.1 and 7.4 and 3 nutrient levels with different N:P ratios, which were 17:1 (close to the Redfield ratio, as a control), 7:1 (N:P <16:1, as N limitation) and 52:1 (N:P >16:1, as P limitation; **Table 1**), and $NaNO_3$ and $Na_2HPO_4{\cdot}7H_2O$ were used to adjust the concentrations of N and P, respectively. All possible combinations were tested with the results of 6 treatments. The other conditions were the same as those in 2.3.1 unless otherwise stated.

TABLE 1 | Seawater acidification and nutrient levels in different groups.

pH level	Nutrient level	NO_3^--N (μmol/L)	PO_4^{3-}-P (μmol/L)	N:P ratios
pH 8.1	Control	35.7	1.45	17:1
	N limitation	14.3	1.45	7:1
	P limitation	35.7	0.48	52:1
pH 7.4	Control	35.7	1.45	17:1
	N limitation	14.3	1.45	7:1
	P limitation	35.7	0.48	52:1

Assay of the Microalgal Population Dynamics

The growth of *K. mikimotoi* was determined according to the method described by Deng et al. (2017). The cell density was determined and quantitatively simulated using a logistic equation. The specific growth rate (μ, d^{-1}) was calculated and analyzed by using the following equation (OECD, 2011):

$$\mu_{i-j}\left(d^{-1}\right) = \frac{\ln X_j - \ln X_i}{t_j - t_i} \ (\mathrm{d}^{-1})$$

where μ_{i-j} represents the average specific growth rate from time i to j, X_i represents the cell density at time I, and X_j represents the cell density at time j.

We evaluated the growth performance of each strain and regressed the population growth curves using the following logistic growth model (Zhao et al., 2015):

$$N_t = K / 1 + e^{a-rt} \quad (1)$$

$$T_p = a/r \quad (2)$$

where N_t (cells ml^{-1}) is the algal density at time t, K (cells mL^{-1}) is the carrying capacity, r (d^{-1}) is the maximum specific growth rate, and T_p is the inflection point of population growth curve.

Transmission Electron Microscopy Observation

On the 8th and 15th days after exposure, 50 mL microalgal medium was sampled from the control and acidification-treated groups and centrifuged at 3000 r/min. Then, the collected microalgal cells were fixed on ice with 3.5% glutaraldehyde in phosphate-buffered saline (PBS; 0.1 mol L^{-1}, pH 7.2). The treated samples were kept at 4°C overnight in fixative liquid and washed 3 times with the same solution. Then, the cells were dehydrated sequentially in graded concentrations of ethanol based on the methods of Zhu et al. (1983), preparing the slides in triplicate. A Hitachi H-7000 (Japan) TEM was utilized to observe the ultrastructure of the algal samples.

Determination of the ROS Levels

The ROS levels were detected by using 2'7'-dichlorofluorescein diacetate (DCFH-DA, Sigma-Aldrich) as a fluorescent probe. Briefly, 2 mL culture medium in each treatment was sampled and centrifuged at 3000 r/min. The supernatants were discarded, and the microalgal cells were resuspended in PBS buffer (pH 7.2). DCFH-DA was added to this suspension to a final

concentration of 10 μM and mixed well. The mixture was incubated at 20°C in the dark for 30 min and washed twice with PBS (Zhou et al., 2019). The fluorescence value was detected by flow cytometry (Beckman Coulter Inc., CA, United States) in the FL1 channel.

Evaluation of Key Enzyme Activities in Mitochondrial Metabolism

The cytochrome c oxidase (COX) and citrate synthase (CS) activities were measured as described in Xiao et al. (2019) with slight modifications. The collected microalgal cells were homogenized in precooled lysis buffer (4°C) by ultrasonication, the mitochondrial suspension was extracted by centrifugation at 6000 r/min, and the enzyme activities of COX and CS were determined by using assay kits (Shanghai Jiemei Gene Pharmaceutical Technology Co., Ltd.; Shanghai Harling Biotechnology Co., Ltd.). The results were all expressed in mg protein/min.

Determination of Nitrate Reductase and Phosphatase Activities

The measurement methods of nitrate reductase (NR) and phosphatase, including alkaline phosphatase (AP) and acid phosphatase (AcP), were conducted as described in Mei et al. (2013) with slight modifications. Microalgal cells were collected onto 0.45 μm pore size glass fiber filter membranes (GF/F, Whatman) and homogenized in precooled lysis buffer (4°C) by the ultrasonic crushing method. The suspension was extracted by centrifugation at 6,000 r/min, and the enzyme activities of NR, AP, and ACP were determined using the corresponding assay kits (Nanjing Jiancheng Bioengineering Institute, Nanjing, China). The results were all expressed in mg protein/min.

Determination of Hemolytic Activity

The microalgal culture medium in both the control and acidification-treated groups was mixed with hemocytes of the blue mussel *Mytilis edulis* according to the method of Li et al. (2018), and the hemolytic activity was evaluated based on the hemolysis rate (Caffrey et al., 1986), which was calculated as:

$$\text{Hemolysis rate}(\%)=\frac{(C_0-C_t)}{C_0}\times 100\%$$

where C_t (cell/ml) denotes the hemocyte density at time t (hour), C_0 is the initial density of the hemocytes, and t is 24 h.

Statistical Analysis

Data analysis was performed using SPSS v. 24, and the data are expressed as the means ± standard deviation (SD). The data under every treatment conformed to a normal distribution (Shapiro–Wilk, $p > 0.05$), and the variances could be considered equal (Levene's test, $p > 0.05$). The effect of pH was analyzed by one-way ANOVA (LSD test). The effects of pH, nutrient status, and their interactions were analyzed by two-way ANOVA. Moreover, significant effects of the nutrient levels at each fixed pH and significant effects of pH at each time point for each nutrient level were analyzed by one-way ANOVA (LSD test). A bivariate Pearson's correlation analysis was performed to analyze the relationship among parameters. For all analyses, significance was assigned at the $p < 0.05$ level. Figures were generated using GraphPad Prism 8.0 software.

RESULTS

Influence of Seawater Acidification on *K. mikimotoi*

Response of Population Dynamics to Seawater Acidification

The population growth of *K. mikimotoi* under different pH levels is shown in **Figure 1A**. The cell density increased over time in all treatment groups and took 20 days for the population to reach the stationary phase. The results of the specific growth rate (**Figure 1B**) showed that on the 8th day after exposure, pH 7.4 conditions promoted the growth

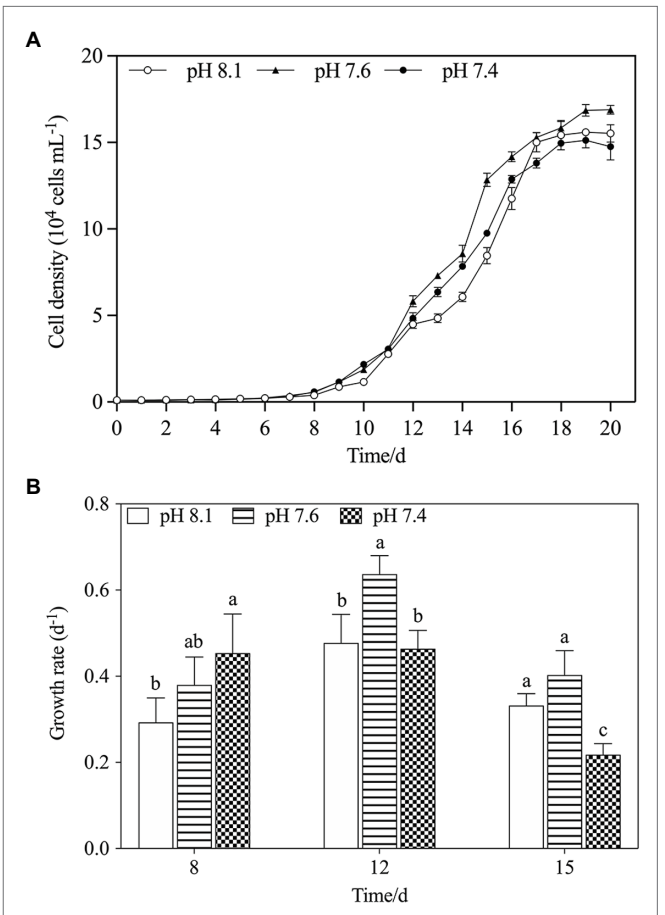

FIGURE 1 | The changes of population dynamics of *K. mikimotoi* when exposed to different pH levels. **(A)** Cell density; **(B)** Specific growth rate. Data are presented as means ± SD. Different lowercase letters indicate significant differences between the treatment and the control at each time point ($p < 0.05$).

TABLE 2 | Regressions of the logistic model on *K. mikimotoi* population growth when exposed to seawater acidification conditions.

Group	*K* (×10^4 cells mL^{-1})	*r* (d^{-1})	*Tp* (d^{-1})
pH 8.1	15.883	0.49325	14.7
pH 7.6	16.983	0.50351	13.6
pH 7.4	15.125	0.46908	13.8

of microalgae ($f = 6.755$; $p = 0.045$), but with time, compared with the pH 8.1, the pH 7.6 condition still significantly promoted the growth of the microalgae, whereas the pH 7.4 condition significantly decreased the growth rate on the 15th day after exposure ($f = 12.237$; $p = 0.025$). Acidification affected the growth of *K. mikimotoi* to a certain extent. We calculated the regressed parameters with a logistic model to quantify the growth dynamics in different treatments (**Table 2**). Based on the calculated Logistic parameters, the carrying capacity (K, reflecting the growth potential of algae) as well as the maximum instantaneous growth rate (r) in the pH 7.6 group was higher than those in the pH 8.1 and pH 7.4 group. These results suggested that *K. mikimotoi* could grow well under pH 7.6 condition.

Effects of Seawater Acidification on the *K. mikimotoi* Cellular Ultrastructure

Transmission electron microscopy images (**Figure 2**) showed that the mitochondria of *K. mikimotoi* cells in the pH 8.1 and pH 7.6 groups on the 8th day after exposure maintained a normal ultrastructure with intact bilayer membranes and abundant cristae (**Figures 2A,C**). Compared with the pH 8.1 group, obvious damage to the mitochondria of *K. mikimotoi* was observed in the pH 7.4 group, which was mainly manifested as the loss of mitochondrial inclusions, damage to the bilayer membrane, and blurring of the internal cristae (**Figure 2E**). On the 15th day after exposure, the mitochondrial membrane structure of the pH 8.1 and pH 7.6 groups remained intact (**Figures 2B,D**). Under pH 7.4 exposure, the mitochondrial membrane structures of *K. mikimotoi* were basically intact, and a few ridges had developed, showing a certain degree of recovery (**Figure 2F**).

Effects of Seawater Acidification on Mitochondrial Metabolism-Related Enzyme Activities

We further explored the effect of pH on mitochondrial function by measuring the activities of key mitochondrial metabolism-related enzymes (**Figure 3**). On the timeline, an increasing trend in COX and CS activities of all treatments was observed from day 8 to day 15 (**Figures 3A,B**). Exposure to pH 7.6 caused increases in the activities of COX and CS, which reached a maximum on day 15 and was significantly higher than that in the pH 8.1 group ($f = 64.125$; $p = 0.0013$ in COX; $f = 5.725$; $p = 0.047$). On the 8th and 12th days, exposure to pH 7.4 inhibited the activities of the two key enzymes to some extent; however, their activities were still higher than that in the pH 8.1group on the 15th day ($f = 27.567$; $p = 0.006$ in COX; $f = 12.237$; $p = 0.025$). During the entire exposure period, the interactive effects of pH and N/P were recorded for COX and CS activities (**Table 2**).

Effects of Seawater Acidification on ROS Production

Overall, ROS levels in *K. mikimotoi* cells increased in a pH-dependent manner, and the highest ROS content was always found in the pH 7.4 group at any set time, especially on the 8th day after exposure, which was significantly higher than that in either the pH 8.1 or the pH 7.6 group ($f = 29.133$; $p = 0.000$). With the extension of time, the ROS level gradually decreased and stabilized on the 12th and 15th days. The assay results indicated that ROS levels in *K. mikimotoi* could be increased by acidification.

Influence of Seawater Acidification on *K. mikimotoi* When Exposed to Different Nutrient Statuses

Response of Population Dynamics to Seawater Acidification With Different Nutrient Statuses

Figure 4A showed variations of *K. mikimotoi* densities exposed to the combination of different pH and nutrient status with time. The population growth was significantly promoted by pH 7.4 with the different nutrient status, and the P limitation exhibited more increased population growth. The results of the specific growth rate (**Figure 1B**) showed that on the 8th day after exposure, only pH 8.1 with P limitation promoted the growth of microalgae ($f = 21.827$; $p = 0.009$). With the extension of time, pH 7.4 with different nutrient levels showed significant ($f = 530.72$; $p = 0.000$) positive effects on the population growth of *K. mikimotoi* by stimulating cell division, and the highest growth rate was found in the pH 7.4 group with P limitation on the 12th day after exposure, which was significantly higher than that in either the control or N limitation groups ($f = 6.644$; $p = 0.041$). Specific growth rate were significantly affected by pH, nutrient status, and their interactions during the whole experiment (**Table 3**). We used a logistic model to calculate the regressed parameters (**Table 4**). Of all the treatments, pH 7.4 with three nutrient status (control, N limitation, and P limitation) showed high *K* values, whereas microalgae grew most slowly under pH 8.1 with N limitation conditions. In addition, pH 7.4 both with control and P limitation groups showed high *r* values and long *Tp*, suggesting possible high total biomass accumulation because of the long growth period. The results indicated that the algal growth of *K. mikimotoi* was promoted significantly by acidification under different nutrient statuses.

Effects of Seawater Acidification With Different Nutrient Statuses on Nutrient Absorption Capacity

The activities of AP in each treatment group increased with time (**Figure 5A**) and reached a peak on the 15th day after exposure, with the highest point at pH 7.4 with P limitation. The activity of ACP (**Figure 5B**) showed a similar trend, but the peak value occurred on the 12th day. The activities of AP

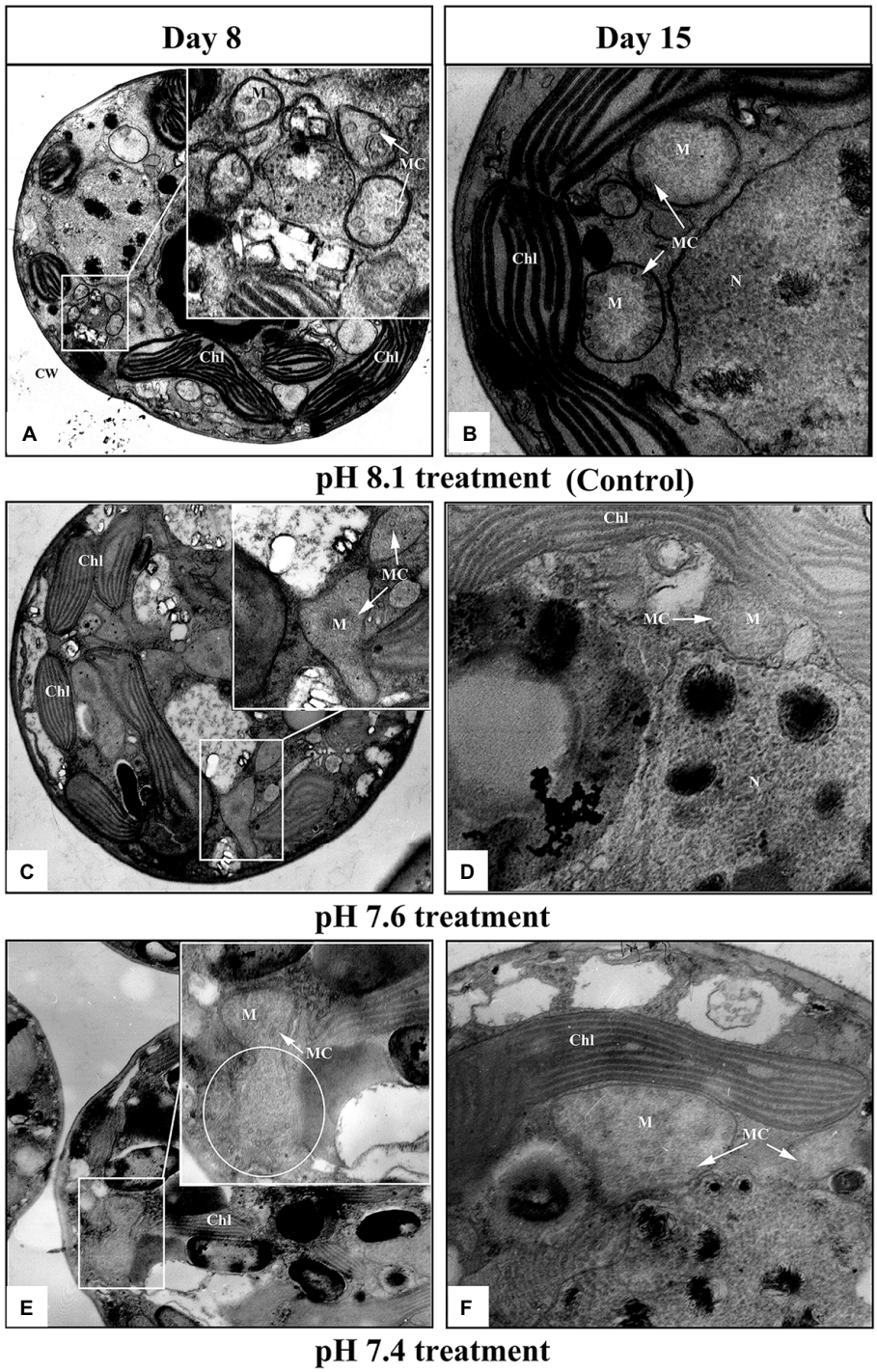

FIGURE 2 | Ultrastructural changes in *K. mikimotoi* cells treated with different pH levels. **(A,B)** Control; **(C,D)** pH 7.6 treatment; **(E,F)** pH 7.4 treatment. CW, Chl, M, MC, and N in each figure denote the cell wall, chloroplast, mitochondria, mitochondrial cristae and nucleus, respectively. The scale of 2 μm is indicated at the bottom of each figure.

and AcP in *K. mikimotoi* increased with decreasing phosphate concentration (**Figures 5A,B**), and significance ($f = 18.753$; $p = 0.012$ in ACP; $f = 2.221$; $p = 0.021$, in AP) was found at pH 7.4 compared to the control of pH 8.1. Specifically, the AP and AcP activities in the P limitation group were much higher than those in the control at the same pH of 7.4, followed by the N limitation group. The results indicated that both low phosphorus and low nitrogen status induced the massive increase of AP and AcP activities under acidification conditions. AP activities were significantly affected by nutrient status and their

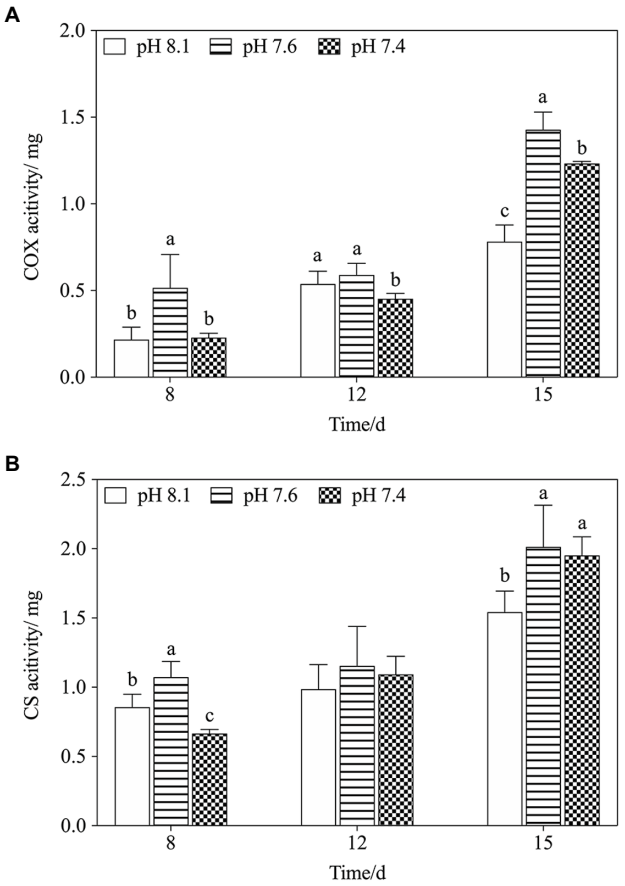

FIGURE 3 | Changes in mitochondrial metabolism-related enzyme activities in *K. mikimotoi* under exposure to different pH levels. **(A)** COX activity; **(B)** CS activity. Data are presented as means ± SD. Different lowercase letters indicate significant differences between the treatment and the control at each time point ($p < 0.05$).

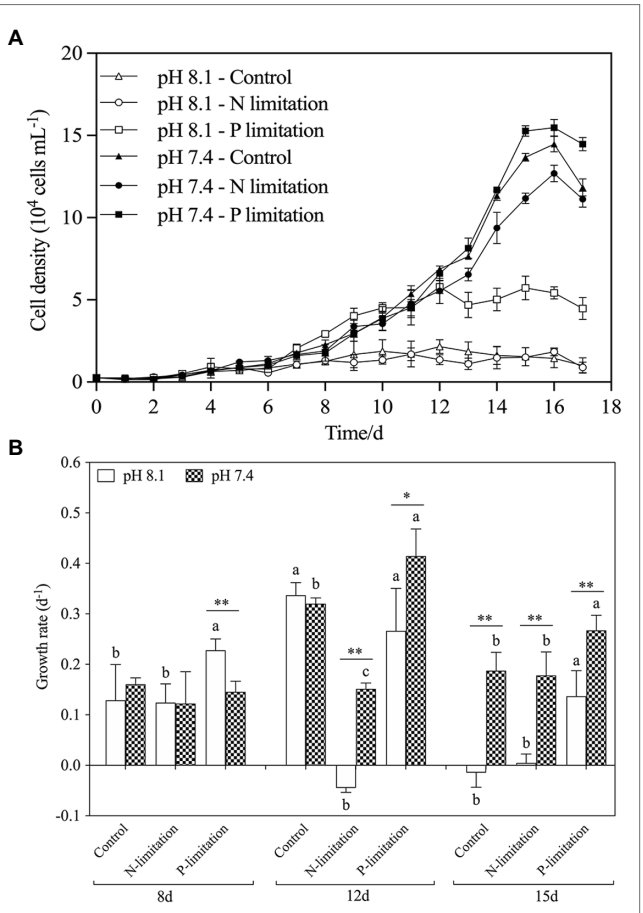

FIGURE 4 | The changes of population dynamics of *K. mikimotoi* under seawater acidification conditions when exposed to different nutrient levels. Data are presented as means ± SD. **(A)** Cell density; **(B)** Specific growth rate. Different lowercase letters indicate significant differences among the three nutrient levels within each pH treatment at each time point ($p < 0.05$). Asterisks indicate significant differences between two pH levels within each nutrient treatment ($p < 0.05$).

interactions at day 12 and day15, and ACP activities were only significantly affected by their interactions at day 12.

On the 8th day after exposure, pH 8.1 with N and P limitations showed a significant positive effect on NR activities compared to pH 7.4. With the extension of time (**Figure 5C**), the NR activities under N and P limitations were lower than those in the control on the 12th and 15th days, and there was no significant change between different pH levels under the same nutrient status. These results indicated that the effect of nutrient limitations on the activity of NR was more dramatic than that of acidification. During the whole experiment, NR activities showed no interactive significant effect. At day 8 and day 15, NR activities were significantly affected by pH and were only affected by nutrient status at day 12 and day15.

Effects of Seawater Acidification With Different Nutrient Statuses on ROS Production

The relative DCF fluorescence demonstrated that the intracellular ROS level was elevated on the 8th day of exposure in each treatment group (**Figure 6**), and the ROS level in the pH 8.1 with N limitation group reached the highest point ($f = 70.54$; $p = 0.001$). With time, the ROS level decreased and then stabilized on the 12th and 15th days. In addition, the ROS levels of all nutrient treatment groups at pH 7.4 were higher than those at pH 8.1 on the 15th day ($f = 31.62$; $p = 0.001$). It is worth noting that the N and P limitation groups at pH 7.4 had no significant difference ($f = 1.205$; $p = 0.363$) in the ROS levels of *K. mikimotoi* compared with the control. The ROS levels showed higher sensitivity to acidification conditions when exposed to different nutrient statuses. ROS levels were significantly affected by nutrient status during the whole experiment. Moreover, interactive effects of pH and nutrient status were observed at day 8 and day 15 (**Table 3**).

Toxicity Responses of *K. mikimotoi* to Seawater Acidification With Different Nutrient Statuses

In general, the hemolysis rate increased with time (**Figure 7**) and reached a peak on the 15th day after exposure, with the highest point at pH 7.4 with P limitation. Specifically, the

TABLE 3 | Two-way ANOVA summary on combined effects of seawater acidification (pH) and nutrient status (N/P) on ROS level, AcP activities, AP activities, growth rate, NR activities, and Hemolysis rate of *K. mikimotoi* at pH 8.1, 7.6, and 7.4; N/P: 7:1, 17:1 and 52:1.

Parameter		ROS			AcP			AP		
df		pH	N/P	pH*N/P	pH	N/P	pH*N/P	pH	N/P	pH*N/P
		1	1	2	1	1	2	1	1	2
8d	F	0.074	6.128	5.500	58.821	31.692	0.732	0.261	3.482	1.145
	P	0.790	**0.015**	**0.020**	**<0.001**	**<0.001**	0.501	0.619	0.064	0.351
12d	F	18.956	15.024	2.048	0.224	76.074	46.057	1.165	20.735	17.981
	P	**0.001**	**0.001**	0.172	0.644	**<0.001**	**<0.001**	0.302	**<0.001**	**<0.001**
15d	F	363.975	58.141	30.917	0.037	16.881	0.000	7.230	15.496	14.736
	P	**<0.001**	**<0.001**	**<0.001**	**0.005**	2.156	0.159	**0.020**	**<0.001**	**0.001**
Parameter		**Growth rate**			**NR**			**Hemolysis**		
df		pH	N/P	pH*N/P	pH	N/P	pH*N/P	pH	N/P	pH*N/P
		1	1	2	1	1	2	1	1	2
8d	F	88.173	40.934	35.092	11.630	0.964	0.572	88.173	40.934	35.092
	P	**<0.001**	**<0.001**	**<0.001**	**0.005**	0.409	0.579	**<0.001**	**<0.001**	**<0.001**
12d	F	5.165	23.363	44.941	0.973	10.154	1.590	0.041	4.518	14.266
	P	**0.042**	**<0.001**	**<0.001**	0.343	**0.003**	0.244	0.843	**0.034**	**0.001**
15d	F	0.365	7.968	15.887	5.976	25.777	2.371	2.703	19.721	41.455
	P	0.557	**0.006**	**<0.001**	**0.031**	**<0.001**	0.136	0.126	**<0.001**	**<0.001**

Significant effects ($p < 0.05$) are indicated in bold.

TABLE 4 | Regressions of the logistic model on *K. mikimotoi* population growth under seawater acidification conditions when exposed to different nutrient statuses.

Group	*K* (×10^4 cells mL^{-1})	*r* (d^{-1})	*Tp* (d^{-1})
pH 8.1			
Control	3.7721	0.4517	5.6
N limitation	2.2478	0.2438	4.7
P limitation	6.0252	0.5088	7.6
pH 7.4			
Control	15.4849	0.4868	12.3
N limitation	15.5869	0.3630	13.2
P limitation	18.2281	0.5794	12.9

hemolysis rate in the P limitation group was much higher than that in the N limitation group at the same pH level, suggesting that *K. mikimotoi* has more adaptability to low phosphate conditions. Interestingly, N limitation conditions inhibited growth but obviously induced hemolytic activity in *K. mikimotoi* at pH 8.1. The results showed that compared to N limitation, P limitation significantly ($f = 70.541$; $p = 0.001$) enhanced the hemolysis rate in hemocytes of mussels under acidification conditions. Hemolysis rates were significantly affected by nutrient status and their interactions during the whole experiment and were only significantly affected by pH at day 8 (**Table 3**).

DISCUSSION

The present study elucidated the impact of acidification on the population dynamics of *K. mikimotoi*, and a possible explanation was proposed from a mitochondrial-metabolic perspective. In addition, the effects of acidification interacting with different nutrient statuses were discussed.

Mitochondrial Metabolism Was Speculated to Alter During the Process of *K. mikimotoi* Coping With Seawater Acidification

In the present study, acidification (pH 7.6) promoted a certain increase in algal growth, but there was no significant stimulating effect at pH 7.4, and even inhibited the growth of algal to some extent ($p < 0.05$). There are two possible explanations for this: First, the cells reallocate intercellular energy for other metabolic activities (Shi et al., 2015) and reduce it for cellular division, and second, acidification impairs the cellular structure (Shi et al., 2009), and this results in a disorder of cell physiological functions (Rost et al., 2010). Mitochondria are organelles responsible for energy production that is essential for cell division and growth (Nunes-Nesi et al., 2014). Energy synthesis in plant mitochondria originates from a sequential set of metabolic processes and then undergoes a series of enzymatic and nonenzymatic reactions to synthesize ATP *via* the tricarboxylic acid cycle (TAC) and oxidative phosphorylation (Jacoby et al., 2012). We measured the activities of two respiratory enzymes, COX and CS, which play key roles in TAC and oxidative phosphorylation and found that pH 7.6 significantly increased their activities ($p < 0.05$). The activation of these enzymes facilitates ATP synthesis and increases ATP production (Xiao et al., 2019). However, pH 7.4 inhibited the activities of COX and CS on the 8th day, indicating an insufficient supply of ATP, which might disrupt cell function (Chivasa et al., 2005). The normal process of cellular biochemical reactions is based on an intact cellular structure, and interference with enzymatic activities could be due to mitochondrial structural damage (Xiao et al., 2019). TEM observations (**Figure 2**) showed that the mitochondria in *K. mikimotoi* cells exhibited normal morphological structures when exposed to pH 7.6 conditions (**Figure 2C**); therefore, the activities of these enzymes were

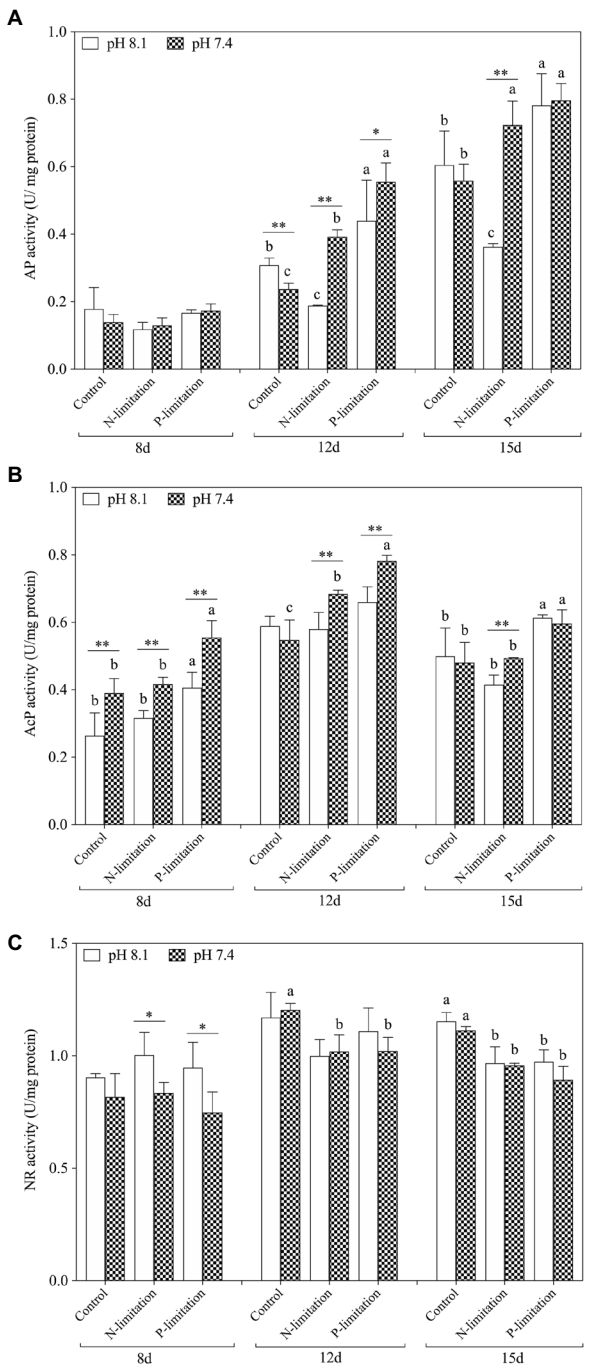

FIGURE 5 | Changes in nutrient absorption-related enzyme activities in *K. mikimotoi* under seawater acidification conditions when exposed to different nutrient levels. **(A)** AP activity; **(B)** AcP activity; **(C)** NR activity. Data are presented as means ± SD. Different lowercase letters indicate significant differences between three nutrient levels within each pH treatment at each time point ($p < 0.05$). Asterisks indicate significant differences between two pH levels within each nutrient treatment ($p < 0.05$).

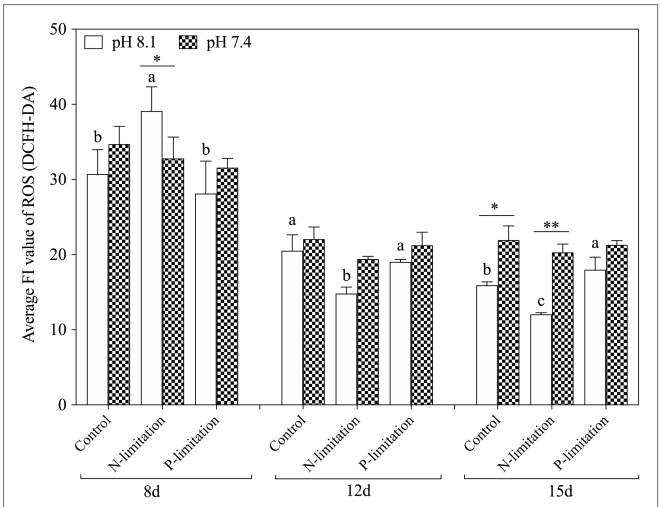

FIGURE 6 | Changes in ROS levels in *K. mikimotoi* under seawater acidification conditions when exposed to different nutrient levels. Data are presented as means ± SD. Different lowercase letters indicate significant differences among three nutrient levels within each pH treatment at each time point ($p < 0.05$). Asterisks indicate significant differences between two pH levels within each nutrient treatment ($p < 0.05$).

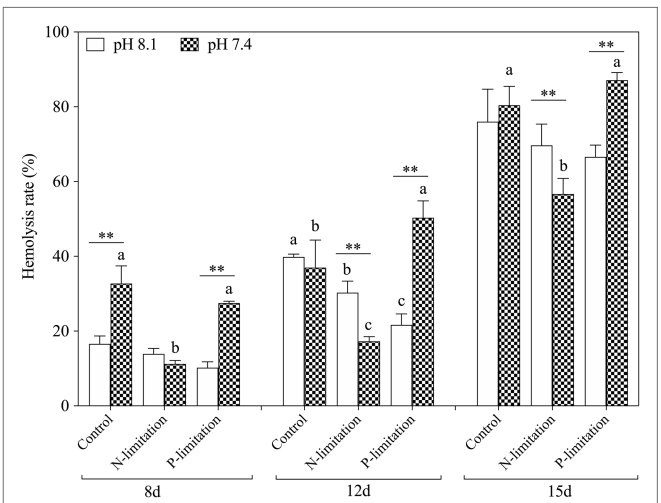

FIGURE 7 | Changes in hemolytic activity in *K. mikimotoi* under seawater acidification conditions when exposed to different nutrient levels. Data are presented as means ± SD. Different lowercase letters indicate significant differences among three nutrient levels within each pH treatment at each time point ($p < 0.05$). Asterisks indicate significant differences between two pH levels within each nutrient treatment ($p < 0.05$).

not negatively affected. However, pH 7.4 destroyed the mitochondrial ultrastructure, damaging the bilayer membrane structure and blurring the cristae (**Figure 2E**). Therefore, changes in the mitochondrial structure at pH 7.4 may affect key mitochondrial enzyme activities and ATP synthesis.

Mitochondria are also responsible for ROS overproduction when aerobic respiration is blocked under stress (Ali et al., 2016; Zhang et al., 2018). It has been reported that acidification stress leads to the accumulation of ROS and results in oxidative damage (Li and Xing, 2011), and we observed similar results in the present study: pH 7.6 induced a slight increase in ROS levels

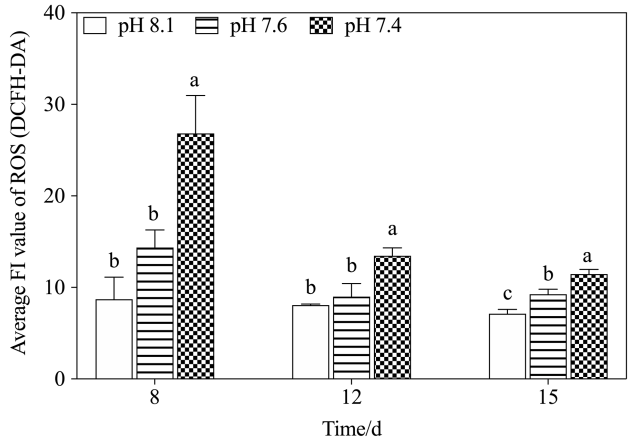

FIGURE 8 | Changes in ROS levels in *K. mikimotoi* under exposure to different pH levels. Data are presented as means ± SD. Different lowercase letters indicate significant differences between the treatment and the control at each time point ($p < 0.05$).

and pH 7.4 stress caused ROS bursts (**Figure 8**), which is an important response of *K. mikimotoi* to acidification exposure on the 8th day, suggesting that pH 7.4 induces mitochondrial oxidative stress. The elevated ROS level damaged the mitochondrial ultrastructure and caused mitochondrial dysfunction in *K. mikimotoi*, which further aggravated the damage. ROS have also been shown to have direct inhibitory effects on a variety of mitochondrial enzymes, including components of the electron transport chain (Chen et al., 2005; Navrot et al., 2007). In this study, ROS were found to have a significantly negative correlation with both COX and CS in all treated groups, and this reached extreme significance ($p < 0.01$) in the pH 7.4 group (**Table 5**). Specifically, Guedouari et al. (2014) found that temporary oxidative stress is associated with an increase in ROS production, which may constitute a signal for adaptive strategies.

It was speculated that the enzymes COX and CS, which are involved in mitochondrial metabolism, are closely related to physiological adaptability at the individual level (Ren et al., 2010). CS activation drives the TCA cycle toward a more energetic metabolism and is necessary to respond to the energetic needs of the cell. Moreover, a significant increase in COX activity may compensate for the inhibition of mitochondria (Guedouari et al., 2014). In this study, the concomitant activation of COX and CS in the pH 7.4 group reflected a shift of the algal cells toward higher levels of energy production on the 15th day, possibly providing the mitochondrial respiratory chain with a larger number of electrons. In addition, activating the key enzymes in mitochondrial metabolism helped to increase ATP production in the algal cells under acidification conditions to run some energy consumption adaptation mechanisms, including activating antioxidant systems to eliminate excessive ROS (Ali et al., 2016; Zhang et al., 2018), thus alleviating ROS damage to mitochondria. As stated above, we thus speculated that mitochondrial metabolism takes part in the active response of *K. mikimotoi* to acidification.

TABLE 5 | Pearson's correlation coefficients between key enzyme activities and ROS levels in *K. mikimotoi* treated with seawater acidification.

		ROS	COX
pH 8.1	COX	−0.983**	
	CS	−0.971**	0.912**
pH 7.6	COX	−0.524*	
	CS	−0.529*	0.992**
pH 7.4	COX	−0.756**	
	CS	−0.828**	0.993**

*Significant differences at the $p < 0.05$ level.
**Significant differences at the $p < 0.01$ level.

Nutrient Alterations Could Drive the Effects of Seawater Acidification on *K. mikimotoi*

We found that a moderate decrease in pH could promote an increase in algal cell density, but a further decrease in pH would damage the cellular structure and function. N and P are the most crucial factors in the growth rate, and algal density increases with increasing N:P ratios in a certain range (Li et al., 2014). It is suggested that high nitrogenous nutrient availability is a prerequisite for *K. mikimotoi* blooms (Chang and Carpenter, 1985). In our study, the condition of acidification with different nutrient statuses significantly increased the population density of *K. mikimotoi*. The growth rate of *K. mikimotoi* was highly sensitive to acidification driven by nutrient alteration, especially under P limitation on the 12th and 15th days (**Figure 4**). Similar results found that the cell density and growth rate of *Conticribra weissflogii* and *Prorocentrum donghaiense* were increased when N/P increase under acidification conditions (Zheng et al., 2016), which was evidenced that the growth rate was controlled not only by the pH but also by the ratio of N to P. Two enzymes closely related to phosphate absorption, AP and AcP, were found to be actively induced simultaneously, and a relatively clear negative correlation was found between the enzymatic activity and the P concentration (**Figure 5**). This result might be a possible explanation for the population dynamics observation of the abovementioned factors and was also consistent with the following statement: acidification promotes the expression of phytoplankton phosphorus deficiency signals, thereby facilitating the absorption and utilization of phosphorus (Ivančić et al., 2010; Fitzsimons et al., 2020). However, the changes in the activities of the two phosphatases differed when exposed to N limitation conditions with acidification. The results showed that N limitation induced a progressive increase in AP activity in a time-dependent manner but only a slight increase in AcP activity on the 12th day ($p < 0.05$). Therefore, both N and P limitations induced an increase in phosphatase activities in *K. mikimotoi* cells under acidification.

Increasing the activity of AP and AcP is one of the important adaptive strategies of plants to enhance P acquisition and utilization (Wang et al., 2009). It is reported that *K. mikimotoi* grows better as nitrate supplied as the only nitrogen source (Lei and Lü, 2011). However, the NR characteristics of different algae are different, which leads to differences in

TABLE 6 | Pearson's correlation coefficients among parameters under seawater acidification conditions when exposed to different nutrient statuses.

	ROS	AP	AcP	NR
pH 8.1				
ROS				
AP	−0.539*			
AcP	−0.641**	0.521*		
NR	−0.278	0.282	0.530*	
Hemolysis rate	−0.708**	0.727**	0.3	0.216
pH 7.4				
ROS				
AP	−0.745**			
AcP	−0.610*	0.589*		
NR	−0.562*	0.172	0.182	
Hemolysis rate	−0.586*	0.799**	0.009	0.202

*Significant differences at the $p<0.05$ level.
**Significant differences at the $p<0.01$ level.

the nitrate utilization efficiency of algae (Berges and Hageman, 1997). In addition, the exact mechanism of nitrate on *K. mikimotoi* algal cell metabolism is still unknown. Our results showed that NR activities in *K. mikimotoi* induced by N and P limitations decreased slightly when exposed to acidification, but the difference between the two nutrient limitations was not significant. We suspect that in the process of external nitrate depletion or after exhaustion, *K. mikimotoi* utilized intracellular reserves of nitrate to maintain a certain NR activity under extremely low nitrate levels in the external environment (Dortch et al., 1979).

Hemolytic toxicity is another effective index indicating the growth status of *K. mikimotoi* (Li et al., 2019), which varies according to the growth stage and nutrient condition of *K. mikimotoi* (Lin et al., 2015). Under nutrient-sufficiency conditions, toxin production is often low, while increased production is associated with different types of nutrient limitation stress. The hemocytes of the blue mussel *M. edulis* were utilized in the present study to determine the hemolytic toxicity, which was different from the routine method that utilizes bovine or rabbit blood cells. We found that the hemolytic activity was increased in a time- and N:P ratio-dependent manner (**Figure 7**), and a significant elevation was seen under P limitation. These results suggest P limitation is an important factor regulating cellular toxicity and adverse impacts. Acidification (pH) and nutrient alteration (N/P) showed statistically (MANOVA) significant interactive effects on hemolytic activity (**Table 3**). The algae cells under high CO_2 and P limitation conditions were the most toxic (**Figure 7**). Similar results showed that cytotoxicity of *Alexandrium catenella* was observed to be significantly increased under P limitation, while acidification conditions further exacerbated this toxicity (Tatters et al., 2013). Significantly, the increase in hemolytic activity is supported by N released within the cell from protein turnover, which was affected by P limitation, so that hemolytic cytotoxin synthesis was enhanced. Negative significance was also observed between hemolytic toxicity and ROS ($p=-0.586$*; **Table 6**). Considering the downregulation of ROS levels over time, we speculated that more energy produced by mitochondrial metabolism was allocated to the accumulation of toxic compounds (Jin et al., 2015), which enhanced the hemolytic activity during exposure to acidification with different nutrient statuses (Wang et al., 2019a). These data further explain why *K. mikimotoi* becomes the dominant species under red tide conditions by enhancing its absorption rate of nutrients and its toxicity.

CONCLUSION

Taken together, seawater acidification plays a critical role in influencing the growth of *K. mikimotoi*, and mitochondrial metabolism is involved in the process of coping with acidification. Nutrient limitations, especially P limitation, could effectively alleviate the negative impacts induced by acidification, which is one of the competitive strategies used by *K. mikimotoi*. Exposure to acidification with different nutrient statuses would lead to changes in the secretion of toxins in *K. mikimotoi*, which is closely related to the formation of red tides under natural conditions.

DATA AVAILABILITY STATEMENT

The raw data supporting the conclusions of this article will be made available by the authors, without undue reservation.

AUTHOR CONTRIBUTIONS

YoW conceived and supervised the project. QL, YaW, and BZ conceived and designed the experiments. QL, YaW, YuL, and YiL performed the experiments. QL and YaW analyzed the data, wrote the manuscript, and contributed to this work. ZZ revised the final manuscript, figures, and tables with input from QL. All authors participated in the discussions of the results and the preparation of the manuscript. All authors contributed to the article and approved the submitted version.

FUNDING

This work was financially supported by the National Key R&D Program of China (No. 2017YFC1404304) and the Fundamental Research Funds for the Central Universities (Nos. 201964024 and 202066001).

ACKNOWLEDGMENTS

The authors thank Dazhi Wang of Xiamen University and Qingchun Zhang of Institute of Oceanography, Chinese Academy of Sciences for providing the *K. mikimotoi* strain (MEL22), and all the members in the lab for their assistance. We also thank the reviewers for numerous valuable suggestions to improve the manuscript.

REFERENCES

Ali, I., Liu, B., Farooq, M. A., Islam, F., Azizullah, A., Yu, C., et al. (2016). Toxicological effects of bisphenol A on growth and antioxidant defense system in *Oryza sativa* as revealed by ultrastructure analysis. *Ecotoxicol. Environ. Saf.* 124, 277–284. doi: 10.1016/j.ecoenv.2015.10.027

Bach, L. T., Taucher, J., Boxhammer, T., Ludwig, A., Achterberg, E. P., Algueró-Muñiz, M., et al. (2016). Influence of ocean acidification on a natural winter-to-summer plankton succession: first insights from a long-term mesocosm study draw attention to periods of low nutrient concentrations. *PLoS One* 11:e0159068. doi: 10.1371/journal.pone.0159068

Bercel, T. L., and Kranz, S. A. (2019). Insights into carbon acquisition and photosynthesis in *Karenia brevis* under a range of CO_2 concentrations. *Prog. Oceanogr.* 172, 65–76. doi: 10.1016/j.pocean.2019.01.011

Berges, J. A., and Hageman, R. H. (1997). Nitrate reductase activity quantitatively predicts the rate of nitrate incorporation under steady state light limitation: a revised assay and characterization of the enzyme in three species of marine phytoplankton. *Limnol. Oceanogr.* 40, 82–93. doi: 10.4319/lo.1995.40.1.0082

Brand, L. E., Campbell, L., and Bresnan, E. (2012). Karenia: the biology and ecology of a toxic genus. *Harmful Algae* 14, 156–178. doi: 10.1016/j.hal.2011.10.020

Brandenburg, K. M., Velthuis, M., and Van de Waal, D. B. (2019). Meta-analysis reveals enhanced growth of marine harmful algae from temperate regions with warming and elevated CO_2 levels. *Glob. Chang. Biol.* 25, 2607–2618. doi: 10.1111/gcb.14678

Caffrey, J. M., Dasmahapatra, A., Smith, H. A., Hede, K., and Frieden, E. (1986). The effect of copper ion on glutathione and hemolysis in rabbit erythrocytes. *Biol. Trace Elem. Res.* 11, 19–26. doi: 10.1007/BF02795519

Chang, J., and Carpenter, E. J. (1985). Blooms of the dinoflagellate *Gyrodinium aureolum* in a long Island estuary: box model analysis of bloom maintenance. *Mar. Biol.* 89, 83–93. doi: 10.1007/BF00392880

Chen, Y. R., Chen, C. L., Zhang, L. W., Greenchurch, K. B., and Zweier, J. L. (2005). Superoxide generation from mitochondrial NADH dehydrogenase induces self-inactivation with specific protein radical formation. *J. Biol. Chem.* 280, 37339–37348. doi: 10.1074/jbc.M503936200

Chen, B., Wang, K., Guo, H., and Lin, H. (2021). *Karenia mikimotoi* blooms in coastal waters of China from 1998 to 2017. *Estuar. Coast. Shelf Sci.* 249:107034. doi: 10.1016/j.ecss.2020.107034

Chivasa, S., Ndimba, B. K., Simon, W. J., Lindsey, K., and Slabas, A. R. (2005). Extracellular ATP functions as an endogenous external metabolite regulating plant cell viability. *Plant Cell* 17, 3019–3034. doi: 10.1105/tpc.105.036806

Deng, X., Li, D., Wang, L., Hu, X., Cheng, J., and Gao, K. (2017). Potential toxicity of ionic liquid ($[C_{12}mim]BF_4$) on the growth and biochemical characteristics of a marine diatom *Phaeodactylum tricornutum*. *Sci. Total Environ.* 586, 675–684. doi: 10.1016/j.scitotenv.2017.02.043

Dortch, Q., Ahmed, S. I., and Packard, T. T. (1979). Nitrate reductase and glutamate dehydrogenase activities in *Skeletonema costatum* as measures of nitrogen assimilation rates. *J. Plankton Res.* 1, 169–186. doi: 10.1093/plankt/1.2.169

Eberlein, T., Van de Waal, D. B., and Rost, B. (2014). Differential effects of ocean acidification on carbon acquisition in two bloom-forming dinoflagellate species. *Physiol. Plant.* 151, 468–479. doi: 10.1111/ppl.12137

Fitzsimons, M. F., Probert, I., Gaillard, F., and Rees, A. P. (2020). Dissolved organic phosphorus uptake by marine phytoplankton is enhanced by the presence of dissolved organic nitrogen. *J. Exp. Mar. Biol. Ecol.* 530-531:151434. doi: 10.1016/j.jembe.2020.151434

Fu, F. X., Place, A. R., Garcia, N. S., and Hutchins, D. A. (2010). CO_2 and phosphate availability control the toxicity of the harmful bloom dinoflagellate *Karlodinium veneficum*. *Aquat. Microb. Ecol.* 59, 55–65. doi: 10.3354/ame01396

Glibert, P. M., Al-Azri, A., Icarus Allen, J., Bouwman, A. F., Beusen, A. H. W., and Burford, M. A. (2018). "Key questions and recent research advances on harmful algal blooms in relation to nutrients and eutrophication," in *Global Ecology and Oceanography of Harmful Algal Blooms. Vol. 232.* eds. P. Glibert, E. Berdalet, M. Burford, G. Pitcher and M. Zhou (Cham: Springer), 229–259.

Glibert, P. M., Harrison, J., Heil, C., and Seitzinger, S. (2006). Escalating worldwide use of urea-A global change contributing to coastal eutrophication. *Biogeochemistry* 77, 441–463. doi: 10.1007/s10533-005-3070-5

Gobler, C. J., Hattenrath-Lehmann, T. K., Doherty, O. M., Griffith, A. W., Kang, Y., and Litaker, R. W. (2017). Reply to Dees et al.: ocean warming promotes species-specific increases in the cellular growth rates of harmful algal blooms. *Proc. Natl. Acad. Sci. U. S. A.* 114, E9765–E9766. doi: 10.1073/pnas.1715749114

Guan, W., and Li, P. (2017). Dependency of UVR-induced photoinhibition on atomic ratio of N to P in the dinoflagellate *Karenia mikimotoi*. *Mar. Biol.* 164, 30–38. doi: 10.1007/s00227-016-3065-x

Guedouari, H., Gergondey, R., Bourdais, A., Vanparis, O., Bulteau, A. L., Camadro, J. M., et al. (2014). Changes in glutathione-dependent redox status and mitochondrial energetic strategies are part of the adaptive response during the filamentation process in *Candida albicans*. *BBA-Mol. Basis Dis.* 1842, 1855–1869. doi: 10.1016/j.bbadis.2014.07.006

Guillard, R. R. L. (1975). "Culture of phytoplankton for feeding marine invertebrates," in *Culture of Marine Invertebrate Animals*. eds. W. L. Smith and M. H. Chanley (US: Springer), 29–60.

Hallegraeff, G. M. (2003). "Harmful algal blooms: a global overview," in *Manual on Harmful Marine Microalgae*. eds. G. M. A. Hallegraeff and A. D. Cembella (Paris, France: UNESCO Publishing), 25–49.

Hallegraeff, G. M., Anderson, D. M., Belin, C., Bottein, M. Y. D., Bresnan, E., Chinain, M., et al. (2021). Perceived global increase in algal blooms is attributable to intensified monitoring and emerging bloom impacts. *Commun. Earth Environ.* 2:117. doi: 10.1038/s43247-021-00178-8

Hardison, D. R., Sunda, W. G., Tester, P. A., Shea, D., and Litaker, R. W. (2014). Increased cellular brevetoxins in the red tide dinoflagellate *Karenia brevis* under CO_2 limitation of growth rate: evolutionary implications and potential effects on bloom toxicity. *Limnol. Oceanogr.* 59, 560–577. doi: 10.4319/lo.2014.59.2.0560

Hu, S., Zhou, B., Wang, Y., Wang, Y., Zhang, X., Zhao, Y., et al. (2017). Effect of CO_2-induced seawater acidification on growth, photosynthesis and inorganic carbon acquisition of the harmful bloom-forming marine microalga, *Karenia mikimotoi*. *Plos One* 12:e0183289. doi: 10.1371/journal.pone.0183289

Ivančić, I., Fuks, D., Radić, T., Lyons, D. M., Šilović, T., Kraus, R., et al. (2010). Phytoplankton and bacterial alkaline phosphatase activity in the northern Adriatic Sea. *Mar. Environ. Res.* 69, 85–94. doi: 10.1016/j.marenvres.2009.08.004

Jacoby, R. P., Li, L., Huang, S., Lee, C. P., Millar, A. H., and Taylor, N. L. (2012). Mitochondrial composition, function and stress response in plants. *J. Integr. Plant Biol.* 54, 887–906. doi: 10.1111/j.1744-7909.2012.01177.x

Jin, P., Wang, T., Liu, N., Dupont, S., Beardall, J., Boyd, P. W., et al. (2015). Ocean acidification increases the accumulation of toxic phenolic compounds across trophic levels. *Nat. Commun.* 6:8714. doi: 10.1038/ncomms9714

Lei, Q. Y., and Lü, S. H. (2011). Molecular ecological responses of dinoflagellate, *Karenia mikimotoi* to environmental nitrate stress. *Mar. Pollut. Bull.* 62, 2692–2699. doi: 10.1016/j.marpolbul.2011.09.021

Leo, E., Graeve, M., Storch, D., Pörtner, H. O., and Mark, F. C. (2020). Impact of ocean acidification and warming on mitochondrial enzymes and membrane lipids in two gadoid species. *Polar Biol.* 43, 1109–1120. doi: 10.1007/s00300-019-02600-6

Li, S., Liu, F., Zheng, F., Huang, X., and Zuo, Y. (2014). Risk assessment of nitrate and petroleum-derived hydrocarbon addition on *Contricriba weissflogii* biomass, lifetime, and nutritional value. *J. Hazard. Mater.* 268, 199–206. doi: 10.1016/j.jhazmat.2014.01.018

Li, Z., and Xing, D. (2011). Mechanistic study of mitochondria-dependent programmed cell death induced by aluminium phytotoxicity using fluorescence techniques. *J. Exp. Bot.* 62, 331–343. doi: 10.1093/jxb/erq279

Li, X., Yan, T., Lin, J., Yu, R., and Zhou, M. (2017). Detrimental impacts of the dinoflagellate *Karenia mikimotoi* in Fujian coastal waters on typical marine organisms. *Harmful Algae* 61, 1–12. doi: 10.1016/j.hal.2016.11.011

Li, X., Yan, T., Yu, R., and Zhou, M. (2019). A review of *Karenia mikimotoi*: bloom events, physiology, toxicity and toxic mechanism. *Harmful Algae* 90:101702. doi: 10.1016/j.hal.2019.101702

Li, Y., Yu, J., Sun, T., Liu, C., Sun, Y., and Wang, Y. (2018). Using the marine rotifer *Brachionus plicatilis* as an endpoint to evaluate whether ROS-dependent hemolytic toxicity is involved in the allelopathy induced by *Karenia mikimotoi*. *Toxins* 10:439. doi: 10.3390/toxins10110439

Lin, J., Yan, T., Zhang, Q., and Zhou, M. (2015). Impact of several harmful algal bloom (HAB) causing species, on life history characteristics of rotifer *Brachionus plicatilis* Müller. *Chin. J. Oceanol. Limnol.* 34, 642–653. doi: 10.1007/s00343-016-5065-6

Mei, F., Song, X. X., Yu, Z. M., and Liu, Y. (2013). Responses of phosphate transporter gene and alkaline phosphatase in *Thalassiosira pseudonana* to phosphine. *PLoS One* 8:e59770. doi: 10.1371/journal.pone.0059770

Navrot, N., Rouhier, N., Gelhaye, E., and Jacquot, J. P. (2007). Reactive oxygen species generation and antioxidant systems in plant mitochondria. *Physiol. Plant.* 129, 185–195. doi: 10.1111/j.1399-3054.2006.00777.x

Nielsen, L. C., Bourg, I. C., and Sposito, G. (2012). Predicting CO_2–water interfacial tension under pressure and temperature conditions of geologic CO_2 storage. *Geochim. Cosmochim. Acta* 81, 28–38. doi: 10.1016/j.gca.2011.12.018

Nimer, N. A., Iglesias Rodriguez, M. D., and Merrett, M. J. (1997). Bicarbonate utilization by marine phytoplankton species. *J. Phycol.* 33, 625–631. doi: 10.1111/j.0022-3646.1997.00625.x

Nunes-Nesi, A., Brito, D. S., Inostroza-Blancheteau, C., Fernie, A. R., and Araújo, W. L. (2014). The complex role of mitochondrial metabolism in plant aluminum resistance. *Trends Plant Sci.* 19, 399–407. doi: 10.1016/j.tplants.2013.12.006

OECD (2011). Test no. 201: OECD guidelines for the testing of chemicals. Freshwater Alga and Cyanobacteria, Growth Inhibition Test. Organisation for Economic Co-operation and Development, Paris.

Radan, R. L., and Cochlan, W. P. (2018). Differential toxin response of *Pseudo-nitzschia multiseries* as a function of nitrogen speciation in batch and continuous cultures, and during a natural assemblage experiment. *Harmful Algae* 73, 12–29. doi: 10.1016/j.hal.2018.01.002

Ren, J. C., Rebrin, I., Klichko, V., Orr, W. C., and Sohal, R. S. (2010). Cytochrome c oxidase loses catalytic activity and structural integrity during the aging process in *Drosophila melanogaster*. *Biochem. Biophys. Res. Commun.* 401, 64–68. doi: 10.1016/j.bbrc.2010.09.009

Riebesell, U., Aberle-Malzahn, N., Achterberg, E. P., Algueró-Muñiz, M., Alvarez-Fernandez, S., Arístegui, J., et al. (2018). Toxic algal bloom induced by ocean acidification disrupts the pelagic food web. *Nat. Clim. Chang.* 8, 1082–1086. doi: 10.1038/s41558-018-0344-1

Rost, B., Richter, K. U., Riebesell, U., and Hansen, P. J. (2010). Inorganic carbon acquisition in red tide dinoflagellates. *Plant Cell Environ.* 29, 810–822. doi: 10.1111/j.1365-3040.2005.01450.x

Sala, M. M., Aparicio, F. L., and Boras, J. (2016). Contrasting effects of ocean acidification on the microbial food web under different trophic conditions. *ICES J. Mar. Sci.* 73, 670–679. doi: 10.1093/icesjms/fsv130

Sett, S., Bach, L. T., Schulz, K. G., Koch-Klavsen, S., Lebrato, M., and Riebesell, U. (2014). Temperature modulates coccolithophorid sensitivity of growth, photosynthesis and calcification to increasing seawater pCO_2. *PLoS One* 9:e88308. doi: 10.1371/journal.pone.0088308

Shi, D., Li, W., Hopkinson, B. M., Hong, H., Li, D., Kao, S. J., et al. (2015). Interactive effects of light, nitrogen source, and carbon dioxide on energy metabolism in the diatom *Thalassiosira pseudonana*. *Limnol. Oceanogr.* 60, 1805–1822. doi: 10.1002/lno.10134

Shi, D. L., Xu, Y. K., and Morel, F. M. M. (2009). Effects of the pH/pCO_2 control method on medium chemistry and phytoplankton growth. *Biogeosciences* 6, 1199–1207. doi: 10.5194/bg-6-1199-2009

Sun, J., Hutchins, D. A., Feng, Y., Seubert, E. L., Caron, D. A., and Fu, F. (2011). Effects of changing pCO_2 and phosphate availability on domoic acid production and physiology of the marine harmful bloom diatom *Pseudo-nitzschia multiseries*. *Limnol. Oceanogr.* 56, 829–840. doi: 10.4319/lo.2011.56.3.0829

Sun, J., Shu, S. Q., Xu, Z. L., Wang, Z. L., and Zhu, M. Y. (2007). The selective grazing of Calanus sinicus during a *Karenia mikimotoi* bloom in the East China Sea. *Oceanol. Limnol. Sin.* 38, 536–542. doi: 10.3321/j.issn:0029-814x.2007.06.008

Sun, T., Tang, X., Jiang, Y., and Wang, Y. (2017). Seawater acidification induced immune function changes of haemocytes in *Mytilus edulis*: a comparative study of CO_2 and HCl enrichment. *Sci. Rep.* 7:41488. doi: 10.1038/srep41488

Sun, T., Tang, X., Zhou, B., and Wang, Y. (2016). Comparative studies on the effects of seawater acidification caused by CO_2 and HCl enrichment on physiological changes in *Mytilus edulis*. *Chemosphere* 144, 2368–2376. doi: 10.1016/j.chemosphere.2015.10.117

Tan, H., Cai, R., Huo, Y., and Guo, H. (2020). Projections of changes in marine environment in coastal China seas over the 21st century based on CMIP5 models. *J. Ocean. Limnol.* 38, 1676–1691. doi: 10.1007/s00343-019-9134-5

Tatters, A. O., Flewelling, L. J., Fu, F., Granholm, A. A., and Hutchins, D. A. (2013). High CO_2 promotes the production of paralytic shellfish poisoning toxins by *Alexandrium catenella* from Southern California waters. *Harmful Algae* 30, 37–43. doi: 10.1016/j.hal.2013.08.007

Taucher, J., Jones, J., James, A. K., Brzezinski, M. A., Carlson, C. A., Riebesell, U., et al. (2015). Combined effects of CO_2 and temperature on carbon uptake and partitioning by the marine diatoms *Thalassiosira weissflogii* and *Dactyliosolen fragilissimus*. *Limnol. Oceanogr.* 60, 901–919. doi: 10.1002/lno.10063

Van de Waal, D. B., Brandenburg, K. M., Keuskamp, J., Trimborn, S., Rokitta, S., Kranz, S. A., et al. (2019). Highest plasticity of carbon-concentrating mechanisms in earliest evolved phytoplankton. *Limnol. Oceanogr. Lett.* 4, 37–43. doi: 10.1002/lol2.10102

Van de Waal, D. B., John, U., Ziveri, P., Reichart, G. J., Hoins, M., Sluijs, A., et al. (2013). Ocean acidification reduces growth and calcification in a marine dinoflagellate. *PLoS One* 8:e65987. doi: 10.1371/journal.pone.0065987

Wang, H., Niu, X., Feng, X., and Goncalves, R. J. (2019a). Effects of ocean acidification and phosphate limitation on physiology and toxicity of the dinoflagellate *Karenia mikimotoi*. *Harmful Algae* 87:101621. doi: 10.1016/j.hal.2019.101621

Wang, X., Feng, X., Zhuang, Y., Lu, J., Wang, Y., Goncalves, R. J., et al. (2019b). Effects of ocean acidification and solar ultraviolet radiation on physiology and toxicity of dinoflagellate *Karenia mikimotoi*. *Harmful Algae* 81, 1–9. doi: 10.1016/j.hal.2018.11.013

Wang, X., Wang, Y., Tian, J., Lim, B. L., Yan, X., and Liao, H. (2009). Overexpressing *AtPAP15* enhances phosphorus efficiency in soybean. *Plant Physiol.* 151, 233–240. doi: 10.1104/pp.109.138891

Wells, M. L., Karlson, B., Wulff, A., Kudela, R., Trick, C., Asnaghi, V., et al. (2019). Future HAB science: directions and challenges in a changing climate. *Harmful Algae* 91:101632. doi: 10.1016/j.hal.2019.101632

Wells, M. L., Trainer, V. L., Smayda, T. J., Karlson, B. S. O., Trick, C. G., Kudela, R. M., et al. (2015). Harmful algal blooms and climate change: learning from the past and present to forecast the future. *Harmful Algae* 49, 68–93. doi: 10.1016/j.hal.2015.07.009

Wohlrab, S., John, U., Klemm, K., Eberlein, T., Grivogiannis, A. M. F., Krock, B., et al. (2020). Ocean acidification increases domoic acid contents during a spring to summer succession of coastal phytoplankton. *Harmful Algae* 92:101697. doi: 10.1016/j.hal.2019.101697

Xiao, C., Wang, L., Hu, D., Zhou, Q., and Huang, X. (2019). Effects of exogenous bisphenol A on the function of mitochondria in root cells of soybean (*Glycine max* L.) seedlings. *Chemosphere* 222, 619–627. doi: 10.1016/j.chemosphere.2019.01.195

Zhang, J., Wang, L., Zhou, Q., and Huang, X. (2018). Reactive oxygen species initiate a protective response in plant roots to stress induced by environmental bisphenol A. *Ecotox. Environ. Saf.* 154, 197–205. doi: 10.1016/j.ecoenv.2018.02.020

Zhao, Y., Tang, X. X., Zhao, X. W., and Wang, Y. (2017). Effect of various nitrogen conditions on population growth, temporary cysts and cellular biochemical compositions of *Karenia mikimotoi*. *PLoS One* 12:e0171996. doi: 10.1371/journal.pone.0171996

Zhao, Y., Wang, Y., and Quigg, A. (2015). Comparison of population growth and photosynthetic apparatus changes in response to different nutrient status in a diatom and a coccolithophore. *J. Phycol.* 51, 872–884. doi: 10.1111/jpy.12327

Zheng, F. Y., Tu, T. X., Liu, F. J., Huang, X., and Li, S. (2016). Influence of acidification and eutrophication on physiological functions of *Conticribra weissflogii* and *Prorocentrum donghaiense*. *Aquat. Toxicol.* 181, 11–21. doi: 10.1016/j.aquatox.2016.10.024

Zhou, Z., Zhou, B., Chen, H., Tang, X., and Wang, Y. (2019). Reactive oxygen species (ROS) and the calcium-(Ca^{2+}) mediated extrinsic and intrinsic pathways underlying BDE-47-induced apoptosis in rainbow trout (*Oncorhynchus mykiss*) gonadal cells. *Sci. Total Environ.* 656, 778–788. doi: 10.1016/j.scitotenv.2018.11.306

Zhu, L.X., Cheng, N.Q., and Gao, X. (1983). *Electron Microscopy in Biology*. Peking University Press, Beijing, China, 286.

Zou, Y. N., Yamasaki, Y., Matsuyama, Y., Yamaguchi, K., Honjo, T., and Oda, T. (2010). Possible involvement of hemolytic activity in the contact-dependent lethal effects of the dinoflagellate Karenia mikimotoi on the rotifer *Brachionus plicatilis*. *Harmful Algae* 9, 367–373. doi: 10.1016/j.hal.2010.01.005

Conflict of Interest: The authors declare that the research was conducted in the absence of any commercial or financial relationships that could be construed as a potential conflict of interest.

Publisher's Note: All claims expressed in this article are solely those of the authors and do not necessarily represent those of their affiliated organizations, or those of the publisher, the editors and the reviewers. Any product that may be evaluated in this article, or claim that may be made by its manufacturer, is not guaranteed or endorsed by the publisher.

frontiers | Frontiers in Plant Science

TYPE Original Research
PUBLISHED 11 November 2022
DOI 10.3389/fpls.2022.1025416

OPEN ACCESS

EDITED BY
Benoit Schoefs,
Le Mans Université, France

REVIEWED BY
Milan Szabo,
Eötvös Loránd Research Network (ELKH), Hungary
Alexandrina Stirbet,
University of Bucharest, Romania

*CORRESPONDENCE
Billur Celebi-Ergin
celebibillur@gmail.com

†PRESENT ADDRESS
Billur Celebi-Ergin,
Department of Molecular Biology and Genetics, Koç University Rumelifeneri Yolu Sariyer, Istanbul, Turkey

SPECIALTY SECTION
This article was submitted to Marine and Freshwater Plants, a section of the journal Frontiers in Plant Science

RECEIVED 22 August 2022
ACCEPTED 10 October 2022
PUBLISHED 11 November 2022

CITATION
Celebi-Ergin B, Zimmerman RC and Hill VJ (2022) Photorespiration in eelgrass (*Zostera marina* L.): A photoprotection mechanism for survival in a CO_2-limited world. *Front. Plant Sci.* 13:1025416. doi: 10.3389/fpls.2022.1025416

Photorespiration in eelgrass (*Zostera marina* L.): A photoprotection mechanism for survival in a CO_2-limited world

Billur Celebi-Ergin *†, Richard C. Zimmerman and Victoria J. Hill

Department of Ocean and Earth Sciences, Old Dominion University, Norfolk, VA, United States

Photorespiration, commonly viewed as a loss in photosynthetic productivity of C3 plants, is expected to decline with increasing atmospheric CO_2, even though photorespiration plays an important role in the oxidative stress responses. This study aimed to quantify the role of photorespiration and alternative photoprotection mechanisms in *Zostera marina* L. (eelgrass), a carbon-limited marine C3 plant, in response to ocean acidification. Plants were grown in controlled outdoor aquaria at different $[CO_2]_{aq}$ ranging from ~55 (ambient) to ~2121 μM for 13 months and compared for differences in leaf photochemistry by simultaneous measurements of O_2 flux and variable fluorescence. At ambient $[CO_2]$, photosynthesis was carbon limited and the excess photon absorption was diverted both to photorespiration and non-photochemical quenching (NPQ). The dynamic range of NPQ regulation in ambient grown plants, in response to instantaneous changes in $[CO_2]_{aq}$, suggested considerable tolerance for fluctuating environmental conditions. However, 60 to 80% of maximum photosynthetic capacity of ambient plants was diverted to photorespiration resulting in limited carbon fixation. The photosynthesis to respiration ratio (P_E : R_D) of ambient grown plants increased 6-fold when measured under high CO_2 because photorespiration was virtually suppressed. Plants acclimated to high CO_2 maintained 4-fold higher P_E : R_D than ambient grown plants as a result of a 60% reduction in photorespiration. The O_2 production efficiency per unit chlorophyll was not affected by the CO_2 environment in which the plants were grown. Yet, CO_2 enrichment decreased the light level to initiate NPQ activity and downregulated the biomass specific pigment content by 50% and area specific pigment content by 30%. Thus, phenotypic acclimation to ocean carbonation in eelgrass, indicating the coupling between the regulation of photosynthetic structure and metabolic carbon demands, involved the downregulation of light harvesting by the photosynthetic apparatus, a reduction in the role of photorespiration and an increase in the role of NPQ in photoprotection. The quasi-mechanistic model developed in this study

permits integration of photosynthetic and morphological acclimation to ocean carbonation into seagrass productivity models, by adjusting the limits of the photosynthetic parameters based on substrate availability and physiological capacity.

KEYWORDS

CO_2, non-photochemical quenching, ocean acidification, photorespiration, photosynthesis, quantum yield, seagrass

Introduction

Photosynthesis and photorespiration are competing processes due to the bi-functionality of ribulose 1,5-biphosphate carboxylase/oxygenase (Rubisco) (Spreitzer and Salvucci, 2002). Since the oxygenation reaction of Rubisco decreases photosynthetic carbon gain, it has been viewed as an inefficient legacy of evolution that might be engineered out of terrestrial plants in a quest for increased productivity (Andrews and Lorimer, 1978; Somerville, 2001; Xin et al., 2015). Recent work, however, suggests that Rubisco's CO_2/O_2 specificity in different species may approach optimal acclimation to their gaseous environment in which the plants are grown (Tcherkez et al., 2006; Bathellier et al., 2018). More importantly, especially for carbon-limited seagrasses, photorespiration may serve as an important metabolic "clutch" to protect the photochemical pathway at high irradiance (Heber and Krause, 1980; Osmond, 1981; Osmond et al., 1997; Igamberdiev et al., 2001). When the Calvin Benson cycle is limited by the availability of CO_2, continuation of light reactions over-reduces the thylakoid electron transport chain and generates O_2 and reactive oxygen species (ROS) that potentiates oxidative stress (Voss et al., 2013). Photorespiration helps to balance the redox state and minimize the accumulation of ROS by dissipating the excess reducing equivalents (NADPH) as well as energy (ATP) (Foyer et al., 2009). By recycling the photorespired CO_2, photorespiration may also facilitate carbon assimilation in CO_2 limited environments, thereby minimizing photosynthetic inefficiencies resulting from C-limitation (Busch et al., 2013; Xin et al., 2015).

Photorespiration is often considered to be of minor importance in aquatic systems as a result of carbon concentrating mechanisms (CCMs) that facilitate the transport of HCO_3^- and its dehydration by algal pyrenoids that effectively deliver CO_2 to Rubisco (Frost-Christensen and Sand-Jensen, 1992; Madsen et al., 1993; Meyer et al., 2017). In today's oceanic water (pH ~8.2), 89% of the DIC is in form of HCO_3^- and only 0.5% exists as dissolved CO_2 (Zeebe, 2012). However, not all aquatic C_3 plants have similar efficiencies to use both forms of DIC for photosynthesis (Raven and Beardall, 2003; Raven et al., 2011; Raven and Beardall, 2014). Additionally, CO_2 acquisition by simple diffusion through the leaf surface is more difficult for submerged plants due to the 10,000-fold lower diffusion rates of gases in a liquid environment relative to air (Borum et al., 2006). Consequently, for aquatic C_3 plants such as seagrasses that do not use CCMs effectively, carbon limitation likely increases the photorespiratory function of Rubisco (Tolbert and Osmond, 1976; Touchette and Burkholder, 2000).

Seagrasses are flowering marine plants that evolved from terrestrial monocots in the middle Cretaceous (Larkum et al., 2006b) when higher atmospheric and oceanic CO_2 concentrations likely supported photosynthesis and minimized photorespiration (Kuypers et al., 1999; Zeebe, 2012). In colonizing the aquatic habitat, seagrass evolved adaptations to a submerged environment that produced important anatomical differences from their terrestrial ancestors (Zimmerman et al., 1997; Larkum et al., 2006a). Seagrass leaves have no stomatal openings as gas exchange occurs across both leaf surfaces by diffusion, which uncouples carbon uptake from water relations. Seagrasses also have a lacunal system with aerenchyma extending from the roots to the leaves that facilitates the transport of O_2 to the roots buried in permanently flooded anoxic sediments, and allows transport of CO_2 from the roots to leaves, providing an alternative carbon source (Madsen and Sand-Jensen, 1991). Like their terrestrial ancestors, however, seagrass chloroplasts lack pyrenoids that serve as an important CCM in most aquatic algae (Meyer et al., 2017) and seagrasses are typically less efficient in utilizing HCO_3^- than macroalgae (Beer et al., 1991). Although Rubisco activity in seagrasses is lower than the typical activities in freshwater emergent angiosperms and marine red algae, it is comparable to that observed in marine green and brown macroalgae (Beer et al., 1991). Simulations of nearshore seawater DIC distribution during the Cretaceous period have predicted that photosynthetic rates of seagrasses would have been similar to macroalgae (Beer and Koch, 1996). However, in today's oceans, seagrass photosynthesis is generally considered to be

carbon limited (Durako, 1993; Beer and Koch, 1996; Zimmerman et al., 1997; Invers et al., 2001).

Carbon limited photosynthesis also restricts seagrasses to shallow, high light environments, where low daytime CO_2:O_2 ratios in the water column may increase seagrass vulnerability to photorespiration (Buapet et al., 2013b). The photorespiratory pathway was confirmed in marine plants and macrophytes by showing that photosynthesis could be inhibited by increasing the O_2 concentration, resulting in higher concentrations of glycolate pathway intermediates (Hough, 1974; Black et al., 1976; Burris et al., 1976; Downton et al., 1976; Hough and Wetzel, 1977; Andrews and Abel, 1979). The decreasing O_2 evolution rates relative to electron transfer rates measured by PAM fluorometry at high irradiances in *Zostera marina* and *Halophila stipulacea* also suggested a role for photorespiration in these seagrass species (Beer et al., 1998). More recent studies demonstrated the influence of oxygen concentrations and temperature on photorespiration in seagrass that fluctuate in natural environment because of eutrophication, high community productivity and elevated ocean temperatures; and therefore, will play a role in predicting the health status of these plants in warmer climate scenarios (Buapet and Björk, 2016; Rasmusson et al., 2020). The plastochron interval, which defines leaf life span, leaf turnover and elongation rates, plays an important role in photoacclimation strategies that differ among species at the chloroplast, leaf and shoot levels (Schubert et al., 2018). However, we still do not understand how long-term acclimation to climate warming and ocean acidification/carbonation will affect photorespiration and photoprotection in seagrasses (Koch et al., 2013).

Several experiments simulating ocean acidification/carbonation impacts on time scales of hours to >1 year have quantified the positive impacts of CO_2 availability on carbon balance, growth, survival and reproductive output in seagrasses (Zimmerman, 2021). During the most recent of these studies, the down-regulation of pigment content with increasing CO_2 resembled the photoacclimation response to high light environment that pointed to the importance of metabolic acclimation regulating the redox state of the chloroplast in eelgrass (Zimmerman et al., 2017; Celebi-Ergin et al., 2021). Therefore, the objectives of this study were to estimate the importance of photorespiration in the marine angiosperm *Zostera marina* L. (eelgrass) under today's oceanic carbon concentrations and explore the potential acclimation response to prolonged ocean acidification/carbonation by 1) quantifying the photochemical rates under different light and CO_2 availability by using eelgrass grown in a high light low CO_2 environment, i.e., representing the baseline photosynthetic capacity under today's oceanic conditions; and 2) comparing the relative contribution of different photochemical pathways in eelgrass after 13 months of acclimation to different CO_2 environments superimposed open daily and seasonal patterns of solar radiation, temperature and salinity.

Materials and methods

Table 1 provides a complete list of all abbreviations, acronyms, and symbols along with their units used throughout this paper.

The experimental facility and sampling from pH treatments

Eelgrass shoots used in this study were grown in an outdoor aquatic climate research facility at the Virginia Aquarium and Marine Science Center, VA, USA. The experimental design and control of manipulations for this-long term project were detailed in Zimmerman et al. (2017). Briefly, eelgrass plants, harvested in May 2013 from a subtidal population growing in South Bay, a coastal lagoon on the Virginia portion of the DelMarVa Peninsula, USA, were transplanted into 20 fiberglass open top aquaria (3 m^3 each) plumbed with running seawater from Owl's Creek, VA and exposed to natural sunlight. Temperature, pH, salinity, and irradiance were monitored continuously in all aquaria. Beverage-grade CO_2 gas was used to enrich the experimental aquaria from June 2013 to October 2014 using a system of pH-controlled solenoid valves. pH treatment levels ranged from pH 6 ($[CO_{2(aq)}] \cong 2121\ \mu M$) to ambient (no CO_2 addition, pH $\cong$ 7.7, $[CO_{2(aq)}] \cong 55\ \mu M$), with 0.5 pH intervals between the treatments (4 aquaria at each pH). The experimental CO_2 manipulation produced consistently different levels of $[CO_{2(aq)}]$ and pH among the treatments day and night throughout the duration of the 13-month experiment. Plant performance was monitored monthly while environmental parameters, which varied daily and seasonally, were recorded at 10-minute intervals.

During July 2014, after 13 months of cultivation in the experimental aquaria, freshly collected 2nd youngest leaves from pH 6.1 (2121 μM $CO_{2(aq)}$), pH 6.9 (371 μM $CO_{2(aq)}$) and ambient pH 7.7 (55 μM $CO_{2(aq)}$) treatments were harvested for laboratory measurements of photochemistry under fully controlled incubation conditions. Hereafter, the three treatments will be referred to as $G_{pH}6$, $G_{pH}7$ and $G_{pH}8$, for simplicity. During these measurements, the daily seawater temperature in aquaria ranged from 25 to 28°C; allowing all the incubation measurements described here to be conducted at the optimal temperature of 25°C without inducing heat stress. The daily total surface irradiance ranged from 10 to 29 mol photons m^{-2} d^{-1}; corresponding to more than 6 h of photosynthetically saturating irradiance (>200 μmol photons m^{-2} s^{-1}) per day, under which conditions the leaves of all plants should have been acclimated to a high light environment (Cummings and Zimmerman, 2003).

Incubation measurements of leaf photochemistry

Photosynthesis and respiration rates were measured using polarographic O_2 electrodes in temperature controlled, water-jacketed glass metabolic incubation chambers (Rank Bros.,

TABLE 1 List of symbols, their definitions, and dimensions.

Symbol	Definition	Dimensions
Chl-*a*	Chlorophyll *a*	μg cm^{-2} or mg g^{-1} FW
Chl-*b*	Chlorophyll *b*	μg cm^{-2} or mg g^{-1} FW
TChl	Total Chlorophyll	μg cm^{-2} or mg g^{-1} FW
TCar	Total Carotenoid	μg cm^{-2} or mg g^{-1} FW
FW	Fresh Weight	mg
LA	Leaf Area	cm^2
$A_L(\lambda)$	Leaf absorptance	Dimensionless
$D(\lambda)$	Leaf absorbance	Dimensionless
$R(\lambda)$	Leaf reflectance	Dimensionless
$a_L^*(\lambda)$	Optical cross-section	m^2 g^{-1} Chl-*a*
λ	Wavelength	nm
PAR	Photosynthetically active radiation	μmol photons s^{-1} m^{-2}
PUR	Photosynthetically usable radiation	μmol photons s^{-1} m^{-2}
E	Incident irradiance	μmol photons s^{-1} m^{-2}
E_k	Photosynthesis-saturating irradiance	μmol photons s^{-1} m^{-2}
P_g	Gross photosynthesis	μmol O$_2$ s^{-1} m^{-2} or μmol O$_2$ hr^{-1} mg^{-1} TChl
P_{net}	Net photosynthesis	μmol O$_2$ hr^{-1} g^{-1} FW or μmol O$_2$ hr^{-1} mg^{-1} TChl
P_E	light-saturated rate of gross photosynthesis	μmol O$_2$ s^{-1} m^{-2} or μmol O$_2$ hr^{-1} g^{-1} FW or μmol O$_2$ hr^{-1} mg^{-1} TChl
P_T	True photosynthesis	
P_R	Photorespiration	μmol O$_2$ hr^{-1} mg^{-1} TChl
R_D	Dark respiration	μmol O$_2$ hr^{-1} g^{-1} FW
α	Photosynthetic efficiency at light-limited region of PE curve	μmol O$_2$ μmol^{-1} photons
Φ_{O2}	Quantum yield of oxygen evolution	μmol O$_2$ μmol^{-1} photons
F_m, $F_{m'}$	Maximum fluorescence from dark and light adapted leaf	Dimensionless
F_0, $F_{0'}$	Minimum fluorescence from dark and light adapted leaf	Dimensionless
F_v	Variable fluorescence	Dimensionless
Φ_{PSII}	Effective Quantum yield of fluorescence ($[F_{m'} - F']/F_{m'}$)	Dimensionless
ETR	Electron transport rate	μmol electrons s^{-1} m^{-2}
NPQ	Nonphotochemical quenching ($[F_m - F_{m'}]/F_{m'}$)	Dimensionless

Parenthetic notation (λ) denotes wavelength dependence of the variable.

Cambridge, UK). Variable fluorescence was measured simultaneously on each leaf using a Pulse Amplitude Modulated (PAM) fluorometer (Mini PAM, Walz, Germany). Incubation seawater pH (a proxy for dissolved inorganic carbon (DIC) concentration) was measured using an epoxy mini-electrode and pH meter (Cole-Parmer) calibrated with NBS buffers. The lid of the incubation chamber was modified to hold the pH electrode in the incubation water and the miniature fiberoptic probe of the PAM device in close proximity to the leaf surface. The chamber was continuously mixed by a magnetic stirrer which homogenized the incubation medium and provided turbulent flow to reduce boundary layer limitation of gas exchange across the leaf surface. Continuous analog signals from the three sensors were recorded digitally using custom software written with LabView (2009 edition, National Instruments). Voltage data were post processed into metabolic rates using MATLAB R2014 (The MathWorks Inc.). A Kodak slide projector fitted with a halogen (ELH) bulb provided photosynthetically active radiation (PAR). The intensity of PAR was adjusted with neutral density filters and calibrated daily with a QSL 2100 scalar radiometer (Biospherical Instruments Inc.).

Concentrations of $CO_{2(aq)}$ in the aquaria and metabolic incubation chambers were determined from measured values of pH, alkalinity, salinity and temperature using CO2SYS (Ver. 2.1; Lewis and Wallace 1998). Leaves, harvested from plants grown at pH/CO_2 treatments $G_{pH}6$ ($[CO_{2(aq)}]$ = 2121 μM), $G_{pH}7$ ($[CO_{2(aq)}]$ = 371 μM) and $G_{pH}8$ ($[CO_{2(aq)}]$ =55 μM), were used to measure the photosynthetic response at pH/$CO_{2(aq)}$ levels of 6 ($M_{pH}6$), 7 ($M_{pH}7$) and 8 ($M_{pH}8$). Seawater [DIC] and pH in the incubation chambers were adjusted by bubbling with a gas mixture of CO_2, O_2 and N_2 that maintained [O_2] at air saturation (~215 μM). Seawater temperature was maintained at 25°C by a circulating water bath. Leaves were cleaned of epiphytes by gently scraping with a razor blade and kept in the dark for 20 minutes before the incubation measurements. A

separate three cm long pieces of leaf tissue, cut approximately one cm above the meristem, was used during each ten min dark (i.e., dark respiration) and ten min light (i.e., net photosynthesis) measurement. The pigment content and optical properties of the leaf tissues (Table 1) were measured after each incubation as described by Celebi-Ergin et al. (2021).

The seawater used during all incubations was collected in April 2014 from Owl's Creek, the tidal estuary used as source water for the experimental facility (Zimmerman et al., 2017). This seawater stock, with salinity of 24 (PSS-78, (Lewis, 1980) was filtered through 0.2 μm Nucleopore membrane filters and stored under refrigeration in dark bottles until used in these experiments. After incubations, alkalinity was determined on aliquots of seawater taken from the chamber using an automated potentiometric titrator (Metrohm). Table 2 summarizes measured parameters of seawater used in metabolic incubation chamber.

Determination of photochemical rates

Oxygen evolution rates of each tissue were separately normalized to fresh weight, leaf area and total pigment concentration to explore the effects of phenotypic differences resulting from acclimation to different growth conditions. Parameters of photosynthesis (P) vs Irradiance (E) curves were estimated by fitting the data to a cumulative one-hit Poisson model pioneered for photosynthesis by Webb et al. (1974):

$$P_{net} = P_g - R_D \quad (1)$$

$$P_{net} = [P_E \cdot (1 - e^{-E/E_k})] - R_D \quad (2)$$

where P_{net} was the measured rate of net photosynthesis and R_D was the measured rate of dark respiration, from which the gross photosynthesis (P_g) was calculated according to Equation (1). P_g was defined as a function of light, where P_E represented the light-saturated rate of gross photosynthesis that varied with [CO_2] and [HCO_3^-] (sensu McPherson et al. (2015)). E_k was the irradiance threshold for photosynthetic saturation. E was separately defined as photosynthetically available radiation (PAR = $\sum_{400}^{700} E[\lambda]$) and as photosynthetically utilized radiation (PUR = $\sum_{400}^{700} [E(\lambda) \cdot A(\lambda)]$), where $A(\lambda)$ was the spectral leaf absorptance that integrated the variability of light capture efficiency due to changes in leaf optical properties and pigment content/composition. The quantum yield of oxygen evolution (Φ_{O2}) at different irradiances (in units of mol O_2 mol^{-1} absorbed photon) was calculated by $\Phi_{O2} = P_g/PUR$. Maximum quantum yield was calculated as $\Phi_{max} = P_E/E_{k\ (PUR)}$.

Although Equation (1) represents the typical method for determining gross photosynthesis from measured values of P_{net} and R_D, the model does not separately account for O_2 consumed by photorespiration in the chloroplast. It also assumes that the Mehler Ascorbate Peroxidase pathway does not affect net O_2

TABLE 2 Distribution of dissolved inorganic carbon and dissolved oxygen concentrations in seawater during the incubation measurements of net photosynthesis at different light levels, including dark respiration measurements.

		At the start of light measurements			At the start of dark measurements		
	Target pH	Growth pH 6	Growth pH 7	Growth pH 8	Growth pH 6	Growth pH 7	Growth pH 8
Sample Size	6	7	7	5	7	7	5
	7	6	6	6	6	6	6
	8	5	5	5	5	5	5
Average pH	6	6.09 ± 0.01	6.08 ± 0.01	6.05 ± 0.01	6.09 ± 0.01	6.08 ± 0.01	6.04 ± 0.01
	7	6.91 ± 0.01	6.85 ± 0.02	6.87 ± 0.02	6.91 ± 0.01	6.84 ± 0.02	6.86 ± 0.02
	8	7.94 ± 0.05	7.95 ± 0.01	7.94 ± 0.02	8.00 ± 0.04	7.98 ± 0.01	7.98 ± 0.02
Average [TCO_2] (µmol/L)	6	3712 ± 28	3131 ± 18	3256 ± 48	3727 ± 27	3153 ± 20	3277 ± 49
	7	2218 ± 9	1874 ± 12	1861 ± 10	2217 ± 10	1876 ± 10	1866 ± 11
	8	1857 ± 15	1534 ± 3	1535 ± 5	1837 ± 14	1526 ± 4	1526 ± 5
Average [HCO^-_3] (µmol/L)	6	1963 ± 0.1	1623 ± 0.0	1624 ± 0.1	1963 ± 0.1	1624 ± 0.0	1624 ± 0.1
	7	1943 ± 0.7	1610 ± 0.7	1609 ± 0.7	1943 ± 0.7	1610 ± 0.6	1609 ± 0.7
	8	1742 ± 21	1442 ± 4	1444 ± 7	1714 ± 20	1431 ± 5	1432 ± 7
Average [CO_2] (µmol/L)	6	1748 ± 28	1506 ± 18	1631 ± 48	1762 ± 27	1528 ± 20	1652 ± 48
	7	265 ± 8	258 ± 11	246 ± 10	264 ± 10	260 ± 10	250 ± 11
	8	23 ± 3	18 ± 0.5	19 ± 0.9	19 ± 2	17 ± 0.5	17 ± 0.8
Average [O_2] (µmol/L)	6	209.5 ± 3.1	215.0 ± 3.5	215.9 ± 2.0	212.6 ± 2.3	214.6 ± 3.0	216.0 ± 2.0
	7	214.6 ± 3.0	218.4 ± 4.3	217.5 ± 3.1	215.7 ± 3.4	219.4 ± 3.3	216.3 ± 1.7
	8	206.4 ± 2.4	215.8 ± 2.4	211.8 ± 2.7	212.2 ± 3.3	218.7 ± 1.6	215.4 ± 2.8

All measurements were conducted at 25°C using seawater with salinity of 24 ppt.

exchange even though it may facilitate ATP generation and electron flow, which might be detected by fluorescence measurements (Larkum et al., 2006a). Following the principle explained by Raghavendra (2000) gross photosynthesis (P_g) can be detailed as the difference between true photosynthesis (P_T) and photorespiration (P_R):

$$P_g = P_T - P_R \quad (3)$$

Under CO_2-saturation (i.e., at low pH that increases CO_2:O_2 ratio in seawater, Table 2), P_R should approach a minimum (~ 0), so that P_g will be an approximate estimate of true photosynthetic O_2 production (P_T). In this study, O_2 production rates measured at pH 6 were assumed to approximate the true photosynthesis (P_T) for each growth condition. Therefore, photorespiration was calculated by subtracting the carbon limited P_g measured at pH > 6 from P_g measured at pH 6:

$$P_{R\ [pH>6]} = P_{g\ [pH6]} - P_{g\ [pH>6]} \quad (4)$$

$$P_{g\ [pH>6]} = \left[P_E \cdot \left(1 - e^{-E/E_k}\right)\right]_{[pH>6]} \quad (5)$$

$$P_{g\ [pH6]} = \left[P_m \cdot \left(1 - e^{-E/E_k}\right)\right]_{[pH6]} \quad (6)$$

Thus, P_g approached P_E when saturated by light and flow, and it approached the true physiological capacity (P_m) when saturated by CO_2, light and flow. In this formulation, the limit of P_m is set by availability of cellular components such as enzyme and pigment concentrations that may change under different growth conditions.

Pulsed Amplitude Modulation (PAM) fluorescence measurements were analyzed following the calculations outlined in Baker (2008). The maximum (F_m) and minimum (F_0) fluorescence emissions were measured in the dark after at least 10 min of acclimation while simultaneously measuring respiration. The maximum variable fluorescence yield ($F_v = F_m - F_0$) was used to quantify the maximum quantum yield of fluorescence (F_v/F_m), which is a measure of maximum efficiency at which absorbed light by photosystem II (PSII) can be used for photochemistry. The maximum (F'_m) and minimum fluorescence (F_t) emissions induced by the short saturating pulse of PAM were measured again in the light while simultaneously measuring P_{net}. Based on these emissions under the presence of the actinic background light, the effective quantum yield of PSII (Φ_{PSII}), also known as photochemical quenching, was determined as:

$$\Phi_{PSII} = \left(F'_m - F_t\right) / F'_m \quad (7)$$

Φ_{PSII} provides an estimate of the quantum yield of linear electron flow through PSII at a given irradiance. The other non-radiative energy loss that quenches fluorescence, called Non-Photochemical Quenching (NPQ), results from the dissipation of excess excitation energy as heat *via* the Xanthophyll cycle. NPQ was estimated as:

$$NPQ = \left(F_m - F'_m\right) / F'_m \quad (8)$$

For comparisons among the treatments and incubations, NPQ and Φ_{PSII} at different light levels were fitted to a four-parameter sigmoid curve, which is commonly used for dose response analysis (Motulsky and Christopoulos, 2004), with the following formula:

$$NPQ = NPQ_{min} + \frac{(NPQ_{max} + NPQ_{min})}{1 + (PUR/EC50)^{-H}} \quad (9)$$

where the exponent H was Hill slope that controlled the steepness of the dose-response curve. *EC50* was the *PUR* level required to provoke a response halfway between the baseline and maximum responses. The threshold for NPQ_{max} was constrained to 10 based on literature values (Kalaji et al., 2014).

The electron transport rate (ETR) was estimated from Φ_{PSII} as:

$$ETR\ (\mu mol\ electrons\ m^{-2}s^{-1}) = PUR \cdot F_{II} \cdot \Phi_{PSII} \quad (10)$$

where F_{II} was the fraction of *PUR* captured by PSII and its light harvesting complexes (LHC). The typical value of F_{II} for Chlorophyta and seagrasses is about 0.5 (Figueroa et al., 2003; Larkum et al., 2006a). Photosynthetic parameters of ETR curves (i.e., ETR_{max}, α_{ETR} and $E_{k\ -ETR}$) were calculated by modifying the model of O_2 based *P* vs *E*. curves (Equation 2):

$$ETR = ETR_{max} \cdot \left(1 - e^{-E/E_k}\right) \quad (11)$$

Linear electron flow through PSII is directly related to photosynthetic oxygen production, therefore the gross photosynthesis based on fluorescence measurements ($P_{g\text{-}ETR}$) were estimated from ETR as:

$$P_{g-ETR}\ (\mu mol\ \ O_2\ m^{-2}s^{-1}) = ETR \cdot \tau \quad (12)$$

where τ was the ratio of oxygen evolved per electron generated at PSII. Since four stable charge separations are necessary to generate one mole of O_2 at PSII, τ is equal to 0.25.

Statistical analysis

Effects of growth [CO_2] on pigment content and optical properties of leaves were analyzed by one-way Analysis of Variance (ANOVA) followed by the Tukey multiple comparison method when significant overall effects were identified. Effects of growth [CO_2] and measurement [CO_2] on

dark respiration rates, measured with the O_2 evolution method, were analyzed by Analysis of Covariance (ANCOVA).

O_2 evolution and fluorescence models were implemented by using the non-linear curve fitting tools in SigmaPlot (Systat Software Inc., Version 13.0). This tool provided the mean estimates of the model parameters with their error estimates and significances using computational procedures described by Draper and Smith (1981) and Zimmerman et al. (1987). Additionally, analysis of variance for the regression models were presented to account for the goodness of fit of the *P* vs *E* curves for each experimental condition (Supplementary Tables 1–3). Significant effects of measurement $[CO_2]$ and growth $[CO_2]$ on model parameters obtained by non-linear regression were analyzed by ANCOVA, with growth pH as the primary (categorial) factor and measurement pH as the continuous covariate.

Results

Photoacclimation to growth CO_2

Pigment content and optical properties varied significantly among the leaves grown in different $[CO_2]$ treatments (Table 3). Both total chlorophyll and carotenoid content decreased with increasing growth $[CO_2]$, while the molar ratio of Total Car : Total Chl remained constant across CO_2 treatments at about 0.27. The decrease in total chlorophyll resulted in an increased optical cross section ($a_L^*(\lambda)$) with growth $[CO_2]$, thereby reducing the package effect that results in Chlorophyll self-shading. Growth $[CO_2]$ increased the thickness of the unpigmented mesophyll, thereby increasing the leaf biomass per unit of surface area. These phenotypic responses, consistent with the long term acclimation responses described by Celebi-Ergin et al. (2021), had important consequences for the comparison of photosynthetic efficiencies when metabolic rates were normalized to different leaf properties.

Light response curves of oxygen flux

Rates of dark respiration, whether normalized to biomass ($R_{D\ (FW)}$) or leaf area ($R_{D\ (LA)}$), were not affected by growth $[CO_2]$ or instantaneous variations of $[CO_2]$ within the metabolic incubation chambers (Table 4). Therefore, the average rate of dark respiration for all samples combined was 5.96 ± 0.31 μmol O_2 hr^{-1} g^{-1} FW or 0.50 ± 0.03 μmol O_2 m^{-2} s^{-1}. Dark respiration rates were also independent of pH within the range examined here, indicating no negative impact of changing ionic composition on respiration.

In contrast, net O_2 production rates increased with light and incubation $[CO_2]$ for all plants, regardless of the CO_2 environment in which they were grown (Figure 1). The biomass specific rate of light-saturated photosynthesis ($P_{E\ (FW)}$) averaged 14.1 μmol O_2 hr^{-1} g^{-1} FW at low incubation $[CO_2]$ for all plants and increased as a function of incubation $[CO_2]$ (Figure 1). However, $P_{E\ (FW)}$ of the plants grown under ambient conditions ($G_{pH}8$) was twice as sensitive to increasing incubation $[CO_2]$ as plants grown under the highest CO_2 enrichment ($G_{pH}6$) (Table 5, 86.8 vs 33.5 μmol O_2 hr^{-1} g^{-1} FW at M_{pH} 6 respectively). This difference was associated with 2-fold higher biomass specific pigment content of the plants grown under ambient $[CO_2]$ (Table 3). Thus, low rates of oxygen evolution by ambient plants in their natural low CO_2 environment resulted mainly from photorespiration and not the lack of photosynthetic capacity characterized by light harvesting, electron transport and carbon fixation.

For all plants, increased incubation $[CO_2]$ also increased the irradiance required to saturate photosynthetic oxygen production ($E_{k\ (PAR)}$ and $E_{k\ (PUR)}$); rather than changing the

TABLE 3 Pigment content and optical properties of leaves used in photosynthesis measurements.

Growth pH (Growth $[CO_2]$)	pH8 (55 μM)	pH7 (371 μM)	pH6 (2121 μM)
Sample Size (n)	16	18	18
FW per LA (mg cm^{-2})	25.8 ± 1.33 ^{a}	27.1 ± 0.92 ^{a}	36.0 ± 1.52 ^{b}
Total Chl per LA (µg Chl cm^{-2})	31.2 ± 1.22 ^{a}	27.0 ± 1.20 ^{b}	20.8 ± 0.86 ^{c}
Total Chl per FW (mg Chl g^{-1} FW)	1.25 ± 0.07 ^{a}	1.01 ± 0.05 ^{b}	0.59 ± 0.03 ^{c}
Total Car per LA (µg Car cm^{-2})	8.16 ± 0.28 ^{a}	7.25 ± 0.25 ^{b}	5.61 ± 0.17 ^{c}
Chl a:b	3.44 ± 0.04 ^{a}	3.73 ± 0.07 ^{b}	3.61 ± 0.04 ^{a,b}
TCar:TChl	0.26 ± 0.00 ^{a}	0.27 ± 0.00 ^{a}	0.27 ± 0.00 ^{a}
Absorptance at 550nm	0.38 ± 0.01 ^{a}	0.37 ± 0.01 ^{a}	0.29 ± 0.01 ^{b}
Absorptance at 680nm	0.75 ± 0.01 ^{a,b}	0.75 ± 0.01 ^{a}	0.73 ± 0.01 ^{b}
$a_L^*(680)$ (m^2 g^{-1} Chl)	5.90 ± 0.33 ^{a}	6.73 ± 0.29 ^{a}	8.10 ± 0.24 ^{b}

Effects of growth pH on mean concentrations (± 1 SE) were analyzed by one-way ANOVA. Different letters represent significant differences among the growth pH for each parameter compared by Tukey method at $p< 0.05$. FW, Fresh Weight; LA, Leaf Area; Chl, Chlorophyll; Car, Carotenoid.

TABLE 4 Dark respiration (R_D) rates measured with O_2 evolution method and estimated by non-linear model fit to *P vs E* curves.

Growth pH	Measurement pH	Measured Dark Respiration Averages (μmol O_2 hr^{-1} g^{-1} FW)	Modeled Dark Respiration (μmol O_2 hr^{-1} g^{-1} FW)	Modeled Dark Respiration (μmol O_2 s^{-1} m^{-2})
6	6	4.61 ± 0.75	4.73 ± 1.34	0.45 ± 0.10
	7	5.31 ± 0.62	5.50 ± 1.15	0.51 ± 0.08
	8	5.84 ± 0.47	5.90 ± 0.63	0.69 ± 0.07
7	6	6.40 ± 1.14	6.90 ± 3.06	0.51 ± 0.12
	7	6.73 ± 1.20	7.08 ± 3.02	0.53 ± 0.22
	8	5.03 ± 0.91	5.04 ± 1.88	0.37 ± 0.12
8	6	6.52 ± 0.93	6.83 ± 2.06	0.46 ± 0.07
	7	6.18 ± 0.75	6.71 ± 2.19	0.46 ± 0.14
	8	7.29 ± 1.26	7.29 ± 1.05	0.56 ± 0.10

ANCOVA of Measured R_D	*df*	SS	MS	F	*p*
Growth pH	2	11.551	5.776	1.173	0.318
Measurement pH	1	0.531	0.531	0.108	0.744
Growth pH x Measurement pH	2	10.206	5.103	1.037	0.363
Residual	46	226.435	4.922	–	–
Total	51	255.682	5.013	–	–

Rates are normalized both to Fresh Weight (FW) and Leaf Area. Effects of measurement pH and growth pH on measured R_D were analyzed by ANCOVA. Sample size for each condition is given in Table 2.

photosynthetic efficiency (α) within the light limited region of *P* versus *E* response curves (Table 5 and Supplementary Table 1). Overall, photoacclimation of eelgrass leaves to ocean carbonation increased $E_{k\ (PUR)}$ values from 17 to 44 and 48 μmol absorbed photon s^{-1} m^{-2} for pH 8 (55 μM $CO_{2(aq)}$), pH 7 (371 μM $CO_{2(aq)}$) and pH 6 (2121 μM $CO_{2(aq)}$) respectively.

Chlorophyll specific rates of light-saturated photosynthesis ($P_{E\ (Chl)}$) were the same for all plants grown at different CO_2 environments and produced an identical response to incubation [CO_2] (Figure 2). Consequently, the O_2 production efficiency per unit chlorophyll was not affected by the CO_2 environment in which the plants were grown (Table 5 and Supplementary Table 2) and the stimulatory effect of [CO_2] on O_2 evolution was instantaneous (Figure 3A). The most likely explanation for this instantaneous response would be a reversible and light dependent O_2 consuming process involving the chloroplast, such as photorespiration (P_R), that is competitively inhibited by increasing [CO_2]. Therefore, for all plants grown under all treatments, $P_{E\ (Chl)}$ rates at high incubation [CO_2] (i.e., at $M_{pH}6$) were assumed to be the true physiological photosynthetic capacity (P_m) under light, carbon and flow saturation. Based on this assumption, photorespiration rates were quantified by solving the Equation 4 with the chlorophyll specific gross photosynthesis models (Figure 3B). Normalizing the models to pigment, rather than biomass or area, eliminated the effect of morphological differences among the plants on net oxygen metabolism.

Like photosynthesis, photorespiration increased with light under constant [CO_2], but decreased with increasing incubation [CO_2], as carboxylation became increasingly favored over oxygenation (Figure 3B). Predicted P_R rates increased rapidly with light to a maximum of 60 to 80% of P_m at low [CO_2] (i.e., $M_{pH}8$) (Figure 3C). When aqueous [CO_2] was equal to aqueous [O_2] (at $M_{pH}7$, Table 2), maximum P_R rates were only 20% of P_m, which is equivalent to the inherent carboxylation: oxygenation ratio of Rubisco.

All plants reached the lowest gross photosynthesis to dark respiration ratio (P_g : R_D) of 2 at low incubation [CO_2] when light saturated (Figure 4A). This ratio increased instantaneously when saturated with CO_2 in the incubation medium, maximally up to 12 for ambient plants ($G_{pH}8$). However, the P_E : R_D ratio of high CO_2 grown plants peaked at 8 when saturated with CO_2 in the incubation medium, illustrating the consequence of pigment acclimation on metabolic balance of plants grown in a high CO_2 environment (Figure 4B, grey arrows). Having excess pigment content in a CO_2-limited environment (as observed in ambient plants) did not improve the P_E : R_D under normal growth conditions even though it allowed the instantaneous 6-fold increase of P_E : R_D when incubation [CO_2] increased. High CO_2 acclimated plants, on the other hand, maintained a 4-fold higher P_E : R_D above ambient plants at their respective growth [CO_2] even though pigment content of the high CO_2 plants decreased by half.

Light response curves of variable fluorescence

Maximum quantum yields of fluorescence by dark-adapted leaves were above 0.7 regardless of incubation [CO_2], indicating leaves from all growth treatments were healthy during the experiments (Φ_{PSII} at PUR 0 μmol absorbed photon s^{-1} m^{-2},

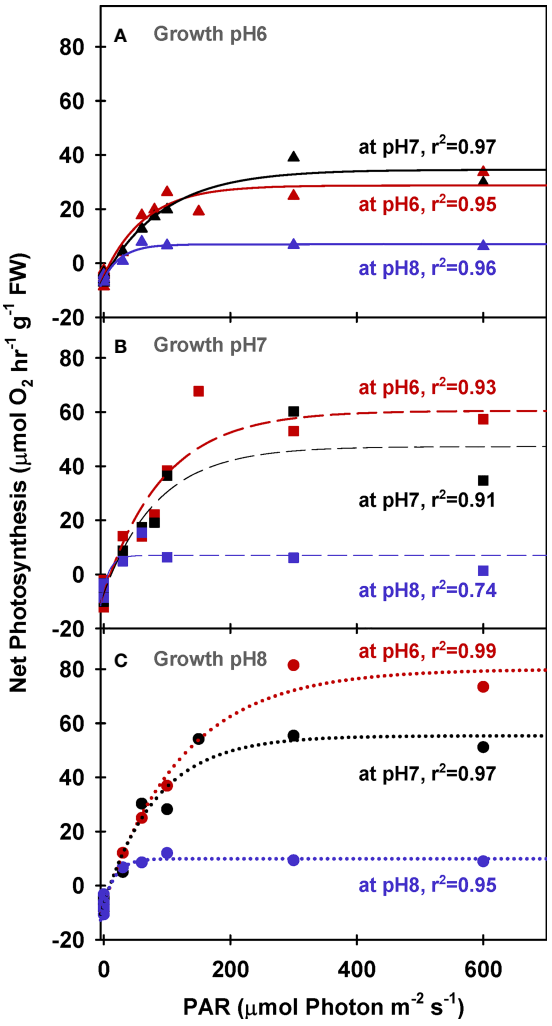

FIGURE 1
Net photosynthesis of eelgrass leaves (biomass normalized) as a function of irradiance. O_2 production rates were measured at different pH levels (red: pH6, black: pH7 and blue: pH8) using leaves grown at pH6 (2121 μM $CO_{2(aq)}$) **(A)**, pH7 (371 μM $CO_{2(aq)}$) **(B)** and ambient pH8 (55 μM $CO_{2(aq)}$) **(C)**. Curves were fit using Equation (2).

Figure 5). For all plants, effective quantum yields of fluorescence (Φ_{PSII}) decreased faster with increasing light when the incubation [CO_2] was low ($M_{pH}8$). The decreased photochemical yield resulted from rapid induction of non-photochemical quenching (NPQ) when [CO_2] was limited under light saturation (Figure 6). Increasing the growth [CO_2], however, caused the light-dependent onset of NPQ to increase, as the NPQ pathway saturated more quickly due the decreased carotenoid content of leaves grown under high [CO_2] (Table 3).

Under saturating irradiance (350 μmol absorbed photon s^{-1} m^{-2}, Figure 6), NPQ values of ambient plants increased 5-fold as incubation [CO_2] became increasingly limiting. In contrast, the plants grown under high [CO_2] ($G_{pH}6$) yielded the same light-saturated NPQ of 2.5 regardless of incubation [CO_2]. The dynamic range of NPQ regulation in ambient grown plants in response to instantaneous changes in [CO_2] suggests considerable tolerance for fluctuating environmental conditions (Figure 6C).

The relation between quantum yield of fluorescence (Φ_{PSII}) and quantum yield of oxygen evolution (Φ_{O2}) was nonlinear, and their ratios were closest to the theoretical value of 8 only at low light and high [CO_2] conditions (Figure 7). For this ratio to be higher than 8, either less than half of the photons are directed to PSII (i.e., F_{II}<0.5, Equation 10), and/or more than four electrons are processed to evolve one mole of oxygen (i.e., τ<0.25, Equation 12). Both outcomes highlight deviation from linear electron flow. For ambient plants, Φ_{O2} decreased faster than Φ_{PSII} with increasing light resulting in a drastic increase in Φ_{PSII}:Φ_{O2}, especially at their growth CO_2 ($G_{pH}8$), suggesting that these plants were using an alternative pathway to maintain electron flow without the production or consumption of O_2.

Similar to net photosynthesis rates, electron transport rates (ETR) of all plants increased with light and were lowest at low incubation [CO_2] (i.e., $M_{pH}8$) (Figure 8 and Table 5). However, the increase of ETR_{max} with incubation CO_2 was not consistent among the plants due to the non-monotonic response of Φ_{PSII} with incubation [CO_2] (Figure 5), in agreement with the findings by Celebi (2016). Only ETR_{max} of plants grown at $G_{pH}7$ increased consistently with increasing incubation [CO_2]. For all incubation experiments, PUR levels required to saturate ETR ($E_{k\text{-}ETR}$) were consistently higher than the E_k values required to saturate O_2 production (Table 5 and Supplementary Table 3). For all plants, estimated gross photosynthesis based on ETR were also higher than the gross photosynthesis measured by the O_2 evolution method (Figure 9). However, this overestimation was not consistent among plants grown at different CO_2 environments. The $P_{E\ (LA)}$ to ETR_{max} ratio was around 0.1 for pH 6 and pH 8 plants when incubated at pH 6 and pH 8, instead of the theoretical value (τ) of 0.25 (Table 5).

Discussion

Long-term growth under high [CO_2] produced a remarkable combination of morphological and metabolic changes in eelgrass. Although pigment content decreased in plants grown at high CO_2, leaf biomass increased as a direct result of the CO_2-stimulated increase in photosynthetic carbon gain. The equivalent responses of chlorophyll normalized O_2 production rates to increased incubation [CO_2], independent of the growth CO_2, allowed us to quantify the impact of [CO_2] on photorespiration in eelgrass because the instantaneous difference in O_2 production rates in CO_2-saturated vs. CO_2-limited incubation media corresponded to the amount of O_2 consumed in the photorespiratory pathway. Thus, photosynthesis and photorespiration as a function of light for

each growth condition were precisely predictable using the *P* versus *E* curves, although the responses to incubation CO_2 differed between biomass and pigment normalization due to changes in leaf morphology. Presently, models of eelgrass performance do not consider these long-term morphological and metabolic acclimation responses (Zimmerman, 2003; Zimmerman, 2006; Zimmerman et al., 2015). Thus, the quasi-mechanistic model developed in this study permits integration of the photosynthetic and morphological acclimation due to ocean carbonation into seagrass productivity models, by adjusting the limits of the photosynthetic parameters based on substrate availability and physiological capacity.

Morphological acclimation and regulation of pigment content, Rubisco activity, light capture and carbon fixation as a function of CO_2 availability have been previously observed in freshwater angiosperms (Madsen et al., 1996). Increasing $P_g : R_D$ due to the enhancing impact of $[CO_2]$ on P_E was detected even in short term (2-6 weeks) studies using temperate and tropical seagrass species without any CO_2 effect on pigment content (Zimmerman et al., 1997; Ow et al., 2015). Long term studies, moreover, reported significant increases in total shoot biomass, carbon allocation to roots and rhizomes (blue carbon), shoot survival and reproductive output by eelgrass in response to CO_2 availability (Palacios and Zimmerman, 2007; Zimmerman et al.,

TABLE 5 Model estimates (mean ± 1 SE) of photosynthesis parameters generated by non-linear regression fit to the experimental data using Equation (2) (N.S. stands for non-significant parameter estimate).

Model Estimates	Growth pH	Measurement pH		
		6.0	7.0	8.0
P_E (μmol O_2 hr^{-1} mg^{-1} Chl)	6	70.2 ± 4.3	55.2 ± 3.7	24.5 ± 2.1
G_{pH} x M_{pH}: p=0.570	7	68.0 ± 3.2	49.3 ± 3.1	12.5 ± 3.1
G_{pH}: p=0.583	8	62.6 ± 2.4	44.9 ± 4.0	20.3 ± 2.4
M_{pH}: p=0.002				
P_E (μmol O_2 hr^{-1} g^{-1} FW)	6	33.5 ± 2.8	40.0 ± 2.5	12.9 ± 1.1
G_{pH} x M_{pH}: p=0.240	7	67.4 ± 7.1	54.3 ± 6.5	12.1 ± 2.9
G_{pH}: p=0.185	8	86.8 ± 4.7	62.1 ± 4.6	17.2 ± 1.7
M_{pH}: p=0.014				
P_E (μmol O_2 s^{-1} m^{-2})	6	3.6 ± 0.2	3.5 ± 0.2	1.5 ± 0.1
G_{pH} x M_{pH}: p=0.233	7	5.8 ± 0.3	4.3 ± 0.5	0.9 ± 0.2
G_{pH}: p=0.199	8	5.8 ± 0.2	4.3 ± 0.3	1.5 ± 0.2
M_{pH}: p=0.007				
ETR_{max} (μmol Electron s^{-1} m^{-2})	6	35.3 ± 0.4	41.0 ± 3.3	22.4 ± 0.5
G_{pH} x M_{pH}: p=0.573	7	93.1 ± 2.6	68.3 ± 4.2	32.4 ± 1.1
G_{pH}: p=0.482	8	58.4 ± 5.8	82.2 ± 5.5	22.8 ± 0.7
M_{pH}: p=0.119				
α_{ETR} (μmol Electron μmol^{-1} absorbed Photon)	6	0.45 ± 0.01	0.50 ± 0.07	0.52 ± 0.03
G_{pH} x M_{pH}: p=0.696	7	0.42 ± 0.01	0.48 ± 0.04	0.44 ± 0.04
G_{pH}: p=0.735	8	0.50 ± 0.08	0.46 ± 0.03	0.52 ± 0.04
M_{pH}: p=0.257				
Φ_{max} (μmol O_2 μmol^{-1} absorbed Photon)	6	0.077 ± 0.01	0.084 ± 0.01	0.107 ± 0.03
G_{pH} x M_{pH}: p=0.263	7	0.079 ± 0.01	0.079 ± 0.02	0.14 ± 0.24
G_{pH}: p=0.314	8	0.083 ± 0.01	0.074 ± 0.01	0.081 ± 0.03
M_{pH}: p=0.100				
E_k (μmol absorbed photon s^{-1} m^{-2}) from 'PG per Chl vs PUR'	6	47.5 ± 7.0	36.4 ± 6.0	14.5 ± 4.9
G_{pH} x M_{pH}: p=0.391	7	64.2 ± 7.4	43.9 ± 6.9	4.7 ± 15.8
G_{pH}: p=0.348	8	68.6 ± 7.2	57.1 ± 13.3	17.4 ± 7.1
M_{pH}: p=0.006				
E_k (μmol photon s^{-1} m^{-2}) from 'PG per FW vs PAR'	6	65.0 ± 14.5	94.7 ± 14.8	28.4 ± 8.6
G_{pH} x M_{pH}: p=0.523	7	94.0 ± 24.2	85.3 ± 25.1	11.6 ± 23.5
G_{pH}: p=0.501	8	124.9 ± 18.6	83.9 ± 16.9	18.3 ± 8.7
M_{pH}: p=0.046				
E_k (μmol absorbed photon s^{-1} m^{-2}) from 'ETR vs PUR'	6	78.5 ± 2.0	82.2 ± 15.6	43.1 ± 2.9
G_{pH} x M_{pH}: p=0.560	7	220.1 ± 10.3	142.6 ± 19.0	72.8 ± 7.3
G_{pH}: p=0.469	8	117.5 ± 27.8	180.1 ± 22.9	44.2 ± 3.8
M_{pH}: p=0.117				

Significant effects of measurement pH (M_{pH}) and growth pH (G_{pH}) on mean estimates were analyzed by ANCOVA.

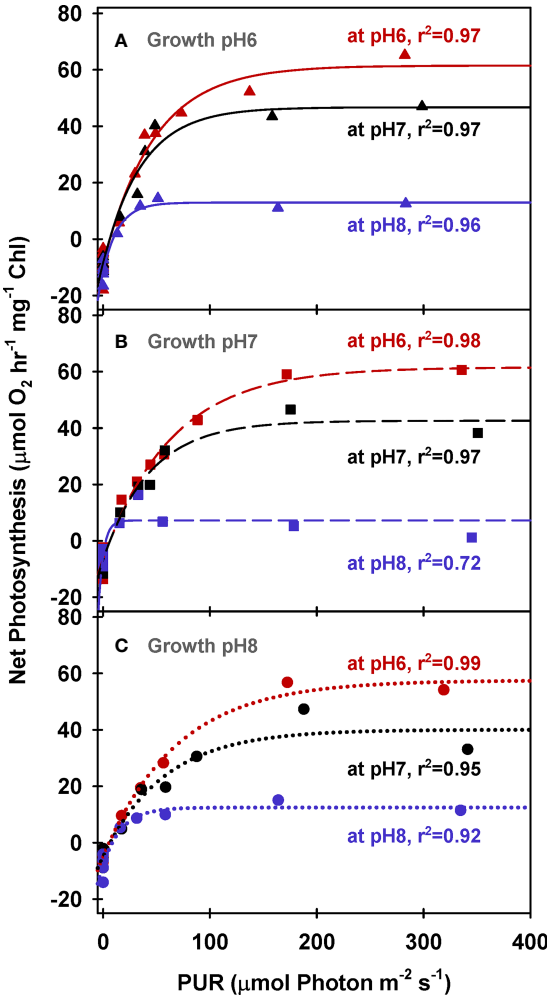

FIGURE 2
Net photosynthesis of eelgrass leaves (Chlorophyll normalized) as a function of absorbed irradiance. O_2 production rates were measured at different pH levels (red: pH6, black: pH7 and blue: pH8) using leaves grown at pH6 (2121 μM $CO_{2(aq)}$) **(A)**, pH7 (371 μM $CO_{2(aq)}$) **(B)** and ambient pH8 (55 μM $CO_{2(aq)}$) **(C)**. Curves were fit using Equation (2).

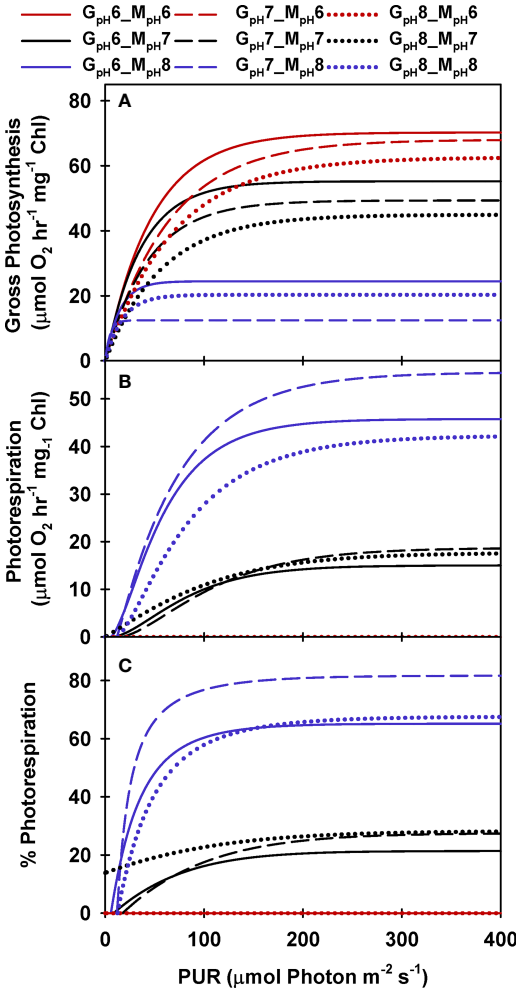

FIGURE 3
Modeled gross photosynthesis **(A)** and photorespiration **(B, C)** of eelgrass leaves as a function of absorbed irradiance. Colors represent different pH/CO_2 levels at which the measurements (M_{pH}) were performed; line styles represent the different pH/CO_2 levels at which the plants were grown (G_{pH}). Photorespiration at M_{pH6} were zero.

2017). Despite the decreases in pigment content and leaf absorptance observed here, plants grown at high CO_2 were able to maintain higher P_g : R_D ratios than plants grown under ambient CO_2; indicating a strong coupling between the regulation of photosynthetic structure and metabolic carbon demands. This coupling between photosynthetic regulation and growth might be poor for organisms that undergo photodamage because photosynthesis might accommodate the biochemical costs associated with protection and recovery rather than fueling the energy towards growth (Barra et al., 2014). On the other hand, the eelgrass used in these experiments show no sign of photodamage, either in the growth aquaria or in laboratory incubations even when photosynthesis was carbon limited but light saturated.

When measured at low [CO_2], plants grown under ambient CO_2 had the same photosynthetic O_2 production as the plants grown at high [CO_2]. These same photosynthetic rates highlighted the apparent lack of carbon concentrating mechanisms inducible by low CO_2 availability in eelgrass, in contrast with marine algae and cyanobacteria that are capable of upregulating their carbon concentrating mechanisms *via* e.g., generation of pyrenoids, carboxysomes and periplasmic carbonic anhydrases when CO_2 availability becomes limiting (Björk et al., 1993; Raghavendra, 2000; Falkowski and Raven, 2007; Meyer et al., 2017). This was also consistent with the

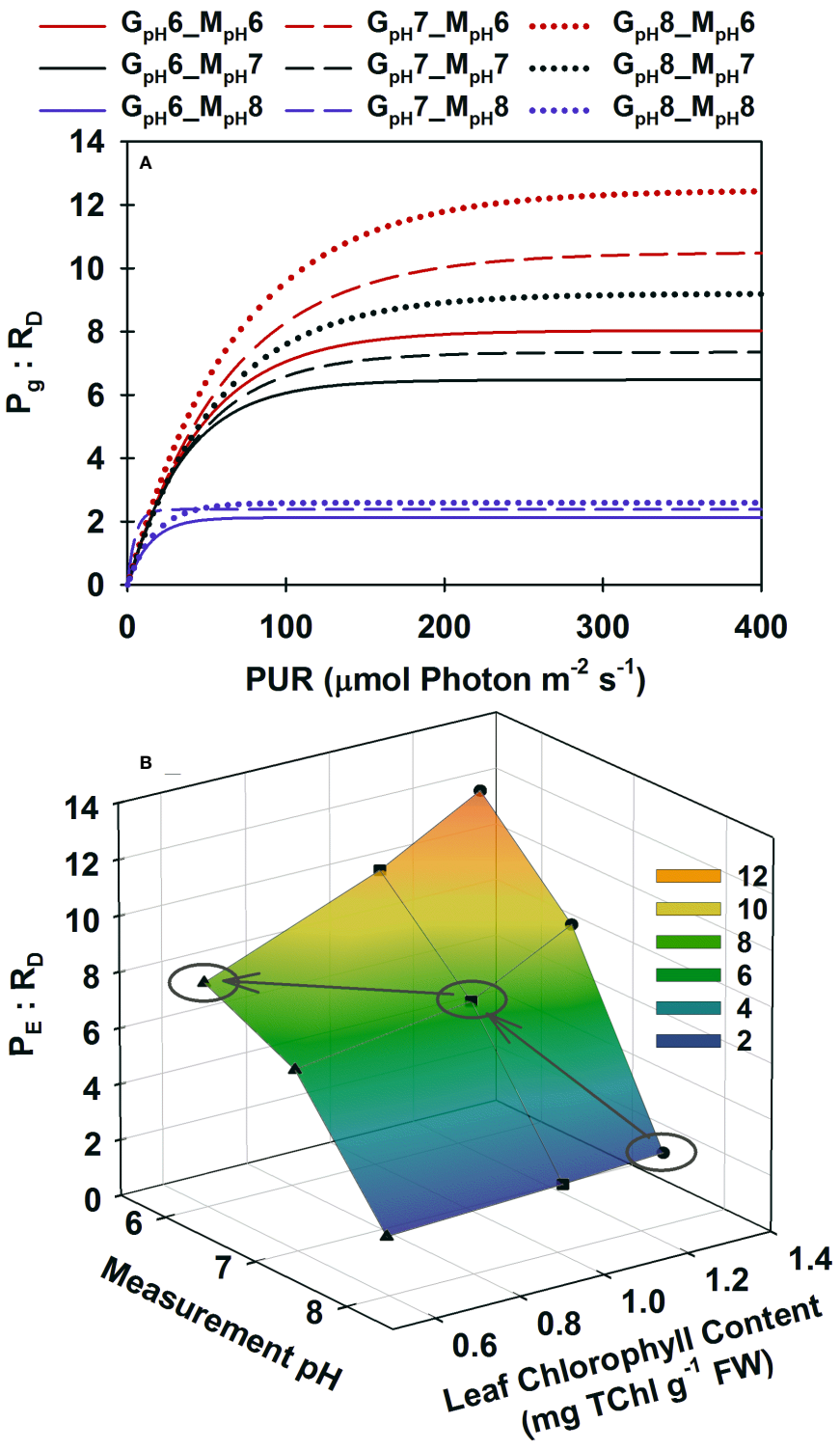

FIGURE 4
Modeled ratio of gross photosynthesis to dark respiration as a function of absorbed irradiance **(A)** and as a function of Chlorophyll content at saturating irradiances **(B)**. Colors represent different pH/CO_2 levels at which the measurements (M_{pH}) were performed; line styles and symbols (▲, at pH6 ■ at pH7, ● at ambient pH) represent the different pH/CO_2 levels at which the plants were grown (G_{pH}). **(B)** Ellipses highlight when plants from different treatments were incubated at their corresponding growth pH/CO_2. Gray arrows show the trajectory of $P_E : R_D$ as a result of phenotypic acclimation to the increasing CO_2 environment.

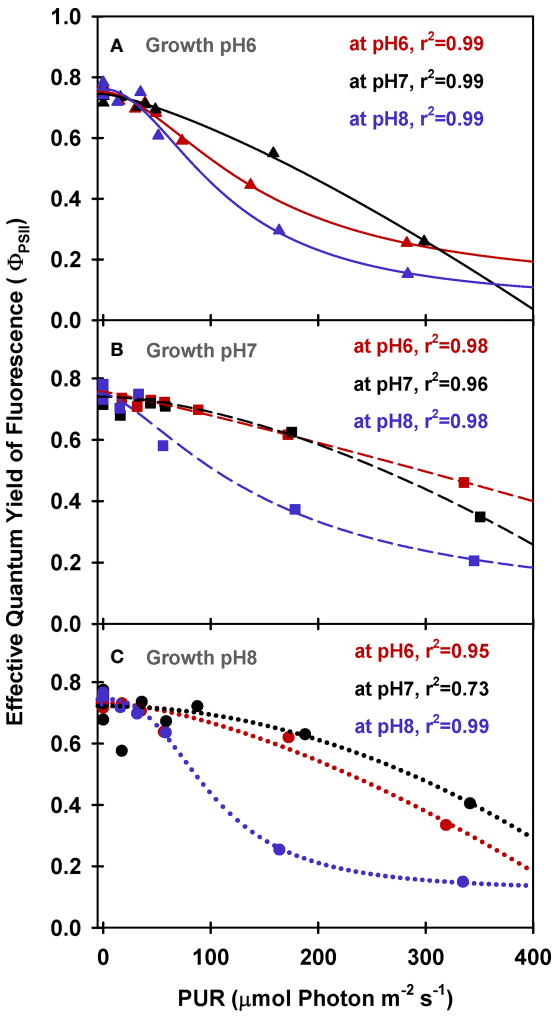

FIGURE 5
PAM fluorescence parameters of eelgrass leaves as a function of absorbed irradiance. PAM fluorescence measurements were performed at different pH/CO_2 levels (red: pH6, black: pH7, blue: pH8) using leaves grown at pH6 (2121 μM $CO_{2(aq)}$) **(A)**, pH7 (371 μM $CO_{2(aq)}$) **(B)** and ambient pH8 (55 μM $CO_{2(aq)}$) **(C)**. Curves were fit using Equation (9).

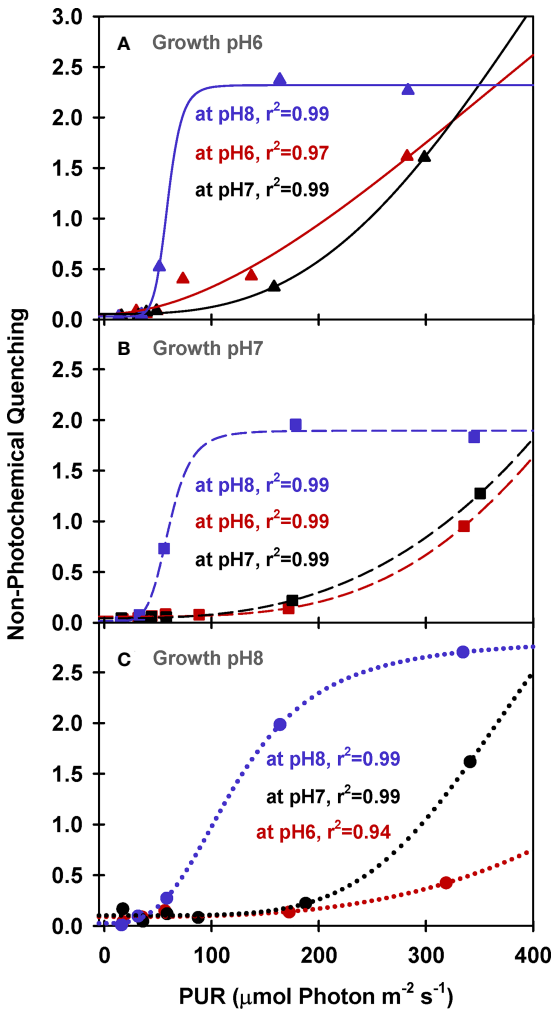

FIGURE 6
PAM fluorescence parameters of eelgrass leaves as a function of absorbed irradiance. PAM fluorescence measurements were performed at different pH/CO_2 levels (red: pH6, black: pH7, blue: pH8) using leaves grown at pH6 (2121 μM $CO_{2(aq)}$) **(A)**, pH7 (371 μM $CO_{2(aq)}$) **(B)** and ambient pH8 (55 μM $CO_{2(aq)}$) **(C)**. Curves were fit using Equation (9).

limited sensitivity of eelgrass photosynthesis to the aqueous presence of acetazolamide, an inhibitor of periplasmic carbonic anhydrase (McPherson et al. (2015) and Celebi-Ergin - unpublished data). Seagrasses living in shallow estuarine environments, like the Chesapeake Bay eelgrass used in this study, are subject to highly variable CO_2/pH levels daily and seasonally, which might explain the unresponsiveness of CCMs for ambient plants (Buapet et al., 2013a; Duarte et al., 2013; Ruesink et al., 2015; Zimmerman et al., 2017; Cyronak et al., 2018). Similarly, all plants had the same $P_{E\ (Chl)}$ when measured at saturating [CO_2] due to minimized P_R, indicating all plants approached the same physiological oxygen production capacity per available photosynthetic apparatus (i.e., $P_{m\ (Chl)}$ was constant across all treatments). Therefore, the difference in P_E : R_D among growth [CO_2] treatments when all were incubated at high [CO_2] resulted from the downregulation of light harvesting components by plants grown in the high CO_2 environment.

Despite phenotypic acclimation across the CO_2 gradient, the maximum photosynthetic efficiency (Φ_{max}) remained constant for all plants (~0.08 mol O_2 mol^{-1} absorbed photon) but photosynthesis-saturating light levels (E_k) increased, as was predicted by the model of McPherson et al. (2015). Photosynthetic efficiency within and among seagrass species vary with efficiency of light absorption and the subsequent conversion of that energy into carbon assimilation (Ralph et al., 2007). Although the observed values of α in this study

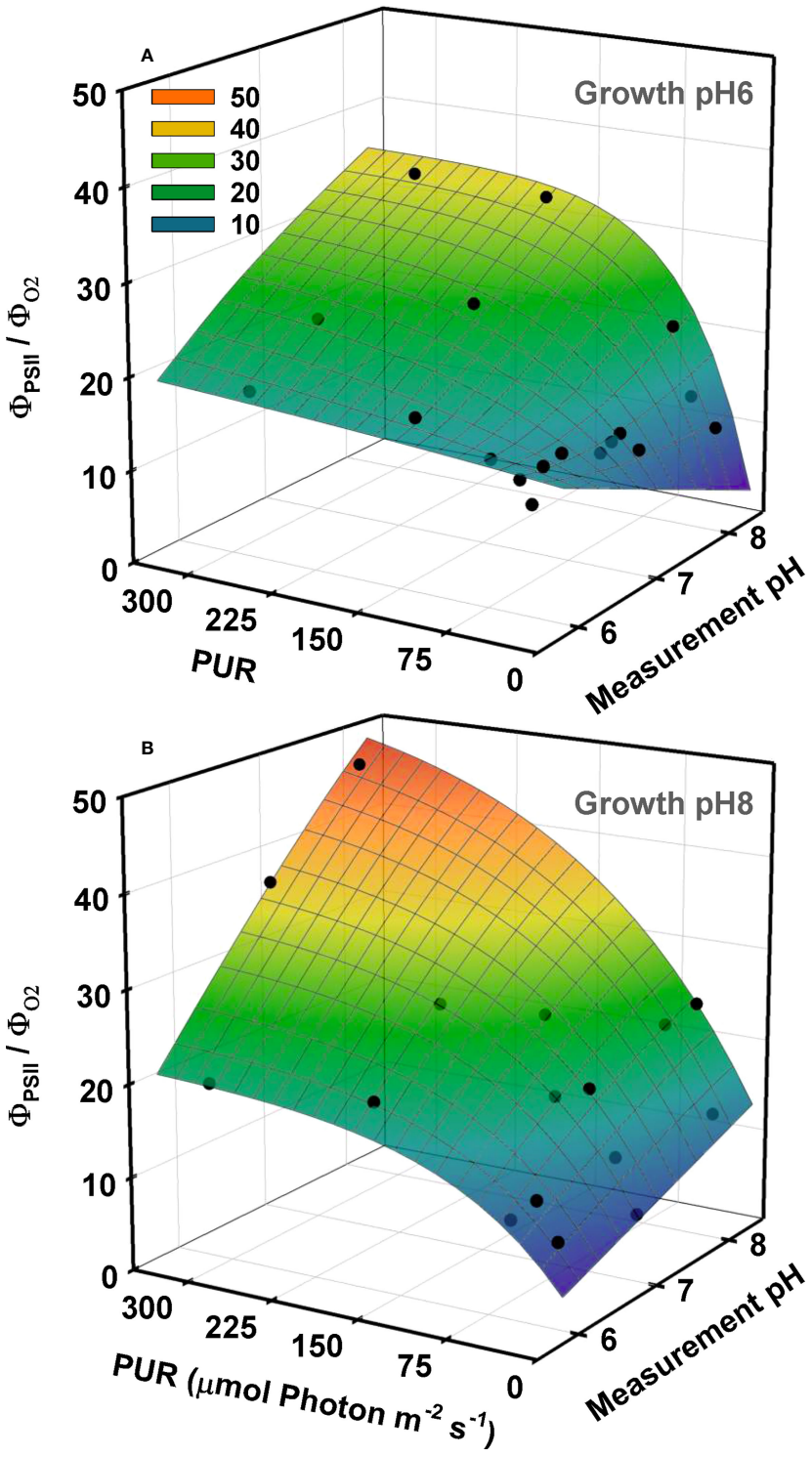

FIGURE 7
Ratio of the quantum yield of fluorescence (Φ_{PSII}) to the quantum yield of oxygen (Φ_{O2}) as a function of light and incubation pH/CO_2. O_2 production and fluorescence were measured simultaneously at different pH levels using eelgrass leaves grown at different CO_2 treatments. Yields were calculated using PUR. Growth specific 3D relationships, at pH6 (2121 μM $CO_{2(aq)}$) **(A)** and ambient pH8 (55 μM $CO_{2(aq)}$) **(B)**, were generated by the combination of non-linear and linear regression fits. First, the Φ_{PSII}/Φ_{O2} ratio as a function of PUR were described by the exponential rise to maximum models separately for each incubation pH/CO_2. Parameter estimates of these non-linear regression models were fitted as a function of incubation pH using linear regression.

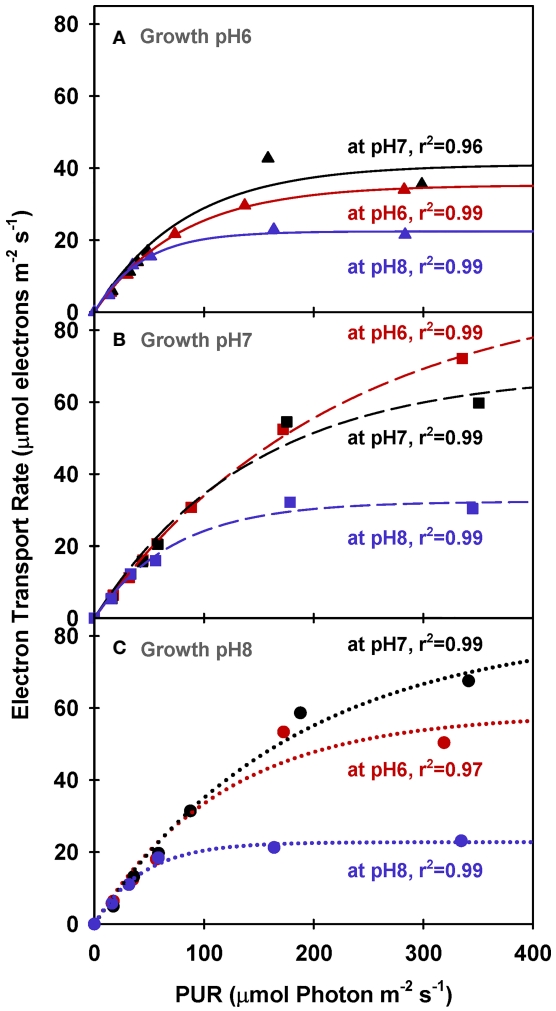

FIGURE 8
Electron transport rates of eelgrass leaves as a function of absorbed irradiance. PAM measurements were performed at different pH/CO_2 levels (red: pH6, black: pH7 and blue: pH8) using leaves grown at pH6 (2121 μM $CO_{2(aq)}$) **(A)**, pH7 (371 μM $CO_{2(aq)}$) **(B)** and ambient pH8 (55 μM $CO_{2(aq)}$) **(C)**. Curves were fit using Equation (11).

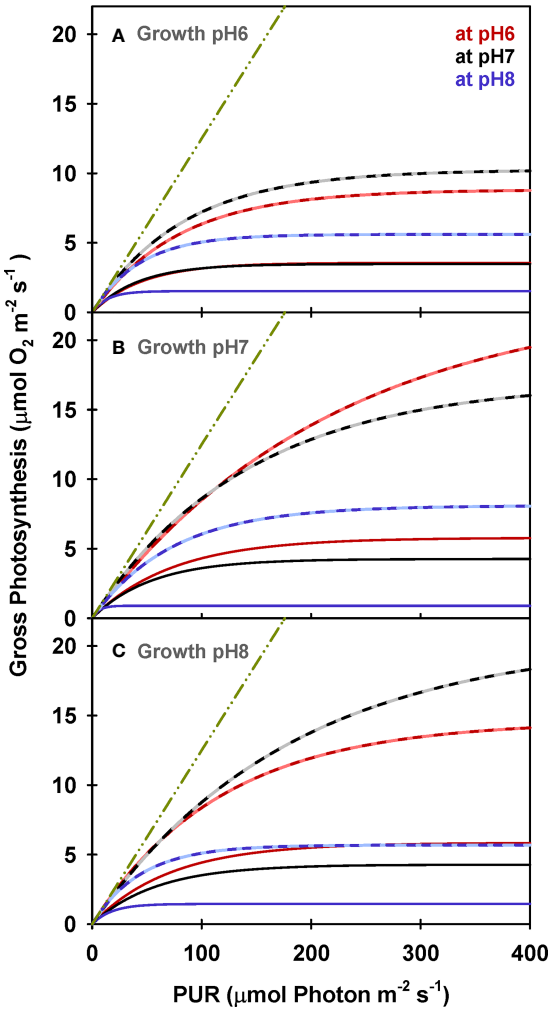

FIGURE 9
Modeled gross photosynthesis of eelgrass leaves as a function of absorbed irradiance for plants growing at pH6 (2121 μM $CO_{2(aq)}$) **(A)**, pH7 (371 μM $CO_{2(aq)}$) **(B)** and ambient pH8 (55 μM $CO_{2(aq)}$) **(C)**. Solid lines are calculated from leaf area normalized O_2 production rates (Equation 1) and dashed lines are estimated from ETR measurements (Equation 12). Colors represent incubation pH/CO_2 levels. Green dot-dashed lines represent the theoretical O_2 production per absorbed photon under non-limiting environmental conditions.

were in agreement with previous estimates for eelgrass (Frost-Christensen and Sand-Jensen, 1992), constant α across different CO_2 regimes represents an interesting contrast to that observed in terrestrial C3 plants in which α increases with [CO_2] availability (Raghavendra, 2000). This difference between responses of aquatic and terrestrial plants may result because CO_2 responses are coupled to water stress in terrestrial plants but not in aquatic plants. The increased E_k and P_E values for high CO_2 acclimated plants will decrease the estimates of H_{sat} (i.e., average daily period of P_E) required to maintain positive carbon balance for the whole plant. The H_{sat} requirement is a useful modeling tool in predicting the depth distribution of eelgrass in variable light environments (Dennison, 1987; Zimmerman et al., 1991; Zimmerman et al., 1994; Zimmerman et al., 1995).

A strong correlation between diurnal NPQ cycle (i.e., xanthophyll cycle) and high light exposure has been confirmed for eelgrass to avoid photodamage under fluctuating light environments (Ralph et al., 2002). High light acclimated eelgrass leaves have higher NPQ activity, and higher photosynthetic capacity, than low light acclimated leaves (Ralph and Gademann, 2005). Here, we demonstrated a similar effect of [CO_2] availability on NPQ activity. Under ambient CO_2 concentrations, the onset of photosynthesis CO_2 limitation (E_k)

occurred at lower irradiance, accelerating the diversion of excess photon absorption to NPQ, likely using the xanthophyll cycle as a photoprotective mechanism to prevent photoinhibition. The high CO_2 incubations reduced this carbon limitation and increased the E_k, consequently reducing NPQ. Due to increased E_k, the same light environment became less damaging at high CO_2, which may explain the reduction in both photosynthetic and photoprotective pigments observed in response to growth CO_2. Thus, by reducing CO_2 limitation of Rubisco, ocean carbonation should also reduce the vulnerability of eelgrass to excess reactive oxygen species (ROS) and therefore the need for photoprotection.

The simultaneous measurements of variable fluorescence, and O_2 flux performed here yielded quantitative estimates of changes in photoprotective pathways of eelgrass acclimated to different CO_2 environments. The difference between the theoretical O_2 evolution (i.e., the linear increase of O_2 with light) and the ETR estimates of gross photosynthesis ($P_{g\text{-}ETR}$) was most pronounced for plants grown at high CO_2, accounting for the absorbed photons that did not contribute to the electron transport pathway (not exciting electrons at PSII), but explained by quenching pathways, such as fluorescence and NPQ. This trend was consistent with their lower area-specific O_2 production rates at high CO_2 incubations when compared to pH7 and ambient pH grown plants. These plants downregulated their pigment content but increased the light-dependent NPQ at lower irradiances even at high incubation [CO_2]. This may indicate that phenotypic acclimation to ocean carbonation by downregulating the photosynthetic apparatus reduces the role of photorespiration but increases the role of NPQ in photoprotection.

On the other hand, as observed in all treatments, the difference between the ETR estimated gross photosynthesis ($P_{g\text{-}ETR}$) and the gross photosynthesis measured by oxygen production (P_g) may result from inaccurate assumptions of F_{ii} and/or τ (Equation 12). In theory, 8 photons absorbed equivalently both by PSI and PSII (F_{ii}= 0.5) excites a total of 4 electrons producing 1 mole of O_2 (τ =0.25). This equilibrium of linear electron flow is valid when there is no limitation of resources such as CO_2 and/or accumulation of byproducts such as reducing equivalents and ROS (Scheibe et al., 2005; Dietz and Pfannschmidt, 2011; Pfannschmidt and Yang, 2012). Under limiting conditions, this balance shifts towards pathways that ensure the optimal redox state of the chloroplast resulting in altered photon: electron: O_2 ratios (Foyer et al., 2012).

Following the linear assumption that 4 electrons produce 1 O_2 (τ = 0.25) resulted in overestimation of the PG_{ETR} in all treatments. Since the molecular chemistry of water splitting at PSII is well-known, τ can only be reduced in an apparent sense. This apparent ratio can result from the excitation of four electrons (as detected with PAM) either without producing O_2, indicating cyclic electron flow around PSII, or consumption of O_2 in the chloroplast that would remain undetected by the gas exchange method (Foyer et al., 2009; Ananyev et al., 2017). Two possible pathways to explain a reduction in τ due to O_2 consumption are (i) the Mehler reaction and (ii) photorespiration. The Mehler reaction increases the pH gradient that may induce NPQ (Demmig-Adams and Adams, 1996; Kanazawa and Kramer, 2002). However, in this study NPQ induction did not happen until Φ_{PSII} values fell below 0.6 while O_2 yield continuously decreased. Therefore, the observed nonlinearity between quantum yield of fluorescence and quantum yield of oxygen most likely resulted from O_2 consumption *via* photorespiration, which probably represents the primary pathway to remove excess O_2 buildup and use the ATP energy from light reactions for this purpose. NPQ was then triggered when photorespiration is incapable of consuming enough ATP to lower the pH gradient forming across lumen at very high irradiances.

Other pathways that keep the electron flow continuous without contributing to CO_2 assimilation are the malate valve and the cyclic electron flow around PSI, which triggers NPQ by generating a pH gradient (Munekage et al., 2004; Johnson, 2005; Miyake, 2010). If PSI cyclic electron flow plays an important role, then the assumption of half of the absorbed photons going to PSII (e.g., F_{ii}=0.5) would be inaccurate. Although PAM measurements are easily made under field conditions (including underwater) and provide non-intrusive information about the photoprotection of eelgrass through NPQ, the fluorescence measurements with PAM overestimate $P_{g\text{-}ETR}$ and therefore are not equivalent to true carbon assimilation. Fluorescence measurements may account for the number of absorbed photons used in electron excitation but not necessarily towards the rates of oxygen production/consumption or carbon assimilation, especially when alternative electron sinks are available (Beer et al., 1998). Still, by having quantified the ratio of Φ_{PSII} to Φ_{O2} as a function of light and carbon availability in response to acclimation to ocean carbonation, the alternative electron pathways can be accounted for in the future estimation of photosynthesis in eelgrass.

To conclude, photorespiration likely provides an important metabolic clutch to protect the photochemical pathway in CO_2-limited eelgrass by maintaining electron flow to prevent the inhibitory damage to photosystems due to light saturation when carbon assimilation is limited by CO_2 supply. In addition to providing a photoprotective role, photorespiration could serve multiple purposes by connecting different metabolic pathways that allow instantaneous energy and reductant modulation under fluctuating environmental conditions. Further, photorespiration may provide a carbon concentrating mechanism *via* recycling of photorespired CO_2 and removing excess intracellular O_2. Therefore, even though carbon limitation causes eelgrass photosynthesis to saturate at relatively low light levels in the modern ocean, longer daily periods of saturating irradiances might be required to keep the photosynthetic apparatus running to produce ATP to support photorespiration. Consequently, understanding photoprotection mechanisms employed by these remarkable plants that are permanently rooted in highly variable shallow-water environments, becomes important when high water

column productivity causes [O_2] to rise and [CO_2] to fall just as daily irradiances begin to peak. More importantly, this study demonstrated that acclimation of photoprotective mechanisms in response to CO_2 availability accounted for the previously reported physiological acclimations of enhanced growth and survival of this species under ocean acidification scenarios.

Data availability statement

The original contributions presented in the study are included in the article/Supplementary Material. Further inquiries can be directed to the corresponding author.

Author contributions

BC-E, RZ and VH conceived the project. BC-E, RZ and VH performed the research. BC-E and RZ analyzed the data. BC-E, RZ and VH wrote the article. All authors contributed to the article and approved the submitted version.

Funding

Financial support for this research was provided by the National Science Foundation (Award OCE-1061823 to RZ and VH), Virginia Sea Grant/NOAA (Award NA14OAR4170093 to RZ and BC-E) and the Department of Ocean, Earth & Atmospheric Sciences, Old Dominion University (to BC-E). This research was performed in partial completion of the requirements for the Ph.D. degree (Oceanography) at Old Dominion University.

Acknowledgments

Thanks to W. M. Swingle and the staff of the Virginia Aquarium & Marine Science Center for assistance with maintenance of the experimental facility, and to D. Ruble, M. Jinuntuya, C. Zayas-Santiago, T. Cedeno and M. Smith for assistance with experimental procedures and maintenance of the experimental plants.

Conflict of interest

The authors declare that the research was conducted in the absence of any commercial or financial relationships that could be construed as a potential conflict of interest.

Publisher's note

Supplementary material

The Supplementary Material for this article can be found online at: https://www.frontiersin.org/articles/10.3389/fpls.2022.1025416/full#supplementary-material

References

Ananyev, G., Gates, C., Kaplan, A., and Dismukes, G. C. (2017). Photosystem II-cyclic electron flow powers exceptional photoprotection and record growth in the microalga chlorella ohadii. *Biochim. Biophys. Acta (BBA) - Bioenergetics* 1858 (11), 873–883. doi: 10.1016/j.bbabio.2017.07.001

Andrews, T. J., and Abel, K. M. (1979). Photosynthetic carbon metabolism in seagrasses 14C-labeling evidence for the C3 pathway. *Plant Physiol.* 63 (4), 650–656. doi: 10.1104/pp.63.4.650

Andrews, T. J., and Lorimer, G. H. (1978). Photorespiration – still unavoidable? *FEBS Lett.* 90 (1), 1–9. doi: 10.1016/0014-5793(78)80286-5

Baker, N. R. (2008). Chlorophyll fluorescence: A probe of photosynthesis *In vivo*. *Annu. Rev. Plant Biol.* 59 (1), 89–113. doi: 10.1146/annurev.arplant.59.032607.092759

Barra, L., Chandrasekaran, R., Corato, F., and Brunet, C. (2014). The challenge of ecophysiological biodiversity for biotechnological applications of marine microalgae. *Mar. Drugs* 12 (3), 1641. doi: 10.3390/md12031641

Bathellier, C., Tcherkez, G., Lorimer, G. H., and Farquhar, G. D. (2018). Rubisco is not really so bad. *Plant Cell Environ.* 41 (4), 705–716. doi: 10.1111/pce.13149

Beer, S., and Koch, E. (1996). Photosynthesis of marine macroalgae and seagrasses in globally changing CO_2 environments. *Mar. Ecol. Prog. Ser.* 141, 199–204. doi: 10.3354/meps141199

Beer, S., Sand-Jensen, K., Madsen, T. V., and Nielsen, S. L. (1991). The carboxylase activity of rubisco and the photosynthetic performance in aquatic plants. *Oecologia* 87 (3), 429–434. doi: 10.1007/BF00634602

Beer, S., Vilenkin, B., Weil, A., Veste, M., Susel, L., and Eshel, A. (1998). Measuring photosynthetic rates in seagrasses by pulse amplitude modulated (PAM) fluorometry. *Mar. Ecology-Progress Ser.* 174, 293–300. doi: 10.3354/meps174293

Björk, M., Haglund, K., Ramazanov, Z., and Pedersén, M. (1993). Inducible mechanisms for HCO_3^- utilization and repression of photorespiration in protoplasts and thalli of three species of ulva (chlorophyta)1. *J. Phycology* 29 (2), 166–173. doi: 10.1111/j.0022-3646.1993.00166.x

Black, C., Burris, J., and Everson, R. (1976). Influence of oxygen concentration on photosynthesis in marine plants. *Funct. Plant Biol.* 3 (1), 81–86. doi: 10.1071/PP9760081

Borum, J., Sand-Jensen, K., Binzer, T., Pedersen, O., and Greve, T. (2006). "Oxygen movement in seagrasses," in *SEAGRASSES: BIOLOGY, ECOLOGYAND CONSERVATION* (Springer, Dordrecht: Springer Netherlands), 255–270. doi: 10.1007/978-1-4020-2983-7_10

Buapet, P., and Björk, M. (2016). The role of O2 as an electron acceptor alternative to CO2 in photosynthesis of the common marine angiosperm zostera marina l. *Photosynthesis Res.* 129 (1), 59–69. doi: 10.1007/s11120-016-0268-4

Buapet, P., Gullström, M., and Björk, M. (2013a). Photosynthetic activity of seagrasses and macroalgae in temperate shallow waters can alter seawater pH and total inorganic carbon content at the scale of a coastal embayment. *Mar. Freshw. Res.* 64 (11), 1040–1048. doi: 10.1071/MF12124

Buapet, P., Rasmusson, L. M., Gullström, M., and Björk, M. (2013b). Photorespiration and carbon limitation determine productivity in temperate seagrasses. *PloS One* 8 (12), e83804. doi: 10.1371/journal.pone.0083804

Burris, J., Holm-Hansen, O., and Black, C. (1976). Glycine and serine production in marine plants as a measure of photorespiration. *Funct. Plant Biol.* 3 (1), 87–92. doi: 10.1071/PP9760087

Busch, F. A., Sage, T. L., Cousins, A. B., and Sage, R. F. (2013). C3 plants enhance rates of photosynthesis by reassimilating photorespired and respired CO_2. *Plant Cell Environ.* 36 (1), 200–212. doi: 10.1111/j.1365-3040.2012.02567.x

Celebi, B. (2016). *Potential impacts of climate change on photochemistry of zostera Marina L.* Doctor of Philosophy (PhD), Dissertation, Ocean & Earth Sciences, (Norfolk, VA: Old Dominion University). doi: 10.25777/8b9x-8303

Celebi-Ergin, B., Zimmerman, R. C., and Hill, V. J. (2021). Impact of ocean carbonation on long-term regulation of light harvesting in eelgrass, *Zostera marina* l. *Mar. Ecol. Prog. Ser.* 671, 111–128. doi: 10.3354/meps13777

Cummings, M. E., and Zimmerman, R. C. (2003). Light harvesting and the package effect in the seagrasses *Thalassia testudinum* banks ex könig and *Zostera marina* l.: optical constraints on photoacclimation. *Aquat. Bot.* 75 (3), 261–274. doi: 10.1016/s0304-3770(02)00180-8

Cyronak, T., Andersson, A. J., D'Angelo, S., Bresnahan, P., Davidson, C., Griffin, A., et al. (2018). Short-term spatial and temporal carbonate chemistry variability in two contrasting seagrass meadows: Implications for pH buffering capacities. *Estuaries Coasts*. 41, 1282–1296. doi: 10.1007/s12237-017-0356-5

Demmig-Adams, B., and Adams, W. W.III (1996). The role of xanthophyll cycle carotenoids in the protection of photosynthesis. *Trends Plant Sci.* 1 (1), 21–26. doi: 10.1016/s1360-1385(96)80019-7

Dennison, W. C. (1987). Effects of light on seagrass photosynthesis, growth and depth distribution. *Aquat. Bot.* 27 (1), 15–26. doi: 10.1016/0304-3770(87)90083-0

Dietz, K.-J., and Pfannschmidt, T. (2011). Novel regulators in photosynthetic redox control of plant metabolism and gene expression. *Plant Physiol.* 155 (4), 1477–1485. doi: 10.1104/pp.110.170043

Downton, W., Bishop, D., Larkum, A., and Osmond, C. (1976). Oxygen inhibition of photosynthetic oxygen evolution in marine plants. *Funct. Plant Biol.* 3 (1), 73–79. doi: 10.1071/PP9760073

Draper, N. R., and Smith, H. (1981). *Applied regression analysis 2nd* Edition (New York: John Wiley & Sons).

Duarte, C. M., Hendriks, I. E., Moore, T. S., Olsen, Y. S., Steckbauer, A., Ramajo, L., et al. (2013). Is ocean acidification an open-ocean syndrome? understanding anthropogenic impacts on seawater pH. *Estuaries Coasts* 36 (2), 221–236. doi: 10.1007/s12237-013-9594-3

Durako, M. J. (1993). Photosynthetic utilization of $CO_{2(aq)}$ and HCO_3^- in *Thalassia testudinum* (Hydrocharitaceae). *Mar. Biol.* 115 (3), 373–380. doi: 10.1007/bf00349834

Falkowski, P. G., and Raven, J. A. (2007). *Aquatic photosynthesis* (Dordrecht: Princeton University Press).

Figueroa, F., Conde-Álvarez, R., and Gómez, I. (2003). Relations between electron transport rates determined by pulse amplitude modulated chlorophyll fluorescence and oxygen evolution in macroalgae under different light conditions. *Photosynthesis Res.* 75 (3), 259–275. doi: 10.1023/A:1023936313544

Foyer, C. H., Bloom, A. J., Queval, G., and Noctor, G. (2009). Photorespiratory metabolism: Genes, mutants, energetics, and redox signaling. *Annu. Rev. Plant Biol.* 60 (1), 455–484. doi: 10.1146/annurev.arplant.043008.091948

Foyer, C. H., Neukermans, J., Queval, G., Noctor, G., and Harbinson, J. (2012). Photosynthetic control of electron transport and the regulation of gene expression. *J. Exp. Bot.* 63 (4), 1637–1661. doi: 10.1093/jxb/ers013

Frost-Christensen, H., and Sand-Jensen, K. (1992). The quantum efficiency of photosynthesis in macroalgae and submerged angiosperms. *Oecologia* 91 (3), 377–384. doi: 10.1007/bf00317627

Heber, U., and Krause, G. H. (1980). What is the physiological role of photorespiration? *Trends Biochem. Sci.* 5 (2), 32–34. doi: 10.1016/s0968-0004(80)80091-0

Hough, R. A. (1974). Photorespiration and productivity in submersed aquatic vascular plants. *Limnology Oceanography* 19 (6), 912–927. doi: 10.4319/lo.1974.19.6.0912

Hough, A. R., and Wetzel, R. G. (1977). Photosynthetic pathways of some aquatic plants. *Aquat. Bot.* 3, 297–313. doi: 10.1016/0304-3770(77)90035-3

Igamberdiev, A. U., Bykova, N. V., Lea, P. J., and Gardestrom, P. (2001). The role of photorespiration in redox and energy balance of photosynthetic plant cells: A study with a barley mutant deficient in glycine decarboxylase. *Physiol. Plant* 111 (4), 427–438. doi: 10.1034/j.1399-3054.2001.1110402.x

Invers, O., Zimmerman, R. C., Alberte, R. S., Pérez, M., and Romero, J. (2001). Inorganic carbon sources for seagrass photosynthesis: an experimental evaluation of bicarbonate use in species inhabiting temperate waters. *J. Exp. Mar. Biol. Ecol.* 265 (2), 203–217. doi: 10.1016/s0022-0981(01)00332-x

Johnson, G. N. (2005). Cyclic electron transport in C3 plants: fact or artefact? *J. Exp. Bot.* 56 (411), 407–416. doi: 10.1093/jxb/eri106

Kalaji, H. M., Schansker, G., Ladle, R. J., Goltsev, V., Bosa, K., Allakhverdiev, S. I., et al. (2014). Frequently asked questions about *in vivo* chlorophyll fluorescence: practical issues. *Photosynthesis Res.* 122 (2), 121–158. doi: 10.1007/s11120-014-0024-6

Kanazawa, A., and Kramer, D. M. (2002). *In vivo* modulation of nonphotochemical exciton quenching (NPQ) by regulation of the chloroplast ATP synthase. *Proc. Natl. Acad. Sci.* 99 (20), 12789–12794. doi: 10.1073/pnas.182427499

Koch, M., Bowes, G., Ross, C., and Zhang, X.-H. (2013). Climate change and ocean acidification effects on seagrasses and marine macroalgae. *Global Change Biol.* 19 (1), 103–132. doi: 10.1111/j.1365-2486.2012.02791.x

Kuypers, M. M. M., Pancost, R. D., and Damste, J. S. S. (1999). A large and abrupt fall in atmospheric CO_2 concentration during Cretaceous times. *Nature* 399 (6734), 342–345. doi: 10.1038/20659

Larkum, A. D., Drew, E., and Ralph, P. (2006a). "Photosynthesis and metabolism in seagrasses at the cellular level," in *Seagrasses: Biology, ecologyand conservation* (Dordrecht: Springer Netherlands), 323–345. doi: 10.1007/978-1-4020-2983-7_14

A. W. D. Larkum, R. J. Orth and C. M. Duarte (Eds.) (2006b). *Seagrasses : biology, ecology, and conservation* (Dordrecht: Springer).

Lewis, E. (1980). The practical salinity scale 1978 and its antecedents. *IEEE J. Oceanic Eng.* 5 (1), 3–8. doi: 10.1109/JOE.1980.1145448

Lewis, E., Wallace, D. W. R., and Allison, L. J. (1998). *Program developed for CO2 system calculations, carbon dioxide information analysis center*. Oak Ridge, Tenn: Oak Ridge National Laboratory.

Madsen, T. V., Maberly, S. C., and Bowes, G. (1996). Photosynthetic acclimation of submersed angiosperms to CO_2 and HCO_3^-. *Aquat. Bot.* 53 (1-2), 15–30. doi: 10.1016/0304-3770(95)01009-2

Madsen, T. V., and Sand-Jensen, K. (1991). Photosynthetic carbon assimilation in aquatic macrophytes. *Aquat. Bot.* 41 (1-3), 5–40. doi: 10.1016/0304-3770(91)90037-6

Madsen, T. V., Sand-Jensen, K., and Beer, S. (1993). Comparison of photosynthetic performance and carboxylation capacity in a range of aquatic macrophytes of different growth forms. *Aquat. Bot.* 44 (4), 373–384. doi: 10.1016/0304-3770(93)90078-B

McPherson, M. L., Zimmerman, R. C., and Hill, V. J. (2015). Predicting carbon isotope discrimination in eelgrass (*Zostera marina* l.) from the environmental parameters–light, flow, and [DIC]. *Limnology Oceanography* 60 (6), 1875–1889. doi: 10.1002/lno.10142

Meyer, M. T., Whittaker, C., and Griffiths, H. (2017). The algal pyrenoid: key unanswered questions. *J. Exp. Bot.* 68 (14), 3739–3749. doi: 10.1093/jxb/erx178

Miyake, C. (2010). Alternative electron flows (Water–water cycle and cyclic electron flow around PSI) in photosynthesis: Molecular mechanisms and physiological functions. *Plant Cell Physiol.* 51 (12), 1951–1963. doi: 10.1093/pcp/pcq173

Motulsky, H., and Christopoulos, A. (2004). *Fitting models to biological data using linear and nonlinear regression : a practical guide to curve fitting* (Oxford: Oxford University Press).

Munekage, Y., Hashimoto, M., Miyake, C., Tomizawa, K.-I., Endo, T., Tasaka, M., et al. (2004). Cyclic electron flow around photosystem I is essential for photosynthesis. *Nature* 429 (6991), 579–582. doi: 10.1038/nature02598

Osmond, C. B. (1981). Photorespiration and photoinhibition : Some implications for the energetics of photosynthesis. *Biochim. Biophys. Acta (BBA) - Rev. Bioenergetics* 639 (2), 77–98. doi: 10.1016/0304-4173(81)90006-9

Osmond, B., Badger, M., Maxwell, K., Björkman, O., and Leegood, R. (1997). Too many photons: photorespiration, photoinhibition and photooxidation. *Trends Plant Sci.* 2 (4), 119–121. doi: 10.1016/s1360-1385(97)80981-8

Ow, Y. X., Collier, C. J., and Uthicke, S. (2015). Responses of three tropical seagrass species to CO_2 enrichment. *Mar. Biol.* 162 (5), 1005–1017. doi: 10.1007/s00227-015-2644-6

Palacios, S., and Zimmerman, R. (2007). Response of eelgrass *Zostera marina* to CO_2 enrichment: possible impacts of climate change and potential for remediation of coastal habitats. *Mar. Ecol. Prog. Ser.* 344, 1–13. doi: 10.3354/meps07084

Pfannschmidt, T., and Yang, C. (2012). The hidden function of photosynthesis: a sensing system for environmental conditions that regulates plant acclimation responses. *Protoplasma* 249 (2), 125–136. doi: 10.1007/s00709-012-0398-2

Raghavendra, A. S. (2000). *Photosynthesis: A comprehensive treatise* (Cambridge, UK: Cambridge University Press).

Ralph, P. J., Durako, M. J., Enríquez, S., Collier, C. J., and Doblin, M. A. (2007). Impact of light limitation on seagrasses. *J. Exp. Mar. Biol. Ecol.* 350 (1-2), 176–193. doi: 10.1016/j.jembe.2007.06.017

Ralph, P. J., and Gademann, R. (2005). Rapid light curves: A powerful tool to assess photosynthetic activity. *Aquat. Bot.* 82 (3), 222–237. doi: 10.1016/j.aquabot.2005.02.006

Ralph, P. J., Polk, S. M., Moore, K. A., Orth, R. J., and Smith, W. O. (2002). Operation of the xanthophyll cycle in the seagrass *Zostera marina* in response to variable irradiance. *J. Exp. Mar. Biol. Ecol.* 271 (2), 189–207. doi: 10.1016/s0022-0981(02)00047-3

Rasmusson, L., Buapet, P., George, R., Gullström, M., Gunnarsson, P., and Björk, M. (2020). Effects of temperature and hypoxia on respiration, photorespiration, and photosynthesis of seagrass leaves from contrasting temperature regimes. *ICES J. Mar. Science.* 2056–2065. doi: 10.1093/icesjms/fsaa093

Raven, J., and Beardall, J. (2003). "Carbon acquisition mechanisms of algae: Carbon dioxide diffusion and carbon dioxide concentrating mechanisms," in *Photosynthesis in algae*. Eds. A. D. Larkum, S. Douglas and J. Raven (Dordrecht: Springer Netherlands), 225–244. doi: 10.1007/978-94-007-1038-2_11

Raven, J. A., and Beardall, J. (2014). CO_2 concentrating mechanisms and environmental change. *Aquat. Bot.* 118 (0), 24–37. doi: 10.1016/j.aquabot.2014.05.008

Raven, J. A., Giordano, M., Beardall, J., and Maberly, S. C. (2011). Algal and aquatic plant carbon concentrating mechanisms in relation to environmental change. *Photosynth Res.* 109 (1-3), 281–296. doi: 10.1007/s11120-011-9632-6

Ruesink, J. L., Yang, S., and Trimble, A. C. (2015). Variability in carbon availability and eelgrass (*Zostera marina*) biometrics along an estuarine gradient in willapa bay, WA, USA. *Estuaries Coasts* 38 (6), 1908–1917. doi: 10.1007/s12237-014-9933-z

Scheibe, R., Backhausen, J. E., Emmerlich, V., and Holtgrefe, S. (2005). Strategies to maintain redox homeostasis during photosynthesis under changing conditions. *J. Exp. Bot.* 56 (416), 1481–1489. doi: 10.1093/jxb/eri181

Schubert, N., Freitas, C., Silva, A., Costa, M. M., Barrote, I., Horta, P. A., et al. (2018). Photoacclimation strategies in northeastern Atlantic seagrasses: Integrating responses across plant organizational levels. *Sci. Rep.* 8 (1), 14825. doi: 10.1038/s41598-018-33259-4

Somerville, C. R. (2001). An early arabidopsis demonstration. resolving a few issues concerning photorespiration. *Plant Physiol.* 125 (1), 20–24. doi: 10.2307/4279600

Spreitzer, R. J., and Salvucci, M. E. (2002). RUBISCO: Structure, regulatory interactions, and possibilities for a better enzyme. *Annu. Rev. Plant Biol.* 53 (1), 449–475. doi: 10.1146/annurev.arplant.53.100301.135233

Tcherkez, G. G. B., Farquhar, G. D., and Andrews, T. J. (2006). Despite slow catalysis and confused substrate specificity, all ribulose bisphosphate carboxylases may be nearly perfectly optimized. *Proc. Natl. Acad. Sci.* 103 (19), 7246–7251. doi: 10.1073/pnas.0600605103

Tolbert, N. E., and Osmond, C. B. (1976). *Photorespiration in marine plants* (Baltimore: CSIRO).

Touchette, B. W., and Burkholder, J. M. (2000). Overview of the physiological ecology of carbon metabolism in seagrasses. *J. Exp. Mar. Biol. Ecol.* 250 (1-2), 169–205. doi: 10.1016/s0022-0981(00)00196-9

Voss, I., Sunil, B., Scheibe, R., and Raghavendra, A. S. (2013). Emerging concept for the role of photorespiration as an important part of abiotic stress response. *Plant Biol.* 15 (4), 713–722. doi: 10.1111/j.1438-8677.2012.00710.x

Webb, W., Newton, M., and Starr, D. (1974). Carbon dioxide exchange of *Alnus rubra* a mathematical model. *Oecologia* 17 (4), 281–291. doi: 10.1007/BF00345747

Xin, C.-P., Tholen, D., Devloo, V., and Zhu, X.-G. (2015). The benefits of photorespiratory bypasses: How can they work? *Plant Physiol.* 167 (2), 574–585. doi: 10.1104/pp.114.248013

Zeebe, R. E. (2012). History of seawater carbonate chemistry, atmospheric CO_2, and ocean acidification. *Annu. Rev. Earth Planetary Sci.* 40 (1), 141–165. doi: 10.1146/annurev-earth-042711-105521

Zimmerman, R. C. (2003). A biooptical model of irradiance distribution and photosynthesis in seagrass canopies. *Limnology Oceanography* 48 (1), 568–585. doi: 10.4319/lo.2003.48.1_part_2.0568

Zimmerman, R. C. (2006). "Light and photosynthesis in seagrass meadows," in seagrasses: Biology, ecology and conservation,". Eds. A. W. D. Larkum, R. J. Orth and C. M. Duarte (Dordrecht: Springer Netherlands), 303–321.

Zimmerman, R. C. (2021). Scaling up: Predicting the impacts of climate change on seagrass ecosystems. *Estuaries Coasts* 44 (2), 558–576. doi: 10.1007/s12237-020-00837-7

Zimmerman, R. C., Cabello-Pasini, A., and Alberte, R. S. (1994). Modeling daily production of aquatic macrophytes from irradiance measurements: a comparative analysis. *Mar. Ecol. Prog. Ser.* 114, 185–196. doi: 10.3354/meps114185

Zimmerman, R. C., Hill, V. J., and Gallegos, C. L. (2015). Predicting effects of ocean warming, acidification, and water quality on Chesapeake region eelgrass. *Limnology Oceanography* 60 (5), 1781–1804. doi: 10.1002/lno.10139

Zimmerman, R. C., Hill, V. J., Jinuntuya, M., Celebi, B., Ruble, D., Smith, M., et al. (2017). Experimental impacts of climate warming and ocean carbonation on eelgrass *Zostera marina*. *Mar. Ecol. Prog. Ser.* 566, 1–15. doi: 10.3354/meps12051

Zimmerman, R. C., Kohrs, D. G., Steller, D. L., and Alberte, R. S. (1997). Impacts of CO_2 enrichment on productivity and light requirements of eelgrass. *Plant Physiol.* 115 (2), 599–607. doi: 10.1104/pp.115.2.599

Zimmerman, R. C., Reguzzoni, J. L., and Alberte, R. S. (1995). Eelgrass (*Zostera marina* l.) transplants in San Francisco bay: Role of light availability on metabolism, growth and survival. *Aquat. Bot.* 51 (1-2), 67–86. doi: 10.1016/0304-3770(95)00472-c

Zimmerman, R. C., Reguzzoni, J. L., Wyllie-Echeverria, S., Josselyn, M., and Alberte, R. S. (1991). Assessment of environmental suitability for growth of *Zostera marina* l. (eelgrass) in San Francisco bay. *Aquat. Bot.* 39 (3-4), 353–366. doi: 10.1016/0304-3770(91)90009-t

Zimmerman, R. C., SooHoo, J. B., Kremer, J. N., and D'Argenio, D. Z. (1987). Evaluation of variance approximation techniques for non-linear photosynthesis–irradiance models. *Mar. Biol.* 95 (2), 209–215. doi: 10.1007/BF00409007

frontiers | Frontiers in Plant Science

TYPE Original Research
PUBLISHED 13 January 2023
DOI 10.3389/fpls.2022.1069842

OPEN ACCESS

EDITED BY
Justine Marchand,
Le Mans Université, France

REVIEWED BY
Gudasalamani Ravikanth,
Ashoka Trust for Research in Ecology and the Environment (ATREE), India
Gonzalo Gajardo,
University of Los Lagos, Chile

*CORRESPONDENCE
Weronika A. Makuch
weronika-agnieszka.makuch@botanik.uni-halle.de

SPECIALTY SECTION
This article was submitted to Marine and Freshwater Plants, a section of the journal Frontiers in Plant Science

RECEIVED 14 October 2022
ACCEPTED 14 December 2022
PUBLISHED 13 January 2023

CITATION
Makuch WA, Wanke S, Ditsch B, Richter F, Herklotz V, Ahlborn J and Ritz CM (2023) Population genetics and plant growth experiments as prerequisite for conservation measures of the rare European aquatic plant *Luronium natans* (Alismataceae). *Front. Plant Sci.* 13:1069842. doi: 10.3389/fpls.2022.1069842

Population genetics and plant growth experiments as prerequisite for conservation measures of the rare European aquatic plant *Luronium natans* (Alismataceae)

Weronika A. Makuch [1,2,3]*, Stefan Wanke [3,4], Barbara Ditsch [5], Frank Richter [6], Veit Herklotz [7], Julian Ahlborn [7] and Christiane M. Ritz [7,8]

[1]Institute of Biology, Geobotany and Botanical Garden, Martin-Luther University Halle, Halle, Germany, [2]German Centre for Integrative Biodiversity Research (iDiv) Halle-Jena-Leipzig, Leipzig, Germany, [3]Institut für Botanik, Fakultät Biologie, Technische Universität Dresden, Dresden, Germany, [4]Departamento de Botanica, Instituto de Biología, Universidad Nacional Autonoma de Mexico, Distrito Federal, Mexico, [5]Botanischer Garten der Technischen Universität Dresden, Dresden, Germany, [6]Sächsisches Landesamt für Umwelt, Landwirtschaft und Geologie, Dresden, Germany, [7]Senckenberg Museum for Natural History Görlitz, Senckenberg – Member of the Leibniz Association, Görlitz, Germany, [8]Professur für Biodiversität der Pflanzen, Internationales Hochschulinstitut (IHI) Zittau, Technische Universität Dresden, Zittau, Germany

Information provided by population genetic studies is often necessary to effectively protect endangered species. In general, such data is scarce for aquatic plants and this holds also for *Luronium natans*, an aquatic macrophyte endemic to northwestern and western Europe. It is threatened across its whole distribution range due to human influences, in particular due to eutrophication and intensive fish farming. In spite of habitat protection populations continue to decline and re-introductions are one possibility to prevent the species' extinction. Therefore, insights in genetic diversity and relatedness of source populations is warranted.

Thus, we performed Amplified Fragment-Length Polymorphism (AFLP) on two large populations in Saxony, Germany (*Großenhainer Pflege* and *Niederspree*), complemented with numerous additional occurrences from Europe. In addition, we conducted experiments on plant growth to assess optimal conditions for *ex-situ* cultivation taking water temperature, water level and substrate into account.

We revealed considerably high levels of genetic diversity within populations (Shannon Indices ranged from 0.367 to 0.416) implying that populations are not restricted to clonal growth only but reproduce also by open-pollinated flowers. Remarkably, the two geographically close Saxon populations were genetically distant to each other but subpopulations within a locality were completely intermingled. Concerning optimal cultivation conditions, longest roots were

obtained at temperatures >14°C and saturated, but not submerging water levels.

Thus, our findings advocate for a re-introduction scheme from nearby source populations and provide detailed information on successful *ex-situ* cultivation.

KEYWORDS

aquatic plant, Alismatales, *Luronium natans*, endangered species, population genetics, conservation, growth form

1 Introduction

The loss of aquatic vegetation has been accelerating in the last four decades (Zhang et al., 2017). Oligotrophic waterbodies such as lakes and ponds are among the most threatened habitats in Europe and they harbor many endangered plant and animal species. However, changes in land use, nutrient inputs, and water pollution represent the main causes of the reduction in species diversity and abundance (Jamin et al., 2020). The dramatic decline in the number of such wetlands and resulting fragmentation is putting further pressure on their flora and fauna, thus these habitats have been protected by European law (Habitats Directive, 1992). In particular, mainly due to eutrophication, aquatic macrophytes belong to the most endangered groups (Preston and Croft, 2001). Anthropogenic increases in nutrients allow plant species adapted to this condition to grow faster and displace rare pioneer species (Kozlowski et al., 2009). Indeed, wetlands are rarely managed to protect threatened species, and it remains incompletely understood which conservation measures are likely to stabilize populations of endangered aquatic plants (Doust and Doust, 1995).

Luronium natans (monotypic genus within Alismataceae) is a typical example of such an aquatic pioneer plant (Greulich et al., 2000; Szańkowski and Kłosowski, 2001) because it can hardly compete with more nitrophilic aquatic and semi-terrestrial plants (Szmeja, 2004). Throughout its distribution area covering the Atlantic and sub-Atlantic climatic zones of western and northwestern Europe, population trends are 'declining' (Preston and Hill, 1997; Greulich, 1999; IUCN, 2021). In Germany, *L. natans* is found mainly in northern lowlands. Since many populations have been lost since 1950, it has been classified as 'critically endangered' and became even extinct in some parts of Germany (Metzing et al., 2018). In the German Federal state Saxony, *L. natans* has suffered a significant population decline during recent decades (Schulz, 2013). Today, only a few populations remain in large, mostly extensively managed ponds in eastern Saxony (Hanspach, 2007), and botanical surveys report a continuous decline in populations (Figure 1). Although historical distribution is not fully documented, it is very likely that isolated populations have existed for the last 100 years. Population declines until 1990 are probably due to loss of suitable habitats, while more recent declines from 1990 onwards are not fully understood and may be caused by changes in water chemistry.

Luronium natans is a perennial herb hibernating by submerged rosettes adapted to both aquatic and semi-terrestrial environments with changing water levels (Szmeja, 2004). The species grows on muddy, usually peaty substrates and is part of the endangered oligotrophic standing water plant communities (Littorelletea uniflorae Br.-Bl. et R. Tx.; Greulich et al., 2000; Reißmann and Dieter, 2015). *Luronium natans* is morphologically highly variable because it develops distinct phenotypes adapted to both aquatic and semi-terrestrial environments (Kay et al., 1999; Szmeja, 2004). These phenotypic adaptations are highly plastic, may occur several times during an individual's life time and these transformations need usually a few weeks only (Glück, 1905; Kay et al., 1999). The aquatic form grows in waters up to about 3 m in depth and is characterized by rosettes of linear submerged leaves and bundled roots. Individuals growing in shallower waters of up to 1.5 m depth may additionally develop floating leaves consisting of long petioles and leathery elliptical to oval blades (Szmeja, 2004). The semi-terrestrial form has well-developed, thread-like, mostly unbranched fine roots and its leaves shape resembles that of floating leaves, however, petioles are wider and shorter (Glück, 1905).

In addition to insect-pollinated flowers above the water level, plants can develop submerged cleistogamous flowers and reproduce vegetatively by stolons and fragmentation (Kay et al., 1999; Szmeja, 2004). However, the relative importance of these reproductive modes has been controversially discussed (Kay et al., 1999; Nielsen et al., 2006; Cox et al., 2014). Nuts do not have special adaptations, but both dispersal by water or birds seems to be likely (Kay et al., 1999; Halvorsen and Grostad, 2002). The species forms a considerable seed bank with seeds germinating after long periods of stasis at considerable rates (Glück, 1905; Nielsen et al., 2006) and the seedbank is

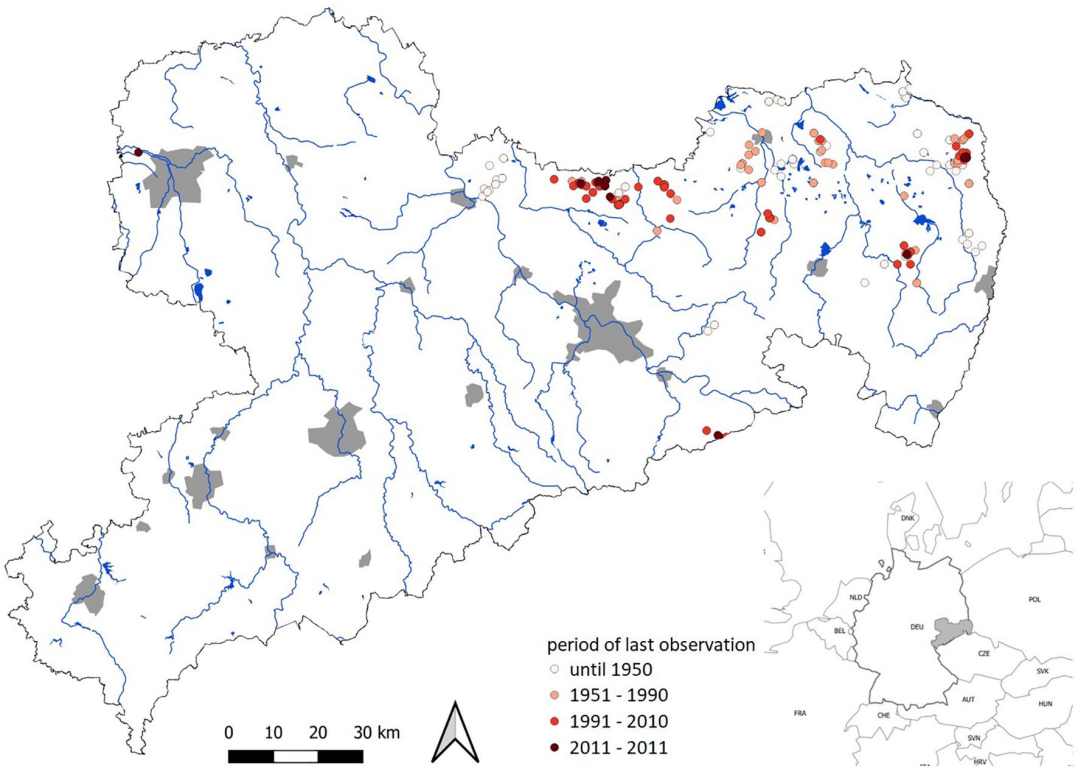

FIGURE 1
Occurrences of *Luronium natans* in Saxony (Germany) based on records from herbaria in Dresden (DR), Görlitz (GLM), Halle (HAL), Jena (JE) and Leipzig (LZ). Main rivers and water reservoirs are marked in blue, cities in grey.

considered to play a key role for surviving periods of inadequate conditions (Kaplan et al., 2014). Particularly in clonal populations, seeds are the major carrier of long-distance spread (Eckert et al., 2016).

Because sufficient genetic variation is the basis for the adaptability to the ever-changing environment (Hoban et al., 2020) and thus for the survival of a species (Hughes et al., 1997; Luck et al., 2003), assessing the extent of genetic diversity in endangered plant species has become a fundamental tool for conservation efforts. Still, the role of genetic diversity for conservation is often under-appreciated in plants and explicit goals for genetic diversity are undeveloped or focus mostly on species of agricultural relevance (Hoban et al., 2020). The importance of intraspecific genetic diversity for the resilience of ecosystems and survival of species is crucial and confirmed by a large body scientific evidence (Laikre et al., 2020). However, estimation of the effective population size (Ne) in natural plant populations with a polymorphic reproductive strategy and a considerable seed bank is not straight-forward at least using easily available dominant marker systems, so most studies rely on simple estimators of genetic diversity (Allendorf et al., 2013). Moreover, dramatic habitat losses due to land use changes may happen so rapidly that they are often not mirrored by lagging changes in genetic diversity (Reichel et al., 2016; Aavik et al., 2019).

Ex-situ collections can be effective measures in conserving plant species (Abeli et al., 2020) by preventing extinction and restoring a species' historic range by re-introductions (He et al., 2016). Therefore, the knowledge of the genetic status and relatedness of source populations can significantly influence re-introduction efforts by maximizing genetic variation in target populations (He et al., 2016; Robinson et al., 2021).

As with many other endangered aquatic plants, neither population genetics nor ecology of *L. natans* has been intensively studied and data are rather anecdotal across its distribution area. So far, population genetic studies have been carried out in the Czech Republic, Germany, Wales and Ireland using isozymes (Kay et al., 1999; Bartuška, 2009) as well as in Belgium and Denmark using Amplified Fragment Length Polymorphism (AFLP; Nielsen et al., 2006; Cox et al., 2014). Bartuška (2009) found little genetic diversity within populations from the Czech Republic and Germany (Saxony: *Großenhainer Pflege* and *Niederspree*). Furthermore, Belgian populations were found to have a high degree of clonal reproduction (Cox et al., 2014).

However, effective reintroduction requires knowledge not only of the genetic status of populations, but ecological experiments on plant growth and survival, which is particularly important for a species with diverse growth forms such as *Luronium*.

To get fundamental genetic and ecological knowledge for successful re-introduction efforts of *Luronium natans*, we investigated population genetics of the remaining Saxon populations using AFLPs. Although this method relies on presence/absence data of anonymous fragments and may have disadvantages compared to sequence-based population genomic methods it still provides reliable and cost-effective data for population genetics in species without prior knowledge on the genome (Woodhead et al., 2005; Allendorf et al., 2013). These markers yield a genome-wide overview about population genetic patterns and robust data can be retrieved when a rigorous scoring and replication scheme is applied (Ley and Hardy, 2013, see below). In addition, previous studies on other European populations of *Luronium natans* were also performed with AFLPs (Cox et al., 2014; Nielsen et al., 2006), allowing for direct comparisons of population genetic estimators.

In particular, we determined the genetic diversity within populations to estimate the degree of clonality and thus the influence of sexual versus vegetative reproduction. We also studied the genetic distance of these populations in comparison to samples covering the species' distribution area and with material from *ex-situ* cultures from various botanical gardens. Since all previous publications indicated a low genetic variability within populations in *L. natans* (Kay et al., 1999; Nielsen et al., 2006; Bartuška, 2009; Cox et al., 2014) and such a pattern seems to hold in general for aquatic plants (Santamaría, 2002) because clonal propagation appears to be common in endangered and aquatic species populations (Silvertown, 2008), we hypothesize low levels of genetic diversity within Saxonian populations but a considerable genetic variance between them.

In addition, we conducted a greenhouse experiment to investigate the influence of temperature, substrate, and water level on plant growth in order to find optimum growing conditions for *ex-situ* cultures potentially used for re-introduction experiments.

2 Material and methods

2.1 Study sites

Our sampling of *L. natans* focused on Saxony (Germany), where the species is found in two pond areas approximately 90 km distant from each other: *Niederspree* (DE_Ni) and *Großenhainer Pflege* (DE_Gr; Hanspach, 2007; Hanspach et al, 2016). The occurrences in the *Niederspree* pond area have been known at least since 1899 and in *Großenhainer Pflege* since 1840.

Both pond areas contain a number of distinct populations in the respective single ponds (Table 1). Within the pond areas several thousand shoots have been detected, in which high fluctuation rates up to 50% were observed (Hanspach et al., 2016, own observations). However, despite historical records (personal communication L. Runge) no occurrences of *Luronium* were found at *Goldgrubenteiche*. The material was collected from the end of September to the beginning of October 2020. In accordance with the collection permit issued by the relevant authorities leaves from 1–28 plants per pound (depending on the size of the subpopulation; minimum distance between samples – 0.8 m) were collected and dried in silica gel. To ensure that the harvested material came from one plant, only a single leaf per plant was harvested. In many cases plants occurred in rather dense patches, from which we sampled only one leaf to avoid collecting clonal plants.

Additionally, leaves from plants of two other localities in Germany (Mecklenburg-Vorpommern: near Rostock; Bavaria: Bad Alexandersbad), as well as several samples from the Czech Republic, Poland, Great Britain, and Norway were investigated (Table 1). Furthermore, leaves from plants cultivated in the Botanical Garden of the TU Dresden were also studied (Table 1).

2.2 Population genetic analyses

DNA was isolated from silica gel dried leaf material using innuPREP Plant DNA Kit (Analytic Jena, Germany) following the manufacturer's instructions except for the elution of DNA, which was eluted in two steps: 1. with 70 µl HPLC grade water, 2. with 30 µl HPLC grade water. The quality of isolates was checked with agarose gel electrophoresis (1%) and DNA quantity was estimated using Qubit Fluorometer (Thermo Fisher Scientific). Extracted DNA was stored at -22°C until further processing.

To investigate genetic diversity within Saxon populations and their relationships to other European populations, AFLP (Vos et al., 1995) was used with minor modifications. One hundred nanograms of isolated DNA were digested with the restriction enzymes *PstI* and *MseI*. Restriction and ligation were performed in a single reaction for 10 hours at 37°C. For selective PCR, we followed Schuelke (2000). We first tested 15 primer combinations based on previous AFLP studies on *L. natans* (Cox et al., 2014; Nielsen et al., 2006) and selected four combinations for further analyses: S7 (*PstI*-ACG/*MseI*-CAC), S8 (*PstI*-ACG/*MseI*-CCG), S11 (*PstI*-ACT/*MseI*-CTC), S12 (*PstI*-ACT/*MseI*-GCT). Samples were randomly distributed on 96-well plates to avoid position effects. Sixty-six of 253 samples were analyzed twice for quality control. In addition, five identical samples were repeated on each of the five 96-well plates, and negative controls for restriction/ligation, pre-selective PCR, and selective PCR were included. Automated detection of AFLP fragments was performed by the Senckenberg Biodiversity and Climate Research Center (SBik-F; Frankfurt am Main, Germany) with

10.3389/fpls.2022.1069842

TABLE 1 Origin of sampled material.

country, state	locality, population	subpopulation	GPS coordinates (WGS 84)		No of samples
Germany, Saxony	*Großenhainer Pflege* (DE_Gr), *Tiergartenteich* (DE_Gr_Tier)	large *Tiergartenteich* (TierL); additional sample from Botanical Garden BG_2: (accession number: 017947-28)	51.338 N	13.746 E	23 1
		small *Tiergartenteich* (TierS); additional sample from Botanical Garden BG_1: (accession number: 017947-28)	51.339 N	13.746 E	8 1
		Schwarzteich[1]; (Sch)			1
	Großenhainer Pflege (DE_Gr), *Raschützwaldteich* (DE_Gr_Ras)	*Kleiner Teich* near *Raschützwald*, eastern part (RasE)	51.342 N	13.670 E	28
		Kleiner Teich near *Raschützwald*, western part (RasW)	51.342 N	13.668 E	13
	Großenhainer Pflege (DE_Gr), *Sergkteich* (DE_Gr_Ser)	southern *Sergkteich* (SerS)	51.345 N	13.724 E	12
		northern *Sergkteich* (SerN)	51.348 N	13.726 E	2
Germany, Saxony	pond area *Niederspree* (DE_Ni), *Großer Tiefzug* (DE_Ni_Tief)	eastern part (TiefE_1)	51.403 N	14.905 E	19
		eastern part, ditch (TiefE_2)	51.403 N	14.905 E	1
	pond area *Niederspree* (DE_Ni), *Froschteich* (DE_Ni_Fro)	*Froschteich* (Fro); additional sample from Botanical Garden BG_4 (accession number: 018092-20)	51.404 N	14.908 E	3 1
Germany, Bavaria	Bad Alexandersbad (DE_By)		50.833 N	14.155 E	6
Germany, Mecklenburg-Pomerania	small patch near to *Entensee* and *Schwarzer See* (DE_Ro)		50.832 N	14.202 E	12
Czech Republic, Ustecky Kraj	Rybník u Králova mlýna (CZ_1)		50.833 N	14.155 E	6
	Hasičská nádrž (CZ_2)		50.832 N	14.202 E	12
	Pruhonice Park (Czech Academy of Sciences) (BG_3)		ex cult., unknown		3
Norway, Oslo	Lake Breisjøen (NO_1)		50.833 N	14.155 E	6
	Lake Maridalsvannet (NO_2)		50.832 N	14.202 E	12
Poland, Pomeranian	Jezioro Smołowskie (PL)		50.833 N	14.155 E	6
United Kingdom, North Wales	Llyn Padarn (UK)		50.832 N	14.202 E	12

[1]Population was newly established based on material from *Tiergartenteich* in 2019 (pers. comm. L. Runge, head of the regional association '*Großenhainer Pflege*' of non-governental organization '*Naturschutzbund Deutschland*').

an ABI 3730 sequencer (ABI Life Technologies, Darmstadt, Germany) using the LIZ-600 size standard (ABI Life Technologies).

Fragment scoring was processed as described in Ley and Hardy (2013). First, scoring was automatically done using PeakScanner 1.0 (Applied Biosystems, ThermoFisher Scientific, Berlin, Germany) on a size range from 100–500 bp, the minimal peak height of 30, and maximal peak width of 1. The program TinyFLP v1.30 (Arthofer, 2010) was then used for a pre-choice of markers. Finally, the software SPAGeDi (Hardy and Vekemans, 2002) was used to estimate the reproducibility of bands by calculating fragment-wise Fst values across repeated samples by combining all combinations within one matrix (see details in Ley and Hardy, 2013). We retained a final data matrix consisting of 151 samples from 22 (sub)populations with 48 fragments with a Fst ≥0.25.

To estimate the genetic diversity within populations (for those with >5 samples) we calculated Expected Heterozygosity (He); Shannon's Index of Diversity (I), and the Percentage of Polymorphic Loci (%P) with GenAlEx v. 6.5 (Peakall and Smouse, 2012). Population structure was analyzed using GenAlEx by performing Analysis of Molecular Variance

(AMOVA) and Principal Coordinate Analysis (PCoA) based on Jaccard distances with the R-Package vegan (Oksanen et al., 2020). In addition, we performed Mantel tests (Mantel, 1967) with GenAIEx to check for a correlation between geographic and genetic distances. Furthermore, Bayesian clustering was conducted with the R-package ParallelStructure (Besnier and Glover, 2013) with 10 iterations for every K from 1 to 10, with a burn-in of 500,000 generations followed by 1,000,000 generations. The best-fitting model was chosen according to the method described by Evanno et al. (2005) using the software Structure Harvester v.0.6.94 (Earl and vonHoldt, 2012). Results were visualized with the program DISTRUCT v.1.1 (Rosenberg, 2003).

2.3 Experiment on plant growth

The experiment started on October 27, 2020 and ended on March 12, 2021. Plant material for the experiment originated from the population *Kleiner Tiergartenteich* (DE_Gr_Tier; Table 1) and had been cultivated since 2019 in the Botanical Garden of the TU Dresden. The plants used for the experiment were propagated by runners from mother plants and were grown after separation from the mother plants for 7 −8 weeks in submerged pots in the outside area of the botanical garden.

Conditions tested in this experiment were selected based on observations from habitat and previous publications (Glück, 1905; Barrat-Segretain and Bornette, 2000; Nielsen et al., 2006). Plants were potted into four types of substrates: clay, sand, mixed, i.e. clay/sand mixture (1:1), and layered, i.e. sand as the top layer and clay as the bottom layer (1:1) to check whether lack of nutrients (especially sand as top layer) will influence root length. Pots were subsequently placed in three different water levels: (1) semi-terrestrial condition (saturated): water up to about 3 cm below the rim of the pot; (2) aquatic condition I: water about 0.5 – 1.0 cm above the rim of the pot; (3) aquatic condition II: water about 7 cm above the rim of the pot. Since seasonal differences in plant growth have been observed previously which are likely related to water temperature (Barrat-Segretain and Bornette, 2000; Nielsen et al., 2006), plants were exposed to two different water temperatures: cold: ~ 5 °C and warm: ~ 14 °C. Four plants each, i.e. biological replications were used for each combination of substrate, water level, and temperature (Supplementary Figure 1), thus the experiment constituted a full-factorial design. Water level (rainwater) was regularly checked and replenished when necessary. The plants were illuminated with assimilation lighting from 7 to 10 a.m. Since not all plants used for the experiments were of the same size, their size classes were recorded in the beginning of the experiment: small (s), medium without floating leaves (m), and medium with floating leaves (wfl). After completion of the experiment roots of each plant were rinsed with water to remove remaining substrate. Then, the length of the longest root and of the longest leaf (floating leaves were excluded) were measured. Typically, roots are cut and weighted, but this procedure could not be performed since the plants had to be kept alive for further *ex situ* conservation.

The effects of the substrate, water level, and temperature on root and leaf length were analyzed using linear regressions. Additionally, we analyzed the effect of the plant size at the onset of the experiment by including the variable as a covariate. For each response variable, we calculated 27 different models (Supplementary Tables 1, 3) with the predictor variables in plausible combinations. For model selection, we used Akaike's information criterion (AIC). The 27 models were ranked *via* AIC and the model with the lowest AIC and a difference of at least 2 to the next model was then considered as the best-fitting model (Burnham and Anderson 2002). All analyses were performed using the R environment (R Core Team, 2020).

3 Results

3.1 Genetic diversity of *Luronium* populations

Genetic diversity of *L. natans* populations was reasonably high Table 2; (grand means He = 0.25; Shannon-Index = 0.387) and differed only little between populations, with highest values found in the population *Raschützteich* (DE_Gr_Ras: He = 0.268) and lowest diversity detected in the Norwegian population (NO: He = 0.234).

3.2 Genetic structure of populations

The Principal Coordinate Analyses including all 151 samples across Europe separated mainly samples from Eastern Europe (Czech Republic = CZ and Poland =PL) and those from Eastern Saxony (pond area *Niederspree* = DE_Ni) from the remaining samples along the first axis (Figure 2). In the left part of the plot samples from the Central Saxon area *Großenhainer Pflege* (DE_Gr) were clustered, whereas samples from Northern and Southern Germany (DE_Ro, DE_By), Great Britain (UK), and Norway (NO) were found in a rather intermediate position. Note that samples obtained from *ex situ* collections of Botanical Gardens clustered according to their geographical origin (Table 1). The PCoA presented in Figure 2 was based on Saxon samples only. Accordingly, samples from *Niederspree* (Eastern Saxony) were clearly separated along the first axis. We observed no genetic structure among the populations within both pond areas, respectively.

TABLE 2 Overview about estimators of genetic diversity in populations >5 samples.

Country	Population ID	N	Shannon-Index	He	%P
Czech Republic	CZ	17	0.379 ± 0.033	0.243 ± 0.024	83.3%
Norway	NO	9	0.367 ± 0.033	0.234 ± 0.024	83.3%
Germany (Saxony)	DE_Ni	21	0.370 ± 0.036	0.240 ± 0.026	81.3%
	DE_Gr_Ras	41	0.416 ± 0.031	0.268 ± 0.023	95.8%
	DE_Gr_Ser	13	0.392 ± 0.035	0.256 ± 0.026	83.3%
	DE_Gr_Tier	31	0.398 ± 0.032	0.256 ± 0.024	93.8%
Total		**132**	**0.387 ± 0.014**	**0.250 ± 0.010**	**86.8% ± 2.6%**

Abbreviations for populations are according to Table 1. He, Expected Heterozygosity, %P, Percentage of Polymorphic Loci.
Values in bold are sums or mean values (total) of the above values.

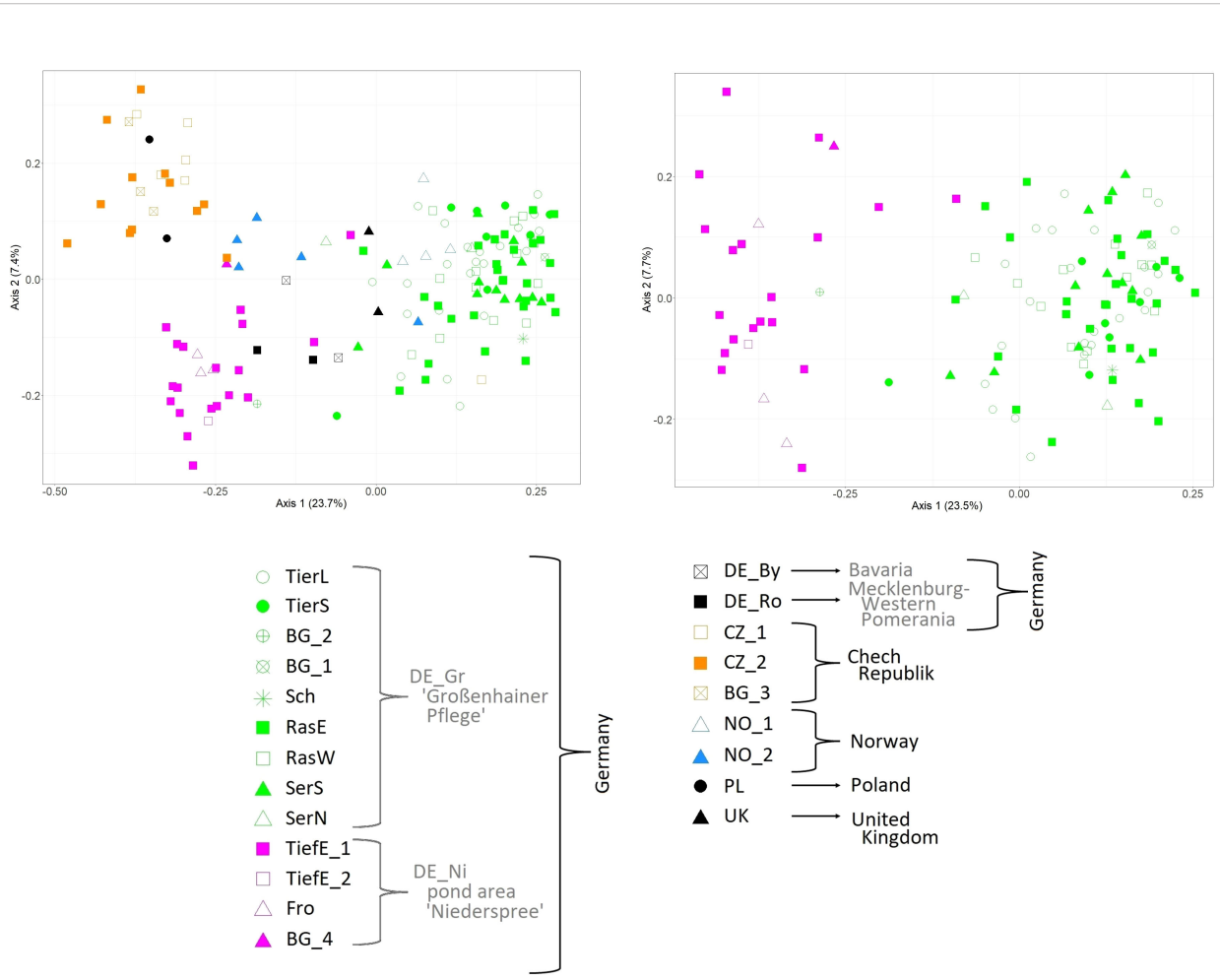

FIGURE 2
Principal Coordinate Analysis based on 48 AFLP loci of 151 individuals from European *L. natans* populations (left), and 113 individuals from Saxon populations only (right). Abbreviations for populations are according to Table 1.

10.3389/fpls.2022.1069842

TABLE 3 Analysis of Molecular Variance based on 48 AFLP loci among and within two Saxon localities of *Luronium natans* (*Niederspree*: DE_Ni and *Großenhain*: DE_Gr).

Source of Variation	Df	Sum of Squares	Mean of Squares	Estimated Variance	% Variance
Among localities	3	122.791	122.791	3.442	33%
Within localities	103	712.511	6.851	6.851	67%
Total	106	835.302		10.294	100%

df, degrees of freedom.

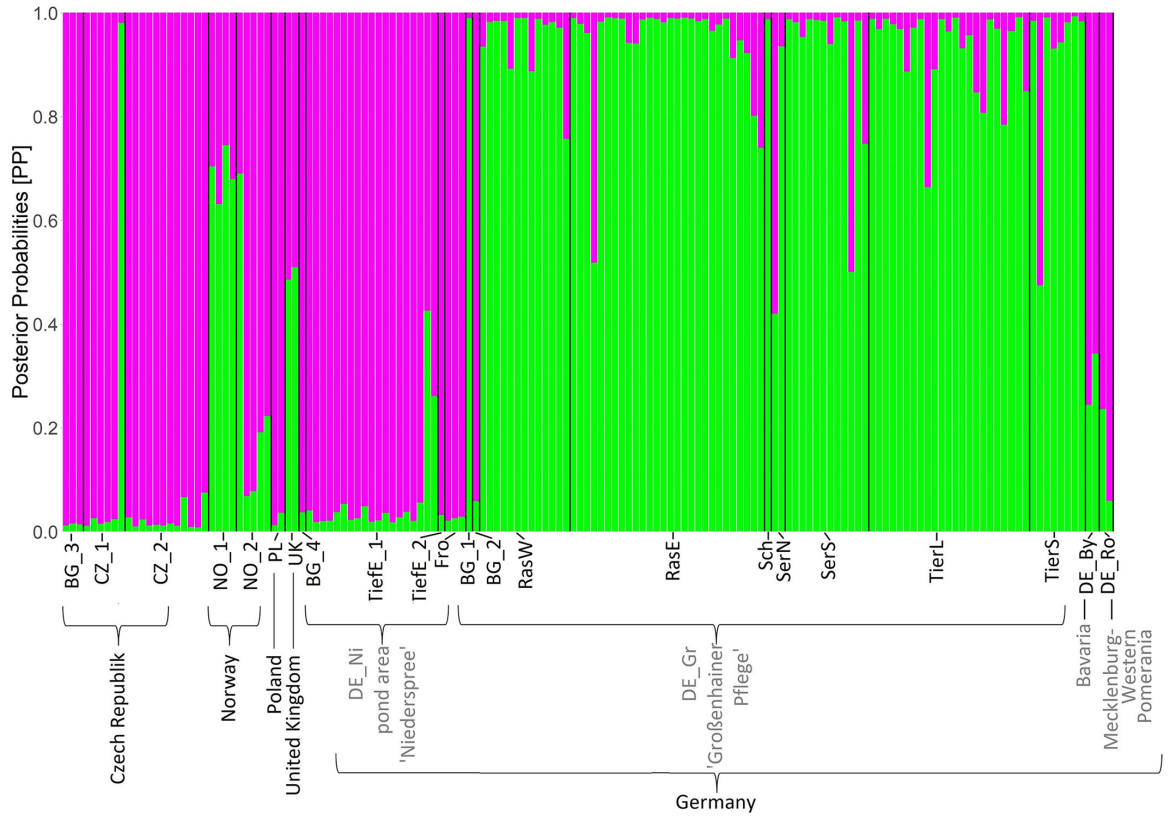

FIGURE 3
Bayesian clustering based on 48 loci AFLP for the model K = 2. Length of the colored bars indicates posterior probabilities (PP) for belonging to one of the two clusters (pink and green). Abbreviations for populations are according to Table 1.

Analyses of Molecular Variance (Table 3) revealed a moderate differentiation (ΦPT = 0.334, P ≥ 0.001) between both Saxon localities (DE_Gr and DE_Ni). Results from Bayesian clustering (Figure 3) with two clusters (K = 2) roughly corresponded to the PCoA analyses of all samples. Accessions from the area *Großenhainer Pflege* (DE_Gr) were assigned to the green cluster, whereas populations from *Niederspree* were found in the same cluster containing most of the Czech (CZ), Polish (PL), and Norwegian (NO) samples. Admixture between both clusters was detected for a few samples from various ponds in Central Saxony and for plants originating from Norway (NO) and Wales (UK). Mantel test did not detect a significant correlation between geographic and genetic distances (all populations: $R^2 = 0.0271$; p = 0.100, Saxon populations: $R^2 = 0.9974$ and p = 0.078).

3.3 Plant growth

The best-fitting model for root length (adjusted r-squared 0.65, $p < 0.001$) included an interaction between temperature and water level (Supplementary Tables 1, 2). The size of the plants at the beginning of the experiment did not have remarkable effects on root length. Roots were longer in plants grown under high water

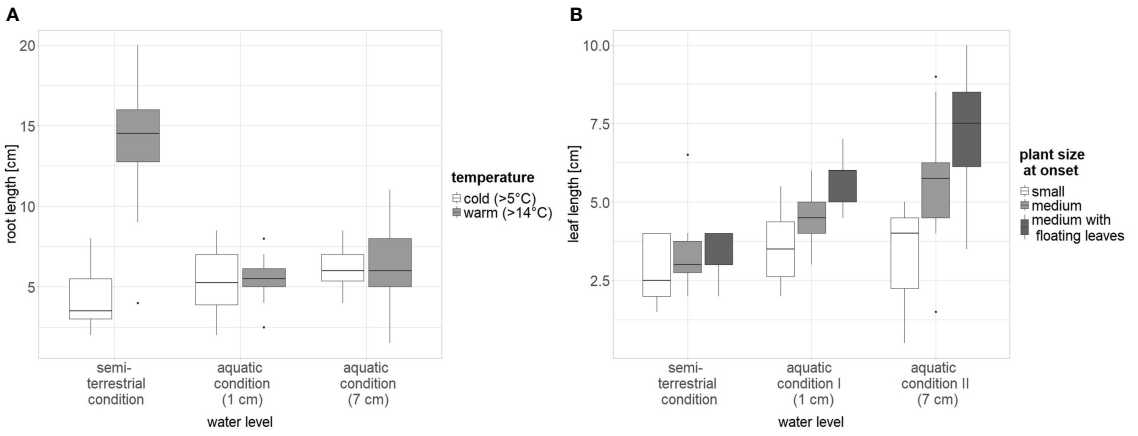

FIGURE 4
The influence of significant factors on plant growth (**A**: root length and **B**: leaf length) of *L. natans*. Water level: "1 cm": water about 0.5 – 1 cm above the rim of the pot; "7 cm": water about 7 cm above the rim of the pot; saturated: semi-terrestrial form, water only up to about 3 cm below the rim of the pot; temperature: cold ~ 5°C, warm ~ 14°C.

levels than under low water levels. The effect of temperature on the root length was restricted to plants grown under saturated water conditions: here, warm temperature led to roots three times longer than those of plants grown under cold temperatures (Figure 4).

The best-fitting model for leaf length (adjusted r-squared 0.47, $p < 0.001$) included an interaction between plant size at the onset of the experiment and water level. According to the best-fitting model (Supplementary Tables 3, 4), leaf length increased with the water level. Plants of medium size and with already developed floating leaves had the longest leaves, and this effect tended to increase with increasing water depths (Figure 4). However, the selected model did not fit much better than the model with plant size at onset and water level lacking interaction, and the model including plant size at onset, water level, and temperature (Δ AIC of the first three models was <2).

4 Discussion

4.1 Genetic diversity in *L. natans* populations

In contrast to our initial hypothesis of low genetic variation within populations, the values of the indices of genetic diversity were quite high (I = 0.367–0.416; Table 2), and these results suggest that Saxon populations are not genetically impoverished and that clonal reproduction does not cover the effect of the sexual reproduction. This finding was rather unexpected and contradicts the results from Bartušek (2009), who reported a moderate to very low (sometimes absent) genetic diversity in Czech and Saxon populations but applied possibly less polymorphic isozyme markers compared to AFLPs (Ipek et al., 2003; Mondini et al., 2009). Similarly, Kay et al. (1999) suggested the dominance of clonal propagation in the United Kingdom and Ireland based on isozyme analyses, and also previous studies from Belgium reported considerably low values (I = 0.0996) based on AFLPs (Cox et al., 2014). In addition, Szmeja (2004) assumed that *L. natans* populations in Poland are mainly represented by multigenerational clones reproducing primarily by fragmentation. However, he observed plants in water reservoirs with deeper water bodies, where cleistogamy occurs more often (Kay et al., 1999). Thus, the high genetic diversity observed in the Saxon populations may be due to marked outcrossing from insect-pollinated chasmogamic flowers above the water surface, which we observed in all ponds studied. Moreover, *L. natans* produces a substantial seed bank and is characterized by high rates of seed germination (average 51-60%; Nielsen et al., 2006). Lansdown and Wade (2003) assumed the seeds to have a capacity for extended dormancy over many years. Germination might take place preferably in shallow waters or on naked mud in empty ponds. The extreme fluctuations of observed shoots (up to 50%) between years (Hanspach et al., 2016, own observations) can be caused by pronounced clonal growth or by high proportion of regeneration from seeds. A much denser sampling design in consecutive years may help to investigate the different ways of population growth. Moreover, estimators of genetic diversity respond often delayed compared to rapid changes in habitats and thus in strong declines in population size (Reichel et al., 2016; Aavik et al., 2019).

In contrast to our results, low values of genetic diversity based on AFLPs (I = 0.025–0.140) were reported within three species of the closely related genus *Baldellia* (Alismataceae) in Europe (Arrigo et al., 2011). However, these authors found varying values depending on the geographic origin of the samples with higher values detected at Iberian Peninsula

compared to France and Switzerland, which were explained by a recent post-glacial re-colonization to the North. Thus, considering a species' biogeographic history might also be crucial regarding conservation approaches.

4.2 Genetic structure of *L. natans* populations

According to our hypothesis of a pronounced genetic structure between Saxon populations, *L. natans* samples clustered mainly according to their geographic origin, whereby we detected three groups of samples: (1) Czech populations, (2) Saxon populations from *Niederspree* and (3) Saxon populations from the pond area *Großenhainer Pflege*, with remaining samples from Germany and Norway in between (Figure 2). This partially coincides with the results reported by Bartuška (2009), who showed that the populations from the Czech Republic, and the two Saxon populations *Großenhainer Pflege* and *Niederspree* constituted three separate groups. Remarkably, sites from Saxony, which are only separated by a distance of approximately 90 km appeared to be rather distantly related because samples from the area *Großenhainer Pflege* formed a separate cluster and those from *Niederspree* were close to remaining samples from various sites across Europe (Figure 3). Most accessions were assigned with high posterior probabilities to one of the two clusters (Figure 3), thus admixture between both Saxon areas played a minor role. Given the rather low geographic distance between Saxon sites the ΦPT value of 0.334 suggests a moderate level of genetic differentiation between populations (Table 3), which was comparable to the values observed in Belgian populations ranging between 0.226 and 0.455 (Cox et al., 2014). Samples from neighboring ponds within each of the respective Saxon areas appeared to be completely intermingled, thus, no genetic structuring on very short distances was observed (Figure 2). While the lack of genetic structure between sub-populations per population (Table 1) may be an effect of water-mediated dispersal (Kay et al., 1999), it does not explain the situation between the three populations in *Großenhainer Pflege* (DE_Gr_Tier, DE_Gr_Ras, and DE_Gr_Ser) as these areas are not connected by ditches but rather suggests zoochoric dispersal, e.g. by birds. Although, Mikkelsen (1943) argued that *Luronium* nuts lack adaptations to bird dispersal, more recent studies reported likely dispersals of 50 to 100 km (Fritz, 1989; Halvorsen and Grostad, 2002; Lansdown and Wade, 2003; Nielsen et al., 2006). Here, bird dispersal would only explain the genetic similarity at the local scale (Table 1) but not between areas, because both areas in Saxony (DE_Gr and DE_Ni) were clearly separated (Figures 2, 3). However, we detected no significant pattern of isolation by distance (Mantel tests for European populations: $R^2 = 0.0271$; $P = 0.100$, for Saxony $R^2 = 0.9974$ and $P = 0.078$) but due to the restricted availability of plant material our sampling was rather unbalanced.

Remarkably the genetic similarity of Polish (PL) and Czech (CZ) samples (Figure 2) is surprising, given the geographic distance between the populations. We would have rather expected a close relationship of the Polish samples with the German population from Rostock (DE_Ro). In Poland, two big geographically separated occurrences, i.e. Pomerania (current populations; closer to Rostock) and Lower Silesia (historical populations; closer to the Czech Republic) are present (Dajdok and Proćków, 2003; Szmeja, 2004). Our findings are in line with the observation of Nischkowsky and Schube (1908) and Suda et al. (2000), who referred to the Lower Silesian occurrences as part of the Jizera Foothills meta-population, which also include the oldest Czech populations. The Czech populations examined in the present study are about 120 km away from these historical occurrences (Nischkowsky and Schube, 1908) but may represent together with scattered populations from *Wielkopolska*, Poland (Szmeja, 2007; Szmeja, 2013) remnants of a former widespread distribution in Poland and the Czech Republic. The closer relationship of samples from *Niederspree* (DE_Ni) to Czech populations rather than to the more western Saxon samples from *Großenhainer Pflege* (DE_Gr) implies a geographic separation of *L. natans* between Eastern and Western Europe, whose border might cross Saxony.

4.3 Growing conditions of *L. natans*

Our experiment showed that *Luronium* plants developed longer roots under semi-terrestrial (saturated) conditions at higher temperature (Figure 4). This is in line with the assumption of Glück (1905) who argued that a more extensive root system of semi-terrestrial forms may be caused by their restricted access to water. The here observed longer roots at higher temperatures fit also with *Luronium's* Ellenberg Indicator Value for temperature (T6; Ellenberg et al., 2001) indicating its adaptation to moderate warm to warm temperatures. In addition, we found longer leaves in plants growing at higher water level, which can be explained by the fact that the aquatic form of *Luronium* has longer leaves than the semi-terrestrial form. In addition, plants which were larger at the onset also produced longer leaves, however, plant size at onset was an uncontrolled factor, and the plants were randomly selected according to size. Thus, the best results for obtaining robust plants for potential reintroduction are obtained under semi-terrestrial conditions and at higher temperatures, as a strong root system can facilitate active planting.

4.4 Implications for conservation

Our study revealed moderate levels of genetic diversities in Saxon populations suggesting that the observed decline in populations is not caused by lacking genetic diversity. We assume

that populations in ponds rely strongly on regeneration by seeds emerged from outcrossing rather than by clonal reproduction or cleistogamous flowers. While we found a considerable genetic differentiation among Saxon populations our results showed no genetic differentiation within pond systems indicating sufficient genetic exchange between neighboring ponds probably mediated by birds or water. Thus, our results imply to use rather nearby populations from the same area as source for reintroductions. Our plant growth experiments demonstrated that possible reintroductions of plants are facilitated by optimal growing conditions in gardens since we obtained plants with longest roots when grown under saturated water conditions and higher temperatures, whereas the tested soil type seems to have less impact.

Data availability statement

The raw data supporting the conclusions of this article will be made available by the authors, without undue reservation.

Author contributions

CR, SW, BD, and FR planned the study, WM and BD collected the samples, WM did the laboratory work, WM, VH, and CR performed population genetic analyses, JA performed statistical analyses on plant growth, WM, JA, CR, and SW wrote the manuscript. All authors read, contributed and approved the final manuscript.

Funding

The work was financed by the core budget of Senckenberg Natural History Museum Görlitz and the Institute of Botany of the TU Dresden, third-party funds were not included.

Acknowledgments

Special thanks go to M. Striese (Boxberg, Germany), L. Runge (Linz, Germany) and F. Ditsch (TU Dresden) who helped with fieldwork, to A. Sembdner (TU Dresden) for the help in the botanical garden and to M. Schwager (Senckenberg Museum für Naturkunde Görlitz) and A. Wenke (TU Dresden) who helped with laboratory work. We also thank the following persons sending plant material from all over Europe, namely M. Čtvrtlíková (Institute of Hydrobiology of the Czech Academy of Sciences), M. Lauerer (Botanical Garden University of Bayreuth), D. Götze (Botanical Garden University of Rostock), Ø. Lofthus (Oslo Botanical Garden), K. Reczek (Botanical Garden of the University of Wrocław) and R. Blackhall-Miles (FossilPlants Gwynedd/UK). We thank P. Gebauer (GLM), J. Mueller (JE), F. Mueller (DR) and P. Otto (LZ) for summarizing herbarium records of the respective collections. In addition, we would also like to thank 'Untere Naturschutzbehörden of Landratsamt Görlitz' and 'Landratsamt Meißen' for granting permission to collect *Luronium* samples. We thank the two reviewers for their thoughtful comments on the manuscript.

Conflict of interest

The authors declare that the research was conducted in the absence of any commercial or financial relationships that could be construed as a potential conflict of interest.

Publisher's note

All claims expressed in this article are solely those of the authors and do not necessarily represent those of their affiliated organizations, or those of the publisher, the editors and the reviewers. Any product that may be evaluated in this article, or claim that may be made by its manufacturer, is not guaranteed or endorsed by the publisher.

Supplementary material

The Supplementary Material for this article can be found online at: https://www.frontiersin.org/articles/10.3389/fpls.2022.1069842/full#supplementary-material

References

Aavik, T., Thetloff, M., Träger, S., Hernández-Agramonte, I. M., Reinula, I., and Pärtel, M. (2019). Delayed and immediate effects of habitat loss on the genetic diversity of the grassland plant *Trifolium montanum*. *Biodivers. Conserv.* 28 (12), 3299–3319. doi: 10.1007/s10531-019-01822-8

Abeli, T., Dalrymple, S., Godefroid, S., Mondoni, A., Müller, J. V., Rossi, G., et al. (2020). *Ex situ* collections and their potential for the restoration of extinct plants. *Conserv. Biol.* 34 (2), 303–313. doi: 10.1111/cobi.13391

Allendorf, F. W., Aitken, S. N., and Luikart, G. (2013). *Conservation and the genetics of populations* (John Wiley & Sons). doi: 10.1111/mec.13948

Arrigo, N., Buerki, S., Sarr, A., Guadagnuolo, R., and Kozlowski, G. (2011). Phylogenetics and phylogeography of the monocot genus *Baldellia* (Alismataceae): Mediterranean refugia, suture zones and implications for conservation. *Mol. Phylogenet. Evol.* 58 (1), 33–42. doi: 10.1016/j.ympev.2010.11.009

Arthofer, W. (2010). tinyFLP and tinyCAT: software for automatic peak selection and scoring of AFLP data tables. *Mol. Ecol. Resour.* 10 (2), 385–388. doi: 10.1111/j.1755-0998.2009.02751.x

Barrat-Segretain, M. H., and Bornette, G. (2000). Regeneration and colonization abilities of aquatic plant fragments: effect of disturbance seasonality. *Hydrobiologia*

421 (1), 31–39. doi: 10.1023/A:1003980927853

Bartuška, M. (2009). *Genetická variabilita kriticky ohroženého žabníčku vzplývavého (Luronium natans (L.) Raf. Alismataceae) na okraji areálu a její význam pro cílenou druhovou ochranu. [master's thesis]* (Prague: Univerzita Karlova v Praze).

Besnier, F., and Glover, K. A. (2013). ParallelStructure: A R package to distribute parallel runs of the population genetics program STRUCTURE on multi-core computers. *PloS One* 8 (7), e70651. doi: 10.1371/journal.pone.0070651

Burnham, K.P., and Anderson, D.R. (2002). *Model selection and multimodel inference: a practical information-theoretic approach, 2nd edn*. New York, Springer.

Cox, K., Leyssen, A., Mergeay, J., Ronse, A., Packet, J., and Denys, L. (2014). Genetic assessment of *Luronium natans* in lower Belgium. *Analysis of population connectivity in an aquatic perennial* 2014 (5021339). (Brussel: Instituut voor Natuur- en Bosonderzoek).

Dajdok, Z., and Proćków, J. (2003). *Flora wodna i błotna dolnego Śląska na tle zagrożeń i możliwości ochrony*. Ed. W. Z. Kącki (Wrocław: Zagrożone gatunki flory naczyniowej Dolnego Śląska), 131–150.

Doust, L. L., and Doust, J. L. (1995). Wetland management and conservation of rare species. *Can. J. Bot.* 73 (7), 1019–1028. doi: 10.1139/b95-11

Earl, D. A., and vonHoldt, B. M. (2012). STRUCTURE HARVESTER: A website and program for visualizing STRUCTURE output and implementing the Evanno method. *Conserv. Genet. Resour.* 4 (2), 359–361. doi: 10.1007/s12686-011-9548-7

Eckert, C. G., Dorken, M. E., and Barrett, S. C. (2016). Ecological and evolutionary consequences of sexual and clonal reproduction in aquatic plants. *Aquat. Bot.* 135, 46–61. doi: 10.1016/j.aquabot.2016.03.006

Ellenberg, H., Weber, H. E., Duell, R., Wirth, V., Werner, W., and Paulissen, D. (2001). *Zeigerwerte von Pflanzen in Mitteleuropa. 3.* edition (Goltze. Scripta Geobotanica: 18 Göttingen).

Evanno, G., Regnaut, S., and Goudet, J. (2005). Detecting the number of clusters of individuals using the software STRUCTURE: a simulation study. *Mol. Ecol.* 14 (8), 2611–2620. doi: 10.1111/j.1365-294X.2005.02553.x

Fritz, O. (1989). A find of *Luronium natans* in the province of Halland, SW Sweden. *Svensk. Botanisk. Tidskrift.* 83 (2), 135–136.

Glück, H. (1905). Biologische und morphologische Untersuchungen über Wasser- und Sumpfgewächse. 118–133.

Greulich, S. (1999). *Compètition, perturbations et productivité potentielle dans la définition de l'habitat d'espèces rares: étude expérimentale du macrophyte aquatique Luronium natans (L) Raf. (Doctoral dissertation, Lyon 1)*. Lyon.

Greulich, S., Bornette, G., Amoros, C., and Roelofs, J. G. (2000). Investigation on the fundamental niche of a rare species: an experiment on establishment of *Luronium natans*. *Aquat. Bot.* 66 (3), 209–224. doi: 10.1016/S0304-3770(99)00073-X

Habitats Directive (1992). Council directive 92/43/EEC of 21 may 1992 on the conservation of natural habitats and of wild fauna and flora. *Off. J. Eur. Union.* 206, 7–50.

Halvorsen, R., and Grostad, T. (2002). Kinnhalvoya i brunlanes, larvik i vestfold og et funn av flytegro *Luronium natans* (L.) Raf. *Blyttia* 60 (2), 117–121.

Hanspach, D. (2007). Zur Bestandsentwicklung des Froschkrautes, *Luronium natans* (L.) Raf. im Niederspreer Teichgebiet. *Ber. Naturforsch. Ges. Oberlausitz.* 15, 149–161.

Hanspach, D., Landgraf, K., and Richter, F. (2016). *Erstellung von Artenschutzkonzepten und Aktionsplänen für Pflanzenarten und wirbellose Tierarten mit besonderer landesweiter Bedeutung, Los 5* (Froschkraut (*Luronium natans*), Abschlussbericht, Landgraf & Richter GbR).

Hardy, O. J., and Vekemans, X. (2002). SPAGeDi: a versatile computer program to analyse spatial genetic structure at the individual or population levels. *Mol. Ecol. Notes* 2 (4), 618–620. doi: 10.1046/j.1471-8286.2002.00305.x

He, X., Johansson, M. L., and Heath, D. D. (2016). Role of genomics and transcriptomics in selection of reintroduction source populations. *Conserv. Biol.* 30 (5), 1010–1018. doi: 10.1111/cobi.12674

Hoban, S., Campbell, C., da Silva, J., Ekblom, R., Funk, W. C., Garner, B., et al. (2020). An analysis of genetic diversity actions, indicators and targets in 114 national reports to the Convention on Biological Diversity. *BioRxiv*. doi: 10.1101/2020.08.28.254672

Hughes, J. B., Daily, G. C., and Ehrlich, P. R. (1997). Population diversity: its extent and extinction. *Science* 278 (5338), 689–692. doi: 10.1126/science.278.5338.689

Ipek, M., Ipek, A., and Simon, P. W. (2003). Comparison of AFLPs, RAPD markers, and isozymes for diversity assessment of garlic and detection of putative duplicates in germplasm collections. *J. Am. Soc. Hortic. Sci.* 128 (2), 246–252. doi: 10.21273/JASHS.128.2.0246

IUCN (2021) *The IUCN Red List of Threatened Species. version 2020-3*. Available at: https://www.iucnredlist.org.

Jamin, A., Peintinger, M., Gimmi, U., Holderegger, R., and Bergamini, A. (2020). Evidence for a possible extinction debt in Swiss wetland specialist plants. *Ecol. Evol.* 10 (3), 1264–1277. doi: 10.1002/ece3.5980

Kay, Q. O. N., John, R. F., and Jones, R. A. (1999). Biology, genetic variation and conservation of *Luronium natans* (L.) Raf. in Britain and Ireland. *Watsonia.* 22 (4), 301–316.

Kaplan, Z., Šumberová, K., Formanová, I., and Ducháček, M. (2014). Re-establishment of an extinct population of the endangered aquatic plant *Potamogeton coloratus*. *Aquat. Bot.*, 119, 91–99. doi: 10.1016/j.aquabot.2014.08.005

Kozlowski, G., Rion, S., Python, A., and Riedo, S. (2009). Global conservation status assessment of the threatened aquatic plant genus *Baldellia* (Alismataceae): challenges and limitations. *Biodivers. Conserv.* 18 (9), 2307–2325. doi: 10.1007/s10531-009-9589-3

Laikre, L., Hoban, S., Bruford, M. W., Segelbacher, G., Allendorf, F. W., Gajardo, G., et al. (2020). Post-2020 goals overlook genetic diversity. *Science* 367 (6482), 1083–1085. doi: 10.1126/science.abb2748

Lansdown, R. V., and Wade, P. M. (2003). Ecology of the floating water-plantain *Luronium natans*. Conserving Natura 2000 rivers. *Ecol. Ser.* 9.

Ley, A. C., and Hardy, O. J. (2013). Improving AFLP analysis of large-scale patterns of genetic variation –a case study with the central African lianas *Haumania* spp. (Marantaceae) showing interspecific gene flow. *Mol. Ecol.* 22 (7), 1984–1997. doi: 10.1111/mec.12214

Luck, G. W., Daily, G. C., and Ehrlich, P. R. (2003). Population diversity and ecosystem services. *Trends Ecol. Evol.* 18 (7), 331–336. doi: 10.1016/S0169-5347(03)00100-9

Mantel, N. (1967). The detection of disease clustering and a generalized regression approach. *Cancer Res.* 27 (2 Part 1), 209–220.

Metzing, D., Hofbauer, N., Ludwig, G., and Matzke-Hajek, G. (2018). Rote Liste gefährdeter Tiere, Pflanzen und Pilze Deutschlands. *Band* 70 (7).

Mikkelsen, V. M. (1943). Udbredelsen af Juncaginaceae, Alismataceae og Hydrocharitaceae i Danmark.

Mondini, L., Noorani, A., and Pagnotta, M. A. (2009). Assessing plant genetic diversity by molecular tools. *Diversity* 1 (1), 19–35. doi: 10.3390/d1010019

Nielsen, U. N., Riis, T., and Brix, H. (2006). The importance of vegetative and sexual dispersal of *Luronium natans*. *Aquat. Bot.* 84 (2), 165–170. doi: 10.1016/j.aquabot.2005.09.002

Nischkowsky, R., and Schube, T. (1908). Ergebnisse der Durchforschung der schlesischen Gefässpflanzenwelt im Jahre 1907. *Jahresber. Schles. Gesellsch. Vaterl. Cult.* 73, 43–61.

Oksanen, J., Blanchet, F. G., Friendly, M., Kindt, R., Legendre, P., McGlinn, D., et al. (2020) *Vegan: Community ecology package. R package version 2.5-7*. Available at: https://CRAN.R-project.org/package=vegan.

Peakall, R. O. D., and Smouse, P. E. (2012). GenAlEx 6.5: Genetic analysis in excel. population genetic software for teaching and research-an up-date. *Bioinformatics* 28, 2537–2539. doi: 10.1111/j.1471-8286.2005.01155.x

Preston, C. D., and Croft, J. M. (2001). *Aquatic plants in Britain and Ireland* (Colchester, Essex, England: Harley Books).

Preston, C. D., and Hill, M. O. (1997). The geographical relationships of British and Irish vascular plants. *Botanical. J. Linn. Soc.* 124 (1), 1–120. doi: 10.1111/j.1095-8339.1997.tb01785.x

R Core Team (2020). *R: A language and environment for statistical computing* (Vienna, Austria: R Foundation for Statistical Computing).

Reißmann, K., and Dieter, F. (2015). 3130 Oligo- bis mesotrophe stehende gewässer mit Vegetation Littorelletea uniflorae und/oder der Isoëto-Nanojuncetea. Available at: http://www.lau.sachsen-anhalt.de/naturschutz/natura-2000/arten-und-lebensraumtypen/lrt-anhang-i-ffh-rl/

Reichel, K., Richter, F., Eichel, L., Kącki, Z., Wesche, K., Welk, E., et al. (2016). Genetic diversity in the locally declining *Laserpitium prutenicum* L. and the more common *Selinum carvifolia* (L.) L.: a "silent goodbye"? *Conserv. Genet.* 17 (4), 847–860. doi: 10.1007/s10592-016-0827-4

Robinson, N. M., Rhoades, C., Pierson, J., Lindenmayer, D. B., and Banks, S. C. (2021). Prioritising source populations for supplementing genetic diversity of reintroduced southern brown bandicoots *Isoodon obesulus obesulus*. *Conserv. Genet.* 22 (3), 341–353. doi: 10.1007/s10592-021-01341-6

Rosenberg, N. A. (2003). Distruct: A program for the graphical display of population structure: PROGRAM NOTE. *Mol. Ecol. Notes* 4 (1), 137–138. doi: 10.1046/j.1471-8286.2003.00566.x

Santamaría, L. (2002). Why are most aquatic plants widely distributed? Dispersal, clonal growth and small-scale heterogeneity in a stressful environment. *Acta Oecol.* 23 (3), 137–154. doi: 10.1016/S1146-609X(02)01146-3

Schuelke, M. (2000). An economic method for the fluorescent labeling of PCR fragments. *Nat. Biotechnol.* 18 (2), 233–234. doi: 10.1038/72708

Schulz, D. (2013) *Rote Liste und Artenliste Sachsens- Farn- und Samenpflanzen*. Available at: https://publikationen.sachsen.de/bdb/artikel/19031.

Silvertown, J. (2008). The evolutionary maintenance of sexual reproduction: evidence from the ecological distribution of asexual reproduction in clonal plants. *Int. J. Plant Sci.* 169 (1), 157–168. doi: 10.1086/523357

Suda, J., Bauer, P., Brabec, J., and Hadinec, J. (2000). Znovunalezené druhy naší květeny–žabníček vzplývavý. *Živa*, 48, 205–207.

Szańkowski, M., and Kłosowski, S. (2001). Habitat conditions of the phytocoenoses dominated by *Luronium natans* (L.) Raf. in Poland. *Hydrobiologia* 455 (1), 213–222. doi: 10.1023/A:1011914607379

Szmeja, J. (2004). *Poradnik ochrony siedlisk i gatunków - Luronium natans (L.) Raf.* (Elisma Wodna).

Szmeja, J. (2007). *Monitoring gatunków i siedlisk przyrodniczych ze szczególnym uwzględnieniem specjalnych obszarów ochrony siedlisk Natura 2000* (Główny Inspektorat Ochrony Środowiska).

Szmeja, J. (2013). *Monitoring gatunków i siedlisk przyrodniczych ze szczególnym uwzględnieniem specjalnych obszarów ochrony siedlisk Natura 2000* (Główny Inspektorat Ochrony Środowiska).

Vos, P., Hogers, R., Bleeker, M., Reijans, M., Lee, T. V. D., Hornes, M., et al. (1995). AFLP: a new technique for DNA fingerprinting. *Nucleic Acids Res.* 23 (21), 4407–4414. doi: 10.1093/nar/23.21.4407

Woodhead, M., Russell, J., Squirrell, J., Hollingsworth, P. M., Mackenzie, K., Gibby, M., et al. (2005). Comparative analysis of population genetic structure in *Athyrium distentifolium* (Pteridophyta) using AFLPs and SSRs from anonymous and transcribed gene regions. *Mol. Ecol.* 14 (6), 1681–1695. doi: 10.1111/j.1365-294X.2005.02543.x

Zhang, Y., Jeppesen, E., Liu, X., Qin, B., Shi, K., Zhou, Y., et al. (2017). Global loss of aquatic vegetation in lakes. *Earth-Sci. Rev.* 173, 259–265. doi: 10.1016/j.earscirev.2017.08.013

frontiers | Frontiers in Plant Science

TYPE Original Research
PUBLISHED 23 January 2023
DOI 10.3389/fpls.2023.1069593

OPEN ACCESS

EDITED BY
Eric Marechal,
UMR5168 Laboratoire de Physiologie Cellulaire Vegetale (LPCV), France

REVIEWED BY
Tian Xie,
Beijing Normal University, China
Lijuan Ren,
Jinan University, China

*CORRESPONDENCE
Tangbin Huo
tbhuo@163.com

SPECIALTY SECTION
This article was submitted to Marine and Freshwater Plants, a section of the journal Frontiers in Plant Science

RECEIVED 14 October 2022
ACCEPTED 02 January 2023
PUBLISHED 23 January 2023

CITATION
Du X, Song D, Wang H, Yang J, Liu H and Huo T (2023) The combined effects of filter-feeding bivalves (*Cristaria plicata*) and submerged macrophytes (*Hydrilla verticillate*) on phytoplankton assemblages in nutrient-enriched freshwater mesocosms.
Front. Plant Sci. 14:1069593.
doi: 10.3389/fpls.2023.1069593

The combined effects of filter-feeding bivalves (*Cristaria plicata*) and submerged macrophytes (*Hydrilla verticillate*) on phytoplankton assemblages in nutrient-enriched freshwater mesocosms

Xue Du[1,2], Dan Song[1,2], Huibo Wang[1,2], Jingshuang Yang[3], Hui Liu[1,2] and Tangbin Huo[1,2]*

[1]Key Laboratory of Aquatic Organism Protection and Ecological Restoration in Cold Waters, Heilongjiang River Fisheries Research Institute, Chinese Academy of Fishery Sciences, Harbin, China, [2]Heilongjiang River Basin Fisheries Ecology Observation and Research Station of Heilongjiang Province, Harbin, China, [3]Jilin Chagan Lake National Nature Reserve Administration, Songyuan, China

Freshwater ecosystems are threatened by eutrophication, which causes persistent and harmful algal blooms. Filter-feeding bivalve mollusks and submerged macrophytes (SMs) alleviate the eutrophication effects by inhibiting phytoplankton biomass blooms. However, very little is known about whether and how the combined manipulation of filter-feeding bivalves and SMs control eutrophication and influence phytoplankton assemblages. Here, we performed a nutrient-enriched freshwater mesocosm experiment to assess the combined effects of the filter-feeding bivalve *Cristaria plicata*, a cockscomb pearl mussel, and the macrophyte *Hydrilla verticillate* on the biomass and composition of phytoplankton assemblages. We found that addition of *C. plicata* and *H. verticillate* decreased the water nutrient concentrations and suppressed overall phytoplankton biomass. Further, distinct differences in taxa between restoration and control treatments were observed and noticeably competitive exclusion of cyanobacteria in the restoration treatments occurred. An antagonistic interaction between filter-feeding bivalves and SMs was only detected for total cyanobacteria biomass demonstrating that a larger magnitude of SM restoration may override the effect of filter-feeding bivalves. Our results suggest that manipulation, through the addition of bivalves as grazers, associated with the restoration of SMs, is an efficient approach for reducing cyanobacterial blooms and alleviating eutrophication.

KEYWORDS

biomanipulation, control of cyanobacteria, eutrophication, filer-feeding bivalves, submerged macrophytes

1 Introduction

Eutrophication of freshwater ecosystems, driven primarily by over enrichment of nitrogen (N) and phosphorus (P) (Carpenter et al., 1998), is a serious threat to water quality, biodiversity and other key ecosystem functions (Smith et al., 2006; Cook et al., 2018; Liu et al., 2021). Nutrient enrichment promotes the appearance and persistence of harmful algal blooms (Heisler et al., 2008; Conley et al., 2009) and the decline of submerged macrophytes (SMs) (Zhang et al., 2017), altering the food web structure (Fujibayashi et al., 2018; Briland et al., 2020). Occurrences of eutrophication are expected to increase with climate and land-use changes (Jeppesen et al., 2010; Bergström and Karlsson, 2019; Le Moal et al., 2019), inducing regime switches from a macrophyte-dominated clear state to phytoplankton-dominated turbid state (Jeppesen et al., 2007a). Considering that human activity is the primary cause of the eutrophication, it is crucial to reduce anthropogenic contributions to aquatic ecosystems and to find effective approaches to control cyanobacterial blooms that usually dominate eutrophic waterbodies.

The restoration of SMs is considered a crucial measure for the rehabilitation of shallow eutrophic lakes (Liu et al., 2020; Li et al., 2021a), as SMs display certain functional traits, that they use to stabilize the clear-water state (Puijalon et al., 2011; Su et al., 2019; Rao et al., 2020). For example, SMs could suppress algal growth by competing for light and nutrients (Lürling et al., 2006), producing algae-inhibiting allelochemicals to interfere the photosynthetic activities (Zhu et al., 2010) and change other physiological and biochemical processes (Zhu et al., 2021; He et al., 2023), and providing grazing zooplankton with a daytime refuge against fish predation (Burks et al., 2001). In addition, SMs can facilitate nutrient uptake from the water column and sediment (Sand-Jensen and Borum, 1991) and reduce sediment resuspension (Horppila and Nurminen, 2003). Earlier studies involving small-scale experiments (Barrow et al., 2019; Amorim and Moura, 2020) and natural aquatic ecosystems (Chao et al., 2022; Peng et al., 2022) have repeatedly reported that the restoration of SMs decreases the phytoplankton abundance and increases water clarity. Thus, usage of SMs is a prospective tool for the elimination of algal blooms (Jeppesen et al., 2007b). The submerged macrophyte restoration is, therefore, expected to prevent or mitigate the expansion of cyanobacterial blooms.

Another restoration technique to improve water quality is the biomanipulation of filter-feeding freshwater animals, such as mussels; however, its effectiveness remains debatable. For example, grazing studies involving filter-feeding mussels, such as zebra mussels and triangle sail mussels, in Europe and China demonstrated that they can efficiently consume pelagic algae and detritus (e.g. MacIsaac et al., 1992; Gao et al., 2017). Further, mussels, as grazers, can reduce or even prevent algal blooms (Gulati et al., 2008). Furthermore, Wu and Culver (1991) found abundant zebra mussels in Lake Erie, and noticed that filter-feeding *Daphnia* were able to reduce edible algal density and enhance water transparency. Interestingly, some mussels display food selectivity and avoid consuming cyanobacteria resulting in dominance of cyanobacteria over other forms (Hwang et al., 2004; Colvin et al., 2015). Contrary to Hwang et al. (2004) and Baker et al. (1998); Colvin et al. (2015) reported that the invasion of zebra mussels led to a decline in *Microcystis* biomass in the Hudson River.

Numerous combined technologies for controlling lake eutrophication have been developed, demonstrating that the combined effect of the two technologies was better than the technology alone. For example, the combination of large herbivorous zooplankton and submerged macrophytes proved to be more efficient at controlling the biomass of cyanobacteria (Amorim and Moura, 2020). In addition, the successful restoration of submersed macrophytes improved the water quality in a eutrophic lake after the removal of common carp (Knopik and Newman, 2018). Despite recent advances on biological restoration methods related to eutrophication, little is known about whether and how the combined manipulation of filter-feeding bivalves and SMs control eutrophication and influence phytoplankton assemblages. Given the complexities of climatically, thermally, ecologically, and hydrologically induced change in natural lakes (Richardson et al., 2019), mesocosm studies have been heralded as a useful means to investigate the effects of multiple factors under manipulated or controlled environmental conditions while supporting realistic levels of biocomplexity (Stewart et al., 2013; Fordham, 2015).

In this study, we designed a 32-day nutrient-enriched freshwater mesocosm experiment to explore the potential interactions between the filter-feeding bivalves and SMs and their impact on the biomass and composition of phytoplankton assemblages. We reasoned that categorizing cyanobacteria based on the adaptations to avoid predation (e.g. colonial and filamentous cyanobacteria) may lead to greater insights into the combined effects of filter-feeding bivalves and SMs on the restoration of eutrophic water bodies. We hypothesized that: (i) biomanipulation *via* addition of filter-feeding bivalves and restoration of submerged macrophyte, under nutrient enrichment, will likely affect phytoplankton assemblages and control the growth of cyanobacteria; (ii) the interactive effects are likely to be superior to either alone for controlling eutrophication.

2 Material and methods

2.1 Study site and experimental design

The outdoor mesocosm experiment was conducted between 25 June and 27 July 2021 in 16 cylindrical polyethylene mesocosms on land – at the Chagan Lake Observation and Research Station near Chagan Lake (45.25°N, 124.28°E). The mesocosms had a diameter of 1 m and a constant water depth of 1.2 m; they contained 0.2 m sediment and 780 L of unfiltered water collected from Chagan Lake (Figure 1). Chagan Lake is a shallow eutrophic freshwater lake (mean depth: 2.5 m) in a catchment area dominant by agricultural lands and grasslands and has relatively high allochthonous inputs of nutrients (especially nitrogen and phosphorus) through precipitation and surface run-off (Liu et al., 2019; Du et al., 2022). Nitrogen and phosphorus, as dissolved mixtures of sodium nitrate ($NaNO_3$) and potassium dihydrogen phosphate (KH_2PO_4), respectively, were added daily to each mesocosm to equate to a nutrient load of 36 µg/L and 5 µg/L, which adhered to the Redfield ratio (Redfield, 1958). The walls of the mesocosms were scrubbed daily to prevent periphyton growth. During the experiment period, evaporation losses from the mesocosms were replaced with unfiltered lake water when not compensated for by rainfall.

The experiment had a factorial design (2 x 2) to evaluate of the effects bivalves, macrophytes, and their interaction, on water nutrient

FIGURE 1
Experimental mesocosms used in our study at the Chagan Lake Observation and Research Station.

concentrations and phytoplankton assemblages in mesocosms. *Cristaria plicata* was chosen as the filter-feeding bivalve in our mesocosms as it is an excellent cleaner of suspended particles (Yu et al., 2020), and *Hydrilla verticillate*, was used as the macrophyte owing to its allelopathic effects on phytoplankton (Gao et al., 2015) and nutrient removal capability (Li et al., 2021b). Three treatments (bivalve: *C. plicata* alone; macrophyte: *H. verticillate* alone; bivalve + macrophyte: *C. plicata* and *H. verticillate* together) and a control (both species absent), each one with four replicates, were randomly assigned to the mesocosms and all received a common nutrient loading over the entire experiment. The bivalve, macrophyte, and bivalve + macrophyte treatments have been proposed as strategies for mitigating eutrophication for many temperate shallow lakes, and consequently, served as the restoration treatments (Søndergaard et al., 2007; Zhang et al., 2014). We added two *C. plicata* with a biomass of 413.8 ± 13.6 standard error (*S.E.*) g/m^2 to the bivalve treatment mesocosms. *C. plicata* were hung with string bags, 30 cm above the sediment surface. Individual *H. verticillate* samples were purchased from a commercial nursery. At the beginning of the experiment, the average stem length of *H. verticillate* was 34 ± 0.8 *S.E.* cm and they were bundled together in groups of five to eight and weighted down in the sediment to encourage root growth. The total wet weight of macrophytes within each mesocosm was 650 ± 10.3 *S.E.* g L^{-1}.

2.2 Sample collection and analysis

Samples of water nutrients and chlorophyll *a* concentrations were collected at the beginning of the experiment (day 0) and on day 4, 8, 12, 16, 20, 24, 28, and 32. The water samples were collected with a tube sampler at two different depths (surface and 5 cm above the sediment), from which subsamples were taken for water nutrients and phytoplankton analysis. We determined concentrations of total phosphorus (TP), phosphate (PO_4-P), total nitrogen (TN), ammonia nitrogen (NH_4-N), nitrate nitrogen (NO_3-N) and nitrite nitrogen (NO_2-N) using standard methods (American Public Health Association, 1992). Chlorophyll *a* (as a proxy of total phytoplankton biomass) concentrations determined spectrophotometrically from matter retained on Whatman GF/C glass microfiber filters after cold ethanol extraction in darkness (Jespersen and Christoffersen, 1987).

To characterize the phytoplankton assemblage composition, we collected phytoplankton from all enclosures. Phytoplankton sampling was done at the beginning (day 0) and at the end of the experiment (day 32). A subsample of the mixed tube sample water was immediately fixed with Lugol's solution. All samples were analyzed using a Sedgewick-Rafter counting chamber and an inverted microscope (RVL-100-G, ECHO, San Diego, California, USA). At least 500 natural units were enumerated and identified to the genus level (Hu and Wei, 2006). Cell volumes of each phytoplankton taxa were calculated after approximation to the nearest geometric standard solid (Hillebrand et al., 1999). The biomass estimates were calculated, assuming that the density of the organisms equals that of water (1 mm^3 L^{-1} = 1 mg L^{-1}) (Wetzel and Likens, 2000). As chlorophyll *a* (μg/L) measured using the spectrophotometric method and total phytoplankton biomass (mm^3/L) estimated from microscope counts and measurements were positively correlated (R^2 = 0.82, p < 0.001), we used the latter measurement to estimate the biomass of cyanobacteria genera. In the case of cyanobacteria, species were classified into colonies and filaments based on their life form.

2.3 Statistical analyses

Prior to analyses, water nutrient and chlorophyll *a* concentration data were natural logarithm-transformed to meet the assumptions of normality and homoscedasticity when necessary. Principal response curve (PRC) method was used to evaluate the time-dependent influence of the bivalve (*C. plicata*), submerged macrophyte (*H. verticillate*) and their potential interactions on key water nutrient concentrations in response to nutrient enrichment. The PRC method is a special case of partial redundancy analysis (RDA) and requires repeated observations from multiple time periods in order to represent the deviation in the treatments from the controls over time (Van den Brink and Braak, 1999; Oksanen et al., 2020). The statistical significance of the PRC models was tested using the Monte Carlo permutation test (Van den Brink and Braak, 1999). The PRC analyses displayed an affinity for the different water nutrient (response) variables with the trajectory by giving each variable a quantitative score. In our study, higher scores of water nutrient variables in a restoration treatment group, resulted in more pronounced responses compared with the control treatment during the experiment (Van den Brink and Braak, 1999). Statistical differences among the control and restoration treatments at the beginning and the end of the experiment were compared using Kruskal-Wallis test. If a significant difference was found, *post hoc* comparisons among treatments were performed using Wilcoxon test.

Subsequently, we investigated the effects of bivalve addition (bivalve), macrophyte addition (macrophyte), and their interaction (bivalve + macrophyte) on phytoplankton biomass (chlorophyll *a* concentration). For chlorophyll *a* concentrations collected multiple times (i.e., on day 0, 4, 8, 12, 16, 20, 24, 28, and 32), we performed a two-way repeated measures ANOVA (RM-ANOVA) using a restricted maximum likelihood (REML) method. If there was a main effect of bivalve, macrophyte, or their interaction, we performed post-hoc analyses on the data under each treatment. If there was a significant ($p < 0.05$) interaction with time, we performed post-hoc analyses on the data within each sampling time.

The shifts in phytoplankton assemblage composition over time and across treatments were evaluated using a multivariate ordination technique: principal coordinate analyses (PCoA). The PCoA was performed using Hellinger-transformed species data (Legendre and Gallagher, 2001) and a Bray-Curtis dissimilarity matrix. The PCoA was paired with a permutational multivariate analysis of variance (PERMANOVA; Anderson, 2001; Oksanen et al., 2020) to test for statistically significant differences in phytoplankton assemblage composition in different treatments with an *F*-type test (999 permutations) using the same dissimilarity matrix (Bray-Curtis) and transformed species data.

The effect of the addition of filter-feeding bivalves and SMs on the biomass of the cyanobacteria genera was tested using a generalised linear mixed-effects model (GLMM; Bolker et al., 2009; Harrison et al., 2018) with a normal distribution. In separate analyses, dependent variable were (i) total biomass of cyanobacteria, (ii) biomass of filamentous cyanobacteria, and (iii) biomass colonial cyanobacteria. Models were fitted using bivalve, macrophyte and their interaction as fixed effects. All models included mesocosm identity as a random effect. We reported the GLMM marginal R^2 (*R2 m*) that describes the variance explained by the fixed effects alone, and the conditional R^2 (*R2 C*) that describes the variance explained by both fixed and random effects (Nakagawa and Schielzeth, 2013).

Statistical analyses were performed using R statistical (version 4.0.3) software (R Core Team, 2020). The PRC, PCoA and PERMANOVA were performed using the *vegan* package version 2.5-7 (Oksanen et al., 2020). The RM-ANOVA was performed using the *ez* package version 4.4-0 (Lawrence, 2016). We conducted GLMM using the *glmmTMB* package version 1.1.3 (Brooks et al., 2017). The *MuMIn* package version 1.46.0 (Bartoń, 2022) was used to generate the R^2 value of each model.

3 Results

3.1 Treatment effects on physicochemical parameters

No significant differences were found for the physicochemical parameters among the treatments at the beginning of the experiment (Kruskal-Wallis test: $P > 0.05$; supplementary Table S1, Figure S1). At the end of the experiment, the biomass of *C. plicata* and the total wet weight of macrophyte increased to 450.2 ± 12.8 standard error (*S.E.*) g/m^2 and 3257.6 ± 52.9 *S.E.* g L^{-1}, respectively. During the experiment, nutrient concentrations in the water shifted in parallel in the restoration treatments (i.e., bivalve, macrophyte and bivalve + macrophyte treatments) relative to the control treatment, with the strongest treatment effects apparent in the bivalve + macrophyte treatment (Figure 2A). The principal response curves (PRC) revealed that 39.2% of the total variance present in water nutrient concentrations is explained by treatment (Monte Carlo, $P < 0.001$). Nitrogen and phosphorus loading led to increased nutrient concentrations in the control treatment, but the decline in the nitrogen to phosphorus ratio (N: P) of restoration treatments. Total phosphorus, total nitrogen, phosphate and nitrate nitrogen had high positive scores (Figure 2B), with the diagram indicating a decrease with the restoration treatment mesocosms. N: P, ammonia nitrogen and nitrite nitrogen had negative scores (Figure 2B), meaning treatment-related increases. At the end of the experiment, addition of filter-feeding bivalves and restoration of submerged macrophyte significantly decreased the concentrations of total phosphorus and total nitrogen (supplementary Table S1).

3.2 Treatment effects on total phytoplankton

The two-way repeated measures ANOVA results revealed that bivalves ($F_{1,\ 3} = 118.6$, $p < 0.001$), macrophytes ($F_{1,\ 3} = 39.7$, $p = 0.008$), and their interactions ($F_{1,\ 3} = 31.2$, $p = 0.011$) had significant effects on phytoplankton biomass. We found a significant decline in chlorophyll *a* concentrations in the bivalve treatment after day 12 ($p < 0.05$), in addition, a significant decline in the bivalve + macrophyte treatment after day 8 ($p < 0.05$). Chlorophyll *a* concentrations

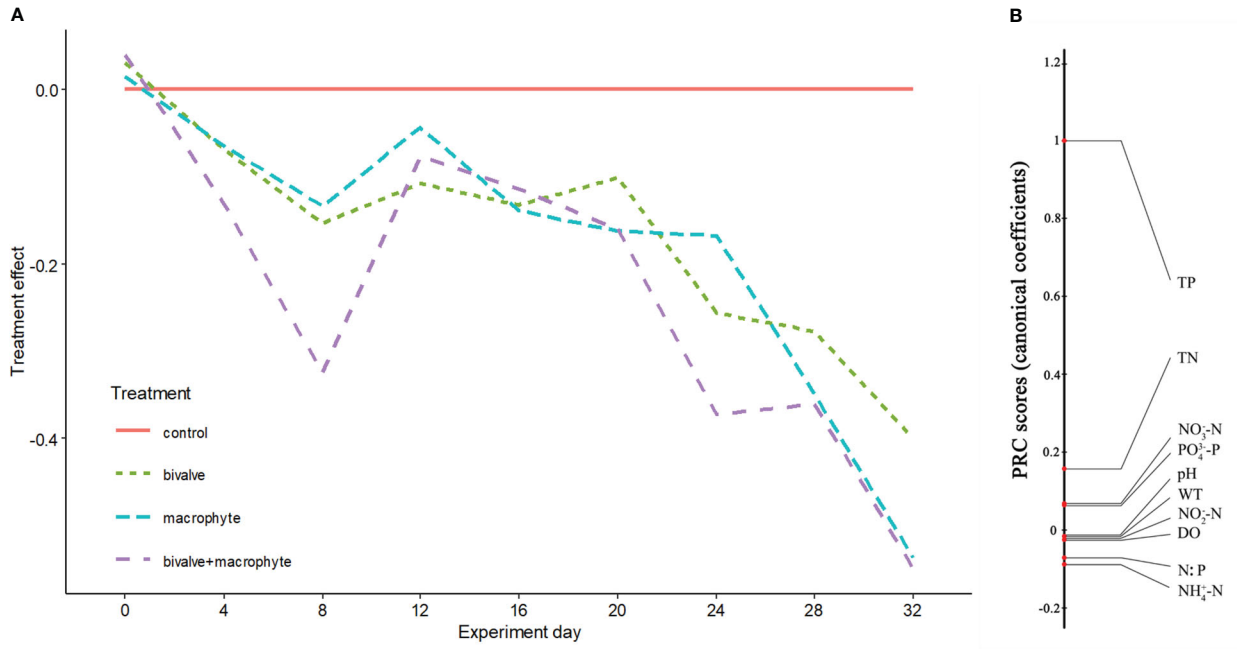

FIGURE 2
Principal response curves resulting from the analysis of water physicochemical variables. Panel **(A)** represents overall deviation from the control treatment mesocosms (control), for the other restoration treatment mesocosms (bivalve, macrophyte, and bivalve + macrophyte). This is expressed as a canonical coefficient of the first principal component axis (PC1), in comparison with the reference control mesocosms, represented by the zero line. Panel **(B)** shows canonical coefficients for the water physicochemical variables interpreted.

markedly increased in the control treatment but decreased in the bivalve, and bivalve + macrophyte treatments (Figure 3). Chlorophyll *a* concentrations remained at a relatively stable level in macrophyte treatment ($p > 0.05$). At the end of the experiment, restoration mesocosms contained 63.7-91.8% less phytoplankton than those of the control treatment. Our analysis indicated a time-by-bivalve interaction ($F_{1, 3} = 12.8$, $p = 0.037$). After day 16, chlorophyll *a* concentrations were significantly lower in both bivalve and bivalve + macrophyte treatments than those in macrophyte treatment (Figure S2).

We found a total of 68 phytoplankton genera throughout the experiment, with representatives from the following classes: Cyanophyceae (14), Bacillariophyceae (14), Chlorophyceae (34), Cryptophyceae (2) and Euglenophyceae (4) (supplementary Table S2). The principal coordinate analysis (PCoA) explained 44.36% of the species composition distribution through the first two axes (Figure 4). Initially (day 0), no treatments differed significantly in phytoplankton composition ($P > 0.05$; Table 1), and chlorophytes dominated the phytoplankton assemblage. By the end of the experiment (day 32), the phytoplankton compositions of the restoration treatments were significantly distinguishable from the controls (Figure 4). Addition of bivalves and/or macrophytes induced significant changes in phytoplankton assemblage structure (Table 1). Specifically, filamentous cyanobacteria, such as *Anabaenopsis*, *Aphanizomenon*, and *Phormidium*, and colonial cyanobacteria, such as *Aphanocapsa*, became abundant and dominant in the control treatment., while symmetrical desmids (e.g. *Cosmarium*, *Micrasterias*) tended to increase over time in the macrophyte treatment, and the large diatoms (e.g. *Cymbella, Fragilaria, Thalassiosira*) became dominant in the treatments with the addition of filter-feeding bivalves.

3.3 Treatment effects on cyanobacteria

By the end of the experiment, the total biomass of cyanobacteria was explained by a positive interaction between bivalve and macrophyte addition. Bivalve and macrophyte addition, as single restoration approaches, resulted in statistically significantly lower cyanobacteria biomass than in the control mesocosms (Figure S3). However, in combination, the effects of bivalves and macrophytes partly counterbalanced each other, resulting in a weak antagonistic interaction, where the total biomass of cyanobacteria was higher than the linearly combined (additive) effects of bivalve and macrophyte additions as single restoration techniques. Decreases in filamentous cyanobacteria and colonial cyanobacteria in response to the addition of bivalves and macrophytes as single restoration approaches were similar (Table 2). Filamentous cyanobacteria were more sensitive to macrophytes than colonial cyanobacteria, that is, filamentous cyanobacteria biomass decreased more in response to the addition of macrophytes, as single restoration techniques, than the addition of bivalves, while colonial cyanobacteria were more sensitive to bivalves.

4 Discussion

The development of SMs is considered as an important restoration strategy in eutrophic shallow lakes. Often restoration experiments do not capture the intricacies related to increased nutrient loading and the amount of filter-feeding animals, instead they primarily focus on assessing the effects of SMs (e.g. Bakker et al., 2013). The use of an experimental mesocosm approach is important for investigating the complexity observed in the field and to gain a

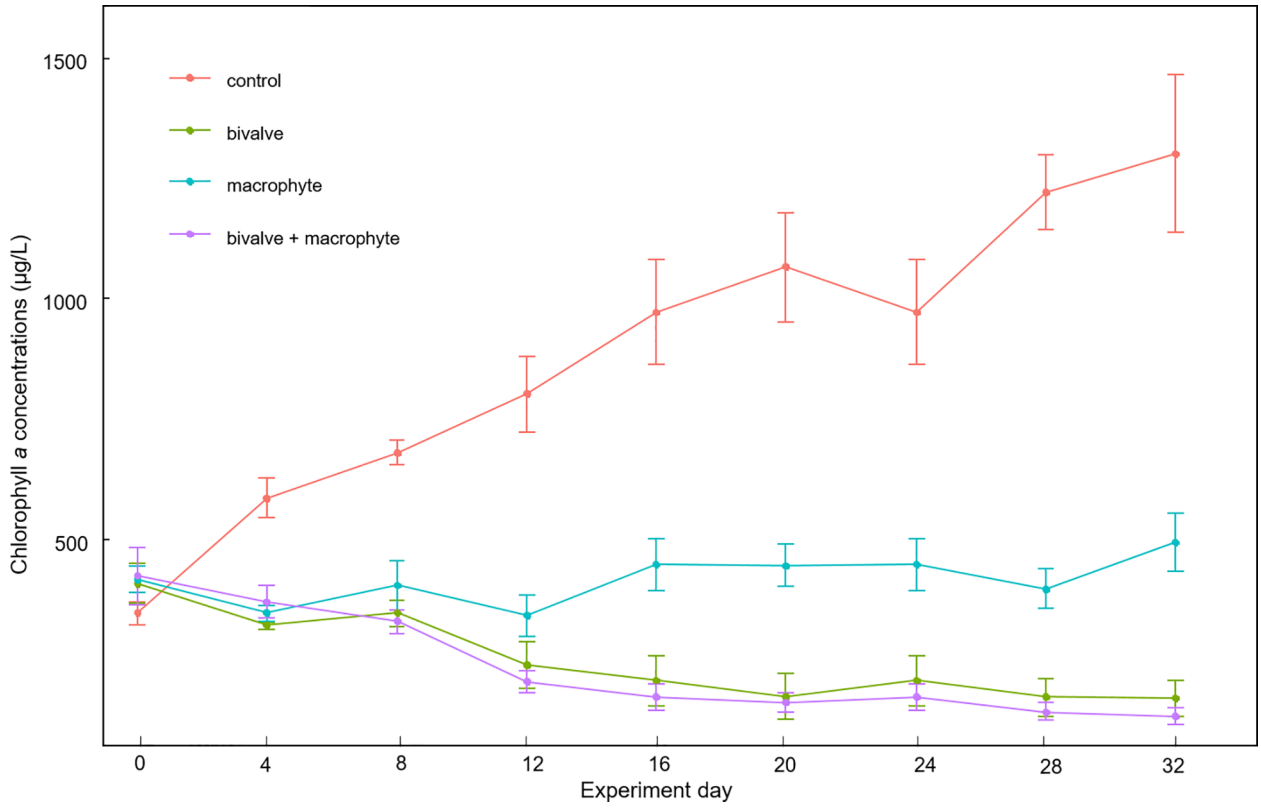

FIGURE 3
Mean values (± standard error) of temporal variations of chlorophyll *a* concentrations throughout the experiment for the different treatments.

mechanistic understanding about the single and interactive effects of multiple restoration measures (Amorim and Moura, 2020; Zhang et al., 2021; Boucher-Carrier et al., 2022). During the loading experiments we noticed that restoration of eutrophic waterbodies by manipulation, i.e., addition of filter-feeding bivalves and SMs, had a marked influence on water quality and algal biomass and community composition.

Our results of TP and TN reduction in the restoration treatments demonstrated that the addition of the filter-feeding bivalve *C. plicata* and the recovery of submerged macrophyte can significantly alleviate eutrophication. Although some species of rooted SMs are sensitive to relatively high nutrients and consequently get suppressed under eutrophic conditions (Søndergaard et al., 2010), in our study, the use of *H. verticillata* reduced the nutrient levels. As a rooted submerged macrophyte, *H. verticillata* can obtain nutrients from sediments *via* root uptake and from the water column *via* foliar uptake (Barko, 1982), thus acting as a major nutrient sink. Moreover, filter-feeding bivalves transfer nutrients (especially P) from the water column to the bottom, through excretion as well as biodeposition of faeces and pseudofaeces (Vaughn and Hoellein, 2018).

As expected, changes in nutrient concentrations and stoichiometry, which were influenced by filter-feeding bivalves and SMs, may have altered the phytoplankton assemblage composition during the mesocosm experiment. In agreement, a previous study observed suppressed Cyanobacterial taxa in lakes under P limitation (Havens et al., 2003). At the end of the experiment, the relatively high TN: TP ratios in the macrophyte (average of 37: 1) and the bivalve + macrophyte (average of 42: 1) treatments likely led to the competitive exclusion of cyanobacteria. These results concur with a previous study by Smith (1983) who noticed suppressed cyanobacterial blooms when the TN: TP ratio exceeded 29 to 1. Algae that are incapable of nitrogen fixation are reported to dominate under P-limited conditions (Schindler, 1977; Amano et al., 2010).

High aquatic N: P ratios in lakes are reported in agricultural regions (Arbuckle and Downing, 2001), suggesting that P is the principal production-limiting nutrient. In our study, relatively high TN: TP ratios (≈29) at the beginning indicated a phosphorus-limitation situation. During the loading experiments addition of N and P close to the Redfield ratio (N: P of 16: 1), relieves nutrient limitation, and promotes a much higher phytoplankton biomass development. Phytoplankton biomass showed a gradual increase under nutrient enrichment (the control treatment). Previous studies have reported a linear relationship between chlorophyll *a* concentration and TP for the lower nutrient ranges (TP < 5–100μgL^{-1}) and asymptotic behavior at higher ranges (TP >100 μgL^{-1}) (Canfield et al., 1984; Phillips et al., 2008; Borics et al., 2013). Noticeably, at the end of the experiment, TP concentration exceeded 100 μgL^{-1}, we noticed an increase in phytoplankton biomass with nutrient enrichment, suggesting nutrients control phytoplankton biomass in nutrient-rich waters (Richardson et al., 2019).

Even in a nutrient-enrichment scenario, as expected, responses to the addition of filter-feeding bivalves (*Cristaria plicata*) alone contributed to the decline in cyanobacterial and total phytoplankton biomass. The overall decline in cyanobacterial and phytoplankton biomass in these mesocosm can be explained by the direct grazing impacts of the filter-feeding bivalves (Gulati et al., 2008). The direct effects of grazing by *C. plicata* led to statistically significant decrease in filamentous or colonial taxa such as the genera *Dolichospermum* (formerly *Anabaena*), *Microcystis*, and

10.3389/fpls.2023.1069593

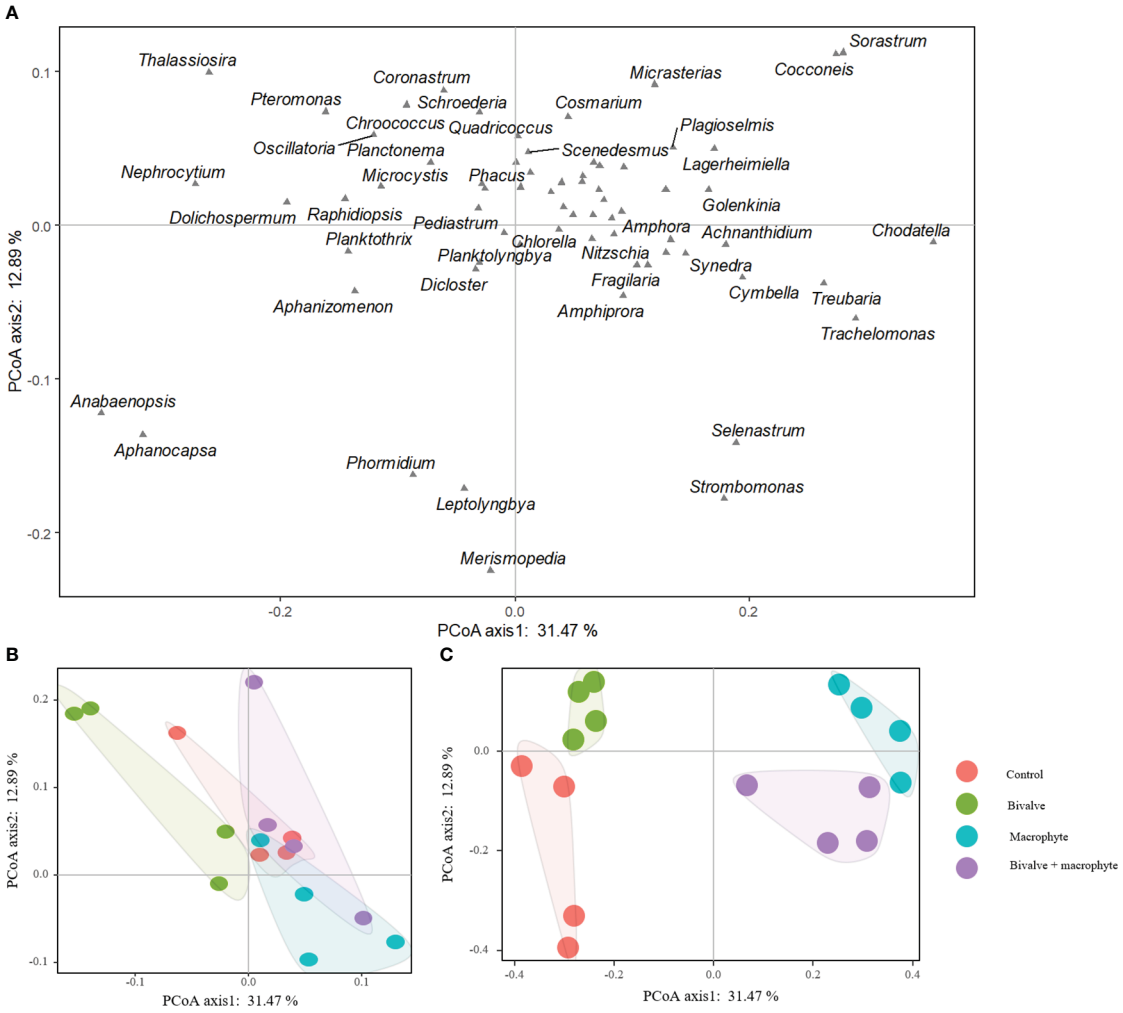

FIGURE 4
Two-dimensional ordination plots resulting from the principal coordinate analysis on the phytoplankton assemblage composition **(A)** comparing the control and restoration treatments on day 0 **(B)** and day 32 **(C)**.

TABLE 1 Pseudo *F*-statistics (above diagonal) and *p* values (below diagonal) for pairwise PERMANOVA tests between the control and restoration treatments on two sampling days (day 0 and day 32). .

	Day 0				Day 32			
	Control	Bivalve	Macrophyte	Bivalve + macrophyte	Control	Bivalve	Macrophyte	Bivalve + macrophyte
Day 0-control		1.073	1.614	0.787	5.284	3.793	3.141	3.015
Day 0-bivalve	0.365		1.547	2.297	4.716	3.694	4.568	4.582
Day 0-macrophyte	0.214	0.098		1.228	6.404	6.029	3.763	2.835
Day 0-bivalve + macrophyte	0.683	0.053	0.317		5.463	3.677	2.98	2.225
Day 32-control	0.029	0.037	0.033	0.034		2.952	8.021	6.204
Day 32-bivalve	0.024	0.041	0.027	0.023	0.026		6.926	6.471
Day 32-macrophyte	0.021	0.038	0.026	0.030	0.039	0.033		4.265
Day 32-bivalve + macrophyte	0.027	0.039	0.029	0.029	0.036	0.031	0.033	

TABLE 2 Summary (coefficients and *SE*) of a generalized linear mixed-effects model to explain variations in cyanobacteria taxa biomass as a function of bivalve (presence and absence) and macrophyte (presence and absence).

Biomass (μg/L)	Intercept	Bivalve	Macrophyte	Bivalve ×Macrophyte	*R2 m*	*R2 C*
ln total cyanobacteria	**2.20**	**-1.34**	**-2.08**	**1.04**	0.82	0.87
ln filamentous cyanobacteria	**2.18**	**-1.38**	**-1.92**		0.84	0.88
ln colonial cyanobacteria	**1.65**	**-1.42**	**-1.09**		0.65	0.79

Significant effects ($p < 0.05$) are highlighted in bold, and nonsignificant effects are left blank.

Planktothrix (Bastviken et al., 1998; Dionisio Pires et al., 2005) which usually form harmful algal blooms. These results are in line with previous studies indicating that cyanobacteria are directly grazed by filter-feeding bivalves (Hwang et al., 2004; Gao et al., 2017), and support the possibility that addition of filter-feeding bivalves will alleviate algal blooms that are associated with eutrophication. Further, several studies have also shown that filter-feeding bivalves are selective feeders and the filtering rate can vary depending on food particle size and bivalve species. Some functional traits of cyanobacteria, including cell size, life form (e.g. single celled, colonial, or filamentous), nutritional deficiency, and toxin production, can prevent them from being grazed by mussels (White and Sarnelle, 2014; Boegehold et al., 2019). For example, *Corbicula fluminea* selectively filtered particles in the range of 0.2–2 μm (Rong et al., 2021), *Dreissena Polymorpha* preferred food particles from 5 to 40 μm (Sprung & Rose, 1988), and *Venerupis corrugatus* filtered out particles of 5 to 13 μm (Stenton-Dozey and Brown, 1992). Although we did not consider selective grazing effects of *C. plicata* on phytoplankton the composition of phytoplankton assemblages significantly differed between the control and the bivalve treatments at the end of the experiment. This result indicates that once nutrient limitation is alleviated, selective grazing would likely be the main factor affecting the structure of the phytoplankton assemblage. Additionally, the phytoplankton assemblages in the filter-feeding bivalve addition treatments appear to have adaptive responses to selective grazing pressure by *C. plicata*, as larger diatoms (e.g. *Cymbella*, *Fragilaria*, *Thalassiosira*) dominated the phytoplankton assemblages.

SMs can also suppress algal growth *via* allelopathic controls and nutrient competition (van Donk and van de Bund, 2002; Mohamed, 2017; Zhu et al., 2021). However, in our experiments, at the end of the experiment a slight, but not significant increase in overall phytoplankton assemblage biomass (chlorophyll *a*) was noticed in the Macrophyte treatment. The phytoplankton blooms occurred when SMs were absent over the course of the nutrient loading experiment (the control treatment). While phytoplankton biomass initially decreased from day 0 to day 4, it then began to slightly increase until day 32, suggesting that SMs did cause a reduction in phytoplankton biomass. The submerged macrophyte *H. verticillate*, has been reported to produce and release allelochemicals that has inhibitory effects on *Chlorella* cell membrane (Zhang et al., 2012) and cyanobacteria (Wang et al., 2006; Gao et al., 2011). Over 32 days, SMs suppressed overall cyanobacteria biomass (Table 2), concurring with findings from other experimental studies (Lürling et al., 2006; Barrow et al., 2019; Amorim and Moura, 2020). Further, factors such as light and nutrient competition likely interacted with allelopathic controls in the mesocosms and led to the competitive exclusion of cyanobacteria.

Although unexpected, we found that filter-feeding bivalves in combination with SMs reduced the biomass of cyanobacteria, and noticeably the effect size of this interaction was less than the sum of their individual effects (i.e., an antagonistic interaction). This result is in line with the widely observed antagonistic interactions in freshwater ecosystems (Jackson et al., 2016; Segurado et al., 2018; He et al., 2021), such as nutrient-pesticide effects on benthic invertebrate richness (Chará-Serna et al., 2019), and fish-shrimp effects on zooplankton biomass (He et al., 2021). The mechanism for the antagonistic interactions is largely unknown, however, a possible explanation could be the asymmetry of mean effect size. In our study, the larger magnitude of the submerged macrophyte restoration may have overridden the effect of stock filter-feeding bivalves (Table 2), thereby negating its contribution to their net impact on the overall biomass of cyanobacteria (Sala et al., 2000; Barrow et al., 2019). An antagonism between filter-feeding bivalves and SMs was only detected for total cyanobacteria. For filamentous or colonial taxa, there was no significant interactive effects; rather filamentous cyanobacteria were more sensitive to macrophytes and colonial cyanobacteria to bivalves. The differential sensitivity of cyanobacterial taxa to different biomanipulation approaches has been noticed previously (Gazulha et al., 2012; Amorim and Moura, 2020), the reason being that cyanobacteria are a diverse and morphologically complex group of prokaryotes with different key ecological traits thus eliciting disparate responses (Mantzouki et al., 2016; Rangel et al., 2020).

5 Conclusions

Our first hypothesis that manipulation *via* addition of filter-feeding bivalves and restoration of submerged macrophyte will likely affect phytoplankton assemblages was confirmed, as this manipulation efficiently decreased water nutrient concentrations and the overall phytoplankton biomass. Since, phytoplankton were dominated by symmetrical desmids (e.g., *Cosmarium*, *Micrasterias*) and the large diatoms (e.g., *Cymbella*, *Fragilaria*, *Thalassiosira*) in the restoration treatments, with the competitive exclusion of cyanobacteria, our results also supported that manipulation could control the growth of cyanobacteria. Contrary to the second hypothesis, an antagonism between filter-feeding bivalves and SMs was detected but only for total cyanobacteria, demonstrating that the larger magnitude of the submerged macrophyte restoration may override the effect of stock filter-feeding bivalves. However, we should also noticed that the addition of bivalves combined with SMs was more efficient at decreasing nutrient concentrations than the isolated addition of bivalves, and at controlling total algal biomass

than the isolated restoration of SMs. Overall, our results suggest that manipulation, through introduction of the stock of bivalves as grazers, associated with the restoration of SMs, is an efficient approach for reducing cyanobacterial blooms and alleviating eutrophication.

Data availability statement

The original contributions presented in the study are included in the article/Supplementary Material. Further inquiries can be directed to the corresponding author.

Author contributions

XD: Conceptualization, Methodology, Investigation, Formal analysis, Writing – original draft, Writing – review & editing, Funding acquisition. DS: Conceptualization, Investigation, Formal analysis, Writing – original draft, Writing – review & editing. HW: Investigation. JY: Resources. HL: Writing – original draft, Investigation. TH: Funding acquisition. All authors contributed to the article and approved the submitted version.

Funding

This work was financially supported by the National Key Research and Development Program of China (2019YFD0900602 and 2019YFD0900605), National Natural Science Foundation of China (No. 31802298) and the Finance Special Fund of Ministry of Agriculture and Rural Affairs (Fisheries Resources and Environment Survey in the Key Water Areas of Northeast China).

Conflict of interest

The authors declare that the research was conducted in the absence of any commercial or financial relationships that could be construed as a potential conflict of interest.

Publisher's note

All claims expressed in this article are solely those of the authors and do not necessarily represent those of their affiliated organizations, or those of the publisher, the editors and the reviewers. Any product that may be evaluated in this article, or claim that may be made by its manufacturer, is not guaranteed or endorsed by the publisher.

Supplementary material

The Supplementary Material for this article can be found online at: https://www.frontiersin.org/articles/10.3389/fpls.2023.1069593/full#supplementary-material

References

Amano, Y., Sakai, Y., Sekiya, T., Takeya, K., Taki, K., and Machida, M. (2010). Effect of phosphorus fluctuation caused by river water dilution in eutrophic lake on competition between blue-green alga *Microcystis aeruginosa* and diatom *Cyclotella* sp. *J. Environ. Sci.* 22 (11), 1666–1673. doi: 10.1016/S1001-0742(09)60304-1

Amorim, C. A., and Moura, A. N. (2020). Effects of the manipulation of submerged macrophytes, large zooplankton, and nutrients on a cyanobacterial bloom: A mesocosm study in a tropical shallow reservoir. *Environ. pollut.* 265, 114997. doi: 10.1016/j.envpol.2020.114997

Anderson, M. J. (2001). A new method for non-parametric multivariate analysis of variance. *Austral Ecol.* 26 (1), 32–46. doi: 10.1111/j.1442-9993.2001.01070.pp.x

American Public Health Association. (1992). *Standard methods for the examination of water and wastewater. 18th ed* (Washington, DC: American Public Health Association).

Arbuckle, K. E., and Downing, J. A. (2001). The influence of watershed land use on lake n: P in a predominantly agricultural landscape. *Limnol. Oceanogr.* 46 (4), 970–975. doi: 10.4319/lo.2001.46.4.0970

Baker, S. M., Levinton, J. S., Kurdziel, J. P., and Shumway, S. E. (1998). Selective feeding and biodeposition by zebra mussels and their relation to changes in phytoplankton composition and seston load. *J. Shellfish Res.* 17 (4), 1207–1214.

Bakker, E. S., Sarneel, J. M., Gulati, R. D., Liu, Z., and van Donk, E. (2013). Restoring macrophyte diversity in shallow temperate lakes: biotic versus abiotic constraints. *Hydrobiologia* 710 (1), 23–37. doi: 10.1007/s10750-012-1142-9

Barko, J. W. (1982). Influence of potassium source (sediment vs. open water) and sediment composition on the growth and nutrition of a submersed freshwater macrophyte (*Hydrilla verticillata*) (L.f.) royle). *Aquat. Bota.* 12, 157–172. doi: 10.1016/0304-3770(82)90011-0

Barrow, J. L., Beisner, B. E., Giles, R., Giani, A., Domaizon, I., and Gregory-Eaves, I. (2019). Macrophytes moderate the taxonomic and functional composition of phytoplankton assemblages during a nutrient loading experiment. *Freshw. Biol.* 64 (8), 1369–1381. doi: 10.1111/fwb.13311

Bartoń, K. (2022). *MuMIn: Multi-model inference* (R package version 1.46.0). Available at: https://CRAN.R-project.org/package=MuMIn.

Bastviken, D. T. E., Caraco, N. F., and Cole, J. J. (1998). Experimental measurements of zebra mussel (*Dreissena polymorpha*) impacts on phytoplankton community composition. *Freshw. Biol.* 39 (2), 375–386. doi: 10.1046/j.1365-2427.1998.00283.x

Bergström, A.-K., and Karlsson, J. (2019). Light and nutrient control phytoplankton biomass responses to global change in northern lakes. *Global Change Biol.* 25 (6), 2021–2029. doi: 10.1111/gcb.14623

Boegehold, A. G., Alame, K., Johnson, N. S., and Kashian, D. R. (2019). Cyanobacteria reduce motility of quagga mussel (*Dreissena rostriformis bugensis*) sperm. *Environ. Toxicol. Chem.* 38 (2), 368–374. doi: 10.1002/etc.4305

Bolker, B. M., Brooks, M. E., Clark, C. J., Geange, S. W., Poulsen, J. R., Stevens, M. H. H., et al. (2009). Generalized linear mixed models: a practical guide for ecology and evolution. *Trends Ecol. Evol.* 24 (3), 127–135. doi: 10.1016/j.tree.2008.10.008

Borics, G., Nagy, L., Miron, S., Grigorszky, I., László-Nagy, Z., Lukács, B. A., et al. (2013). Which factors affect phytoplankton biomass in shallow eutrophic lakes? *Hydrobiologia* 714 (1), 93–104. doi: 10.1007/s10750-013-1525-6

Boucher-Carrier, O., Brisson, J., Abas, K., Duy, S. V., Sauvé, S., and Kõiv-Vainik, M. (2022). Effects of macrophyte species and biochar on the performance of treatment wetlands for the removal of glyphosate from agricultural runoff. *Sci. Total Environ.* 838, 156061. doi: 10.1016/j.scitotenv.2022.156061

Briland, R. D., Stone, J. P., Manubolu, M., Lee, J., and Ludsin, S. A. (2020). Cyanobacterial blooms modify food web structure and interactions in western lake Erie. *Harmful Algae* 92, 101586. doi: 10.1016/j.hal.2019.03.004

Brooks, M. E., Kristensen, K., van Benthem, K. J., Magnusson, A., Berg, C. W., Nielsen, A., et al (2017). Glmmtmb balances speed and flexibility among packages for zero-inflated generalized linear mixed modeling. *R J* 2 (2), 378–400. doi: 10.3929/ethz-b-000240890

Burks, R. L., Jeppesen, E., and Lodge, D. M. (2001). Littoral zone structures as *Daphnia* refugia against fish predators. *Limnol. Oceanogr.* 46 (2), 230–237. doi: 10.4319/lo.2001.46.2.0230

Canfield, D., Shireman, J. V., Colle, D. E., Haller, W. T., Watkins, C. E., and Maceina, M. J. (1984). Prediction of chlorophyll *a* concentrations in Florida lakes: Importance of aquatic macrophytes. *Can. J. Fish. Aquat. Sci.* 41 (3), 497–501. doi: 10.1139/f84-059

Carpenter, S. R., Caraco, N. F., Correll, D. L., Howarth, R. W., Sharpley, A. N., and Smith, V. H. (1998). Nonpoint pollution of surface waters with phosphorus and nitrogen. *Ecol. Appl.* 8 (3), 559–568. doi: 10.1890/1051-0761(1998)008[0559:NPOSWW]2.0.CO;2

Chao, C., Lv, T., Wang, L., Li, Y., Han, C., Yu, W., et al. (2022). The spatiotemporal characteristics of water quality and phytoplankton community in a shallow eutrophic lake: Implications for submerged vegetation restoration. *Sci. Total Environ.* 821, 153460. doi: 10.1016/j.scitotenv.2022.153460

Chará-Serna, A. M., Epele, L. B., Morrissey, C. A., and Richardson, J. S. (2019). Nutrients and sediment modify the impacts of a neonicotinoid insecticide on freshwater community structure and ecosystem functioning. *Sci. Total Environ.* 692, 1291–1303. doi: 10.1016/j.scitotenv.2019.06.301

Colvin, M. E., Pierce, C., and Stewart, T. W. (2015). A food web modeling analysis of a Midwestern, USA eutrophic lake dominated by non-native common carp and zebra mussels. *Ecol. Model.* 312, 26–40. doi: 10.1016/j.ecolmodel.2015.05.016

Conley, D. J., Paerl, H. W., Howarth, R. W., Boesch, D. F., Seitzinger, S. P., Havens, K. E., et al. (2009). Controlling eutrophication: Nitrogen and phosphorus. *Science* 323(5917), 1014–1015. doi: 10.1126/science.1167755

Cook, S. C., Housley, L., Back, J. A., and King, R. S. (2018). Freshwater eutrophication drives sharp reductions in temporal beta diversity. *Ecology* 99 (1), 47–56. doi: 10.1002/ecy.2069

Core Team., R. (2020). *R: A language and environment for statistical computing* (Vienna, Austria: R Foundation for Statistical Computing). Available at: https://www.R-project.org/.

Dionisio Pires, L. M., Bontes, B. M., Van Donk, E., and Ibelings, B. W. (2005). Grazing on colonial and filamentous, toxic and non-toxic cyanobacteria by the zebra mussel *Dreissena polymorpha*. J. *Plankton Res.* 27 (4), 331–339. doi: 10.1093/plankt/fbi008

Du, X., Song, D., Ming, K., Yang, J., Jin, X., Wang, H., et al. (2022). Functional responses of phytoplankton assemblages to watershed land use and environmental gradients. *Front. Ecol. E* 9. doi: 10.3389/fevo.2021.819252

Fordham, D. A. (2015). Mesocosms reveal ecological surprises from climate change. *PloS Biol.* 13 (12), e1002323. doi: 10.1371/journal.pbio.1002323

Fujibayashi, M., Okano, K., Takada, Y., Mizutani, H., Uchida, N., Nishimura, O., et al. (2018). Transfer of cyanobacterial carbon to a higher trophic-level fish community in a eutrophic lake food web: fatty acid and stable isotope analyses. *Oecologia* 188 (3), 901–912. doi: 10.1007/s00442-018-4257-5

Gao, Y.-N., Liu, B.-Y., Xu, D., Zhou, Q.-H., Hu, C.-Y., Ge, F.-J., et al. (2011). Phenolic compounds exuded from two submerged freshwater macrophytes and their allelopathic effects on *Microcystis aeruginosa*. *Pol. J. Environ. Stud.* 20 (5), 1153–1159.

Gao, H., Qian, X., Wu, H., Li, H., Pan, H., and Han, C. (2017). Combined effects of submerged macrophytes and aquatic animals on the restoration of a eutrophic water body–a case study of gonghu bay, lake taihu. *Ecol. Eng.* 102, 15–23. doi: 10.1016/j.ecoleng.2017.01.013

Gao, H., Song, Y., Lv, C., Chen, X., Yu, H., Peng, J., et al. (2015). The possible allelopathic effect of *Hydrilla verticillata* on phytoplankton in nutrient-rich water. *Environ. Earth Sci.* 73 (9), 5141–5151. doi: 10.1007/s12665-015-4316-8

Gazulha, V., Mansur, M. C. D., Cybis, L. F., and Azevedo, S. M. F. O. (2012). Grazing impacts of the invasive bivalve *Limnoperna fortunei* (Dunker 1857) on single-celled, colonial and filamentous cyanobacteria. *Braz. J. Biol.* 72, 33–39. doi: 10.1590/S1519-69842012000100004

Gulati, R. D., Dionisio Pires, L. M., and Van Donk, E. (2008). Lake restoration studies: Failures, bottlenecks and prospects of new ecotechnological measures. *Limnologica* 38 (3), 233–247. doi: 10.1016/j.limno.2008.05.008

Harrison, X. A., Donaldson, L., Correa-Cano, M. E., Evans, J., Fisher, D. N., Goodwin, C. E., et al. (2018). A brief introduction to mixed effects modelling and multi-model inference in ecology. *PeerJ* 6, e4794. doi: 10.7717/peerj.4794

Havens, K. E., James, R. T., East, T. L., and Smith, V. H. (2003). N:P ratios, light limitation, and cyanobacterial dominance in a subtropical lake impacted by non-point source nutrient pollution. *Environ. pollut.* 122 (3), 379–390. doi: 10.1016/S0269-7491(02)00304-4

Heisler, J., Glibert, P. M., Burkholder, J. M., Anderson, D. M., Cochlan, W., Dennison, W. C., et al. (2008). Eutrophication and harmful algal blooms: A scientific consensus. *Harmful Algae* 8 (1), 3–13. doi: 10.1016/j.hal.2008.08.006

He, H., Ning, X., Chen, K., Li, Q., Li, K., Liu, Z., et al. (2021). Intraguild predation dampens trophic cascades in shallow aquatic mesocosms in the subtropics: Implications for lake restoration by biomanipulation. *Freshw. Biol.* 66 (8), 1571–1580. doi: 10.1111/fwb.13739

He, Y., Zhou, Y., Zhou, Z., Liu, Y., Xiao, Y., Long, L., et al. (2023). Allelopathic effect of pyrogallic acid on cyanobacterium *Microcystis aeruginosa*: The regulatory role of nitric oxide and its significance for controlling harmful algal blooms (HABs). *Sci. Total Environ.* 858, 159785. doi: 10.1016/j.scitotenv.2022.159785

Hillebrand, H., Dürselen, C. D., Kirschtel, D., Pollingher, U., and Zohary, T. (1999). Biovolume calculation for pelagic and benthic microalgae. *J. Phycol.* 35 (2), 403–424. doi: 10.1046/j.1529-8817.1999.3520403.x

Horppila, J., and Nurminen, L. (2003). Effects of submerged macrophytes on sediment resuspension and internal phosphorus loading in lake hiidenvesi (southern Finland). *Water Res.* 37 (18), 4468–4474. doi: 10.1016/S0043-1354(03)00405-6

Hu, H., and Wei, Y. (2006). The freshwater algae of China-systematics, taxonomy and ecology. (Beijing: Science Press).

Hwang, S.-J., Kim, H.-S., Shin, J.-K., Oh, J.-M., and Kong, D.-S. (2004). Grazing effects of a freshwater bivalve (*Corbicula leana* prime) and large zooplankton on phytoplankton communities in two Korean lakes. *Hydrobiologia* 515 (1), 161–179. doi: 10.1023/B:HYDR.0000027327.06471.1e

Jackson, M. C., Loewen, C. J. G., Vinebrooke, R. D., and Chimimba, C. T. (2016). Net effects of multiple stressors in freshwater ecosystems: a meta-analysis. *Global Change Biol.* 22 (1), 180–189. doi: 10.1111/gcb.13028

Jeppesen, E., Meerhoff, M., Jacobsen, B. A., Hansen, R. S., Søndergaard, M., Jensen, J. P., et al. (2007b). Restoration of shallow lakes by nutrient control and biomanipulation–the successful strategy varies with lake size and climate. *Hydrobiologia* 581 (1), 269–285. doi: 10.1007/s10750-006-0507-3

Jeppesen, E., Moss, B., Bennion, H., Carvalho, L., DeMeester, L., Feuchtmayr, H., et al. (2010). "Interaction of climate change and eutrophication," in *Climate change impacts on freshwater ecosystems*. Eds. M. Kernan, R. W. Battarbee and B. Moss (Oxford: Wiley-Blackwell), 119–151. doi: 10.1002/9781444327397.ch6

Jeppesen, E., Søndergaard, M., Meerhoff, M., Lauridsen, T. L., and Jensen, J. P. (2007a). Shallow lake restoration by nutrient loading reduction–some recent findings and challenges ahead. *Hydrobiologia* 584, 239–252. doi: 10.1007/s10750-007-0596-7

Jespersen, A. M., and Christoffersen, K. (1987). Measurements of chlorophyll-*a* from phytoplankton using ethanol as extraction solvent. *Arch. Hydrobiologie* 109 (3), 445–454. doi: 10.1127/archiv-hydrobiol/109/1987/445

Knopik, J. M., and Newman, R. M. (2018). Transplanting aquatic macrophytes to restore the littoral community of a eutrophic lake after the removal of common carp. *Lake Reservoir Manage.* 34 (4), 365–375. doi: 10.1080/10402381.2018.1477885

Lawrence, M. (2016). *Ez: Easy analysis and visualization of factorial experiments* (R Package Version 4.4-0). Available at: https://CRAN.R-project.org/package=ez.

Legendre, P., and Gallagher, E. D. (2001). Ecologically meaningful transformations for ordination of species data. *Oecologia* 129 (2), 271–280. doi: 10.1007/s004420100716

Le Moal, M., Gascuel-Odoux, C., Ménesguen, A., Souchon, Y., Étrillard, C., Levain, A., et al. (2019). Eutrophication: A new wine in an old bottle? *Sci. Total Environ.* 651, 1–11. doi: 10.1016/j.scitotenv.2018.09.139

Li, H., Li, Y., Huang, D., Zhang, L., Lu, J., and Zhang, J. (2021a). The response mechanism of *Hydrilla verticillata* and leaf epiphytic biofilms to depth and nutrient removal. *Environ. Sci. pollut. R.* 28 (35), 49032–49041. doi: 10.1007/s11356-021-14131-x

Liu, H., Liu, G., and Xing, W. (2021). Functional traits of submerged macrophytes in eutrophic shallow lakes affect their ecological functions. *Sci. Total Environ.* 760, 143332. doi: 10.1016/j.scitotenv.2020.143332

Liu, X., Zhang, G., Sun, G., Wu, Y., and Chen, Y. (2019). Assessment of lake water quality and eutrophication risk in an agricultural irrigation area: A case study of the chagan lake in northeast China. *Water* 11 (11), 2380. doi: 10.3390/w11112380

Liu, H., Zhou, W., Li, X., Chu, Q., Tang, N., Shu, B., et al. (2020). How many submerged macrophyte species are needed to improve water clarity and quality in Yangtze floodplain lakes? *Sci. Total Environ.* 724, 138267. doi: 10.1016/j.scitotenv.2020.138267

Li, Y., Wang, L., Chao, C., Yu, H., Yu, D., and Liu, C. (2021b). Submerged macrophytes successfully restored a subtropical aquacultural lake by controlling its internal phosphorus loading. *Environ. pollut.* 268, 115949. doi: 10.1016/j.envpol.2020.115949

Lürling, M., van Geest, G., and Scheffer, M. (2006). Importance of nutrient competition and allelopathic effects in suppression of the green alga *Scenedesmus obliquus* by the macrophytes *Chara*, *Elodea* and *Myriophyllum*. *Hydrobiologia* 556 (1), 209–220. doi: 10.1007/s10750-005-1168-3

MacIsaac, H. J., Sprules, G., Johannson, O. E., and Leach, J. H. (1992). Filtering impacts of larval and sessile zebra mussels (*Dreissena polymorpha*) in western lake Erie. *Oecologia* 92 (1), 30–39. doi: 10.1007/bf00317259

Mantzouki, E., Visser, P. M., Bormans, M., and Ibelings, B. W. (2016). Understanding the key ecological traits of cyanobacteria as a basis for their management and control in changing lakes. *Aquat. Ecol.* 50 (3), 333–350. doi: 10.1007/s10452-015-9526-3

Mohamed, Z. A. (2017). Macrophytes-cyanobacteria allelopathic interactions and their implications for water resources management–a review. *Limnologica* 63, 122–132. doi: 10.1016/j.limno.2017.02.006

Nakagawa, S., and Schielzeth, H. (2013). A general and simple method for obtaining R^2 from generalized linear mixed-effects models. *Methods Ecol. Evol.* 4 (2), 133–142. doi: 10.1111/j.2041-210x.2012.00261.x

Oksanen, J., Blanchet, F. G., Friendly, M., Kindt, R., Legendre, P., McGlinn, D., et al. (2020). *Vegan: Community ecology package* (R package version 2.5-7). Available at: https://CRAN.R-project.org/package=vegan.

Peng, X., Lin, Q., Liu, B., Huang, S., Yan, W., Zhang, L., et al. (2022). Effect of submerged plant coverage on phytoplankton community dynamics and photosynthetic activity *in situ*. *J. Environ. Manage.* 301, 113822. doi: 10.1016/j.jenvman.2021.113822

Phillips, G., Pietiläinen, O. P., Carvalho, L., Solimini, A., Lyche Solheim, A., and Cardoso, A. C. (2008). Chlorophyll–nutrient relationships of different lake types using a large European dataset. *Aquat. Ecol.* 42 (2), 213–226. doi: 10.1007/s10452-008-9180-0

Puijalon, S., Bouma, T. J., Douady, C. J., van Groenendael, J., Anten, N. P. R., Martel, E., et al. (2011). Plant resistance to mechanical stress: evidence of an avoidance–tolerance trade-off. *New Phytol.* 191 (4), 1141–1149. doi: 10.1111/j.1469-8137.2011.03763.x

Rangel, L. M., Silva, L. H. S., Faassen, E. J., Lürling, M., and Ger, K. A. (2020). Copepod prey selection and grazing efficiency mediated by chemical and morphological defensive traits of cyanobacteria. *Toxins* 12 (7), 465. doi: 10.3390/toxins12070465

Rao, Q., Su, H., Deng, X., Xia, W., Wang, L., Cui, W., et al. (2020). Carbon, nitrogen, and phosphorus allocation strategy among organs in submerged macrophytes is altered by eutrophication. *Front. Plant Sci.* 11. doi: 10.3389/fpls.2020.524450

Redfield, A. C. (1958). The biological control of chemical factors in the environment. *Am. Sci.* 46 (3), 205–221.

Richardson, J., Feuchtmayr, H., Miller, C., Hunter, P. D., Maberly, S. C., and Carvalho, L. (2019). Response of cyanobacteria and phytoplankton abundance to warming, extreme rainfall events and nutrient enrichment. *Global Change Biol.* 25 (10), 3365–3380. doi: 10.1111/gcb.14701

Rong, Y., Tang, Y., Ren, L., Taylor, W. D., Razlutskij, V., Naselli-Flores, L., et al. (2021). Effects of the filter-feeding benthic bivalve *Corbicula fluminea* on plankton community and water quality in aquatic ecosystems: A mesocosm study. *Water* 13 (13), 1827. doi: 10.3390/w13131827

Søndergaard, M., Jeppesen, E., Lauridsen, T. L., Skov, C., Van Nes, E. H., Roijackers, R., et al. (2007). Lake restoration: successes, failures and long-term effects. *J. Appl. Ecol.* 44 (6), 1095–1105. doi: 10.1111/j.1365-2664.2007.01363.x

Søndergaard, M., Johansson, L. S., Lauridsen, T. L., Jørgensen, T. B., Liboriussen, L., and Jeppesen, E. (2010). Submerged macrophytes as indicators of the ecological quality of lakes. *Freshw. Biol.* 55 (4), 893–908. doi: 10.1111/j.1365-2427.2009.02331.x

Sala, O. E., Chapin, F. S.III, Armesto, J. J., Berlow, E., Bloomfield, J., Dirzo, R., et al. (2000). Global biodiversity scenarios for the year 2100. *Science* 287 (5459), 1770–1774. doi: 10.1126/science.287.5459.1770

Sand-Jensen, K., and Borum, J. (1991). Interactions among phytoplankton, periphyton, and macrophytes in temperate freshwaters and estuaries. *Aquat. Bota.* 41 (1), 137–175. doi: 10.1016/0304-3770(91)90042-4

Schindler, D. W. (1977). Evolution of phosphorus limitation in lakes. *Science* 195 (4275), 260–262. doi: 10.1126/science.195.4275.260

Segurado, P., Almeida, C., Neves, R., Ferreira, M. T., and Branco, P. (2018). Understanding multiple stressors in a Mediterranean basin: Combined effects of land use, water scarcity and nutrient enrichment. *Sci. Total Environ.* 624, 1221–1233. doi: 10.1016/j.scitotenv.2017.12.201

Smith, V. H. (1983). Low nitrogen to phosphorus ratios favor dominance by blue-green algae in lake phytoplankton. *Science* 221 (4611), 669–671. doi: 10.1126/science.221.4611.669

Smith, V. H., Joye, S. B., and Howarth, R. W. (2006). Eutrophication of freshwater and marine ecosystems. *Limnol. Oceanogr* 51 (1part2), 351–355. doi: 10.4319/lo.2006.51.1_part_2.0351

Sprung, M., and Rose, U. (1988). Influence of food size and food quantity on the feeding of the mussel *Dreissena polymorpha*. *Oecologia* 77 (4), 526–532. doi: 10.1007/BF00377269

Stenton-Dozey, J., and Brown, A. C. (1992). Clearance and retention efficiency of natural suspended particles by the rock-pool bivalve *Venerupis corrugatus* in relation to tidal availability. *Mar. Ecol. Prog. Ser.* 82, 175–186. doi: 10.3354/meps082175

Stewart, R. I. A., Dossena, M., Bohan, D. A., Jeppesen, E., Kordas, R. L., Ledger, M. E., et al. (2013). Mesocosm experiments as a tool for ecological climate-change research. *Adv. Ecol. Res.* 48, 1–181. doi: 10.1016/B978-0-12-417199-2.00002-1

Su, H., Chen, J., Wu, Y., Chen, J., Guo, X., Yan, Z., et al. (2019). Morphological traits of submerged macrophytes reveal specific positive feedbacks to water clarity in freshwater ecosystems. *Sci. Total Environ.* 684, 578–586. doi: 10.1016/j.scitotenv.2019.05.267

Van den Brink, P. J., and Braak, C. J. F. T. (1999). Principal response curves: Analysis of time-dependent multivariate responses of biological community to stress. *Environ. Toxicol. Chem.* 18 (2), 138–148. doi: 10.1002/etc.5620180207

van Donk, E., and van de Bund, W. J. (2002). Impact of submerged macrophytes including charophytes on phyto- and zooplankton communities: allelopathy versus other mechanisms. *Aquat. Bota.* 72 (3), 261–274. doi: 10.1016/S0304-3770(01)00205-4

Vaughn, C. A., and Hoellein, T. J. (2018). Bivalve impacts in freshwater and marine ecosystems. *Annu. Rev. Ecol. Evol. Syst.* 49 (1), 183–208. doi: 10.1146/annurev-ecolsys-110617-062703

Wang, L.-X., Zhang, L., Zhang, Y.-X., Jin, C.-Y., Lu, C.-M., and Wu, G.-R. (2006). The inhibitory effect of *Hydrilla verticillata* culture water on *Microcystic aeruginosa* and its mechanism. *J. Plant Physiol. Mol. Biol.* 32 (6), 672–678.

Wetzel, R. G., and Likens, G. E. (2000). *Limnological analyses*. *3rd edition*. (New York: Springer-Verlag).

White, J. D., and Sarnelle, O. (2014). Size-structured vulnerability of the colonial cyanobacterium, *Microcystis aeruginosa*, to grazing by zebra mussels (*Dreissena polymorpha*). *Freshw. Biol.* 59 (3), 514–525. doi: 10.1111/fwb.12282

Wu, L., and Culver, D. A. (1991). Zooplankton grazing and phytoplankton abundance: an assessment before and after invasion of *Dreissena polymorpha*. *J. Great Lakes Res.* 17 (4), 425–436. doi: 10.1016/S0380-1330(91)71378-6

Yu, J., Xia, M., He, H., Jeppesen, E., Guan, B., Ren, Z., et al. (2020). The host mussel *Sinanodonta woodiana* alleviates negative effects of a small omnivorous fish (*Acheilognathus macropterus*) on water quality: A mesocosm experiment. *Freshw. Sci.* 39 (4), 752–761. doi: 10.1086/711295

Zhang, T. T., He, M., Wu, A. P., and Nie, L. W. (2012). Inhibitory effects and mechanisms of *Hydrilla verticillata* (Linn.f.) royle extracts on freshwater algae. *B. Environ. Contam. Tox.* 88 (3), 477–481. doi: 10.1007/s00128-011-0500-z

Zhang, Y., Jeppesen, E., Liu, X., Qin, B., Shi, K., Zhou, Y., et al. (2017). Global loss of aquatic vegetation in lakes. *Earth-Sci. Rev.* 173, 259–265. doi: 10.1016/j.earscirev.2017.08.013

Zhang, X., Liu, Z., Jeppesen, E., and Taylor, W. D. (2014). Effects of deposit-feeding tubificid worms and filter-feeding bivalves on benthic-pelagic coupling: Implications for the restoration of eutrophic shallow lakes. *Water Res.* 50, 135–146. doi: 10.1016/j.watres.2013.12.003

Zhang, X., Zhen, W., Jensen, H. S., Reitzel, K., Jeppesen, E., and Liu, Z. (2021). The combined effects of macrophytes (*Vallisneria denseserrulata*) and a lanthanum-modified bentonite on water quality of shallow eutrophic lakes: A mesocosm study. *Environ. pollut.* 277, 116720. doi: 10.1016/j.envpol.2021.116720

Zhu, X., Dao, G., Tao, Y., Zhan, X., and Hu, H. (2021). A review on control of harmful algal blooms by plant-derived allelochemicals. *J. Hazard. Mater.* 401, 123403. doi: 10.1016/j.jhazmat.2020.123403

Zhu, J., Liu, B., Wang, J., Gao, Y., and Wu, Z. (2010). Study on the mechanism of allelopathic influence on cyanobacteria and chlorophytes by submerged macrophyte (*Myriophyllum spicatum*) and its secretion. *Aquat. Toxicol.* 98 (2), 196–203. doi: 10.1016/j.aquatox.2010.02.011

frontiers | Frontiers in Plant Science

TYPE Original Research
PUBLISHED 24 March 2023
DOI 10.3389/fpls.2023.1142848

OPEN ACCESS

EDITED BY
Benoit Schoefs,
Le Mans Université, France

REVIEWED BY
Sanqiang Gong,
South China Sea Institute of Oceanology (CAS), China
John Raven,
University of Dundee, United Kingdom

*CORRESPONDENCE
Hong Sheng Jiang
jhs@wbgcas.cn

SPECIALTY SECTION
This article was submitted to Marine and Freshwater Plants, a section of the journal Frontiers in Plant Science

RECEIVED 12 January 2023
ACCEPTED 03 March 2023
PUBLISHED 24 March 2023

CITATION
Liao Z, Li P, Zhou J, Li W and Jiang HS (2023) Different photosynthetic inorganic carbon utilization strategies in the heteroblastic leaves of an aquatic plant *Ottelia ovalifolia*. *Front. Plant Sci.* 14:1142848. doi: 10.3389/fpls.2023.1142848

Different photosynthetic inorganic carbon utilization strategies in the heteroblastic leaves of an aquatic plant *Ottelia ovalifolia*

Zuying Liao[1,2], Pengpeng Li[1,3], Jingzhe Zhou[1,2], Wei Li[1,4] and Hong Sheng Jiang[1]*

[1]Aquatic Plant Research Center, Wuhan Botanical Garden, Chinese Academy of Sciences, Wuhan, China, [2]University of Chinese Academy of Sciences, Beijing, China, [3]Hainan Key Laboratory for Sustainable Utilization of Tropical Bioresources, School of Life Sciences, Hainan University, Haikou, China, [4]Research Center for Ecology, College of Science, Tibet University, Lhasa, China

The leaves of the heteroblastic aquatic plant *Ottelia ovalifolia* faces submerged and aerial environments during its life history. However, the acclimation of the submerged leaves and floating leaves to these two environments in morphology, physiology, and biochemistry remain unclear. In the present study, we investigated the acclimation of the CO_2-concentrating mechanisms in these two types of leaves. We found that the submerged leaves were longer, narrower, and thinner than the floating leaves, which increased the specific surface area of the leaves and lead to better absorption of the inorganic carbon underwater. Meanwhile, the floating leaves absorbed atmospheric CO_2 directly through the stomata to acclimate to the aerial environment. Both the leaf types had the ability to use HCO_3^-, but the capacity in submerged leaves was stronger than that in floating leaves. The extracellular carbonic anhydrase and anion exchanger were responsible for the HCO_3^- use in both types of leaves. The higher ratio of chlorophyll a/b and content of anthocyanin in floating leaves than that in submerged leaves indicated that the acclimation of aerial and submerged photosynthesis depended on changes in the photosynthetic pigments. Based on the stable carbon isotope ratio, key enzyme activities of the C4 pathway indicated that submerged leaves might have the ability to perform C4 metabolism while floating leaves only performed C3 metabolism. In summary, *O. ovalifolia* acclimates to submerged and aerial environments through changes in morphology, physiology, and biochemistry during different growth stages.

KEYWORDS

***Ottelia ovalifolia*, heteroblastic plant, bicarbonate use, C4, carbon isotope ratio**

Introduction

The distribution of plants is driven by the ability of plants to disperse, establish, and maintain in their specific environments (Cavalli et al., 2012). Species that acclimate well to different environments are better able to take up positions in habitats and may displace other species or even alter the habitats (Cavalli et al., 2012). Due to the high transport resistance, high water pH and the external boundary layer (Raven, 1970; Maberly and Madsen, 1998), CO_2 shortage is considered to be one of the limiting factors for photosynthesis of submerged plants (Maberly and Madsen, 1998) that play an important role in aquatic ecosystem, as they provide food, habitat and shelter for invertebrates and fish (Chambers et al., 2008). Although CO_2 is the preferred carbon source for submerged photosynthesis, it only contributes to a very small proportion of dissolved inorganic carbon (DIC) and HCO_3^- is the main form of DIC in most natural water body. It is generally believed that the acquisition and utilization of limited resources by plants is highly competitive, which have an important effect on plants distribution (James et al., 1999). Adapting to the shortage of CO_2 under water, submerged plants develop several CO_2 concentrating mechanisms (CCMs) that enrich the available concentration of CO_2 at the active site of ribulose 1,5-bisphosphate carboxylase/oxygenase (Rubisco) in physiological and biochemical response including HCO_3^- use, crassulacean acid metabolism (CAM)-like and C4 (or C4-like) metabolism (Klavsen et al., 2011). Abundant HCO_3^- in field freshwater can serve as an additional carbon source for photosynthesis in about 44% of tested aquatic plants and reduce photorespiration under low CO_2 availability (Maberly and Gontero, 2017; Yin et al., 2017; Iversen et al., 2019; Jiang et al., 2021; Li et al., 2021). Two mechanisms of HCO_3^- use have been studied in detail in microalgae, macroalgae, seagrasses and a small range of freshwater aquatic plants (Giordano et al., 2005; Axelsson et al., 1995; Huang et al., 2020a; Jiang et al., 2021): I) Extracellular carbonic anhydrase (CAext) catalyzes the conversion of HCO_3^- into CO_2 that enters the cell and participates in photosynthesis. This mechanism of HCO_3^- use was widespread in aquatic plants (Huang et al., 2020a); II) HCO_3^- is directly absorbed *via* an anion exchanger (AE) protein located at the plasmalemma. These two mechanisms are not mutually exclusive but complementary in some species, and they will be responsible for the HCO_3^- uptake under different DIC environments that could cope with the variation of DIC in the natural waterbody (Axelsson et al., 1995; Huang et al., 2020a; Jiang et al., 2021). Both CAM and C4 perform the first step of carbon fixation with phosphoenolpyruvate carboxylase (PEPC) whose active is temporal separation for CAM plants or spatial separation for C4 plants (Maberly and Gontero, 2017). CAM is a malleable metabolism in aquatic plants compared to land plants (Bowes and Salvucci, 1989) and 9% of aquatic plant perform CAM (Maberly and Gontero, 2018). For instance, CAM could be induced under low CO_2 conditions, but not under high CO_2 conditions in the submerged macrophyte *Ottelia alismoides* (Shao et al., 2017). On the other hand, C4 metabolism was found in about 4% of the tested aquatic plants (Maberly and Gontero, 2018) and it typically involves a PEPC catalyzing phosphoenolpyruvate (PEP) and HCO_3^- to form a 4-carbon acid, which is then cleft by a decarboxylase to produce CO_2 in the vicinity of Rubisco (Clement et al., 2016). C4 metabolism in terrestrial plants is often associated with Kranz-type anatomy, but some submerged plants lacking Kranz-type structures also possess C4 metabolism, such as *Hydrilla verticillata*, *Egeria densa*, and *O. alismoides* (Bowes et al., 2002; Lara et al., 2002; Zhang et al., 2014). Compared to CCMs in terrestrial plants that are adapted to high temperature and drought, aquatic plants develop CCMs most widely in low CO_2, high HCO_3^-, high pH, and high light environments (Maberly and Gontero, 2017) and perform changes in morphology and physiological function.

The leaf is the main photosynthetic organ in higher plants and its morphology and anatomy could also reflect the influences of their growth environments (Vogelmann and Gorton, 2014). For instance, the heteroblastic species, *O. cordata*, grew submerged leaves at the juvenile stage and floating or aerial leaves at the adult stage (Wang et al., 2022). Floating and aerial leaves are directly exposed to the air, and they have similar anatomical structures to terrestrial plants, with palisade tissue and spongy tissues differentiated, and stomata in the upper and/or lower epidermis (Han et al., 2021; Horiguchi et al., 2021; Wang et al., 2022). The morphology and anatomical structure of submerged leaves indicate that they are adapted to water habitat: submerged leaves are thin, with normally two to three layers of cells and their morphologies are whorled, dissected whorled, dissected, linear, linear strap-like and filiform, which could increase the specific surface area and better exploit DIC in the water (Shao et al., 2017; Maberly and Gontero, 2018; Horiguchi et al., 2021; Wang et al., 2022).

Ottelia ovalifolia (R. Br.) Rich, a species from the Hydrocharitaceae and native to Australia (Paice et al., 2017a), is a heteroblastic plant with submerged leaves at the juvenile stage and floating leaves at the adult stage (Arber, 1919; Paice et al., 2017b). This species was the first invasive aquatic plant recorded in New Zealand and had a large biomass in slow water, affecting the drinking water of livestock (McCullough, 1997). Previous study also found that the aquatic plant *O. alismoides* from the same genus has invaded Europe (Hussner, 2012). In addition, the aquatic plants in the Hydrocharitaceae, the same family of *O. ovalifolia*, such as *E. densa* invaded East Asia and Europe (Hussner, 2012; Wang et al., 2016), and *H. verticillata* invaded America (Sousa, 2011), they all showed highly invasive capacity in East Asia, Europe, North America and New Zealand (McCullough, 1997). It is interesting to find that these aquatic plants were reported to possess at least one of the CCMs, and previous studies showed that the ability of CCMs has an impact on aquatic plant distribution and species composition in the CO_2 shortage natural water (Maberly and Gontero, 2018; Iversen et al., 2019; Jiang et al., 2021). Current studies on *O. ovalifolia* mainly focus on the factors influencing plant distribution and the potential of submerged plants to support food webs (Paice et al., 2017a; Paice et al., 2017b), but little is known of its CCMs. Therefore, in the present study, we will investigate the CCMs on *O. ovalifolia* and we hypothesized that both submerged and floating leaves of *O. ovalifolia* had CCMs: HCO_3^- use, C4 and CAM.

Materials and methods

Plant materials

O. ovalifolia was collected from the resource nursery of Wuhan Botanical Garden, Chinese Academy of Sciences. Three growth stages were found in resource nursery: juvenile growth stage (with only submerged leaves), transition growth stage (with submerged and floating leaves), and adult growth stage (with only floating leaves). In this study, submerged leaves were selected from healthy plants at the juvenile growth stage to avoid the effects from floating leaves and floating leaves were selected from healthy plants at the adult growth stage to exclude the effect from submerged leaves. The experiments were conducted from June to September 2021. The pH of the *in-situ* water was measured by a hand-held pH meter with an accuracy of ± 0.05 (az8886, AZ Instrument, China) at 9:30, and the alkalinity of the water was determined by the Gran titration with 0.1 M HCl (Zhang et al., 2014). The chemical characteristics of inorganic carbon *in-situ* water were shown in Table 1.

Morphology, anatomy, ultrastructure and photosynthetic pigments

Leaf morphology was described as fresh weight, area, length, width, leaf mass per area (LMA) and aspect ratio. Fresh leaves were photographed with a digital camera (Huawei Mate30pro, China), and the length, width and area of five independent individual leaves were measured using Image J software 1.50 (NIH, USA). The stomatal density of the leaf epidermis of five independent individual leaves was observed under light microscopy (PH100-341L-PL, Purkinje General, China). After cleaning, the leaf fragments (2 cm × 1 cm, length × width) were fixed in 2 mL FAA fixative solution (FAA, 50% ethanol: glacial acetic acid: 40% formaldehyde = 90:5:5, v/v). Subsequently, the paraffin sections were obtained from the fixed slides (Khan et al., 2022) and then the cells length, width and area were measured by Image J software. Fragments of floating and submerged leaves (3 mm × 3 mm, length × width) were fixed overnight in 2.5% glutaraldehyde solution prepared with 0.1M phosphate buffer (pH7.4) at 4 °C and then post-fixed in 1% OsO_4 solution for 2.5h at 4 °C (Farnese et al., 2017). Ultrathin sections (72 nm) were obtained on a Leica EM UC7 ultramicrotome, and the operation procedure was referred to Han et al. (2020). Chlorophyll content was measured by a spectrophotometer (TU-1810PC, Purkinje General, China) at the absorbance of 470, 665 and 649 nm after 0.1 g fresh weight leaves were extracted in 5 mL 95% ethanol at 4 °C for 24 hours (Shao et al., 2017), each type of leaf had 15 replicates. The anthocyanin content of 0.1 g fresh weight leaves was performed as described by (Solfanelli et al., 2006). Anthocyanin content was expressed by A535/g (FW), each type of leaf had 5 replicates.

TABLE 1 Inorganic carbon chemistry in the growth culture in the field.

pH	Alkalinity (mequiv L^{-1})	CO_2 (mM)	HCO_3^- (mM)
7.59 (7.41–7.7)	1.11 (1.09–1.13)	0.055 (0.041–0.078)	1.102 (1.086–1.121)

pH-drift experiments

The ability of HCO_3^- use of floating and submerged leaves was assessed by pH-drift experiments as described in a previous study (Zhang et al., 2014). In addition, previous studies have shown that some *Ottelia* plants are able to utilize HCO_3^- through CAext and AE (Huang et al., 2020a; Jiang et al., 2021; Wang et al., 2022). The CAext inhibitor acetazolamide (AZA) and AE inhibitor 4,4'-diisothio-cyanatostilbene-2,2'-disulfonate (DIDS) (Beer et al., 2002) were added to the pH-drift system to verify the HCO_3^- utilization pathway in *O. ovalifolia*. One treatment without inhibitors was named control, one treatment containing 0.2 mM AZA was named AZA, and the other treatment containing 0.3 mM DIDS was named DIDS. After 24 h illumination determined the endpoint pH in each treatment with eight replicates for the control and five replicates for AZA and four replicates for DIDS treatments.

Measurement of stable ^{13}C isotope

Four submerged leaves and five floating leaves were oven dried and then the stable ^{13}C isotope was determined as described in previous studies (Jiang et al., 2021; Wang et al., 2022) by using a Delta Plus Advantage isotope ratio mass spectrometer (Thermo Fisher Scientific, Bremen, Germany). For the $\delta^{13}C$ DIC analysis of *in-situ* water, the method of Li et al. (2008) was used, with a precision of 0.1 ‰. Isotope data was shown in the conventional delta notion (‰) versus Vienna Pee Dee Belemnite (V-PDB).

Measurement of photosynthesis enzymes activities

The key enzymes (Rubisco, PEPC and pyruvate phosphate dikinase (PPDK)) activities of carboxylation and decarboxylation in C3 and C4 metabolism of five individuals in submerged and floating leaves were measured by using the method described in Zhang et al. (2014).

Measurement of acidity

Diurnal variation of titratable acidity was calculated as the difference between the minimum (samples collected at dusk: 18:00) and maximum (samples collected at dawn: 4:30) titratable acidity per unit of fresh mass (Zhang et al., 2014). Each treatment had five replicates.

Statistical analysis

Data were shown as mean and standard deviation (SD). The statistical analyses were performed in software R version 4.0.5. In

the absence of special instructions, we generally used t-test for difference analysis between submerged and floating leaves. Analysis of pH drift experiments without (control) or with inhibitors (AZA, DIDS) were determined by a one-way ANOVA with a Tukey's HSD test when $p<0.05$.

Results

Morphological, anatomic and photosynthetic features

The morphology of *O. ovalifolia* leaves was dramatically different between the floating and submerged leaves. The floating leaves were oval or broadly cordate shape while the submerged leaves were linear (Figures 1A, B). Significant differences in leaf length, leaf width, leaf length/width, leaf area and LMA were found between floating and submerged leaves (Table 2). The floating leaves were wider, heavier and had a larger area and LMA (Table 2). The submerged leaves, however, were longer and had a larger leaf length/width (Table 2).

The anatomical structure of floating and submerged leaves was shown in Figures 1C, D. The observation of the transverse section showed that the upper and lower epidermal cells of both floating and submerged leaves were composed of single-layered rectangular cells, neatly and closely arranged (Figures 1C, D). The mesophyll cells of floating leaves were differentiated into palisade tissue and spongy tissue (Figure 1C), while the submerged leaves were not (Figure 1D). The length of mesophyll cells and the upper epidermis of floating leaves was significantly larger than that of submerged leaves (Table 2). Only the length of upper, the length of lower mesophyll cells and the width of lower mesophyll cells in floating leaves were significantly higher than in submerged leaves (Table 2). There were air spaces between the mesophyll cells of floating and submerged leaves, however, no significant difference was found in the air space transection area of floating and submerged leaves (Table 2). In the floating leaves, chloroplasts were only found in lower epidermal cells and mesophyll cells, but did not occur in the upper epidermal cells (Figures 1E–G). However, chloroplasts were found in both upper and lower epidermal cells, and mesophyll cells of submerged leaves (Figures 1H–J). Stomata appeared on the upper surface, and the stomata density was 65 individuals per mm^2, but there were no stomata on the upper and lower surfaces of the transverse sections of the submerged leaf (Table 2; Figure S1).

No significant difference in Chl-a content was found between floating and submerged leaves (Table 2). However, the Chl-b content in submerged leaves was significantly higher than that in floating leaves (Table 2) and the Chl-a/b in floating leaves weas significantly higher than that in submerged leaves (Table 2). In contrast to Chl-b, the content of anthocyanin in floating leaves was significantly higher than that in submerged leaves (Table 2). The content of anthocyanin in floating leaves was significantly lower than that in submerged leaves (Table 2).

$\delta^{13}C$ isotope values

The $\delta^{13}C$ isotope of DIC in water was –10.92 ‰, and the $\delta^{13}C$ isotope in floating leaves (–30.07‰) was significantly lower than that in submerged leaves (–25.33‰) (Table 2). On the basis of the isotope fractionation between HCO_3^- and CO_2 (Mook et al., 1974), when the $\delta^{13}C$ isotope of DIC was –10.92 ‰, the value of $\delta^{13}C$ for HCO_3^- calculated to be –10.5‰, while the value of $\delta^{13}C$ for dissolved free CO_2 was –18.4‰.

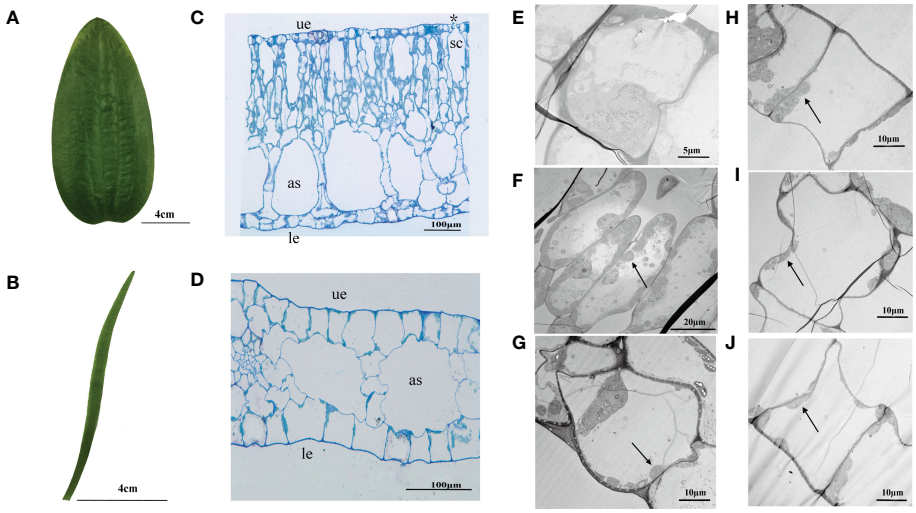

FIGURE 1
Leaf morphology and anatomical structure in transverse sections of *O. ovalifolia*. **(A)** Morphology of floating leaf; **(B)** Morphology of submerged leaf; **(C)** Transection structure of floating leaf; **(D)** Transection structure of submerged leaf; **(E)** TEM image showing the ultrastructure of upper epidermal cell in floating leaf; **(F)** TEM image showing the ultrastructure of mesophyll cell in floating leaf; **(G)** TEM image showing the ultrastructure of lower epidermal cell in floating leaf; **(H)** TEM image showing the ultrastructure of upper epidermal cell in submerged leaf; **(I)** TEM image showing the ultrastructure of mesophyll cell in submerged leaf; **(J)** TEM image showing the ultrastructure of lower epidermal cell in submerged leaf. as, air space; le, lower epidermis; sc, stomatic chamber; ue, upper epidermis; asterisk indicates stoma; black arrows indicate chloroplasts.

TABLE 2 Morphological, anatomic, photosynthetic and carbon isotope characters in floating and submerged leave of *O. ovalifolia*.

Parameters	Floating leaf	Submerged leaf
Leaf length (cm)	14.9 ± 1.4 b	21.2 ± 3.51 a
Leaf width (cm)	5.86 ± 0.63 a	0.54 ± 0.08 b
Leaf length/width	2.57 ± 0.27 b	39.79 ± 4.84 a
Leaf area (cm^2)	70.0 ± 13.4 a	10.2 ± 2.3 b
Leaf FW (g)	2.49 ± 0.38 a	0.12 ± 0.03 b
LMA g m^{-2}	358.1 ± 19.9 a	111.2 ± 14.2 b
Upper epidermis cell length (μm)	29.6 ± 5.1a	38.0 ± 2.3 a
Upper epidermis cell width (μm)	17.8 ± 4.9 a	12.8 ± 3.7 a
Lower epidermis cell length (μm)	42.45 ± 6.0 a	36.4 ± 7.5 a
Lower epidermis cell width (μm)	23.0 ± 4.9 a	12.0 ± 3.0 a
Upper epidermis cell area (mm^2)	767 ± 143 a	483 ± 100 a
Lower epidermis cell area ($μm^2$)	1156 ± 233 a	434 ± 153 a
Upper mesophyll cell length (μm)	65.1 ± 8.5 a	38.8 ± 11.8 b
Upper mesophyll cell width (μm)	17.2 ± 6.2 a	15.1 ± 0.7 a
Upper mesophyll cell area ($μm^2$)	1381 ± 275 a	514 ± 98 a
Lower mesophyll cell length (μm)	62.8 ± 11.1a	38. 8 ± 11.8 b
Lower mesophyll cell width (μm)	27.2 ± 7.1 a	15.1 ± 0.7 b
Lower mesophyll cell area ($μm^2$)	2023 ± 9883 a	5143 ± 983 a
Air space area ($μm^2$)	14361 ± 38081 a	9850 ± 5559 a
Stomatic chamber area ($μm^2$)	13561 ± 4711	
Stomatal density surface (individual mm^2)	65.4 ± 14.5	
Chl–a (mg g^{-1})	0.60 ± 0.11 a	0.60 ± 0.06 a
Chl–b (mg g^{-1})	0.21 ± 0.04 b	0.25 ± 0.04 a
Chl–a/b	2.80 ± 0.16 a	2.39 ± 0.14 b
Car (mg g^{-1})	0.05 ± 0.02 a	0.05 ± 0.02 a
anthocyanin content (A535 g^{-1})	10.10 ± 1.84 a	1.07 ± 0.29 b
Leaf δ ^{13}C (‰)	−30.07 ± 0.54 a	−25.33 ± 0.51 b
DIC δ ^{13}C (‰)	−10.92 ± 2.14	−10.92 ± 2.14

Data were expressed as mean ± standard deviation. Different letters indicated significant difference between floating and submerged leaves by t-test ($p<0.05$).
FW, fresh weigh; LMA, leaf mass per area; Chl-a, b, chlorophyll a and chlorophyll b.

pH-drift experiments

The average final pH in submerged leaves was 10.2 and was significantly higher than that in floating leaves (9.7) (Figure 2A). The remained concentration of CT, HCO_3^-, CO_2 and CT/Alk in the pH-drift system of floating leaves was significantly higher than that of submerged leaves (Figures 2B–D, F). The concentration of CO_3^{2-} was not significantly different between floating and submerged leaves (Figure 2E). The inhibitors adding pH-drift experiments showed that 0.2mM AZA and 0.3mM DIDS significantly decreased the final pH both in floating and submerged leaves (Figure 3).

Photosynthesis enzymes activities

Rubisco activity, a key enzyme of the Calvin cycle, was significantly higher in floating leaves than that in submerged leaves (Figure 4A). However, the activity of another carboxylase, PEPC, was not significantly different between floating leaves and submerged leaves (Figure 4B). As a consequence, the ratio of PEPC/Rubisco activities in submerged leaves (2.24) was significantly higher than that in floating leaves (0.988) (Figure 4C). Similarly, the activity of PPDK performed the same pattern as PEPC based on the fact that the activity of PPDK in floating leaves was significantly higher than that in submerged leaves (Figure 4D).

10.3389/fpls.2023.1142848

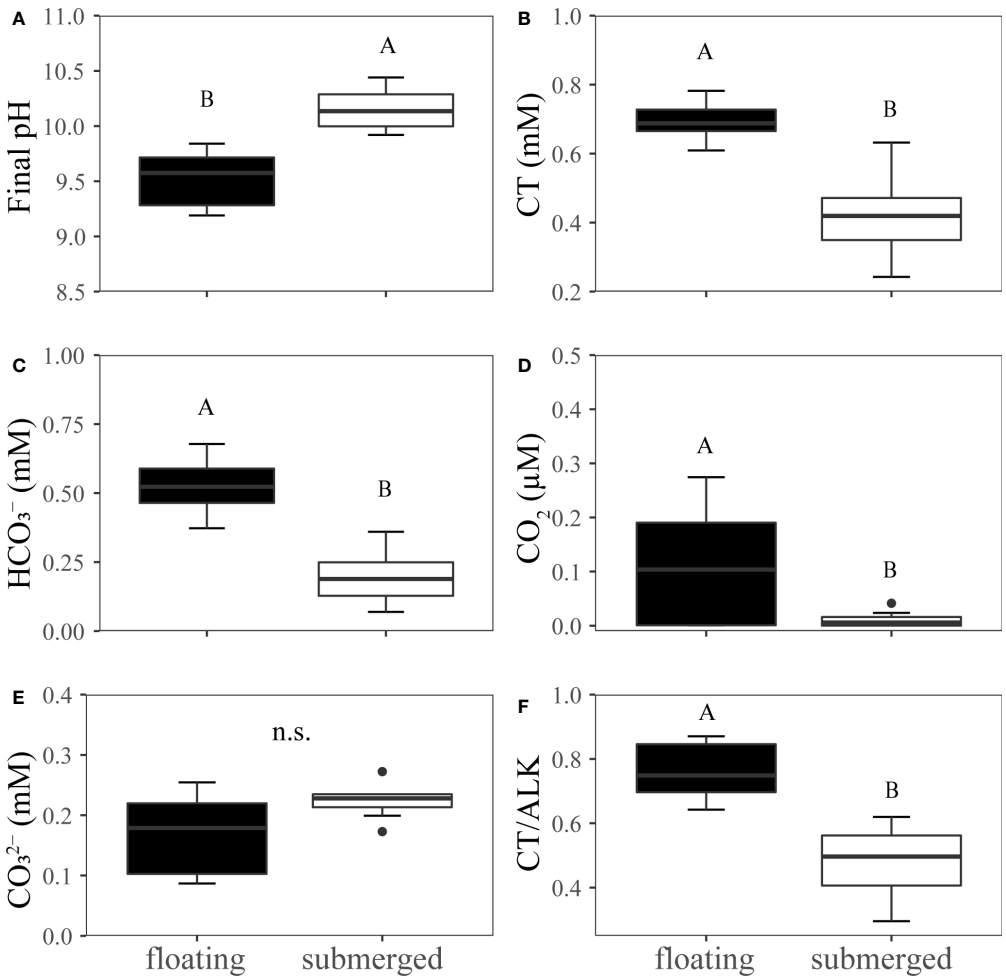

FIGURE 2
Experimental analysis of pH drift in floating and submerged leaves of *O. ovalifolia*. **(A)** Final pH. **(B)** CT. **(C)** HCO_3^-. **(D)** CO_2. **(E)** CO_3^{2-}. **(F)** CT/Alk. CT, total inorganic carbon; Alk, alkalinity. n.s., not significant. n=8. The different uppercase letters indicate significant differences ($p < 0.05$) between floating leaf and submerged leaf.

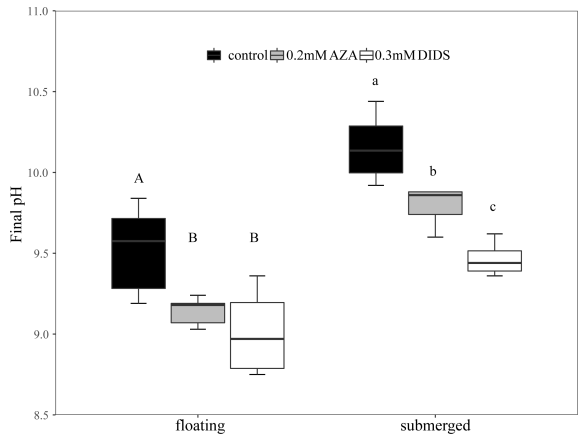

FIGURE 3
Final pH in the inhibitors adding pH-drift experiments. The different uppercase letters in floating leaves indicate significant differences among control, 0.2 mM AZA and 0.3 mM DIDS. The different lowercase letters in submerged leaves indicate significant differences among control, 0.2mM AZA and 0.3 mM DIDS. n= 4~8.

Titrated acidity

The titratable acidity at dusk and dawn was 14.34 and 14.54 μequiv g^{-1} FW in floating leaves, and there was no significant difference between dusk and dawn (Figure 5). Additionally, the titratable acidity of submerged leaves at dusk and dawn was 8.95 and 9.42 μequiv g^{-1} FW respectively, and there was no significant difference between them (Figure 5).

Discussion

In the present study, floating leaves were shorter, wider and thicker than submerged leaves in acclimating to the aerial environment. However, the morphology of submerged leaves was longer, narrower and thinner than floating leaves, which increases specific leaf area, enhanced the absorption capacity of DIC in water and decrease water flow resistance in flowing water (Maberly and Gontero, 2018; Li et al., 2019). The anatomical structure results were in line with the previous studies showing that the growth

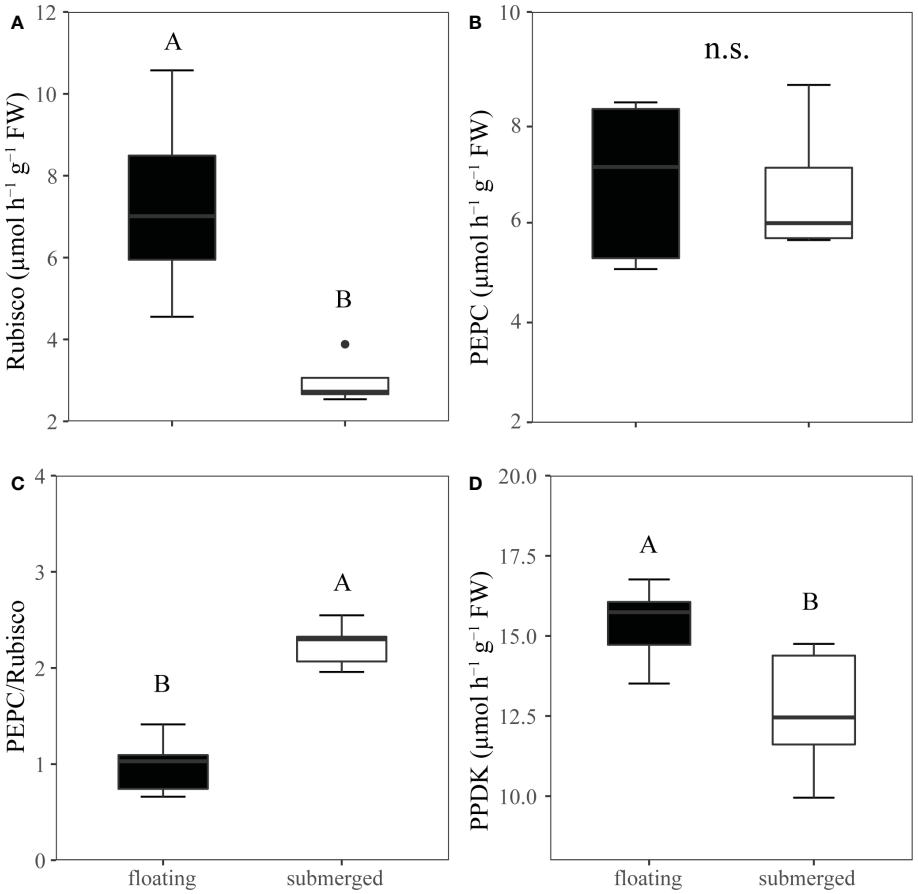

FIGURE 4
Comparison the crude extracts of C3 and C4 metabolic enzyme activities from *O. ovalifolia* in floating and submerged leaves. **(A)** Rubisco, ribulose 1,5-bisphosphate carboxylase–oxygenase. **(B)** PEPC, PEP carboxylase. **(C)** Ratio of PEPC to Rubisco activity. **(D)** PPDK, pyruvate phosphate dikinase. n=5. The different uppercase letters indicate significant differences ($p < 0.05$) between floating leaf and submerged leaf. n.s., not significant.

environment affected the morphology and anatomical structure of submerged and floating leaves (Li et al., 2019; Han et al., 2021; Horiguchi et al., 2021; Wang et al., 2022). Besides, the stomata are important for gas exchange and water loss in the atmosphere. The biggest difference between submerged leaves and floating leaves was that floating leaves had stomata on the adaxial leaf surfaces, while submerged leaves had no stomata, indicating that floating leaves have the ability to directly use atmospheric CO_2 for photosynthesis. The floating leaves can efficiently obtain a stable carbon source through stomata which is one of the development exploitation strategies of aquatic plants to overcome carbon limitation (Maberly and Gontero, 2018; Huang et al., 2020b). This genetic capacity to produce stomata on the upper epidermis of floating leaves is inherited from their terrestrial ancestors and expressed under suitable conditions (Harris et al., 2020) to acclimate to the aerial environment.

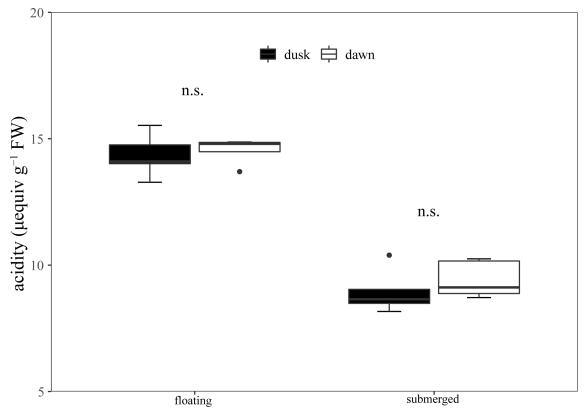

FIGURE 5
Diel changes of titrated acidity in the floating and submerged leaves of *O. ovalifolia*. n.s.: not significant. n = 5.

Photosynthetic pigments are responsible for light absorption and transformation during photosynthesis (Rosevear et al., 2001). The higher content of Chl-b in submerged leaves is in line with the previous studies showing that the chlorophyll content was higher in submerged leaves than that in aerial leaves in hydrophytes (Johnson et al., 1993; Nekrasova et al., 1998). The ratio of Chl-a/b decreases under light limitation (Dale and Causton, 1992; Ronzhina et al., 2004), which can increase the efficiency of light harvesting at very low irradiation (Rosevear et al., 2001). In the present study, the ratio of Chl-a/b in submerged leaves was lower than that in floating leaves, indicating that submerged leaves better adapted to the underwater shading environment (Baig et al., 2005). Meanwhile,

in comparison to the terrestrial plants, the ratio of Chl-a/b was 2.89 in floating leaves that was close to 3 for sunny plants and 2.38 in submerged leaves that was close to 2.3 for shady plants (Lichtenthaler et al., 2007). Both upper and lower epidermal cells containing chloroplasts were presumably beneficial to the submerged leaves absorbing light under a low-irradiance submerged environment. Additionally, transcriptomics studies have found that submerged leaves increase the number of photosynthesis-antenna proteins by increasing the expression of light-harvesting proteins to improve their light-harvesting capacity and better to adapt to the underwater low-light environment (Han et al., 2021). However, in the floating leaves, the absence of chloroplast in the upper epidermal cells could protect against photo-damage under high irradiance. Further, the higher content of anthocyanins also suggested that the floating leaves of *O. ovalifolia* adapted to the strong optical radiation in aerial environments and could quench the free radicals formed by light (Nielsen and Nielsen, 2006). Our present result was in accordance with the results showing that the higher expression of anthocyanins synthetic genes in floating leaves of the heterophyllous plant *Potamogeton wrightii* and which could be responsible for the higher saturated irradiance of floating leaves than that of submerged leaves (Han et al., 2021).

Previous studies reported that HCO_3^- utilization by aquatic plants provided an additional carbon source for photosynthesis and effectively reduced photorespiration increasing plant primary productivity and growth (Iversen et al., 2019; Li et al., 2021). It was found that HCO_3^- could be utilized in both floating and submerged leaves of *O. cordata* (Cao et al., 2019; Huang et al., 2020b; Wang et al., 2022), a heteroblastic plant from the same genus. In the present study, the final pH of submerged and floating leaves pH-drift experiment of *O. ovalifolia* was higher than 9.5 indicating that both types of leaves had the ability to use HCO_3^- (Fernández et al., 2014; Jiang et al., 2021). The value of CT/Alk after the pH-drift experiment could be used to indicate the HCO_3^- utilization capacity of plants, and the smaller the value, the stronger the utilization capacity (Maberly and Spence, 1983; Madsen and Sand-Jensen, 1991). The lower values of CT/Alk and higher final pH in submerged leaves were similar to previous studies, which suggested that submerged leaves had a stronger ability to use HCO_3^- than floating leaves. Our present results are in accordance with previous studies on *Potamogeton wrightii* and *O. cordata* (Han et al., 2021; Wang et al., 2022).

In this study, the decrease of the final pH of submerged and floating leaves in AZA treatment indicated that the HCO_3^- utilization in *O. ovalifolia* depended on the catalytic activity of CAext. This result was consistent with the catalytic utilization of bicarbonate by CAext in submerged plants of the same genus, *O. alismoides* and *O. cordata* (Huang et al., 2020a; Wang et al., 2022). DIDS, an anion exchanger inhibitor, also inhibited the final pH in the pH-drift experiment, indicating that there was a direct absorption of HCO_3^- by *O. ovalifolia* under our current experimental conditions, which was the same as the result of *O. alismoides* and *O. guanyangensis* (Huang et al., 2020a; Jiang et al., 2021). However, the present result of the DIDS treatment was different from *O. cordata* under DIDS treatment showing that DIDS had no inhibitory effect on the HCO_3^- use in *O. cordata* (Wang et al., 2022). A previous study reported that submerged plants tended to use HCO_3^- through the AE pathway only under very low CO_2 conditions (Axelsson et al., 1995). While the concentration of CO_2 *in-situ* water was ~55 μM that was much lower than that in *O. cordata* growth conditions (510 μM). In addition, studies on *O. guanyangensis* at different locations in a karst river supplied by underground water found that the plant did not induce AE pathway to use HCO_3^- at the upstream with a higher concentration of CO_2, while the AE pathway was induced at the downstream with lower concentrations of CO_2 (Jiang et al., 2021). Thus, the low concentration of CO_2 in the growth conditions could be responsible for the direct use of HCO_3^- *via* AE in the present study.

Besides HCO_3^- use, C4 and CAM pathways are also important amelioration strategies in submerged plants, which can improve the concentration of CO_2 at Rubisco active site and adapt to CO_2 deficiency under water (Madsen and Sand-Jensen, 1991; Klavsen et al., 2011; Maberly and Gontero, 2018; Wang et al., 2022). The slight changes in diel titratable acid of *O. ovalifolia* suggested that both submerged and floating leaves did not perform CAM pathway. It was found that CAM metabolism was induced in *O. alismoides* under high light and low CO_2 conditions (11 μM), while it then disappeared under high light and high CO_2 conditions (286 μM) (Shao et al., 2017). Similar results were found in the floating leaves of *O. cordata* research which the CAM appear in low carbon conditions (15 μM) (Huang et al., 2020b). Nevertheless, when the CO_2 concentration was extremely high in the plants growing environment (510 μM), the CAM was absent in *O. cordata* (Wang et al., 2022). In the present study, the CO_2 concentration of plant growth water was 55 μM, 3.67-fold higher than that in water at air equilibrium conditions (15 μM), which might be the reason why there was no CAM in *O. ovalifolia*. Meanwhile, floating leaves exposed to air use CO_2 more easily in the air for photosynthesis and without water deficiency, so the lack of CAM pathway in *O. ovalifolia* was reasonable.

The $\delta^{13}C$ of atmospheric CO_2 was usually maintained at about −8‰. When plants used atmospheric CO_2 as the sole carbon source for photosynthesis, the $\delta^{13}C$ of C3 plants in the range of −20‰ to −37.5‰ and C4 plants in the range of −10‰ to −17‰ had been reported (Farquhar et al., 1989; von Caemmerer et al., 2014). In our present research, $\delta^{13}C$ of the floating leaf was −30.07‰, indicating that the floating leaf may perform C3 metabolism and utilize atmospheric CO_2 as the main carbon source. Different from floating leaves, submerged leaves are completely immersed in water and cannot contact the atmosphere which results in free CO_2 and HCO_3^- underwater being their potential carbon sources. In the present study, if free CO_2 was the only inorganic carbon source, the $\delta^{13}C$ of C3 and C4 were −37.65‰ and −23.96‰, respectively; if HCO_3^- was the only inorganic carbon source, the $\delta^{13}C$ of C3 and C4 were −29.9‰ and −16.11‰, respectively. However, the free CO_2 concentration in the study water was 55 μM, which was much less than the inorganic carbon of half-saturated photosynthesis (100–200 μM) in submerged plants that force the plant to use heavier ^{13}C isotope and affects the isotope fractionation effect (Farquhar et al., 1989), therefore, it cannot be directly concluded that submerged leaves have a C4 pathway through the $\delta^{13}C$ value. However, based

on the enzyme activity analysis, the submerged leaves of *O. ovalifolia* exhibited carboxylase, PEP regeneration enzyme and decarboxylase activities, which are key enzymes in the C4 process. In addition, the PEPC/Rubisco ratio was 2.24 in submerged leaves and 0.988 in floating leaves. The PEPC/Rubisco ratio in typical terrestrial C3 plants and aquatic plants lacking biochemical concentrating mechanisms was generally less than 1 (Zhang et al., 2014). However, previous studies reported that PEPC and PPDK not only contribute to the C4 pathway, but also could participate in other metabolisms in both C4 and C3 plants (Sheen, 1991; Kawamura et al., 1992; Dong et al., 1998; Rao et al., 2008). The different isoforms of PEPC and PPDK genes expressed patterns and posttranslational regulation (Sheen, 1991; Kawamura et al., 1992; Dong et al., 1998; Rao et al., 2008). In the present study, we did not analyze the sequences of PEPC and PPDK or the gene expression of the different isoforms. Thus, the activities of enzymes seemed to imply that submerged leaves might have the ability to perform C4 metabolic pathway, but it needs more evidence to support it in future works. Further, the PEPC/Rubisco ratio, and the $\delta^{13}C$ isotopic abundance both proved that floating leaves do not have a C4 pathway.

The present study found that *O. ovalifolia* possessed the capacity to use HCO_3^- and the juvenile leaves of *O. ovalifolia* also could perform the C4 pathway to acclimate to low CO_2 underwater and at the adult stage, the floating leave of *O. ovalifolia* could directly use CO_2 from the air, which increases the adaptation range of CO_2 conditions. It is widely accepted that the ability of plants to access and utilize limiting resources, eventually affecting their competitive advantages, is important for their distribution (James et al., 1999; Cavalli et al., 2012). As for the invasive ability of *O. ovalifolia*, it is still necessary to compare its utilization efficiency of inorganic carbon with that of native species and to understand its reproductive strategy and the mechanism of population formation.

Conclusions

In the present study, we investigated how an invasive heteroblastic aquatic plant, *O. ovalifolia*, adapts to aquatic and aerial environments. In morphology and anatomical features, submerged leaves are thinner, narrower and longer to increase inorganic carbon absorption in water by increasing specific surface area, while floating leaves directly absorb CO_2 from the atmosphere through stomata. The difference in chlorophyll and anthocyanin content between submerged and floating leaves is an adaptation to aquatic and aerial environments. There are also differences in CCMs between submerged and floating leaves. Both floating and submerged leaves had the ability to use HCO_3^- by the external carbonic anhydrase catalysis and the AE pathway. Furthermore, the enzyme results implied that submerged leaves might perform C4 metabolism while floating leaves perform the C3 pathway for photosynthesis. In general, HCO_3^- utilization, C4 metabolism and CO_2 absorption are the inorganic carbon utilization strategies for *O. ovalifolia* to cope with the inorganic carbon between aquatic and terrestrial environments, which is conducive to better adaptation to aquatic and terrestrial habitats.

Data availability statement

The raw data supporting the conclusions of this article will be made available by the authors, without undue reservation.

Author contributions

HJ and WL designed the experiments. HJ and ZL performed the experiments. ZL analyzed data and wrote the first edition of the manuscript. PL and JZ modified the manuscript. All authors contributed to the article and approved the submitted version.

Funding

This research was supported by the National Natural Science Foundation of China (32120103002), the Strategic Priority Research Program of Chinese Academy of Sciences (XDB31000000), and the Youth Innovation Promotion Association CAS (2021340).

Acknowledgments

We would like to thank Li Chen from the Public Laboratory Platform, WBGCAS for helping with instruments operation.

Conflict of interest

The authors declare that the research was conducted in the absence of any commercial or financial relationships that could be construed as a potential conflict of interest.

Publisher's note

Supplementary material

The Supplementary Material for this article can be found online at: https://www.frontiersin.org/articles/10.3389/fpls.2023.1142848/full#supplementary-material

References

Arber, A. (1919). On heterophylly in water plants. *Am. Nat.* 53, 272–278. doi: 10.1086/279712

Axelsson, L., Ryberg, H., and Beer, S. (1995). Two modes of bicarbonate utilization in the marine green macroalga *Ulva lactuca*. *Plant Cell Environ.* 18, 439–445. doi: 10.1111/j.1365-3040.1995.tb00378.x

Baig, M. J., Anand, A., Mandal, P. K., and Bhatt, R. K. (2005). Irradiance influences contents of photosynthetic pigments and proteins in tropical grasses and legumes. *Photosynthetica* 43 (1), 47–53. doi: 10.1007/s11099-005-7053-5

Beer, S., Bjork, M., Hellblom, F., and Axelsson, L. (2002). Inorganic carbon utilization in marine angiosperms (seagrasses). *Funct. Plant Biol.* 29, 349–354. doi: 10.1071/PP01185

Bowes, G., Rao, S. K., Estavillo, G. M., and Reiskind, J. B. (2002). C4 mechanisms in aquatic angiosperms: Comparisons with terrestrial C4 systems. *Funct. Plant Biol.* 29, 379–392. doi: 10.1071/PP01219

Bowes, G., and Salvucci, M. E. (1989). Plasticity in the photosynthetic carbon metabolism of submerged aquatic macrophytes. *Aquat. Bot.* 34, 233–266. doi: 10.1016/0304-3770(89)90058-2

Cao, Y., Liu, Y., Ndirangu, L., Li, W., Xian, L., and Jiang, H. S. (2019). The analysis of leaf traits of eight *Ottelia* populations and their potential ecosystem functions in karst freshwaters in China. *Front. Plant Sci.* 9. doi: 10.3389/fpls.2018.01938

Cavalli, G., Riis, T., and Baattrup-Pedersen, A. (2012). Bicarbonate use in three aquatic plants. *Aquat. Bot.* 98 (1), 57–60. doi: 10.1016/j.aquabot.2011.12.007

Chambers, P. A., Lacoul, P., Murphy, K. J., and Thomaz, S. M. (2008). Global diversity of aquatic macrophytes in freshwater. *Hydrobiologia* 595, 9–26. doi: 10.1007/s10750-007-9154-6

Clement, R., Dimnet, L., Maberly, S. C., and Gontero, B. (2016). The nature of the CO_2-concentrating mechanisms in a marine diatom, *Thalassiosira pseudonana*. *New Phytol.* 209 (4), 1417–1427. doi: 10.1111/nph.13728

Dale, M., and Causton, D. (1992). Use of the chlorophyll a-b ratio as a bioassay for the light environment of a plant. *Funct. Ecol.* 6, 190–196. doi: 10.2307/2389754

Dong, L., Masuda, T., Kawamura, T., Hata, S., and Izui, K. (1998). Cloning, expression, and characterization of a root-form phosphoenolpyruvate carboxylase from *Zea mays*: Comparison with the c-4 form enzyme. *Plant Cell Physiol.* 39, 865–873. doi: 10.1093/oxfordjournals.pcp.a029446

Farnese, F. S., Oliveira, J. A., Paiva, E. A. S., Menezes-Silva, P. E., da Silva, A. A., Campos, F. V., et al. (2017). The involvement of nitricoxide in integration of plant physiological and ultrastructural adjustments in response to arsenic. *Front. Plant Sci.* 8. doi: 10.3389/fpls.2017.00516

Farquhar, G. D., Ehleringer, R., and Hubic, K. T. (1989). Carbon isotope discrimination and photosynthesis. *Annu. Rev. Plant Physiol. Plant Mol. Bio.* 40, 503–537. doi: 10.1146/annurev.pp.40.060189.002443

Fernández, P. A., Hurd, C. L., and Roleda, M. Y. (2014). Bicarbonate uptake *via* an anion exchange protein is the main mechanism of inorganic carbon acquisition by the giant kelp *Macrocystis pyrifera* (Laminariales, phaeophyceae) under variable pH. *J. Phycol.* 50 (6), 998–1008. doi: 10.1111/jpy.12247

Giordano, M., Beardall, J., and Raven, J. A. (2005). CO2 concentrating mechanisms in algae: Mechanisms, environmental modulation, and evolution. *Annu. Rev. Plant Biol.* 56, 99–131. doi: 10.1146/annurev.arplant.56.032604.144052

Han, S., Maberly, S. C., Gontero, B., Xing, Z., Li, W., Jiang, H. S., et al. (2020). Structural basis for C4 photosynthesis without kranz anatomy in leaves of the submerged freshwater plant *Ottelia alismoides*. *Ann. Bot.* 125, 869–879. doi: 10.1093/aob/mcaa005

Han, S., Xing, Z., Jiang, H. S., Li, W., and Huang, W. (2021). Biological adaptive mechanisms displayed by a freshwater plant to live in aquatic and terrestrial environments. *Environ. Exp. Bot.* 191. doi: 10.1016/j.envexpbot.2021.104623

Harris, B. J., Harrison, C. J., Hetherington, A. M., and Williams, T. A. (2020). Phylogenomic evidence for the monophyly of bryophytes and the reductive evolution of stomata. *Curr. Biol.* 30, 2001–2012. doi: 10.1016/j.cub.2020.03.048

Horiguchi, G., Matsumoto, K., Nemoto, K., Inokuchi, M., and Hirotsu, N. (2021). Transition from proto-kranz-type photosynthesis to HCO_3^- use photosynthesis in the amphibious plant *Hygrophila polysperma*. *Front. Plant Sci.* 12. doi: 10.3389/fpls.2021.675507

Huang, W., Han, S., Jiang, H. S., Gu, S., Li, W., Gontero, B., et al. (2020a). External alpha-carbonic anhydrase and solute carrier 4 are required for bicarbonate uptake in a freshwater angiosperm. *J. Exp. Bot.* 71 (19), 6004–6014. doi: 10.1093/jxb/eraa351

Huang, W., Han, S., Xing, Z., and Li, W. (2020b). Responses of leaf anatomy and CO_2 concentrating mechanisms of the aquatic plant *Ottelia cordata* to variable CO_2. *Front. Plant Sci.* 11. doi: 10.3389/fpls.2020.01261

Hussner, A. (2012). Alien aquatic plant species in European countries. *Weed Res.* 52 (4), 297–306. doi: 10.1111/j.1365-3180.2012.00926.x

Iversen, L. L., Winkel, A., Baastrup-Spohr, L., Hinke, B. A., Alahuhta, J., Baattrup-Pedersen, A., et al. (2019). Catchment properties and the photosynthetic trait composition of freshwater plant communities. *Science* 366 (6467), 878–881. doi: 10.1126/science.aay5945

James, C. S., Eaton, J. W., and Hardwick, K. (1999). Competition between three submerged macrophytes, *Elodea canadensis* michx, *Elodea nuttallii* (Planch.) St John and *Lagarosiphon major* (Ridl.) moss. *Hydrobiologia* 415, 35–40. doi: 10.1023/A:1003802205092

Jiang, H. S., Jin, Q., Li, P., Zhao, S., Liao, Z., Yin, L., et al. (2021). Different mechanisms of bicarbonate use affect carbon isotope composition in *Ottelia guayangensis* and *Vallisneria denseserrulata* in a karst stream. *Aquat. Bot.* 168. doi: 10.1016/j.aquabot.2020.103310

Johnson, G. N., Scholes, J. D., Horton, P., and Young, A. J. (1993). Relationships between carotenoid composition and growthhabit in British plant species. *Plant Cell Environ.* 16, 681–686. doi: 10.1111/j.1365-3040.1993.tb00486.x

Kawamura, T., Shigesada, K., Toh, H., Okumura, S., Yanagisawa, S., and Izui, K. (1992). Molecular evolution of phosphoenolpyruvate carboxylase for C4 photosynthesis in maize comparison of its cDNA sequence with a newly isolated cDNA encoding an isozyme involved in the anaplerotic function. *J. Biochem.* 112, 147–154. doi: 10.1093/oxfordjournals.jbchem.a123855

Khan, R., Ma, X., Hussain, Q., Asim, M., Iqbal, A., Ren., X., et al. (2022). Application of 2,4-epibrassinolide improves drought tolerance in tobacco through physiological and biochemical mechanisms. *Biol. (Basel)* 11, (8). doi: 10.3390/biology11081192

Klavsen, S. K., Madsen, T. V., and Maberly, S. C. (2011). Crassulacean acid metabolism in the context of other carbon-concentrating mechanisms in freshwater plants: a review. *Photosynth. Res.* 109 (1-3), 269–279. doi: 10.1007/s11120-011-9630-8

Lara, M. V., Casati, P., and Andreo, C. S. (2002). CO_2-concentrating mechanisms in *Egeria densa*, a submersed aquatic plant. *Physiol. Plant* 115, 487–495. doi: 10.1034/j.1399-3054.2002.1150402.x

Li, S. L., Calmels, D., Han, G., Gaillardet, J., and Liu, C. Q. (2008). Sulfuric acid as an agent of carbonate weathering constrained by $\delta^{13}C$ DIC: Examples from southwest China. *Earth Planet. Sci. Lett.* 270 (3-4), 189–199. doi: 10.1016/j.epsl.2008.02.039

Li, G., Hu, S., Hou, H., and Kimura, S. (2019). Heterophylly: Phenotypic plasticity of leaf shape in aquatic and amphibious plants. *Plants (Basel)* 8, 420. doi: 10.3390/plants8100420

Li, P., Liao, Z., Zhou, J., Yin, L., Jiang, H. S., and Li, W. (2021). Bicarbonate-use by aquatic macrophytes allows a reduction in photorespiration at low CO_2 concentrations. *Environ. Exp. Bot.* 188. doi: 10.1016/j.envexpbot.2021.104520

Lichtenthaler, H. K., Ac, A., Marek, M. V., Kalina, J., and Urban, O. (2007). Differences in pigment composition, photosynthetic rates and chlorophyll fluorescence images of sun and shade leaves of four tree species. *Plant Physiol. Biochem.* 45 (8), 577–588. doi: 10.1016/j.plaphy.2007.04.006

Maberly, S. C., and Gontero, B. (2017). Ecological imperatives for aquatic CO_2-concentrating mechanisms. *J. Exp. Bot.* 68 (14), 3797–3814. doi: 10.1093/jxb/erx201

Maberly, S. C., and Gontero, B. (2018). "Trade-offs and synergies in the structural and functional characteristics of leaves photosynthesizing in aquatic environments," in *The leaf: A platform for performing photosynthesis*. Eds. III. W.W. Adams and I. Terashima (Cham: Springer International Publishing), 307–343. doi: 10.1007/978-3-319-93594-2_11

Maberly, S., and Madsen, T. (1998). Affinity for CO_2 in relation to the ability of freshwater macrophytes to use HCO_3^-. *Funct. Ecol.* 12, 99–106. doi: 10.1046/j.1365-2435.1998.00172.x

Maberly, S. C., and Spence, D. H. N. (1983). Photosynthetic inorganic carbon use by freshwater plants. *J. Ecol.* 71, 705–724. doi: 10.2307/2259587

Madsen, T., and Sand-Jensen, K. (1991). Photosynthetic carbon assimilation in aquatic macrophytes. *Aquat. Bot.* 41, 5–40. doi: 10.1016/0304-3770(91)90037-6

McCullough, C. (1997). A review of the aquatic macrophyte family hydrocharitaceae (angiospermae) in new Zealand. *Tane* 36, 181–195.

Mook, W. G., Bommerson, J. C., and Staverman, W. H. (1974). Carbon isotope fractionation between dissolved bicarbonate and gaseous carbon dioxide. *Earth Planet. Sci. Lett.* 22, 169–176. doi: 10.1016/0012-821X(74)90078-8

Nekrasova, G. F., Ronzhina, D. A., and Korobitsina, E. B. (1998). Photosynthetic apparatus in developing submerged, floating, and aerial leaves of hydrophytes. *Russ J. Plant Physl+* 45 (4), 456–464. doi: 10.1016/S0034-6667(98)00012-8

Nielsen, S. L., and Nielsen, H. D. (2006). Pigments, photosynthesis and photoinhibition in two amphibious plants: consequences of varying carbon availability. *New Phytol.* 170 (2), 311–319. doi: 10.1111/j.1469-8137.2006.01670.x

Paice, R. L., Chambers, J. M., and Robson, B. J. (2017a). Native submerged macrophyte distribution in seasonally-flowing, south-western Australian streams in relation to stream condition. *Aquat. Sci.* 79 (1), 171–185. doi: 10.1007/s00027-016-0488-x

Paice, R. L., Chambers, J. M., and Robson, B. J. (2017b). Potential of submerged macrophytes to support food webs in lowland agricultural streams. *Mar. Freshw. Res.* 68, (3). doi: 10.1071/mf15391

Rao, S. K., Reiskind, J. B., and Bowes, G. (2008). Kinetic analyses of recombinant isoforms of phosphoenolpyruvate carboxylase from *Hydrilla verticillata* leaves and the impact of substituting a C4-signature serine. *Plant Sci.* 174, 475–483. doi: 10.1016/j.plantsci.2008.01.010

Raven, J. A. (1970). Exogenous inorganic caron sources in plant photosynthesis. *Biol. Rev. Biol. Proc. Camb. Philos. Soc* 45, 167–221. doi: 10.1111/j.1469-185X.1970.tb01629.x

Ronzhina, D. A., Nekrasova, G. F., and P'yankov, V. I. (2004). Comparative characterization of the pigment complex in emergen floating and submerged leaves of hydrophytes. *Russ J. Plant Physl+* 51 (1), 21–24. doi: 10.1023/B:RUPP.0000011299.93961.8f

Rosevear, M. J., Young, A. J., and Johnson, G. N. (2001). Growth conditions are more important than species origin in determining leaf pigment content of British plant species. *Funct. Ecol.* 15, 474–480. doi: 10.1046/j.0269-8463.2001.00540.x

Shao, H., Gontero, B., Maberly, S. C., Jiang, H. S., Cao, Y., Li, W., et al. (2017). Responses of *Ottelia alismoides*, an aquatic plant with three CCMs, to variable CO_2 and light. *J. Exp. Bot.* 68 (14), 3985–3995. doi: 10.1093/jxb/erx064

Sheen, J. (1991). Molecular mechanisms underlying the differential expression of maize pyruvate, orthophosphate dikinase genes. *Plant Cell* 3, 225–245. doi: 10.1105/tpc.3.3.225

Solfanelli, C., Poggi, A., Loreti, E., Alpi, A., and Perata, P. (2006). Sucrose-specific induction of the anthocyanin biosynthetic pathway in arabidopsis. *Plant Physiol.* 140 (2), 637–646. doi: 10.1104/pp.105.072579

Sousa, W. T. Z. (2011). *Hydrilla verticillata* (Hydrocharitaceae), a recent invader threatening brazil's freshwater environments: A review of the extent of the problem. *Hydrobiologia* 669 (1), 1–20. doi: 10.1007/s10750-011-0696-2

Vogelmann, T. C., and Gorton, H. L. (2014). "Leaf: Light capture in the photosynthetic organ," in *Advances in photosynthesis and respiration*, vol. 39 . Ed. M. Hohmann-Marriott (U.S.A.: Dordrecht: Springer), 363–377. doi: 10.1007/978-94-017-8742-0_19

von Caemmerer, S., Ghannoum, O., Pengelly, J. J., and Cousins, A. B. (2014). Carbon isotope discrimination as a tool to explore C4 photosynthesis. *J. Exp. Bot.* 65 (13), 3459–3470. doi: 10.1093/jxb/eru127

Wang, S., Li, P., Liao, Z., Wang, W., Chen, T., Yin, L., et al. (2022). Adaptation of inorganic carbon utilization strategies in submerged and floating leaves of heteroblastic plant *Ottelia cordata*. *Envir. Exp. Bot.* 196. doi: 10.1016/j.envexpbot.2022.104818

Wang, H., Wang, Q., Bowler, P., and Xiong, W. (2016). Invasive aquatic plants in China. *Aquat. Invasions* 11 (1), 1–9. doi: 10.3391/ai.2016.11.1.01

Yin, L., Li, W., Madsen, T. V., Maberly, S. C., and Bowes, G. (2017). Photosynthetic inorganic carbon acquisition in 30 freshwater macrophytes. *Aquat. Bot.* 140, 48–54. doi: 10.1016/j.aquabot.2016.05.002

Zhang, Y., Yin, L., Jiang, H. S., Li, W., Gontero, B., and Maberly, S. C. (2014). Biochemical and biophysical CO_2 concentrating mechanisms in two species of freshwater macrophyte within the genus *Ottelia* (Hydrocharitaceae). *Photosynth. Res.* 121 (2-3), 285–297. doi: 10.1007/s11120-013-9950-y

frontiers | Frontiers in Plant Science

TYPE Original Research
PUBLISHED 12 June 2023
DOI 10.3389/fpls.2023.1186537

OPEN ACCESS

EDITED BY
Justine Marchand,
Le Mans Université, France

REVIEWED BY
Gallo Carmela,
National Research Council (CNR), Italy
Manoj Kumar,
University of Technology Sydney, Australia

*CORRESPONDENCE
Valeria Villanova
valeria.villanova@unipa.it
Jonathan Armand Charles Roques
jonathan.roques@bioenv.gu.se

RECEIVED 14 March 2023
ACCEPTED 17 May 2023
PUBLISHED 12 June 2023

CITATION
Villanova V, Roques JAC, Forghani B, Shaikh KM, Undeland I and Spetea C (2023) Two-phase microalgae cultivation for RAS water remediation and high-value biomass production.
Front. Plant Sci. 14:1186537.
doi: 10.3389/fpls.2023.1186537

Two-phase microalgae cultivation for RAS water remediation and high-value biomass production

Valeria Villanova[1,2]*, Jonathan Armand Charles Roques[1,3]*, Bita Forghani[4], Kashif Mohd Shaikh[1], Ingrid Undeland[4] and Cornelia Spetea[1]

[1]Department of Biological and Environmental Sciences, University of Gothenburg, Gothenburg, Sweden, [2]Department of Biological, Chemical and Pharmaceutical Sciences and Technologies (STEBICEF), University of Palermo, Palermo, Italy, [3]SWEMARC, The Swedish Mariculture Research Center, University of Gothenburg, Gothenburg, Sweden, [4]Department of Life Sciences-Food and Nutrition Science, Chalmers University of Technology, Gothenburg, Sweden

The overall goal of this study was to provide solutions to innovative microalgae-based technology for wastewater remediation in a cold-water recirculating marine aquaculture system (RAS). This is based on the novel concept of integrated aquaculture systems in which fish nutrient-rich rearing water will be used for microalgae cultivation. The produced biomass can be used as fish feed, while the cleaned water can be reused, to create a highly eco-sustainable circular economy. Here, we tested three microalgae species *Nannochloropis granulata* (*Ng*), *Phaeodactylum tricornutum* (*Pt*), and *Chlorella sp* (*Csp*) for their ability to remove nitrogen and phosphate from the RAS wastewater and simultaneously produce high-value biomass, i.e., containing amino acids (AA), carotenoids, and polyunsaturated fatty acids (PUFAs). A high yield and value of biomass were achieved for all species in a two-phase cultivation strategy: *i)* a first phase using a medium optimized for best growth (f/2 14x, control); *ii)* a second "stress" phase using the RAS wastewater to enhance the production of high-value metabolites. *Ng* and *Pt* performed best in terms of biomass yield (i.e., 5-6 g of dry weight, DW.L^{-1}) and efficient cleaning of the RAS wastewater from nitrite, nitrate, and phosphate (i.e., 100% removal). *Csp* produced about 3 g L^{-1} of DW and reduced efficiently only nitrate, and phosphate (i.e., about 76% and 100% removal, respectively). The biomass of all strains was rich in protein (30-40 % of DW) containing all the essential AA except Methionine. The biomass of all three species was also rich in PUFAs. Finally, all tested species are excellent sources of antioxidant carotenoids, including fucoxanthin (*Pt*), lutein (*Ng* and *Csp*) and *β*-carotene (*Csp*). All tested species in our novel two-phase cultivation strategy thus showed great potential to treat marine RAS wastewater and provide sustainable alternatives to animal and plant proteins with extra added values.

KEYWORDS

Carotenoids, *Chlorella*, *Nannochloropsis*, *Phaedactylum tricornum*, proteins, PUFA, RAS wastewater, two-phase cultivation

1 Introduction

Over the last 40 years, aquaculture has become one of the fastest-developing food-production activities worldwide (FAO, 2022). To satisfy the growing demands for fish with high nutritional values (i.e., high content of proteins and long chain omega-3 (n-3) polyunsaturated fatty acids, LC n-3 PUFAs), the aquaculture sector needs sustainable development. Two of the main current bottlenecks encountered by this industry are the treatment of the wastes produced by the fish, and the need for fish sustainably produced feed (Lenzi, 2013).

The intensification of the aquaculture industry mostly using open-water systems has led to some environmental concerns, such as the eutrophication caused by the leakage of nitrogen-rich nutrients into the environment, (Pahri et al., 2015). Land-based closed containment systems such as recirculating aquaculture systems (RAS) are better alternatives as they allow for a high degree of water reuse as well as ensure better control of the farming practices (Van Rijn, 2013; Ahmad et al., 2021; Ahmed and Turchini, 2021; Øvrebø et al., 2022).

At present, in RAS, nitrifying bacteria convert the ammonium (NH_4^+) produced by the fish into nitrate (NO_3^-), *via* nitrite (NO_2^-), in the presence of oxygen (O_2). As a result, NO_3^- can slowly accumulate over time and reach concentrations that could affect the fish's health and welfare (Camargo et al., 2005; Roques, 2013; Van Rijn, 2013; Roques et al., 2021). High NO_3^- can later be managed through the biological conversion of NO_3^- to nitrogen gas (N_2) in anaerobic biofilters with denitrifying bacteria, anammox bacteria, or by regular water exchanges (Chen, 2002; Preena et al., 2021; Micolucci et al., 2023). The use of microalgae as a filter could be a promising alternative or complement to the current water remediation techniques, and in addition the biomass obtained could, later, be valorised into animal feed or feed supplements (Tejido-Nuñez et al., 2019; Tossavainen et al., 2019; Villar-Navarro et al., 2022).

In the last decades, the demand for fish meal and oils, mainly produced from the catch of small pelagic fish species, as aquaculture feedstock has increased tremendously (World Bank, 2013; FAO, 2020). However, the massive use of fish at the base of the marine food chain has led to increased prices and a shortage of natural fish stocks. Rapidly, plant-derived protein and oils have therefore been introduced as fish feed ingredients. However, their utilization is limited by the presence of a wide variety of anti-nutritional substances (Francis et al., 2001). In addition, the production of plant-derived protein and oils for fish feed requires arable lands and freshwater, which are both limited and could be instead directly used for human consumption (Hardy, 2010; Flachowsky et al., 2017; FAO, 2020). Therefore, alternative technologies such as microalgae cultivation has great potential as an eco-sustainable source of fish feed (Camacho-Rodríguez et al., 2018).

Microalgae are currently used in the aquaculture sector as live feed for different marine organisms, such as zooplankton, molluscs, crustaceans, and some species of fish (Koyande et al., 2019). The interest for use of microalgae in the food sector is because some species are as rich in proteins as food sources of animal (e.g., meat, fish, eggs, and milk) and vegetable origin (e.g., soy, Bleakley and Hayes, 2017). Microalgae are also a source of LC n-3 PUFAs (e.g., eicosapentaenoic acid, EPA, and docosahexaenoic acid, DHA), important for both fish and human health. However, the cultivation and harvesting of large volumes of microalgae, as well as the extraction of the molecules of interest, are energy-consuming and expensive processes. For this reason, despite their abundant presence in nature, to date, only a few marine species are marketed and used in the food industry as biomass (e.g. including species from the genus *Nannochloropsis*, *Phaeodactylum*, and *Chlorella*) or as extracts (e.g., β- carotene, fucoxanthin, EPA, DHA, proteins) (Sathasivam et al., 2019). Microalgae are also a sustainable alternative to heterotrophic bacteria and chemicals in wastewater treatment. Indeed, some microalgae species can convert both inorganic and organic pollutants from wastewater into high-value molecules (Samer, 2015).

Here, we investigated the ability of three industrially relevant microalgae species; *Nannochloropsis granulata* (*Ng*), *Phaeodactylum tricornutum* (*Pt*) and *Chlorella sp* (*Csp*) to grow in wastewater from a RAS producing high-value metabolites and at the same time cleaning the water. *Ng* and *Pt* are marine microalgae able to produce biomass enriched in EPA-rich lipids if grown under specific conditions (Abida et al., 2015; Villanova et al., 2017; Cheregi et al., 2021; Villanova et al., 2022). *Csp* can grow and significantly reduce both inorganic nitrogen and phosphorus in various types of wastewater (Asadi et al., 2019; Lima et al., 2020). For this reason, a strain of the genus previously isolated from a Sicilian coastline *Csp* was also included in this study (Arena et al., 2021). Moreover, the three selected species are rich in high-value carotenoids such as fucoxanthin and β-carotene, whose concentrations vary with the growth conditions (Arena et al., 2021; Villanova et al., 2021b; Villanova et al., 2022). A two-phase cultivation strategy was applied to obtain high-yield and high-quality biomass. At the end of the 19-22 days cultivation, the biochemical composition of the biomass and the nutrient removal efficiency were determined and compared among the strains.

2 Materials and methods

2.1 Microalgal species and preculture cultivation

The microalgae species used in this study were *Ng*, *Pt*, and *Csp*, obtained from the Gothenburg University Marine Algal Culture Collection (GUMACC https://www.gu.se/en/marina-vetenskaper/about-us/algal-bankgumacc, accessed on 1 March 2023). The cultures were not axenic, but 100 μg L^{-1} of ampicillin was added at the beginning of the cultivation to control the bacterial growth.

Precultures were maintained in 100 mL flasks at 16°C, with a light intensity of about 20 μmol photons m^{-2} s^{-1} and a 12/12 h light/dark cycle. The medium used was natural seawater collected from a depth of 30 m at the Tjärnö Research Station (University of Gothenburg, Strömstad, Sweden) supplemented with 14-fold concentrated nutrients (f/2 14x) to obtain a high concentration of biomass (Villanova et al., 2022). The seawater was filtered using two 0.4 μm GF/F glass fibre filters, the salinity was adjusted with deionized water to 26 practical salinity units (PSU), and it was

sterilized by autoclaving at 121°C for 20 min. Finally, the nutrient stock solution from the standard f/2 marine cultivation medium ($NaNO_3$, NaH_2PO_4, microelements, vitamins, Guillard and Ryther, 1962) was sterilized with cellulose filter paper (with a pore size of 0.22 µm) and 14 mL of each stock solution was added to 1 L of autoclaved seawater.

2.2 RAS wastewater

RAS wastewater (10 L, Table 1) was collected from the aquarium facilities of the University of Gothenburg (Gothenburg, Sweden), hosting a pilot scale research and development facility for the development of land-based seawater RAS at low temperatures (ca. 10°C). The fish species in the marine RAS were rainbow trout (*Oncorhynchus mykiss*) and Atlantic wolffish (*Anarhichas lupus*). In June 2020, the RAS wastewater was first filtered and then stored in 5 L plastic containers at 4°C until use. A subsample of filtered water was used for physiochemical characterization. The pH and salinity were measured using a Multimeter (pHenomenal MU 6100 H, VWR International, Radnor, PA, USA). The subsample was subsequently frozen (-80°C) and sent for determination of NH_4^+-N, NO_2^--N, NO_3^--N, and PO_4^{3-}-P to an accredited laboratory (Eurofins, Linköping, Sweden). Table 1 shows the physiochemical characterization of both RAS wastewater and f/2 14x before algae cultivation. Nitrogen is one of the most important nutrients for microalgae growth (Abida et al., 2015) for this reason the same concentration of $NaNO_3$ in f/2 14x was added to RAS wastewater in one-phase cultivation.

2.3 One-phase cultivation

Ng and *Pt* were grown in f/2 14x or RAS wastewater added with 14-fold concentrated $NaNO_3$ (14N) using a Multicultivator MC 1000 OD (Photon System Instruments, Drásov, Check Republic) in flasks containing 80 mL of liquid culture at 22°C with a constant light intensity of 100 µmol photons m^{-2} s^{-1} and with air bubbling. The cultures were grown in triplicates until the stationary phase was reached (i.e., 18 days).

2.4 Two-phase cultivation

Ng, *Pt*, and *Csp* were grown in the Multicultivator system described above. A two-phase-cultivation mode was used, which includes a first phase (phase I) using a medium and conditions for optimized growth to reach high biomass, and a second phase (phase II) using the RAS wastewater and stress conditions to stimulate the production of secondary metabolites. The experimental design of the two-phase cultivation is summarized in Figure 1. In phase I, the cultures were grown in f/2 14x at 22°C and the intensity of the light (cool white light) was increased over 19-22 days gradually from 100 to 800 µmol photons m^{-2} s^{-1}, according to the specific algal growth performance. Phase I ended when the stationary phase was reached (19-22 days). In phase II, 40 mL cultures from phase I were inoculated in new flasks containing 40 mL of RAS wastewater. It contains inorganic nitrogen only in low concentrations and is relatively high in salinity, factors that can be stressful for microalgae growth but can produce high concentrations of certain molecules of interest, e.g., lipids and carotenoids. By contrast the phosphate concentration was the same in both 14x and RAS wastewater. These new cultures were grown at the same temperature as the RAS was maintained (10°C) and at a constant light intensity of 40 µmol photons m^{-2} s^{-1}. The experiment ended when the stationary phase was reached (9-12 days). Four replicates of *Ng* and *Pt*, and two replicates of *Csp* were grown in parallel.

Algal growth was monitored every two days by measuring chlorophyll *a* fluorescence expressed in relative fluorescence units (RFU), using a Varioscan Flash Multimode Reader (Thermo Fisher Scientific, Vantaa, Finland), in a 96-well microplate. A total of 250 µL of each sample was added into separate wells of the microplate (in triplicate) and incubated for 10 min in darkness. Dilutions were performed when required (i.e., RFU > 30). Chlorophyll fluorescence was detected using a wavelength of 425 nm for excitation and 680 nm for emission (Cheregi et al., 2021; Villanova et al., 2022). In addition, the growth of both bacteria and algae was monitored as absorbance at 750 nm using a Thermo Scientific Evolution 60S UV-Visible Spectrophotometer (Thermo Fisher Scientific, Vantaa, Finland).

After the stationary phase was reached in both cultivation phases, the biomass yield was determined and expressed as g of dry weight (DW) L^{-1}. A total of 5 mL of final cultures was filtered through pre-weighted dried GF/F (47 mm) Whatman filters (Cytiva, Marlborough, MA, USA), and then washed with 10 mL of 0.5 M ammonium carbonate to remove the excess salt. Finally, the filters containing the culture were incubated at 100°C for 24 h and weighed for DW determination according to the following formula:

$$DW\ (g) = \frac{(weight\ (filter + biomass,\ in\ g)) - (weight\ of\ filter,\ in\ g)}{0.005\ L\ (volume\ of\ filtered\ culture)}$$

Moreover, at the end of the two-phase cultivation, cells were collected by centrifugation and the pellets were immediately freeze-dried for further analysis.

TABLE 1 Physicochemical characteristics of the RAS wastewater and f/2 14x prior algae cultivation.

Parameter	Salinity (PSU)	pH	NH_4^+ (mg-N L^{-1})	NO_2^- (mg-N L^{-1})	NO_3^- (mg-N L^{-1})	PO_4^{3-} (mg-P L^{-1})
Method	Multimeter	Multimeter	ISO 15923-1:2013 Annex B	SS-EN ISO 13395:1997	SS-EN ISO 13395:1997	ISO 15923-1:2013 Annex F
RAS wastewater	34	5.45	0.87	0.0021	100	70
f/2 14x medium	26	8	0	0	1050	70

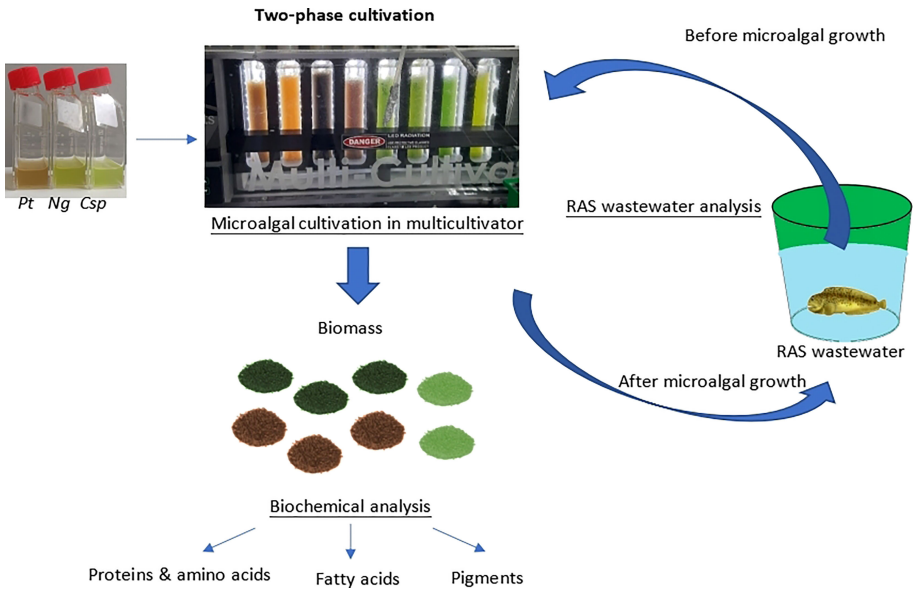

FIGURE 1
Overview of two-phase microalgae cultivation for cleaning of RAS wastewater and production of high-value biomass. *Ng*, *Nannochloropsis granulata*, *Pt*, *Phaeodactylum tricornutum*, and *Csp*, *Chlorella sp.*

2.5 RAS wastewater analysis before and after cultivation

On the first and last day of growth in phase II cultivation, cells were centrifuged for 5 min at 4000 *g* and the supernatant was collected and filtered. The supernatants were analysed immediately or preserved at -20°C until analysis.

The total nitrogen (TN) was calculated based on the concentrations of NH_4^+, NO_2^-, and NO_3^-. Salinity and pH were measured using a multimeter (pHenomenal MU 6100 H, VWR International, PA, Radnor, USA). The NH_4^+ and NO_2^- concentrations were determined using the powder pillow methods (salicylate method, 8155, and diazotization method, 8507, respectively, Hach-Lange, Dusseldorf, Germany) and the DR-2800 (Hach-Lange, Dusseldorf, Germany). The concentrations of (NO_3^- were determined using ion-exchange chromatography (HPLC 20A; Shimadzu, Kyoto, Japan) with a Shodex Asahipak NH2P-50 4D anion column (Showa Denko, Tokyo, Japan) and UV-VIS detector (SPD-20AV, Shimadzu) after filtration of samples through 0.2-µm pore-size PTFE membranes (Advantec, Tokyo, Japan) (Mojiri et al., 2020). The detection limits were 0.01, 0.002, and 0.5 mg-N L^{-1} for NH_4^+, NO_2^- and NO_3^-, respectively. Finally, PO_4^{3-} analysis was done using a commercial kit (114842 Spectroquant, Merck, Darmstadt, Germany) according to the manufacturer's recommendations (detection limit: 0.5 mg-P P L^{-1}). The data are presented as means ± standard deviation of four replicates of the supernatant from *Ng* and *Pt*, and two replicates of *Csp* and expressed as removal efficiency relative to the initial nutrient concentration (Table 2).

2.6 Biochemical analysis of the biomass

2.6.1 Protein content and amino acid composition

Freeze-dried biomass was bead-beaten for 2 min at 30 Hz (QIAGEN Tissuelyser II, Qiagen, Hilden, Germany) before the determination of total protein content. The total protein content of microalgal extracts was then determined by colorimetric analysis at 750 nm using the DC protein kit (Bio-Rad Laboratories, Hercules, CA, USA) following a sequential hot trichloroacetic acid (TCA) and alkaline extraction of the biomass (Slocombe et al., 2013). For the quantification, a standard curve of bovine serum albumin in the range of 0.225–1.35 mg L^{-1} was used.

For the determination of amino acid (AA) content, a known amount of freeze-dried biomass was resuspended in 4 mL of 6 N HCl in glass tubes followed by flushing with nitrogen gas for 30 s.

TABLE 2 Removal efficiency of total nitrogen (TN), NH_4^+, NO_2^-, NO_3^- ad PO_4^{3-} at the end of phase II.

Species	TN removal (%)	NH_4^+ removal (%)	NO_2^- removal (%)	NO_3^- removal (%)	PO_4^{3-} removal (%)
Nannochloropsis granulata	85.4 ± 11.4	41.2 ± 18.0	100.0 ± 0.0	100.0 ± 0.0	100.0 ± 0.0
Phaeodactylum tricornutum	86.7 ± 3.5	27.5 ± 14.8	100.0 ± 0.0	100.0 ± 0.0	100.0 ± 0.0
Chlorella sp	50.0 ± 2.8	-*	-*	75.7 ± 1.4	100.0 ± 0.0

Data are presented as means ± standard deviation of two to four biological replicates. *Increase of in the nutrient concentration as compared to the initial condition.

The samples were then hydrolysed at 110°C for 24 h, after which they were filtered (syringe filter, PES, 0.2 µm) (VWR, Radnor, PA, USA) and diluted before AA determination using LC/APCI-MS as described previously (Forghani et al., 2022). All analyses were performed in duplicate.

2.6.2 Fatty acid content and composition

Freeze-dried biomass was powdered and put into pre-weighed furnaced glass tubes. Fatty acids (FAs) were then extracted and methylated as previously described (Forghani et al., 2022). A known amount of powdered biomass was suspended in 400 µL of chloroform, and 200 µL of internal standard (i.e., heptadecanoic acid 100 µL mL^{-1}) was added to the tubes. Samples were sonicated on ice for 1 h and transesterification was performed by adding 0.75 mL of HCl/MeOH (5% v/v) and incubating at 90°C for 90 min. After cooling, FA methyl esters (FAMEs) were extracted by adding 2 mL of hexane and mixing vigorously for 30 s followed by shaking at 300g for 20 min. The samples were then centrifugated at 2000g for 5 min and the upper phase was transferred into a clean tube. The extraction was repeated one more time for increasing the recovery of FAMEs. After the evaporation of hexane, measurement of FAMEs was carried out by using an Agilent Technologies 7890 A GC system connected to Agilent Technologies 5975 inert MSD (Kista, Sweden). Acquisition, identification, and quantification of FAME peaks were performed by their comparison with the 37-component FAME standard mix (Supelco, Bellefonte, PA, USA, Cavonius et al., 2014) by using Masshunter Quantitative Analysis software (version B.09.00, Agilent Technologies, Santa Clara, CA, USA). FA analyses were done in duplicate.

2.6.3 Pigment composition

A known amount of freeze-dried biomass was mixed with 5 mL of 90% (v/v) acetone in falcon tubes covered with aluminium foil to prevent light penetration. The samples were ground in a glass homogenizer and incubated at 4°C for 4 h. After this period, the samples were centrifuged at 3000 g for 5 min. The supernatant was filtered using a filter with a pore size of 0.2 µm and used for pigment analysis. The pigment composition was obtained by using HPLC coupled with a PDA detector (Villanova et al., 2022). 100 µL of samples were analysed in a Shimadzu UFLC system (Shimadzu corporation, Kyoto, Japan) equipped with an Alltima C18 (RP18, ODS, Octadecyl) 150 × 4.6 mm column. The pigments were eluted through a low-pressure gradient system constituted by solvent A with methanol and 0.5 M ammonium acetate buffer (85:15, v/v), solvent B with acetonitrile and milliQ water (90:10, v/v), and solvent C with 100% ethyl acetate. The following program was used: 100% B:0% C: (8 min), 90% B:10% C: (8.6 min), 65% B:35% C (13.1 min), 31% B:69% C (21 min), and 100% B:0% C (27 min). The identification of pigments was done by comparison of their retention time and spectra with standards (DHI, Hørsholm, Denmark) run under the same conditions. The quantification of the pigment concentration was then obtained by comparing the area of the corresponding standard. The pigment concentration was then normalized for freeze-dried biomass and expressed as µg mg^{-1} of DW. Four replicates were processed for *Ng* and *Pt*, and duplicates for *Csp* were used.

2.6.4 Statistical analysis

The biochemical composition of the biomass was compared among the different species using a two-way analysis of variance (ANOVA) test (GraphPad 9.5.1 Software, San Diego, CA, USA). *p*-values were used to quantify the variability among the three different species. Differences were considered significant for *p*-values< 0.05.

3 Results

3.1 Microalgal growth in f/2 and RAS wastewater

The physicochemical characteristics of the RAS wastewater and f/2 14x before the start of the algae cultivation were different (Table 1). For this reason, the RAS wastewater composition was slightly adjusted for optimal algae cultivation and the modified substrate named RAS wastewater 14N. As nitrogen compounds, the RAS wastewater contained NH_4^+, NO_2^-, and NO_3^-, but the latter was much less abundant than in f/2 14x. Moreover, RAS wastewater was characterized by lower pH and slightly higher salinity than f/2 14x (Table 1). Therefore, the RAS water was supplemented with NO_3^- and pH was adjusted to reach the same levels as in f/2 14x. In a one-stage cultivation, *Pt* and *Ng* were able to grow in undiluted RAS wastewater 14N similarly to f/2 14x, which can be explained by their similar nutrient composition (Table 1) after a lag phase during the first eight cultivation days (Supplementary File 1A, B). The biomass yields were similar, but *Pt* showed a higher yield than *Ng* in the tested conditions (i.e., 3 and 2 g DW L^{-1}, respectively) (Supplementary File 1C).

To reduce the lag phase and produce a high yield and value of biomass, the three microalgal strains were grown using a two-phase cultivation strategy. The growth conditions used for the different species in two-phase cultivation are shown in Figure 2A-C. Figure 2D-F shows the growth monitored as chlorophyll fluorescence (RFU) along the cultivation time in the two-phase cultivation. *Ng* and *Pt* grew better than *Csp* in phase I. Moreover, after the 1:1 dilution in RAS wastewater in phase II, *Ng* and *Pt* reached a similar RFU as at the end of phase I. In contrast, *Csp* in phase II was not able to recover the maximum RFU obtained in phase I. The dry weight (DW) of the biomass was determined at the end of phase I and phase II (Figure 2G). *Ng* and *Pt* reached significantly higher DW than *Csp* (5-6 and 3 g L^{-1}, respectively) in phase I. Moreover, both *Pt* and *Ng* yielded similar DW at the end of phase II. In contrast, *Csp* produced only about 2 g DW L^{-1} after phase II, confirming previous observations on growth profiles. This can be explained by the fact that *Chlorella* species are mostly freshwater microalgae, hence not adapted to the high salinity of f/2 and RAS wastewater (i.e., 26 and 34 PSU, respectively) (Darienko et al., 2019).

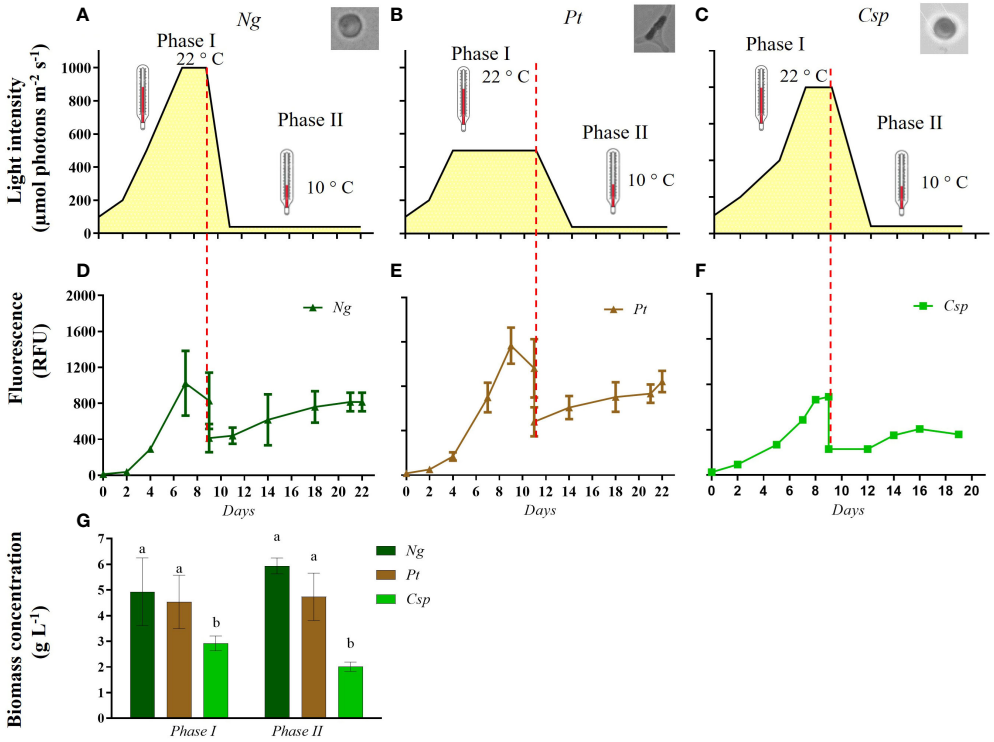

FIGURE 2
Growth conditions **(A–C)** and growth curve of **(D)** *Nannochloropsis granulata* (*Ng*, dark green line), **(E)** *Phaeodactylum tricornutum* (*Pt*, brown line), and **(F)** *Chlorella sp* (*Csp*, light green line) in a two-phase system in Multicultivator. **(G)** Biomass concentration obtained at the end of phase I and phase II cultivation in *Ng* (dark green bar), *Pt* (brown bar), and *Csp* (light green bar). Data shown in **(D–G)** are the means ± standard deviation of four biological replicates for *Ng* and *Pt*, and two biological replicates for *Csp*. Different letters indicate significant differences among the species ($p < 0.05$).

3.2 Biochemical composition of the biomass

To determine the industrial potential of the tested microalgae species as fish feed, a biochemical analysis of the biomass collected at the end of phase II was performed. In particular, to test the microalgae as an eco-sustainable alternative to terrestrial animal and plant proteins, the protein content and AA profile were determined. The biomass of *Ng* and *Csp* contained about 40% protein of DW as compared to 30% in *Pt* (Figure 3A). The proteins from the all three species contained all essential AA (i.e., Arginine, Arg; Histidine, Hys; Isoleucine, Ile; Leucine, Leu; Lysine, Lys; Phenylalanine, Phe; Threonine, Thr; and Valine, Val) except for Methionine (Met) and Tryptophane (Trp), the latter, which is not captured by the applied method. Only slight differences in the content of essential AA were detected between the three species. Both *Ng* and *Pt* contained Glutamic acid (Glu) and Aspartic acid (Asp) as main AA, with about 13-14% and 10-11% of the total, respectively. *Csp* contained Proline (Pro) and Glu as the main amino acids, with about 16% and 11 % of the total, respectively (Figure 3B).

FA content and profile were also analyzed due to their importance in both fish and human nutrition. The highest FA content was obtained in *Ng* followed by *Pt* and *Csp* with about 13, 9, and 8 % of DW, respectively (Figure 4A). FAs can be classified as saturated (SFAs), monounsaturated (MUFAs), and PUFAs to indicate the presence of only carbon single bonds, one double bond, and two or more double bonds respectively. SFAs were more abundant in *Pt* and *Csp* (i.e., about 50% of total FA) as compared to *Ng* (i.e., about 30% of total FA). *Pt* and *Ng* showed higher MUFAs (i.e., about 27-28% of the total) than *Csp* (i.e., about 16% of the total). Finally, *Ng* showed the highest content of PUFAs followed by *Csp* and *Pt* with 39, 32, and 27% of the total, respectively (Figure 4B). The FA profile was similar for *Ng* and *Pt* and dominated by C13:0 (i.e., about 13 and 23% of TFA, respectively), C16:0 (i.e., about 12 and 10 %, respectively), C16:1 (i.e., about 24 and 26%, respectively), and EPA (i.e., 25-30%). The main FAs in *Csp* were C16:0 (i.e., about 10% of TFA), C17:1 (i.e., about 13%), and alpha-linolenic acid (C18:3 n-3, i.e., about 42%). Moreover, *Pt* also contained a low concentration of DHA (about 1%) (Figure 4C). The relative content of n-3 PUFAs was about 30, 26, and 29%, respectively in *Ng*, *Pt*, and *Csp*. The corresponding percentages of LC n-3 PUFAs (i.e., EPA+DHA) were about 29 and 26%, in *Ng* and *Pt*, respectively. LC n-3 PUFAs were not detected in *Csp*.

Finally, the pigment content was analyzed as an important source of antioxidants for stabilization of the microalgae biomass or products derived thereof. Also, some studies have revealed importance of antioxidants in animal and human nutrition (Miyashita et al., 2011; Tan and Hou, 2014; Petrushkina et al.,

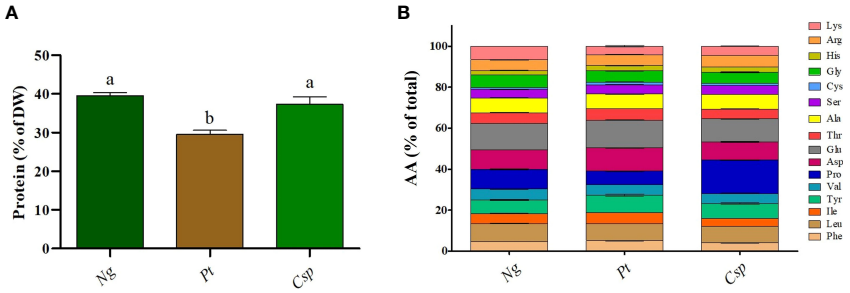

FIGURE 3
Protein content **(A)** and amino acid profile **(B)** of *Nannochloropsis granulata* (*Ng*, dark green bar), *Phaeodactylum tricornutum* (*Pt*, brown bar), and *Chlorella sp* (*Csp*, light green bar) grown in two-phase system in Multicultivator. Data shown are the means ± standard deviation of four biological replicates for *Ng* and *Pt*, and two biological replicates for *Csp*. Different letters indicate significant differences among the species ($p < 0.05$).

2017; Dawood et al., 2018). *Pt* had as main pigments chlorophyll *a*, fucoxanthin, and *β*-carotene with about 6, 10, and 0.4 µg per mg of DW, respectively. *Ng* was characterized by about 1.5 µg of chlorophyll *a*, 0.01 µg of lutein/zeaxanthin, and 0.07 µg of *β*-carotene per mg of DW. *Ng* also showed traces of astaxanthin and canthaxanthin. Finally, *Csp* contained chlorophyll *a*, lutein/zeaxanthin, and *β*-carotene as main pigments with about 6, 1, and 0.3 µg per mg of DW, respectively (Figure 5). *Csp* also produced a small amount of astaxanthin. Raw data for all biochemical analyses are available in Supplementary File 2.

3.3 Nutrient removal from RAS wastewater

To determine the potential of the different microalgae species to clean the RAS wastewater, the removal efficiency of each nitrogen compound was calculated at the end of phase II. *Ng* and *Pt* performed best in terms of cleaning the RAS wastewater from NO_2^-, NO_3^- (i.e., 100% removal) as compared to *Csp* which reduced about 76% of NO_3^- and none of the NO_2^-. NH_4^+ was reduced by 41.2 and 27.5% in *Ng* and *Pt*, respectively. The concentration of NH_4^+ was instead increased in *Csp* at the end of phase II, indicating some different nitrogen degradation pathways in *Chlorella* species. The sum of nitrogen compounds (NH_4^+, NO_2^-, NO_3^-) was not equal to the total nitrogen (TN) in all the tested samples, indicating that many organic nitrogen compounds (e.g., protein and AA origin) are released in the medium by the microalgae. Finally, all tested species efficiently and completely removed all PO_4^{3-} contained in the RAS wastewater (Table 2).

4 Discussion

In this study, we demonstrate the ability of three microalgal species (i.e., *Ng*, *Pt*, and *Csp*) to grow in RAS wastewater. Our results are in line with previous studies for *Nannochloropsis*, *Phaeodactylum tricornutum*, and *Chlorella* species, along with other species (Sirakov and Velichkova, 2014; Tejido-Nuñez et al., 2019; Villar-Navarro et al., 2021). However, *Pt*, *Ng*, and *Csp* showed about 10, 22, and 2.5-fold, respectively, higher biomass productivity than related species grown in RAS wastewater to date (Table 3). These results demonstrate the importance of two-phase cultivation to increase algal production capabilities in terms of high-quality and quantity of biomass. This novel strategy is based on the concept that each microalgae species grows best in certain (optimal) conditions, which however do not necessarily correspond to the conditions for the highest production of molecules of interest (e.g., PUFAs and carotenoids). Here, we grew *Ng*, *Pt*, and *Csp* in the following conditions: *i)* Phase I: each species was cultivated at 22°C with a gradual increase along growth to avoid photoinhibition phenomena (Aléman-Nava et al., 2017; Ali et al., 2021; Karpagam et al., 2022) and in enriched medium (i.e., f/2 14x); *ii)* phase II: the cells were transferred to a medium containing RAS wastewater in stress conditions (e.g., low nutrients, low temperature, high salinity) to

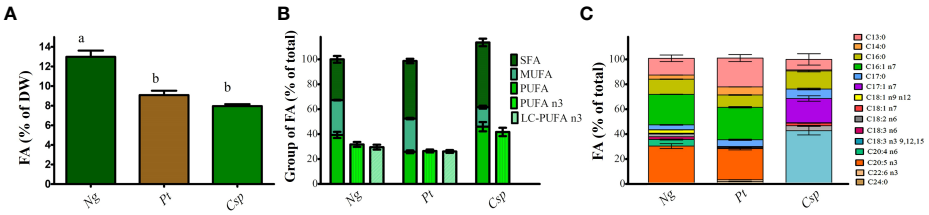

FIGURE 4
Fatty acid content **(A)**, Saturated, monounsaturated and polyunsaturated fatty acid **(B)** and fatty acid profile **(C)** of *Nannochloropsis granulata* (*Ng*, dark green bar), *Phaeodactylum tricornutum* (*Pt*, brown bar), and *Chlorella sp* (*Csp*, light green bar) grown in a two-phase cultivation in Multicultivator. Data showed are the means ± standard deviation of biological replicates for *Ng* and *Pt*, and two biological replicates for *Csp*. Different letters indicate significant differences among the species ($p < 0.05$).

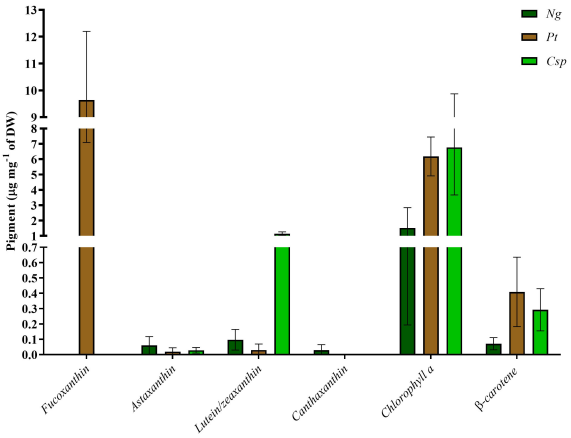

FIGURE 5
Pigment profile of *Nannochloropsis granulata* (*Ng*, dark green bar), *Phaeodactylum tricornutum* (*Pt*, brown bar), and *Chlorella sp* (*Csp*, light green bar) grown in a two-phase system in Multicultivator. Data shown are the means ± standard deviation of four biological replicates for *Ng* and *Pt*, and two biological replicates for *Csp*. Different letters indicate significant differences among the species ($p<0.05$).

increase the production of molecules of interest. Similar strategies were previously used for *Nannochloropsis oculata*, *Pt*, and *Chlorella vulgaris* resulting in increased lipid and carotenoid productivity (Sirakov and Velichkova, 2014; Villar-Navarro et al., 2021). To our knowledge, this is the first time that a two-phase cultivation strategy was applied for growing microalgae in RAS wastewater. Moreover, we show that by using this strategy the algal biomass yield can increase in *Ng* and *Pt* by a factor of about 3 and 2, respectively, as compared to one-phase cultivation (Supplementary File 1C; Figure 2G).

Microalgae are good candidates to partially replace fishmeal and fish oil in fish feed. For instance, inclusions levels of 7.5-30% of *Nanochloropsis oceanica* extracts gave promising results in cold-water species such as Atlantic salmon (*Salmo salar*) and spotted wolffish (*Anarhichas minor*) (Sørensen et al., 2017; Gong et al., 2018; Knutsen et al., 2019). However, only a few studies focused on the biomass composition of microalgae grown in RAS wastewater to date (Sirakov and Velichkova, 2014; Villar-Navarro et al., 2021). Here, we determined the content of proteins, AA, FA, and carotenoids in the biomass derived from phase II cultivation of *Ng*, *Pt*, and *Csp* to evaluate their potential as alternative sustainable fish feed. We found a higher protein content in all tested microalgae (30-40% of DW) than previous results obtained in other species or strains grown in similar conditions (i.e., 14-37% of DW) Cho and Kim, 2011). However, all these values are significantly lower than the average protein content found in fish feed (i.e., 60-72%, Cho and Kim, 2011), calling for downstream up-concentration of the proteins. This can be done for example with the pH-shift process commonly applied to e.g. soybeans and peas (Dumoulin et al., 2021), but also to algae (Cavonius et al., 2015; Trigo et al., 2023). It is well known that under nitrogen deplete conditions (i.e., conditions found in phase II of this work), protein concentration can be reduced in several microalgae species, explaining our results (Jia et al., 2015; Canelli et al., 2020; Latsos et al., 2020). Moreover, the proteins of *Pt*, *Ng* and *Csp* were constituted by almost all essential AA, confirming previous results for closely related species (Villar-Navarro et al., 2021; Forghani et al., 2022).

Ng, *Pt*, and *Csp* showed higher PUFAs content as compared to related species when grown in RAS wastewater (Villar-Navarro et al., 2021; Forghani et al., 2022). The increase in PUFAs can be explained by the use of low temperatures (i.e., 10°C) during phase II cultivation, as concentration of PUFAs generally decreases at increasing temperatures in microalgae, including in *Pt* (Qiao et al., 2016; Santin et al., 2021). The biomasses were also rich in n-3 PUFAs, i.e., 25-30% of FAs were constituted by EPA in *Pt* and *Ng* and by C18:3 n-3 in *Csp*. These amounts were higher than the reference values for fish oil, confirming the potential of these microalgal strains as a substitute for fish feed (Villar-Navarro et al., 2021).

Finally, the pigment content of the microalgae biomass was evaluated based on their beneficial effect on animals and humans for blocking macrophage-mediated inflammation and inflammation-induced obesity in both *in-vivo* and *in-vitro* assays (Tan and Hou, 2014; Petrushkina et al., 2017). Fucoxanthin is the most abundant pigment carotenoid in diatoms and can make up to 1-2.5 % of DW (Yi et al., 2015; Guo et al., 2016). A similar fucoxanthin content was found in *Pt* in our study and was 3-fold higher than in previous results for the same species (Villanova et al., 2021b). This finding can be explained by the use of low light intensity in phase II, often correlated to an increase in the fucoxanthin content in *Pt* (Khaw et al., 2022). Other valuable carotenoids detected in *Pt*, *Csp*, and *Ng* were β-carotene and lutein/zeaxanthin, confirming previous results (Serra et al., 2021; Villanova et al., 2022). It is known that β-carotene concentration content can increase in microalgae

TABLE 3 Comparison of microalgal biomass productivity from this study with previous studies in RAS wastewater.

Species	Biomass productivity (mg DW L^{-1} d^{-1})	Cultivation condition	Reference
Nannochloropsis granulata	270 ± 13	Two-phase cultivation	This study
Phaeodactylum tricornutum	225 ± 49	Two-phase cultivation	This study
Chlorella sp	105 ± 7	Two-phase cultivation	This study
Nannochloropsis gaditana	23 ± 1	Batch cultivation	(Villar-Navarro et al., 2021)
Phaeodactylum tricornutum	32 ± 1	Batch cultivation	(Villar-Navarro et al., 2021)
Chlorella vulgaris	42.6	Continuous cultivation	(Gao et al., 2016)

cultivated under salt stress (Villanova et al., 2021a). The salinity in the tested RAS wastewater was only slightly higher than in the microalgae cultivation medium (Table 1). This can explain why we did not detect a significant increase in the concentration content of this carotenoid.

The last part of this work was focused on the determination of the capability of *Ng*, *Pt*, and *Csp* to remove the nutrients present in RAS wastewater. In RAS, NH_4^+ is oxidized into NO_3^- *via* NO_2^- by nitrifying bacteria in a biofilm reactor. All these compounds can accumulate over time in RAS and if not appropriately managed through regular water changes or denitrification, may negatively affect the fish. High NH_4^+ is neurotoxic for fish (Wilkie, 2002). NO_2^- converts hemoglobin into methemoglobin, which is not capable to bind O_2 (Russo and Thurston, 1977; Williams and Eddy, 1986). NO_3^- toxicity is thought to be similar to that of NO_2^-, but to a lower extent (Stormer et al., 1996; Camargo et al., 2005). As most of the RAS nowadays are partial RAS (i.e., without denitrification), (NO_3^- can slowly accumulate over time and reach concentrations which could affect fish health and welfare (Russo and Thurston, 1977; Wilkie, 2002). High NO_3^- can be managed through the biological conversion of NO_3^- to nitrogen gas (N_2) in anaerobic denitrifying biofilters, or by regular water exchanges (Williams and Eddy, 1986; Camargo et al., 2005). The concentration of NH_4^+, NO_2^- and NO_3^- measured in our RAS wastewater are quite typical for a conventional RAS with only nitrification, with NH_4^+ values below 1 mg-N L^{-1}, NO_2^- below 0.5 mg-N L^{-1} and accumulation of NO_3^- up to 100-1000 mg-N L^{-1} (Brazil et al., 1996; Krumins et al., 2001; Van Rijn and Ebeling, 2007; Roques, 2013; Ciji and Akhtar, 2020; Sikora et al., 2022). Our results showed that all three microalgae species were able to remove efficiently NO_3^- from their environment. In particular, *Pt* and *Ng* were able to completely remove NO_3^- and NO_2^- and are therefore the two most promising candidates to treat RAS wastewater. Despite a decent removal efficiency of NO_3^- (75.7%), *Csp* did not remove any other nitrogenous waste compounds, and even increased the concentration of NH_4^+ and NO_2^-. This relatively low performance could again be linked to the fact that *Csp* is a mostly freshwater microalgae species and its performance in this study was probably affected by the exposure to the relatively high salinity of both f/2 and RAS wastewater (Darienko et al., 2019). The NH_4^+ removal efficiencies of *Pt* and *Ng* were also quite limited (27.5 and 41.2%, respectively), which was quite expected as NO_3^- seems to be the preferred substrate of these microalgae. NH_4^+ seems to inhibit the uptake of NO_3^- in *Pt* (Cresswell and Syrett, 1979). Yongmanitchai and Ward (1991) used NH_4^+, NO_3^- and urea as nitrogen sources for *Pt*, showing that the growth was inhibited in the culture supplemented with NH_4^+ alone or in combination with NO_3^- or urea *Nannochloropis* species can use either NH_4^+, NO_2^- or NO_3^- as the sole nitrogen source, but NO_3^- and NO_2^- seem to be the preferred substrates for these species, as introduced NH_4^+ acidify the pH conditions of the medium (Sauer et al., 2001; Liu et al., 2017). As a result, *Pt* and *Ng* are great candidates to remove NO_3^- from marine RAS wastewater, but they should be used in combination with other treatment solutions to also remove excess NH_4^+ (e.g., nitrifying bacteria).

To conclude, all species tested in this study showed great potential as a sustainable alternative to fish oil and meal and as a source of antioxidants for fish feed. These species also showed great potential as a multifunctional vegan protein ingredient for various food products in which also n-3 PUFAs and antioxidants are wanted. Moreover, the two-phase cultivation can be used as a strategy to *i)* increase the productivity and content of high-value molecules in the biomass of the tested strains, and *ii*) recycle the RAS wastewater. Different growth conditions and microbial species should be tested to further optimize this process.

Data availability statement

The original contributions presented in the study are included in the article/Supplementary Material. Further inquiries can be directed to the corresponding authors.

Author contributions

VV, JR, and CS contributed to the conception and design of the study. VV performed the experiments. VV, JR, BF, and KS performed sample analyses. VV performed the statistical analyses. IU and CS supervised the project. VV, JR, IU, and CS secured funding. VV and JR wrote the first draft of the manuscript. All authors contributed to the manuscript revision, and read, and approved the submitted version.

Funding

This research was supported by the European Union's Horizon 2020 research and innovation programme under the Marie Sklodowska-Curie Grant Agreement No. 844909, The Swedish Research Council for Sustainable Development FORMAS (2020-00867 and 2018-01839), Stockholm, Sweden, the Royal Swedish Academy of Agriculture and Forestry (KSLA), Stockholm, Sweden (VAT2020-0007), The Birgit och Birger Wåhlströms Minnesfond för den bohuslänska havs-och insjömiljön, Stockholm, Sweden, STINT, Stockholm, Sweden (mobility grant for internationalization, MG2019-8483), SWEMARC, the Swedish mariculture research center, strategic funding university of Gothenburg, Gothenburg, Sweden, JSPS KAKENHI Grant Numbers JP20KK0244 Tokyo, Japan. KS was a recipient of a postdoctoral fellowship from the Carl Tryggers Foundation CTS20:406.

Acknowledgments

The authors are grateful to Professor Tomonori Kindaichi and M.Sc. Naoki Fujii (Hiroshima University, Japan) for their technical assistance with the measurement of NO_3^-. We thank Olga Kourtchenko from the Department of Marine Sciences, University of Gothenburg for providing the *Ng, Pt*, and *Csp* from the GUMACC collection.

Conflict of interest

The authors declare that the research was conducted in the absence of any commercial or financial relationships that could be construed as a potential conflict of interest.

Publisher's note

Supplementary material

The Supplementary Material for this article can be found online at: https://www.frontiersin.org/articles/10.3389/fpls.2023.1186537/full#supplementary-material

SUPPLEMENTARY FILE 1
Growth curve and final biomass of microalgal strains from GUMACC collection in one-phase cultivation. Growth curve of **(A)** *Phaeodactylum tricornutum* (*Pt*, brown lines) and **(B)** *Nannochloropsis granulata* (*Ng*, dark green lines) in f/2 14x (continuous lines) and RAS wastewater 14N (dotted lines). **(C)** Final biomass concentration of *Ng* and *Pt* grown in both f/2 14x and RAS wastewater 14N. Data shown are the means ± standard deviation of three biological replicates.

SUPPLEMENTARY FILE 2
Biochemical analysis of the biomass produced in phase II cultivation.

References

Abida, H., Dolch, L.-J., Meï, C., Villanova, V., Conte, M., Block, M. A., et al. (2015). Membrane glycerolipid remodeling triggered by nitrogen and phosphorus starvation in phaeodactylum tricornutum. *Plant Physiol.* 167, 118–136. doi: 10.1104/pp.114.252395

Ahmad, A., Abdullah, S. R. S., Hasan, H. A., Othman, A. R., and Ismail, N. I. (2021). Aquaculture industry: supply and demand, best practices, effluent and its current issues and treatment technology. *J. Environ. Manage.* 287, 112271. doi: 10.1016/j.jenvman.2021.112271

Ahmed, N., and Turchini, G. M. (2021). Recirculating aquaculture systems (RAS): environmental solution and climate change adaptation. *J. Clean. Prod.* 297, 126604. doi: 10.1016/j.jclepro.2021.126604

Aléman-Nava, G. S., Muylaert, K., Bermudez, S. P. C., Depraetere, O., Rittmann, B., Parra-Saldívar, R., et al. (2017). Two-stage cultivation of nannochloropsis oculata for lipid production using reversible alkaline flocculation. *Biores. Technol.* 226, 18–23. doi: 10.1016/j.biortech.2016.11.121

Ali, H. E. A., El-Fayoumy, E. A., Rasmy, W. E., Soliman, R. M., and Abdullah, M. A. (2021). Two-stage cultivation of chlorella vulgaris using light and salt stress conditions for simultaneous production of lipid, carotenoids, and antioxidants. *J. Appl. Phycol.* 33, 227–239. doi: 10.1007/s10811-020-02308-9

Arena, R., Lima, S., Villanova, V., Moukri, N., Curcuraci, E., Messina, C., et al. (2021). Cultivation and biochemical characterization of isolated Sicilian microalgal species in salt and temperature stress conditions. *Algal Res.* 59, 102430. doi: 10.1016/j.algal.2021.102430

Asadi, P., Rad, H. A., and Qaderi, F. (2019). Comparison of chlorella vulgaris and chlorella sorokiniana pa. 91 in post treatment of dairy wastewater treatment plant effluents. *Environ. Sci. pollut. R.* 26, 29473–29489. doi: 10.1007/s11356-019-06051-8

Bleakley, S., and Hayes, M. (2017). Algal proteins: extraction, application, and challenges concerning production. *Foods* 6, 33. doi: 10.3390/foods6050033

Brazil, B. L., Summerfelt, S. T., and Libey, G. S. (1996). "Application of ozone to recirculating aquaculture systems," *Proceeding from the Successes and Failures in Commercial Recirculating Aquaculture Conference. Roanoke, VA*. (152 Riley-Robb Hall, Ithaca, New York: Northeast Regional Agricultural Engineering Service) 1996.

Camacho-Rodríguez, J., Macías-Sánchez, M., Cerón-García, M., Alarcón, F., and Molina-Grima, E. (2018). Microalgae as a potential ingredient for partial fish meal replacement in aquafeeds: nutrient stability under different storage conditions. *J. Appl. Phycol.* 30, 1049–1059. doi: 10.1007/s10811-017-1281-5

Camargo, J. A., Alonso, A., and Salamanca, A. (2005). Nitrate toxicity to aquatic animals: a review with new data for freshwater invertebrates. *Chemosphere* 58, 1255–1267. doi: 10.1016/j.chemosphere.2004.10.044

Canelli, G., Tarnutzer, C., Carpine, R., Neutsch, L., Bolten, C. J., Dionisi, F., et al. (2020). Biochemical and nutritional evaluation of chlorella and auxenochlorella biomasses relevant for food application. *Front. Nutr.* 7, 565996. doi: 10.3389/fnut.2020.565996

Cavonius, L. R., Albers, E., and Undeland, I. (2015). pH-shift processing of nannochloropsis oculata microalgal biomass to obtain a protein-enriched food or feed ingredient. *Algal Res.* 11, 95–102. doi: 10.1016/j.algal.2015.05.022

Cavonius, L. R., Carlsson, N.-G., and Undeland, I. (2014). Quantification of total fatty acids in microalgae: comparison of extraction and transesterification methods. *Anal. Bioanal. Chem.* 406, 7313–7322. doi: 10.1007/s00216-014-8155-3

Chen, S. (2002). Recirculating systems effluents and treatments. In: Tumasso, J. (ed). *Aquaculture and the Environment in the United States. A Chapter of the World Aquaculture Society*. (Baton Rouge: US Aquaculture Society), pp. 119–140.

Cheregi, O., Engelbrektsson, J., Andersson, M. X., Strömberg, N., Ekendahl, S., Godhe, A., et al. (2021). Marine microalgae for outdoor biomass production–a laboratory study simulating seasonal light and temperature for the west coast of Sweden. *Physiol. Plant.* 173, 543–554. doi: 10.1111/ppl.13412

Cho, J., and Kim, I. (2011). Fish meal–nutritive value. *J. Anim. Physiol. An. N.* 95, 685–692. doi: 10.1111/j.1439-0396.2010.01109.x

Ciji, A., and Akhtar, M. S. (2020). Nitrite implications and its management strategies in aquaculture: a review. *Rev. Aquacult.* 12, 878–908. doi: 10.1111/raq.12354

Cresswell, R., and Syrett, P. (1979). Ammonium inhibition of nitrate uptake by the diatom, phaeodactylum tricornutum. *Plant Sci. Lett.* 14, 321–325. doi: 10.1016/S0304-4211(79)90263-3

Darienko, T., Rad-Menéndez, C., Campbell, C., and Pröschold, T. (2019). Are there any true marine chlorella species? molecular phylogenetic assessment and ecology of marine chlorella-like organisms, including a description of droopiella gen. nov. *Syst. Biodivers.* 17, 811–829. doi: 10.1080/14772000.2019.1690597

Dawood, M. A., Koshio, S., and Esteban, M. Á. (2018). Beneficial roles of feed additives as immunostimulants in aquaculture: a review. *Rev. Aquacult.* 10, 950–974. doi: 10.1111/raq.12209

Dumoulin, L., Jacquet, N., Malumba, P., Richel, A., and Blecker, C. (2021). Dry and wet fractionation of plant proteins: how a hybrid process increases yield and impacts nutritional value of faba beans proteins. *Innov. Food Sci. Emerg.* 72, 102747. doi: 10.1016/j.ifset.2021.102747

FAO (2020). *The state of food and agriculture 2020. overcoming water challenges in agriculture* (Rome, Italy: FAO).

FAO (2022). *The state of world fisheries and aquaculture (SOFIA) 2022* (Rome: Food and Agriculture Organization of the United Nations).

Flachowsky, G., Meyer, U., and Südekum, K.-H. (2017). Land use for edible protein of animal origin–a review. *Animals* 7, 25. doi: 10.3390/ani7030025

Forghani, B., Mayers, J. J., Albers, E., and Undeland, I. (2022). Cultivation of microalgae-chlorella sorokiniana and auxenochlorella protothecoides-in shrimp boiling water residues. *Algal Res.* 65, 102753. doi: 10.1016/j.algal.2022.102753

Francis, G., Makkar, H. P., and Becker, K. (2001). Antinutritional factors present in plant-derived alternate fish feed ingredients and their effects in fish. *Aquaculture* 199, 197–227. doi: 10.1016/S0044-8486(01)00526-9

Gao, F., Li, C., Yang, Z.-H., Zeng, G.-M., Feng, L.-J., Liu, J.-Z., et al. (2016). Continuous microalgae cultivation in aquaculture wastewater by a membrane photobioreactor for biomass production and nutrients removal. *Ecol. Eng.* 92, 55–61. doi: 10.1016/j.ecoleng.2016.03.046

Gong, Y., Guterres, H., Huntley, M., Sørensen, M., and Kiron, V. (2018). Digestibility of the defatted microalgae nannochloropsis sp. and desmodesmus sp. when fed to a tlantic salmon, Salmo salar. *Aquacult. Nutr.* 24, 56–64. doi: 10.1111/anu.12533

Guillard, R. R., and Ryther, J. H. (1962). Studies of marine planktonic diatoms: i. cyclotella nana hustedt, and detonula confervacea (Cleve) gran. can. *J. Microbiol.* 8, 229–239. doi: 10.1139/m62-029

Guo, B., Liu, B., Yang, B., Sun, P., Lu, X., Liu, J., et al. (2016). Screening of diatom strains and characterization of cyclotella cryptica as a potential fucoxanthin producer. *Mar. Drugs* 14, 125. doi: 10.3390/md14070125

Hardy, R. W. (2010). Utilization of plant proteins in fish diets: effects of global demand and supplies of fishmeal. *Aquac. Res.* 41, 770–776. doi: 10.1111/j.1365-2109.2009.02349.x

Jia, J., Han, D., Gerken, H. G., Li, Y., Sommerfeld, M., Hu, Q., et al. (2015). Molecular mechanisms for photosynthetic carbon partitioning into storage neutral lipids in nannochloropsis oceanica under nitrogen-depletion conditions. *Algal Res.* 7, 66–77. doi: 10.1016/j.algal.2014.11.005

Karpagam, R., Jawaharraj, K., Ashokkumar, B., Pugazhendhi, A., and Varalakshmi, P. (2022). A cheap two-step cultivation of phaeodactylum tricornutum for increased TAG production and differential expression of TAG biosynthesis associated genes. *J. Biotechnol.* 354, 53–62. doi: 10.1016/j.jbiotec.2022.06.002

Khaw, Y. S., Yusoff, F. M., Tan, H. T., Noor Mazli, N., Nazarudin, M. F., Shaharuddin, N. A., et al. (2022). Fucoxanthin production of microalgae under different culture factors: a systematic review. *Mar. Drugs* 20, 592. doi: 10.3390/md20100592

Knutsen, H., Johnsen, I., Keizer, S., Sørensen, M., Roques, J., Hedén, I., et al. (2019). Fish welfare, fast muscle cellularity, fatty acid and body-composition of juvenile spotted wolffish (Anarhichas minor) fed a combination of plant proteins and microalgae (Nannochloropsis oceanica). *Aquaculture* 506, 212–223. doi: 10.1016/j.aquaculture.2019.03.043

Koyande, A. K., Chew, K. W., Rambabu, K., Tao, Y., Chu, D.-T., and Show, P.-L. (2019). Microalgae: a potential alternative to health supplementation for humans. *Food Sci. Hum. Wellness* 8, 16–24. doi: 10.1016/j.fshw.2019.03.001

Krumins, V., Ebeling, J., and Wheaton, F. (2001). Part-day ozonation for nitrogen and organic carbon control in recirculating aquaculture systems. *Aquacult. Eng.* 24, 231–241. doi: 10.1016/S0144-8609(01)00061-9

Latsos, C., Van Houcke, J., and Timmermans, K. R. (2020). The effect of nitrogen starvation on biomass yield and biochemical constituents of rhodomonas sp. *Front. Mar. Sci.* 7, 563333. doi: 10.3389/fmars.2020.563333

Lenzi, M. (2013). The future of aquaculture. *J. Aquac. Res. Dev.* 4, e106. doi: 10.4172/2155-9546.1000e106

Lima, S., Villanova, V., Grisafi, F., Caputo, G., Brucato, A., and Scargiali, F. (2020). Autochthonous microalgae grown in municipal wastewaters as a tool for effectively removing nitrogen and phosphorous. *J. Water Process. Eng.* 38, 101647. doi: 10.1016/j.jwpe.2020.101647

Liu, J., Song, Y., and Qiu, W. (2017). Oleaginous microalgae nannochloropsis as a new model for biofuel production: review & analysis. *Renew. Sustain. Energy Rev.* 72, 154–162. doi: 10.1016/j.rser.2016.12.120

Micolucci, F., Roques, J. A., Ziccardi, G. S., Fujii, N., Sundell, K., and Kindaichi, T. (2023). Candidatus scalindua, a biological solution to treat saline recirculating aquaculture system wastewater. *Processes* 11, 690. doi: 10.3390/pr11030690

Miyashita, K., Nishikawa, S., Beppu, F., Tsukui, T., Abe, M., and Hosokawa, M. (2011). The allenic carotenoid fucoxanthin, a novel marine nutraceutical from brown seaweeds. *J. Sci. Food Agr.* 91, 1166–1174. doi: 10.1002/jsfa.4353

Mojiri, A., Ohashi, A., Ozaki, N., Aoi, Y., and Kindaichi, T. (2020). Integrated anammox-biochar in synthetic wastewater treatment: performance and optimization by artificial neural network. *J. Clean. Prod.* 243, 118638. doi: 10.1016/j.jclepro.2019.118638

Øvrebø, T. K., Balseiro, P., Imsland, A. K. D., Stefansson, S. O., Tveterås, R., Sveier, H., et al. (2022). Investigation of growth performance of post-smolt Atlantic salmon (Salmo salar l.) in semi closed containment system: a big-scale benchmark study. *Aquac. Res.* 53, 4178–4189. doi: 10.1111/are.15919

Pahri, S. D. R., Mohamed, A. F., and Samat, A. (2015). LCA for open systems: a review of the influence of natural and anthropogenic factors on aquaculture systems. *Int. J. Life Cycle Assess.* 20, 1324–1337. doi: 10.1007/s11367-015-0929-0

Petrushkina, M., Gusev, E., Sorokin, B., Zotko, N., Mamaeva, A., Filimonova, A., et al. (2017). Fucoxanthin production by heterokont microalgae. *Algal Res.* 24, 387–393. doi: 10.1016/j.algal.2017.03.016

Preena, P. G., Rejish Kumar, V. J., and Singh, I. S. B. (2021). Nitrification and denitrification in recirculating aquaculture systems: the processes and players. *Rev. Aquacult.* 13, 2053–2075. doi: 10.1111/raq.12558

Qiao, H., Cong, C., Sun, C., Li, B., Wang, J., and Zhang, L. (2016). Effect of culture conditions on growth, fatty acid composition and DHA/EPA ratio of phaeodactylum tricornutum. *Aquaculture* 452, 311–317. doi: 10.1016/j.aquaculture.2015.11.011

Roques, J. (2013). *Apects of fish welfare in aquaculture practices* (The Netherlands: Radboud University Nijmegen).

Roques, J. A., Micolucci, F., Hosokawa, S., Sundell, K., and Kindaichi, T. (2021). Effects of recirculating aquaculture system wastewater on anammox performance and community structure. *Processes* 9, 1183. doi: 10.3390/pr9071183

Russo, R., and Thurston, R. (1977). The acute toxicity of nitrite to fishes. In: Tubb, R. A. (ed). *Recent Advances in Fish Toxicity* (Corvallis, OR, USA: US Environmental protection Agency). EPA-600/3-77-085, 118–131.

Samer, M. (2015). Biological and chemical wastewater treatment processes. *Wastewater Treat. Eng.* 150, 212. doi: 10.5772/61250

Santin, A., Russo, M. T., Ferrante, M. I., Balzano, S., Orefice, I., and Sardo, A. (2021). Highly valuable polyunsaturated fatty acids from microalgae: strategies to improve their yields and their potential exploitation in aquaculture. *Molecules* 26, 7697. doi: 10.3390/molecules26247697

Sathasivam, R., Radhakrishnan, R., Hashem, A., and Abd_Allah, E. F. (2019). Microalgae metabolites: a rich source for food and medicine. *Saudi J. Biol. Sci.* 26, 709–722. doi: 10.1016/j.sjbs.2017.11.003

Sauer, J. R., Schreiber, U., Schmid, R., VöLker, U., and Forchhammer, K. (2001). Nitrogen starvation-induced chlorosis in synechococcus PCC 7942. low-level photosynthesis as a mechanism of long-term survival. *Plant Physiol.* 126, 233–243. doi: 10.1104/pp.126.1.233

Serra, A. T., Silva, S. D., Pleno De Gouveia, L., Alexandre, A. M., Pereira, C. V., Pereira, A. B., et al. (2021). A single dose of marine chlorella vulgaris increases plasma concentrations of lutein, β-carotene and zeaxanthin in healthy Male volunteers. *Antioxidants* 10, 1164. doi: 10.3390/antiox10081164

Sikora, M., Nowosad, J., and Kucharczyk, D. (2022). Nitrogen compound oxidation rate in recirculation systems using three biological filter medias in rearing common carp (Cyprinus carpio l.) juveniles. *Aquaculture* 547, 737532. doi: 10.1016/j.aquaculture.2021.737532

Sirakov, I., and Velichkova, K. (2014). Bioremediation of wastewater originate from aquaculture and biomass production from microalgae species-nannochloropsis oculata and tetraselmis chuii. *Bulg. J. Agric. Sci.* (Agricultural Academy - Bulgaria) 20, 66–72. Available at: http://agrojournal.org/20/01-12.pdf.

Slocombe, S. P., Ross, M., Thomas, N., Mcneill, S., and Stanley, M. S. (2013). A rapid and general method for measurement of protein in micro-algal biomass. *Biores. Technol.* 129, 51–57. doi: 10.1016/j.biortech.2012.10.163

Sørensen, M., Gong, Y., Bjarnason, F., Vasanth, G. K., Dahle, D., Huntley, M., et al. (2017). Nannochloropsis oceania-derived defatted meal as an alternative to fishmeal in Atlantic salmon feeds. *PloS One* 12, e0179907. doi: 10.1371/journal.pone.0179907

Stormer, J., Jensen, F. B., and Rankin, J. C. (1996). Uptake of nitrite, nitrate, and bromide in rainbow trout,(Oncorhynchus mykiss): effects on ionic balance. *Can. J. Fish. Aquat. Sci.* 53, 1943–1950. doi: 10.1139/cjfas-53-9-1943

Tan, C.-P., and Hou, Y.-H. (2014). First evidence for the anti-inflammatory activity of fucoxanthin in high-fat-diet-induced obesity in mice and the antioxidant functions in PC12 cells. *Inflammation* 37, 443–450. doi: 10.1007/s10753-013-9757-1

Tejido-Nuñez, Y., Aymerich, E., Sancho, L., and Refardt, D. (2019). Treatment of aquaculture effluent with chlorella vulgaris and tetradesmus obliquus: the effect of pretreatment on microalgae growth and nutrient removal efficiency. *Ecol. Eng.* 136, 1–9. doi: 10.1016/j.ecoleng.2019.05.021

Tossavainen, M., Lahti, K., Edelmann, M., Eskola, R., Lampi, A.-M., Piironen, V., et al. (2019). Integrated utilization of microalgae cultured in aquaculture wastewater: wastewater treatment and production of valuable fatty acids and tocopherols. *J. Appl. Phycol.* 31, 1753–1763. doi: 10.1007/s10811-018-1689-6

Trigo, J. P., Stedt, K., Schmidt, A. E., Kollander, B., Edlund, U., Nylund, G., et al. (2023). Mild blanching prior to pH-shift processing of saccharina latissima retains protein extraction yields and amino acid levels of extracts while minimizing iodine content. *Food Chem.* 404, 134576. doi: 10.1016/j.foodchem.2022.134576

Van Rijn, J. (2013). Waste treatment in recirculating aquaculture systems. *Aquacult. Eng.* 53, 49–56. doi: 10.1016/j.aquaeng.2012.11.010

Van Rijn, J., and Ebeling, J. (2007). Denitrification. *Recirculating Aquac.* (New York, NY, USA: Cayuga Aqua Ventures, Ithaca), 387–424.

Villanova, V., Fortunato, A. E., Singh, D., Bo, D. D., Conte, M., Obata, T., et al. (2017). Investigating mixotrophic metabolism in the model diatom phaeodactylum tricornutum. *Philos. T. R.* 372, 20160404. doi: 10.1098/rstb.2016.0404

Villanova, V., Galasso, C., Fiorini, F., Lima, S., Brönstrup, M., Sansone, C., et al. (2021a). Biological and chemical characterization of new isolated halophilic microorganisms from saltern ponds of trapani, Sicily. *Algal Res.* 54, 102192. doi: 10.1016/j.algal.2021.102192

Villanova, V., Galasso, C., Vitale, G. A., Della Sala, G., Engelbrektsson, J., Strömberg, N., et al. (2022). Mixotrophy in a local strain of nannochloropsis granulata for renewable high-value biomass production on the West coast of Sweden. *Mar. Drugs* 20, 424. doi: 10.3390/md20070424

Villanova, V., Singh, D., Pagliardini, J., Fell, D., Le Monnier, A., Finazzi, G., et al. (2021b). Boosting biomass quantity and quality by improved mixotrophic culture of the diatom phaeodactylum tricornutum. *Front- Plant Sci.* 12, 642199. doi: 10.3389/fpls.2021.642199

Villar-Navarro, E., Garrido-Pérez, C., and Perales, J. A. (2021). The potential of different marine microalgae species to recycle nutrients from recirculating aquaculture systems (RAS) fish farms and produce feed additives. *Algal Res.* 58, 102389. doi: 10.1016/j.algal.2021.102389

Villar-Navarro, E., Ruiz, J., Garrido-Pérez, C., and Perales, J. A. (2022). Microalgae biotechnology for simultaneous water treatment and feed ingredient production in aquaculture. *J. Water Process. Eng.* 49, 103115. doi: 10.1016/j.jwpe.2022.103115

Wilkie, M. P. (2002). Ammonia excretion and urea handling by fish gills: present understanding and future research challenges. *J. Exp. Zool.* 293, 284–301. doi: 10.1002/jez.10123

Williams, E., and Eddy, F. (1986). Chloride uptake in freshwater teleosts and its relationship to nitrite uptake and toxicity. *J. Comp. Physiol. B.* 156, 867–872. doi: 10.1007/BF00694263

World Bank (2013). *FISH TO 2030 prospects for fisheries and aquaculture WORLD BANK REPORT NUMBER 83177-GLB* (Washington, DC: World bank).

Yi, Z., Xu, M., Magnusdottir, M., Zhang, Y., Brynjolfsson, S., and Fu, W. (2015). Photo-oxidative stress-driven mutagenesis and adaptive evolution on the marine diatom phaeodactylum tricornutum for enhanced carotenoid accumulation. *Mar. Drugs* 13, 6138–6151. doi: 10.3390/md13106138

Yongmanitchai, W., and Ward, O. P. (1991). Growth of and omega-3 fatty acid production by phaeodactylum tricornutum under different culture conditions. *Appl. Environ. Microb.* 57, 419–425. doi: 10.1128/aem.57.2.419-425.1991

Frontiers in Plant Science

Cultivates the science of plant biology and its applications

The most cited plant science journal, which advances our understanding of plant biology for sustainable food security, functional ecosystems and human health.

Discover the latest Research Topics

See more →

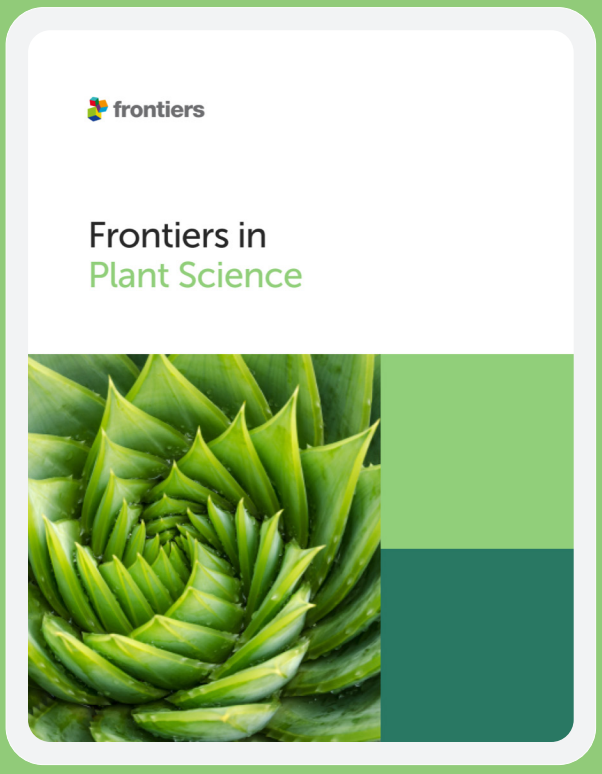

Frontiers

Avenue du Tribunal-Fédéral 34
1005 Lausanne, Switzerland
frontiersin.org

Contact us

+41 (0)21 510 17 00
frontiersin.org/about/contact